



Title	Regulations and functions of rho-kinases in hepatocellular carcinoma
Advisor(s)	Ng, IOL
Author(s)	Wong, Chak-lui, Carmen.; 黃澤薈.
Citation	Wong, C. C. [黃澤薈]. (2009). Regulations and functions of rho-kinases in hepatocellular carcinoma. (Thesis). University of Hong Kong, Pokfulam, Hong Kong SAR. Retrieved from http://dx.doi.org/10.5353/th_b4218200
Issued Date	2009
URL	http://hdl.handle.net/10722/61132
Rights	The author retains all proprietary rights, (such as patent rights) and the right to use in future works.

Abstract of thesis entitled

**Regulations and Functions of Rho-kinases in
Hepatocellular Carcinoma**

Submitted by

Wong, Carmen Chak-Lui

For the degree of Doctor of Philosophy

At the University of Hong Kong

April 2009

Hepatocellular carcinoma (HCC) is the fifth most prevalent cancer in the world causing more than 500, 000 deaths per annum. Metastasis is a major cause of mortality in HCC patients, and understanding the molecular mechanisms involved is of crucial significance. Acquisition of cell migration is an indispensable step involved in cancer metastasis. In this study, we aimed to investigate the migratory pathway regulating HCC cell movement hence leading to HCC invasion.

Previously, we characterized a tumor suppressor gene, Deleted in Liver Cancer 1 (DLC1), a RhoGAP protein which suppressed the activity of RhoA. Rho-kinases, ROCK1 and ROCK2 are immediate down-stream effectors of RhoA in regulating various cytoskeletal events, and are implicated in cell motility and cancer metastasis. Therefore, we examined the effect of DLC1 on ROCK in HCC. We found that DLC1 suppressed ROCK-mediated cytoskeletal reorganization including the formation of focal adhesions



stress fibers network, and the cortical phosphorylation of myosin light chain in a RhoGAP dependent manner and eventually resulted in cytoskeletal collapse. Dominant active ROCK reversed the DLC1 induced cytoskeletal collapse. This part of our findings suggested that DLC1/Rho/ROCK might be an important pathway regulating HCC cell movement and HCC invasion.

In a continuous effort to delineate the functional implication of the DLC1/Rho/ROCK pathway, we examined the molecular impact of ROCK in HCC. We showed that ROCK2 but not ROCK1 was frequently overexpressed in primary HCC. Overexpression of ROCK2 was closely associated with presence of tumor microsatellite formation, an indicator of intrahepatic metastasis in HCC. Stable knockdown of ROCK2 resulted in a significant reduction of cell migration and invasion *in vitro* and *in vivo*. We also observed significant reduction of myosin phosphatase phosphorylation and disruption of actin polymerization when ROCK2 was stably knocked down. This part of our findings indicated that ROCK2 played an important role in coordinating cytoskeletal events and contributed to the invasion of HCC.

ROCK2 was overexpressed at protein but not mRNA level. Thus, we aimed to investigate the post-transcriptional mechanism that might contribute to the deregulation of ROCK2 in human HCC. First, we found that the 3' untranslated region (UTR) of ROCK2 suppressed gene translation. It has been widely reported that a group of non-coding RNAs, microRNAs, interacts with the 3'UTR of the target genes and suppresses gene translation. By *in silico* study, we identified a microRNA, miR139, that harbored



potential interacting ability with the 3'UTR of ROCK2. Overexpression of miR139 suppressed ROCK2 protein expression in HCC cell line. miR139 was found to be frequently underexpressed in human HCC and the expression of miR139 was inversely correlated with the ROCK2 protein expression in human HCC samples. Clinicopathologic correlation showed that underexpression of miR139 in human HCC was significantly associated with multistep hepatocarcinogenesis and aggressive HCC features. Our findings demonstrated that miR139 regulated ROCK2 protein expression in hepatocarcinogenesis and suggested a post-transcriptional mechanism involved in the deregulation of ROCK2 leading to HCC progression.

Overall, we delineated the DLC1/Rho/ROCK migratory pathway and demonstrated that deregulation of ROCK played an important role in HCC progression and invasion.

An abstract of exactly 500 words



**Regulations and Functions of
Rho-kinases
in Hepatocellular Carcinoma**

By

Wong, Carmen Chak-Lui

B.Sc., M.Sc.

A thesis submitted in partial fulfillment of the requirements for the

Degree of Doctor of Philosophy

At the University of Hong Kong

April 2009



Declaration

I declare that this thesis entitled “Regulations and functions of rho-kinases in hepatocellular carcinoma” represents my original work unless acknowledgements were made. The content of this thesis has never been submitted to this University and other institutions for a degree or any other qualifications in the form of thesis or other report.

Signature _____

Wong, Carmen Chak Lui



Acknowledgements

I would like to express my deepest gratitude to my supervisor and mentor, Professor Irene O.L. Ng, for her invaluable guidance, support, and encouragement throughout my PhD study.

Massive thanks to all my labmates for their advice, technical support, and friendship. I would like to especially thank Dr. Edmund K.K. Tung for his support on the animal work and Ms. Joyce M.F. Lee for her support on the immunohistochemistry study.

I would also like to express my sincere appreciation to Dr. Kwan Man and her research team for their expertise and support on the orthotopic implantation and the xenogen imaging.

Special thanks to Dr. Wilson Y.P. Ching and Dr. Judy W.P. Yam for their valuable advice and ideas for my research, and Dr. Raven K.H. Kok for his valuable advice on the small RNA work.

I genuinely thank Dr. Jack C.M. Wong for his tremendous contribution and support all the way through my study.

Last but not least, I would like to thank my parents and my brother. I am incredibly fortunate to have my family for their love and indulgence in my life. I am indebted to their unconditional and unwavering understanding, support, and encouragement throughout my study.



Table of Contents

Abstract	i-iii
Title Page	iv
Declaration	v
Acknowledgements	vi
Table of Contents	vii-xv
List of Figures	xvi-xviii
List of Tables	xix
List of Abbreviations	xx-xxi
Chapter 1 General Introduction	1-40
1.1 Epidemiology and etiology of hepatocellular carcinoma (HCC)	1-7
1.1.1 Epidemiology of HCC	1
1.1.2 Etiology of HCC	2
1.1.2.1 Hepatitis B virus (HBV)	2
1.1.2.2 Hepatitis C virus (HCV)	5
1.1.2.3 Cirrhosis	6
1.1.2.4 Aflatoxin B1	6
1.1.2.5 Alcohol abuse	7
1.1.2.6 Additional Risk Factors	7
1.2 Cancer Metastasis and HCC Metastasis	8-19
1.2.1 Cancer Metastasis	8
1.2.2 Liver Metastasis	8



1.2.3 Molecular Mechanisms of Cancer Metastasis	10
1.2.3.1 Invasion Beyond the Basement Membrane	10
1.2.3.2 Intravasation and Survival	11
1.2.3.3 Extravasation and Colonization to distant organs	12
1.2.3.4 Principal Steps in Cell Motility	13
1.2.3.5 Cell Polarity	17
1.3 Rho-kinase (ROCK)	20-38
1.3.1 RhoGTPases and Rho-kinases (ROCK) in Cancer	20
1.3.2 Background Information of ROCK	22
1.3.2.1 Identification of ROCK	22
1.3.2.2 Tissue Distribution of ROCK	23
1.3.2.3 Cellular Distribution of ROCK	23
1.3.2.4 Molecular Structure of ROCK	23
1.3.2.5 Functions of ROCK Domains	24
1.3.2.6 Regulation of ROCK	26
1.3.2.7 Substrates of ROCK	30
1.3.2.8 Functions of ROCK	35
1.3.2.9 ROCK Inhibitors	37
1.4 Objectives	39
Chapter 2 General Methodology	41-65
2.1 HCC Patients	41-43
2.1.1 Patients	41



2.1.2 HCC and Non-Tumorous Liver Samples	41
2.1.3 Clinical Pathological Study	41
2.2 Tissue Culture	44-48
2.2.1 Cell Lines	44
2.2.2 Maintenance of Cells	46
2.2.3 Trypsinization	47
2.2.4 Cell Counting	47
2.2.5 Transfection with Mammalian Cell Lines	47
2.2.6 Stocking and Thawing Frozen Cells	48
2.3 Preparation of RNA and cDNA Samples	49-50
2.3.1 Extraction of Total RNA from Frozen Tissues	49
2.3.2 Extraction of Total RNA from Cell Lines	49
2.3.3 Complementary DNA Synthesis	50
2.4 Western Blot Analysis	51-55
2.4.1 Extraction of Protein from Frozen Tissues	51
2.4.2 Extraction of Protein from Cell Lines	51
2.4.2.1 Extraction by NETN Buffer	51
2.4.2.2 Extraction by SDS Buffer	52
2.4.3 Measurement of Protein Concentration	52
2.4.4 Polyacrylamide Gel Electrophoresis	52
2.4.4.1 Protein Preparation for Loading	52
2.4.4.2 Polyacrylamide Gel Preparation	53
2.4.5 Immunoblotting	54



2.4.5.1	Western Transfer	54
2.4.5.2	Stripping and Reprobing of Western Blot	55
2.5	Gene Cloning	56-60
2.5.1	Cloning of PCR Products into pGEM-T Easy or pCR4-TOPO Vectors	56
2.5.2	Restriction Enzyme Digestion, Alkaline Phosphatase Treatment, and DNA Ligation	57
2.5.3	Transformation	57
2.5.4	Minipreparation and Midipreparation of Plasmid DNA	58
2.5.5	DNA Sequencing	59
2.6	Cell Migration and Invasion Assays	61-65
2.6.1	Wound Healing Assay	61
2.6.2	Transwell Assay	61
2.6.3	Invasion Assay	63
2.6.4	<i>In Vivo</i> Metastasis Assay (Orthotopic Liver Implantation in Nude Mice)	63
Chapter 3 Regulation of ROCK: Signal Transduction Pathway		66-102
3.1	Introduction	66-70
3.1.1	DLC1 is a RhoGAP protein that Downregulates RhoA in HCC	67
3.1.2	Implications of DLC1 in HCC and Cancers	69
3.1.3	Objectives	70



3.2 Materials and Methods	71-74
3.2.1 Cell Lines and Plasmids	71
3.2.2 Drug Treatment and Transfection	72
3.2.3 Immunofluorescence Microscopy	72
3.2.4 Cell Migration Assay	73
3.2.5 Cell Proliferation Assay	74
3.2.6 mRNA Extraction, Protein Extraction, Western Blots	74
3.3 Results	75-94
3.3.1 DLC1 Abolished Formation of ROCK-mediated Stress fibers and Focal Adhesion Network	75
3.3.2 DLC1 Abolished ROCK-mediated Cortical Myosin Light Chain 2 Phosphorylation	81
3.3.3 DLC1 Attenuated Myosin Phosphatase Activity by Reducing Phosphorylation of Myosin Phosphatase Target Subunit 1	84
3.3.4 ROCK Inhibitor Suppressed HCC Cell Motility	88
3.3.5 ROCK Reversed the Cell Morphological Alteration of DLC1	92
3.4 Discussion	95-100
3.4.1 DLC1 Negatively Regulated ROCK-mediated Actomyosin Contractility	95
3.4.2 DLC1 Abolished Focal Adhesion Formation and Also Localized to Focal Adhesion Complex	96
3.4.3 Cytoskeletal Collapse Induced Cell Shrinkage and the Impact	97



of DLC1 on Cytoskeletal Collapse	
3.5 Summary	101-102
Chapter 4 Functions of ROCK in Hepatocellular Carcinoma	103-148
4.1 Introduction	103-104
4.1.1 Objectives	104
4.2 Materials and Methods	105-110
4.2.1 Cell Lines and Patient Samples	105
4.2.2 Semi-quantitative PCR and Real time-quantitative PCR	105
4.2.3 Antibodies	105
4.2.4 Protein Extraction and Western Blotting	106
4.2.5 Clinopathologic Correlation and Statistical Analysis	106
4.2.6 Plasmid Construction	107
4.2.7 Establishment of ROCK2 Stably Expressing Cells and ROCK2 Stable Knockdown Cells	107
4.2.8 Cell Migration and Invasion Assays	108
4.2.9 Immunofluorescence Microscopy and Scanning Electron Microscopy	108
4.2.10 Orthotopic Liver Implantation in Nude Mice	109
4.2.11 Histologic Analysis	110
4.2.12 Golgi Reorientation Assay	110
4.3 Results	111-144
4.3.1 Expression of ROCK1 and ROCK2 Expression in human	111



HCC	
4.3.2 Overexpression of ROCK2 in Human HCC was Associated With Aggressive Tumor Behavior	116
4.3.3 Expression of ROCK1 and ROCK2 Expression in HCC Cell Lines	118
4.3.4 ROCK2 Enhanced Cell Migration and Invasion of HCC Cells <i>in Vitro</i>	118
4.3.5 Stable Knockdown of ROCK2 in HCC Cell Line Suppressed Invasion and Metastasis in Nude Mice	121
4.3.6 Knockdown of ROCK2 Inhibited Stress Fiber Formation and Attenuated Phosphorylation of Myosin Phosphatase Target Subunit (MYPT1)	135
4.3.7 Knockdown of ROCK2 Inhibited Filopodia and Membrane Bleb Formation	138
4.3.8 Knockdown of ROCK2 Disrupted HCC Cell Polarity	138
4.4 Discussion	145-147
4.5 Summary	148

Chapter 5 Post-translational Modifications of ROCK in Hepatocellular Carcinoma **149-183**

5.1 Introduction	149-155
5.1.1 MicroRNA Biogenesis	149
5.1.2 MicroRNA and Cancer	153



5.1.3	MicroRNA Signature in HCC	154
5.1.4	Objectives	155
5.2	Materials and Methods	156-159
5.2.1	Luciferase Reporter Assay	156
5.2.2	Bioinformatics	156
5.2.3	Cell Lines, Plasmids, microRNA Precursors, and Drug Treatment	157
5.2.4	HCC Patient Samples and Microdissection	157
5.2.5	Clinicopathologic Correlation and Statistical Analysis	158
5.2.6	MicroRNA Extraction and microRNA Reverse Transcription and MicroRNA Real-time Quantitative PCR	159
5.3	Results	160-178
5.3.1	3'UTR of ROCK2 Regulates Translational Control of Gene Expression	160
5.3.2	Expression of ROCK2 was Deregulated in Post-transcriptional Level and miR139 Potentially Targets 3' Untranslated Region (3'UTR) of ROCK2	160
5.3.3	Overexpression of miR139 Caused a Decrease in ROCK2 Protein Expression and Suppressed HCC Cell Migration and Invasion	162
5.3.4	Expression of miR139 in HCC Inversely Correlated with Expression of ROCK2 Protein in Human HCC Samples	164
5.3.5	Underexpression of miR139 was Correlated with Aggressive	171



Human HCC and Hepatocarcinogenesis	
5.3.6 Expression of miR139 was Further Decreased in Venous Invasion and Extrahepatic Metastases	175
5.4 Discussion	179-182
5.5 Summary	183
Chapter 6 General Discussion	184-191
References	192-203
List of Publications (Journals/ Abstract Proceedings)	204-207
List of Academic Awards	208



List of Figures

Figure 1.1 Global distributions of HBV carriers and HCC incidence	4
Figure 1.2 Processes in metastasis	9
Figure 1.3 Principal steps in cell movement	15
Figure 1.4 Stress fibers are composed of actin and myosin	16
Figure 1.5 Golgi reorientation in polarized cell during cell migration	19
Figure 1.6 Members of the RhoGTPases family exhibited distinctive functions in the rearrangement of actin cytoskeleton	21
Figure 1.7 Molecular structures of ROCK	25
Figure 1.8 Regulation of ROCK activity	27
Figure 1.9 Regulation of Rho activity	29
Figure 1.10 ROCK regulates phosphorylation of MLC2 and MYPT1 and regulates actomyosin contractility	31
Figure 1.11 Chemical structure of Y27632	38
Figure 2.1 Cell migration assay (transwell)	62
Figure 2.2 Orthotopic liver tumor implantation	64
Figure 3.1 DLC1 possessed RhoGAP activity specific for RhoA	68
Figure 3.2 ROCK inhibitor suppressed formation of stress fiber and focal adhesion	76
Figure 3.3 DLC1 suppressed ROCK-mediated stress fiber formation in HCC cells	77
Figure 3.4 DLC1 suppressed ROCK-mediated focal adhesion formation in HCC cells (SMMC-7721)	78
Figure 3.5 DLC1 suppressed ROCK-mediated focal adhesion formation in HCC cells (BEL7402)	79
Figure 3.6 DLC1 and focal adhesions	80
Figure 3.7 ROCK inhibitor suppressed cortical phosphorylation of MLC2	82
Figure 3.8 ROCK mediated cortical phosphorylation of MLC2	83
Figure 3.9 DLC1 expression in cell lines	85
Figure 3.10 DLC1 expression was associated with phospho-MLC2 staining pattern	86
Figure 3.11 DLC1 RhoGAP was responsible for regulating cortical phosphorylation of MLC2	87
Figure 3.12 ROCK inhibitor suppressed MYPT phosphorylation	89
Figure 3.13 DLC1 and ROCK regulated MYPT phosphorylation	90
Figure 3.14 ROCK inhibitor suppressed HCC cell migration	91
Figure 3.15 ROCK reversed the cell morphological alteration of DLC1	93
Figure 3.16 ROCK reversed the cell morphological alteration of DLC1	94
Figure 3.17 Prolonged ROCK inhibitor treatment induced HCC cell collapse	98
Figure 3.18 Model of DLC1 induced cytoskeletal collapse	99
Figure 3.19 DLC1 suppressed RhoA/ROCK/MLC2 pathway	102
Figure 4.1 ROCK1 and ROCK2 mRNA expression in human HCC (semi-quantitative PCR)	112



Figure 4.2	ROCK2 protein expression in human HCC	113
Figure 4.3	ROCK1 protein expression in human HCC	114
Figure 4.4	ROCK2 mRNA expression in human HCC (real-time quantitative PCR)	115
Figure 4.5	ROCK1 and ROCK2 protein expression in HCC cell lines	119
Figure 4.6	Overexpression of ROCK2 enhanced HCC cell migration and invasion	120
Figure 4.7	ROCK2 expression in BEL7402 ROCK2 stable knockdown cells	122
Figure 4.8	Knockdown of ROCK2 suppressed HCC cell migration (transwell)	123
Figure 4.9	Knockdown of ROCK suppressed HCC cell migration (wound healing)	124
Figure 4.10	Knockdown of ROCK2 suppressed HCC cell invasion	125
Figure 4.11	ROCK2 expression in MHCC97L ROCK2 knockdown stable clone	127
Figure 4.12	Knockdown of ROCK2 suppressed HCC metastasis <i>in vivo</i>	128
Figure 4.13	Histologies showing knockdown of ROCK2 in MHCC97L suppressed HCC invasion <i>in vivo</i>	129
Figure 4.14	Knockdown of ROCK2 in BEL7402 suppressed HCC invasion <i>in vivo</i>	132
Figure 4.15	Knockdown of ROCK2 did not affect HCC cell proliferation <i>in vitro</i> and <i>in vivo</i>	134
Figure 4.16	Knockdown of ROCK2 impaired stress fibers formation	136
Figure 4.17	Knockdown of ROCK2 inhibited MYPT phosphorylation at Thr 853	137
Figure 4.18	Knockdown of ROCK2 suppressed formation of membrane blebs and filopodia	139
Figure 4.19	BEL7402 cells exhibited Golgi reorientation 6 hours after wound creation	141
Figure 4.20	SMMC-7721 cells did not exhibit Golgi reorientation 6 hours after wound creation	142
Figure 4.21	CHO cells exhibited Golgi reorientation 6 hours after wound creation	143
Figure 4.22	Knockdown of ROCK2 suppressed HCC cell polarity	144
Figure 5.1	Biogenesis of microRNAs	150
Figure 5.2	Interaction of 5' cap and 3' poly A tail induced circularization of mRNA	152
Figure 5.3	The 3' untranslated region (3' UTR) of ROCK2 suppressed gene translation	161
Figure 5.4	Predicted binding site of miR139 on the 3' UTR of ROCK2	163
Figure 5.5	miR139 suppressed ROCK2 protein expression	165
Figure 5.6	miR139 suppressed HCC cell invasion	166
Figure 5.7	miR139 could not suppress cell migration in ROCK2 knockdown HCC cells	167
Figure 5.8	Underexpression of miR139 in HCC	169



Figure 5.9 Expression of miR139 progressively decreased in hepatocarcinogenesis	173
Figure 5.10 miR139 was further downregulated in veins invaded HCC	176
Figure 5.11 miR139 was further downregulated in extrahepatic metastases	177
Figure 5.12 ROCK2 was not affected by MG132 treatment	180



List of Tables

Table 1.1	ROCK phosphorylatable substrates	34
Table 2.1	Clinicopathological features of 71 HCC patients included in this study.	43
Table 2.2	Properties of HCC cell lines used in this study	45
Table 4.1	Clinicopathologic correlation of ROCK2 overexpression in human HCC	117
Table 4.2	Results of orthotopic liver implantation from MHCC97L vector and ROCK2 knockdown clones	130
Table 4.3	Results of orthotopic liver implantation from BEL7402 vector and ROCK2 knockdown clones	133
Table 5.1	Expression of miR139 reversely correlated with ROCK2 protein expression in human HCC	170
Table 5.2	Clinicopathologic correlation of miR139 underexpression in human HCC	172
Table 5.3	miR139 underexpression is associated with multistep hepatocarcinogenesis	174



List of Abbreviations

a.a.	Amino acid
Ab	Antibody
Ago	Argonaute
ATP	Adenosine triphosphate
bp	basepair
cDNA	Complementary deoxyribonucleic acid
CO ₂	Carbon dioxide
CRD	Cysteine rich domain
CRMP	Collapsin response mediator protein
DAPI	4'-6-diamidino-2-phenylindole
DLC1	Deleted in Liver Cancer 1
DLC2	Deleted in Liver Cancer 2
DLC3	Deleted in Liver Cancer 3
DA	Dominant active
DMEM	Dulbecco's Modified Eagle Minimal medium
DN	Dominant negative
DNA	Deoxyribonucleic acid
eIF	Eukaryotic translation initiation factor
ECM	Extracellular matrix
EMT	Epithelial mesenchymal transition
ERM	Ezrin-radixin-moesin
FBS	Fetal bovine serum
FFPE	Formalin fixed paraffin embedded
GDP	Guanosine diphosphate
GFAP	Glial fibrillary acidic protein
GTP	Guanosine triphosphate
GST	Glutathione S-transferase
HBV	Hepatitis B virus
HCC	Hepatocellular carcinoma
HCV	Hepatitis C virus
HG	High glucose
ICAP-1	Integrin cytoplasmic domain associated protein-1
IPA	Isopropanol
LB	Luria-Bertani
LUC	Luciferase
LOH	Loss of heterozygosity
MARCK	Myristoylated alanine-rich C-kinase substrate
miRISC	MicroRNA induced silencing complex
miRNA	Micro RNA
MLC2	Myosin light chain 2
MMP	Matrix metalloproteinase
MYPT1	Myosin phosphatase (myosin phosphatase target subunit 1)
NF-L	Neuronal intermediate filament reorganization
PAGE	Polyacrylamide gel electrophoresis



PBS	Phosphate buffered saline
PCR	Polymerase chain reaction
PH	Pleckstrin homology
Pre-miRNA	Precursor microRNA
Pri-miRNA	Primary microRNA
Poly A	Poly adenine
RBD	Rho binding domain
RNA	Ribonucleic acid
Rho	Rho GTPase
RhoGAP	Rho GTPase Activating Protein
RhoGEF	Rho Guanine Nucleotide Exchange Factor
ROCK	Rho-kinase
ROCK1	Rho-kinase 1
ROCK2	Rho-kinase 2
RT	Reverse transcription
RT	Real time
RTK	Receptor tyrosine kinase
SAM	Sterile alpha motif
SDS	Sodium dodecyl sulfate
Ser	Serine
ShRNA	Short-hairpin RNA
Thr	Threonine
3' UTR	3' untranslated region
5' cap	5'-terminal 7-methylguanosine cap



Chapter 1

General Introduction

1.1 Epidemiology and etiology of hepatocellular carcinoma (HCC)

1.1.1 Epidemiology of HCC

Primary liver cancer is the fifth most prevalent cancer in the world, with approximate 564,000 new cases in year 2000 (1, 2). Primary liver cancer mainly includes hepatocellular carcinoma (HCC), cholangiocarcinoma, and angiosarcoma. HCC accounts for 90% of liver cancer (3). HCC refers to the primary malignancy of the liver arises from liver cells, hepatocytes (3). HCC distributed characteristically throughout the world. High incidence geographic regions (>20/ 100,000 annually) include Southeast Asia, Japan, China, Hong Kong, Taiwan, and sub-Saharan Africa (3). Low incidence geographic regions (<5/ 100,000 annually) include North and South America, Northern and Western Europe, Oceania (3). Although decreased incidence among Chinese populations in Hong Kong, Shanghai, Singapore, and Japan was reported in 1997, the occurrence of HCC has increased in the western countries including the United States, United Kingdom, and Australia (3). In the United States, the incidence of HCC increased from 1.4/ 100,000 population to 2.4/ 100,000 population from year 1976 to year 1995 (3).



Like many other cancers, HCC incidence increases progressively with age. This trend suggests the accumulation of genetic alterations over time is requisite for HCC development. Early HCC onset is observed in countries with endemic hepatitis infection due to the possibility of increased genome alterations during extensive liver regeneration (4). In almost all populations, males apparently have more frequent incidence of HCC than females in all geographical regions, with a male to female ratio from 2:1 to 4:1 (3). In Hong Kong, the incidence of HCC is 29.9/ 100,000 male population and 8.3/ 100,000 female population and the death rate for HCC is 14.9/ 100,000 male population and 8/ 100,000 female population, ranked the highest mortality rate only after lung cancer and colorectal cancer in year 2005. (Hong Kong Hospital Authority: <http://www3.ha.org.hk/cancereg/eng/default.asp>)

1.1.2 Etiology of HCC

Despite the etiology of HCC is multi-causative, the key risk factors of HCC are clearly identified. The major risk factors of HCC include chronic viral hepatitis B (HBV) and hepatitis C (HCV) infection, cirrhosis, aflatoxin B1 intake, alcohol abuse, and inherited metabolic disorders.

1.1.2.1 Hepatitis B virus (HBV)

HBV, a DNA virus with size of about 3.2 kb, undoubtedly is the most important risk factor of HCC in Hong Kong, China, Southeast Asia, and sub-Saharan Africa. HBV holds an intimate relationship with HCC as clearly demonstrated first by epidemiological studies. The global distribution of HBV infection incidence matches closely with the



global distribution of HCC incidence (Figure 1.1). Studies further demonstrated that a 5-15 fold increased chance for chronic HBV carriers to develop HCC as compared with the non-infected population (3). In spite of the fact that most of the HBV associated HCC patients (about 70% - 90%) bear cirrhotic background, HBV may also induce HCC in patients without going through cirrhosis stage.

Mounting studies demonstrated that HBV possessed oncogenic properties important for HCC development. Long term chronic HBV infection is shown to be associated with integration of the HBV DNA into genomes of the host DNA (5). Although the underlying mechanisms of HBV integration is still elusive, studies reported that HBV integration usually occurred at cancer associated sites of the human genome (5) and the genetic instability created might result in aberrant gene expressions in HCC. Woodchuck hepatitis virus (WHV), a DNA virus belonging to the same class with HBV, was found to integrate frequently into a protooncogene, *N-myc* gene, of the woodchuck genome (6).

HBV encompasses large envelope protein, viral polymerase, and transactivator protein called HBx. HBx is the viral component that contributes to HCC. HBx physically interacts with and inactivates the tumor suppressor p53 (7). Moreover, HBx has been reported to activate NF- κ B transcription factor pathway and some growth regulatory genes including c-fos, c-jun, c-myc, and EGF (8). Furthermore, a recent study has shown that HBX is able to induce epigenetic events including promoter hypermethylation of a tumor suppressor gene IGFBP3 and global genome hypomethylation (9).



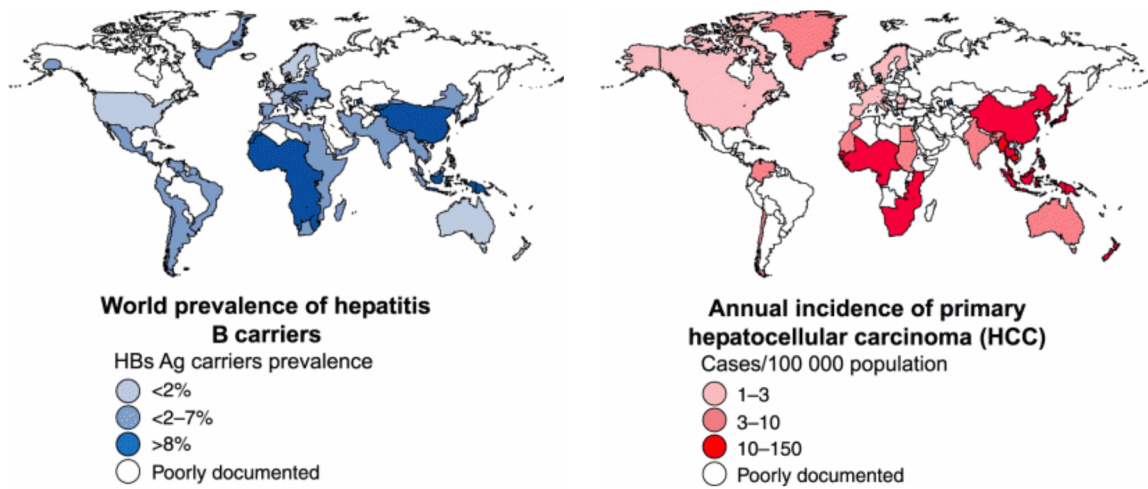


Figure 1.1 Global distributions of HBV carriers and HCC incidence

(A) Global distribution of HBV carriers. (B) Global distribution of HCC incidence.

(Journal of Viral Hepatology. 2004)

1.1.2.2 Hepatitis C virus (HCV)

HCV, a RNA virus with size of about 10 kb, is the main risk factor of HCC in Japan, Europe, and the United States. The correlations of HCV incidence and HCC incidence in different regions vary. Studies demonstrated that a 17 fold increased chance for HCV infected carriers to develop HCC as compared with the non-infected population (10). A prospective study revealed that HCC incidence in patients infected with chronic hepatitis C is approximately 2.7 times higher than patients infected with chronic hepatitis B (11). Unlike HBV, HCV does not integrate into the host genome since HCV replicates from one strand of RNA into a new strand of RNA without synthesizing DNA. HCV composed of core protein, E1, E2, p7, NS2, NS3, NS4A, NS4B, NS5A, and NS5b. It was shown that HCV core and NS4B protein are the viral protein components responsible for HCC. HCV core protein not only interacted with Ras in transformation (12) but also suppressed p53 transcriptional activity (13). Furthermore, HCV core protein and NS4B protein are important in triggering NF-κB, SRE, and AP1 (14, 15). The induction of these pathways will functionally enhance cell proliferation and inflammatory cytokines generation that will eventually contribute to HCC development. Transgenic mouse model provided further evidence for the oncogenic property of HCV core protein. The HCC incidence in transgenic mice carrying HCV core gene was profoundly increased when compared with non-transgenic control mice (16). These transgenic mice developed HCC in a multistep sequence from hepatic steatosis, to adenomas, finally to HCC which is similar to the histopathological characteristics of HCC patients with chronic hepatitis C (16).



1.1.2.3 Cirrhosis

Cirrhosis results from chronic liver diseases and most HCC cases (~80-90%) are associated with a recognized background of cirrhosis (17). Cirrhosis describes the phenomenon which liver tissue is replaced by fibrous scar tissue and widespread regenerative nodules, lumps formed by regenerating damaged tissues. The regenerative nodules are believed to have enhanced DNA synthesis in hepatocytes and more DNA rearrangements, and are more prone to mutations when induced by other risk factors. Cirrhosis is a precancerous phenomenon; nevertheless, cirrhosis is not necessarily an obligation for HCC development, while HCC may not necessarily be a consequence of cirrhosis. Cirrhosis and HCC, nonetheless, share similar causes such as chronic HBV infection. The underlying cellular mechanism of the development of cirrhosis to hepatocarcinogenesis is still obscure, but it is believed to be related to extensive liver cell regeneration which creates a selective environment favoring clonal expansion of the committed cells.

1.1.2.4 Aflatoxin B1

Aflatoxin B1, a mycotoxin that is recognized as hepatocarcinogen, which is produced by *Asperigillus flavis* and *A. parasitans*. These fungi grow favorably on grains and peanuts and are especially abundant in the humid subtropical and tropical areas. Field studies demonstrated a close relationship between aflatoxin exposure and high HCC incidence in poor districts where fungal contamination in food is common. The active metabolite of aflatoxin B1 can bind to DNA and cause DNA damage such as mutation. Aflatoxin B1 was found to induce a selective mutation of p53 at codon 249 from G to T in 30% - 60%



of HCC tissues in aflatoxin prevalent regions (18, 19). This mutation has nearly become a signature of aflatoxin B1 infection. The exposure of aflatoxin B1 to populations of 10 villages in China was associated with HCC mortality (20). Furthermore, a prospective report in Shanghai, China showed that detection of aflatoxin B1 metabolite in patients increased HCC risk up to 4 fold; and together with HBV infection, HCC risk was increased strikingly up to 60 fold (21).

1.1.2.5 Alcohol Abuse

Prolonged heavy alcohol intake (50-70 g/day) is a risk factor for HCC. Alcohol is not a carcinogen itself, but is closely related to cirrhosis development. Heavy alcohol intake, together with HBV or HCV, synergistically increases the risk of HCC through enhancing cirrhosis. For example, it was reported that daily intake of more than 60 g of alcohol and HCC risk related linearly in heavy alcohol drinkers and a 2 fold increase of HCC risk was found in HCV infected alcohol drinkers (10).

1.1.2.6 Additional Risk Factors

There are some other additional HCC risk factors reported. Cigarette smoking enhanced HCC risk factor of about 2.1 fold (22, 23). Intake of pesticide such as DDT from ditch water was reported to increase HCC risk in Qidong province in China (17). Also, steroid sex hormone and oral contraceptive have been reported to be HCC risk factors (22, 23).



1.2 Cancer Metastasis and HCC Metastasis

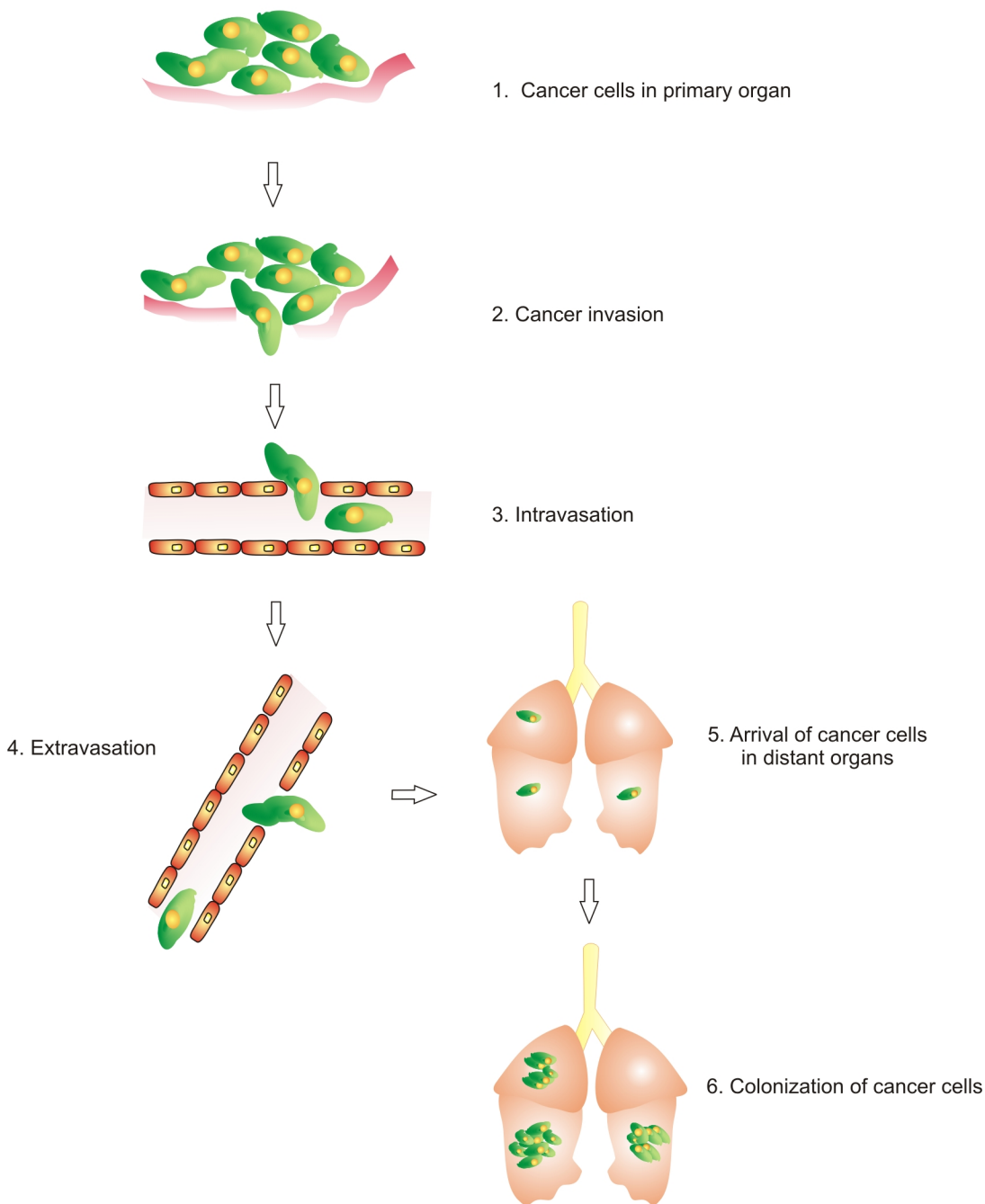
1.2.1 Cancer Metastasis

Cancer metastasis is responsible for 90% of mortality from solid tumors (24). Tumor metastasis involves sequential biological steps enabling cancer cells to move from its primary tumor site to another distant location (24). Cancer cells from its primary tumor site needs to acquire the ability to intravasate, to invade its surrounding tissue and enter the circulatory or lymphatic system (Figure 1.2). Then, the cancer cells acquire the ability to survive along the circulation, extravasate into the new tissue site, and eventually colonize and grow at the new site. The extravasated cancer cells could colonize at tissues of the same organ or other organs. Recently, a provocative hypothesis suggested that disseminated cancer cells can return to their primary site, described as self-seeding (25), may contribute to extensive accumulation of aggressive cancer cells at the primary site resulting in local recurrence.

1.2.2 Liver Metastasis

HCC is the third leading cause of mortality among cancer patients. The high mortality rate is greatly attributed to the late symptom presentations from HCC patients, mostly at advanced stages, and the high incidence of postoperative recurrence. Since the presence of vascular invasion in the liver or extrahepatic metastases is the classic symptoms for advanced HCC, metastasis undoubtedly is the most significant cause of liver failure and mortality in HCC patients. In HCC, the metastasized cancer cells can colonize to other region of the liver, intrahepatic metastasis, or to other distant organs such as lung, brain, and bones, extrahepatic metastasis. So far, there is no promising curative therapy to target





(Modified and redrawn from Steeg PS. Nature Medicine. 2006) (31)

Figure 1.2 Processes in metastasis

Tumor cells at the primary tumor site invade and intravasate into the blood stream or lymphatics. Bloodstream and lymphatics are harsh environments for tumor cells to survive. For example, tumor cells need to avoid the immune attack in the lymphatics and size restriction and pressure in the blood stream. After the tumor cells extravasate from the circulation and enter new sites, micrometastases develop to macrometastases after colonization of cancer cells in the new sites.

metastatic HCC; only Sorafenib, a receptor tyrosine kinase inhibitor targeting the Raf/Mek/Erk pathway and angiogenesis, was shown to improve the overall survival for advanced stage HCC patients for 3 months in a randomized trial (26).

1.2.3 Molecular Mechanisms of Cancer Metastasis

Cancer metastasis is a multistep process (Figure 1.2) and includes fundamental molecular mechanisms which will be described in this section.

1.2.3.1 Invasion Beyond the Basement Membrane

Invasion is the first step of metastasis. Invasion requires cancer cells to de-adhere from other cells and enter the extracellular matrix (ECM) by proteolytic degradation at the invasion front of surrounding tissue and enhanced cell motility to propel the cancer cells through the matrix and the surrounding tissues. First, the cell cell adhesions need to be disrupted. Cell cell adhesions are regulated by cadherins which adhere cells through binding extracellularly. The entrance of tumor cells to the ECM requires engagement of integrins, the transmembrane proteins that are composed of heterodimers of α and β subunits. Integrins bind to ECM proteins and initiate a series of intracellular signal transduction to facilitate cell invasion including the triggering of integrin-linked kinase (ILK)/ Snail pathway to downregulate E-cadherin causing cell de-adhesion (27). Then, proteolytic degradation of the extracellular matrix follows which largely relies on a group of proteases called matrix metalloproteinases (MMPs) (28). MMPs are produced as inactive form and are activated by proteolytic cleavage of its autoinhibitory domain (28). Activated MMPs degrade numerous ECM proteins such as elastin, laminin, collagen, and



proteoglycan (28). Degradation of the extracellular matrix is not sufficient enough for cancer cell invasion, but it also requires substantial alterations of the cell cytoskeletons and the establishment of cell polarity, both require RhoGTPases and will be further elaborated in Section 1.2.3.4 and 1.2.3.5, respectively.

Interestingly, an atypical form of cancer cell movement, amoeboid mode invasion, is independent of proteolysis of the ECM was reported by Sahai E *et al* in the lymphoma model in three-dimensional migration study (29). This amoeboid mode of movement is controlled by the cell shape which allows the cell to glide through the matrix without involvement of proteolytic degradation of the ECM. Instead of protease inhibitor treatment, only treatment of Rho effector, Rho kinase (ROCK), inhibitor profoundly suppressed the amoeboid mode of movement (29). Although this amoeboid movement is uncommon and was only demonstrated in particular cell lines, this suggests that Rho/ROCK signaling is an important pathway employed by different cell types and modes of movements.

1.2.3.2 Intravasation and Survival

As mentioned earlier, tumor cells metastasize to another site of tissues require invasion by entering the vasculature. A study has demonstrated that a transcription factor, TWIST, is crucial for intravasation, the entrance of cancer cells into the circulation, by triggering epithelial mesenchymal transition (EMT) in lung metastasis (30). Once the tumor cells have invaded into the bloodstream, tumor cells have to overcome the adverse environment in the bloodstream or the lymphatic system. Abundant immune cells, fluidic



pressure, and the lack of substrate attachment create a harsh environment for the cells to survive in the circulatory system. Anoikis, cell death following detachment or loss of substrate adhesions, in the blood stream often occurs to cancer cells and impedes the progress of metastasis. *In vitro* study demonstrated that a number of receptor tyrosine kinases (RTKs) and their signaling effectors are responsible in triggering cell anoikis resistance which is believed to allow cancer cells to tolerate and live in the harsh environment in the bloodstream (31).

1.2.3.3 Extravasation and Colonization to distant organs

Cancer cells need to undergo extravasation upon bloodstream survival. Cancer cells extravasate, exit the blood stream, and colonize into new favorable sites in the same organ or distant organs. The microenvironments of the secondary organs or sites are essential in determining the efficiency of colonization. For instance, the site of colonization may be determined by receptors on the surface of the cancer cells and their complementary ligands in the secondary targeted sites, or vice versa. For example, $\alpha_3\beta_1$ integrins interact with the ligand, laminin 5, at the vascular basement membrane inducing pulmonary metastasis (31); breast cancer cells with CXCR4 chemokine receptor (C-X-C motif chemokine receptor 4) expression was shown to metastasize to sites such as lungs, with abundant CXCL12 (C-X-C motif chemokine ligand 12), a chemokine specific for CXCR4 (32). After colonization, the cancer cells can propagate and form macroscopic metastases. The cancer cells can also remain dormant in the distant sites and propagate later which may be the cause of tumor recurrence (25). Nonetheless, the underlying



molecular mechanism driving the fate of cancer cells in the distant organs remains elusive.

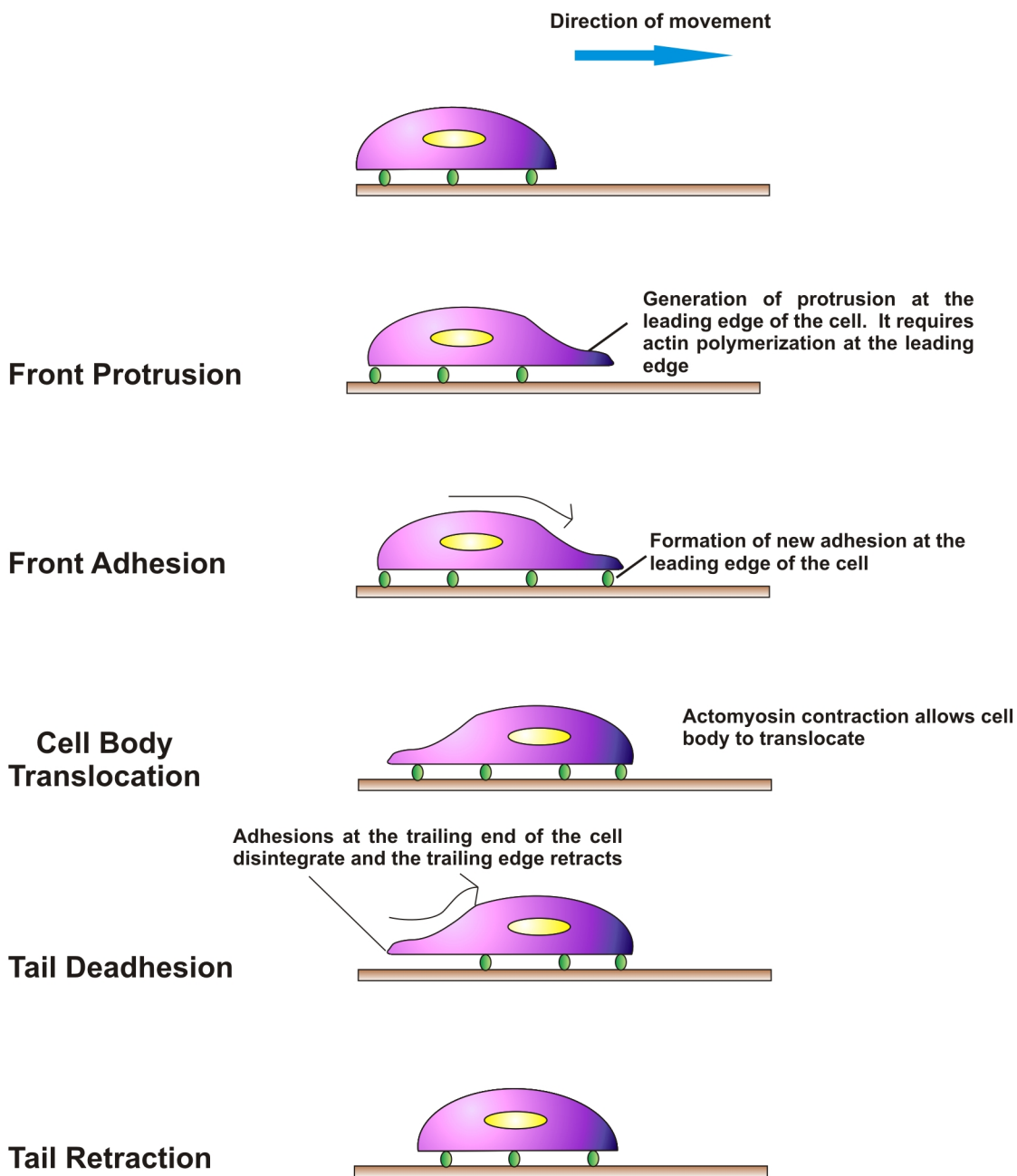
1.2.3.4 Principal Steps in Cell Motility

Cell motility is vital for many steps involved in cancer metastasis such as invasion, intravasation, and extravasation. External signal such as chemoattractant initiates cell movement by stimulating the cell receptors of cell membrane and hence triggers a series of signaling events. Then, cell migration can be simplified in three important steps (Figure 1.3). The first step requires the extension of the cell by generating protrusions towards the direction of cell migration at the front of the cell, the anterior end. This protruding step includes formation of new adhesions that anchor the protrusions and the substratum. Formation of new adhesions and protrusions requires actin polymerization which recycles the actin monomer from dissolving the existing actin filament. The second step requires actomyosin contraction that drives the cell body to move forward toward the protrusive end. Actomyosin contraction refers to the force generated by actin filaments, also called stress fibers, which are actually composed of polymerized actin and myosin (Figure 1.4). Stress fibers stretch across the cells anchoring to a group of macromolecules called focal adhesion molecules. The focal adhesion molecules anchor the cells to the substratum and act as mechanical linkages to the ECM. Following actomyosin contraction, the third step emerges concomitantly and involves the release of the attached adhesions at the rear end of the cell, the posterior end. This de-adhering step facilitates the actomyosin contraction in dragging the cell to move forward. Migration is



often referred as a cyclical mechanism which involves the above three steps that involve the disassembling and assembling of actin filaments (33, 34).





(Modified and redrawn from Ananthakrishnan R et al. International Journal of Biological Sciences Review. 2007) (33)

Figure 1.3 Principal steps in cell movement

Cell migration involves pivotal steps including cell protrusion at the leading/ anterior edge (front). Front protrusion: at the new protrusion, actin polymerization is required and new focal adhesion molecules are recruited to adhere the cell front to the substratum. Cell body translocation: the cell body (including the nucleus) translocates by actomyosin contraction. Tail deadhesion and retraction: the focal adhesion molecules at the trailing/ posterior edge (tail) disassemble and the trailing edge retracts.

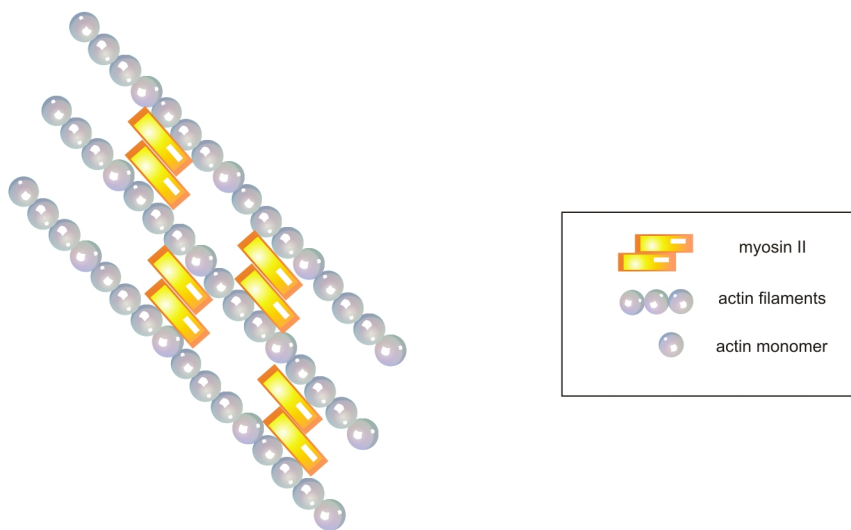


Figure 1.4 Stress fibers are composed of actin and myosin

Stress fibers are composed of myosin II and actin. Actin are polymerized in forming actin filaments while myosin II are present discontinuously along the actin filaments. Together, they create actomyosin contraction for cell movement.

1.2.3.5 Cell Polarity

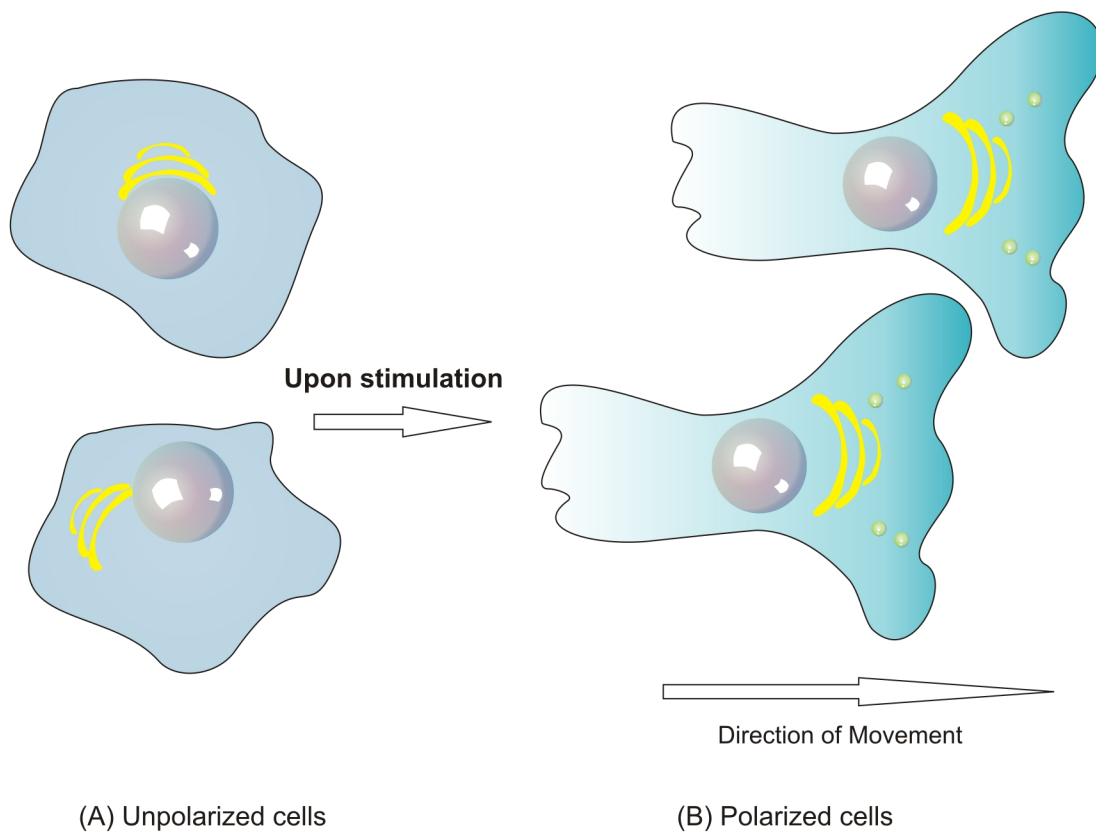
The three fundamental steps involved in cell motility have been described in the preceding section; however, how the cell determines its direction upon stimulation and signals different cellular regions to perform their according functions has not been covered. The direction of movement of motile cells is determined by cell polarity. Each cellular region of a polarized cell is different from another region of the cell morphologically and functionally. Polarity of the cell is established when the anterior end of the cell protrudes, the posterior end of the cell retracts, and the cell body contracts and relaxes to propel the cell forward. Cell polarity is a crucial step for cell migration and involves multiple transduction signaling events. Demonstrated in neutrophils, a highly motile cell type, the achievement of cell polarity requires collaboration of multiple Rho GTPases signaling pathway (35, 36).

Motile cells respond to external cues such as growth factors and available space by moving towards the cues. In this directional movement, a cell becomes polarized as described above and its Golgi apparatus and microtubule organizing center (MTOC) also reposition to the front of the nucleus facing towards the direction of movement (Figure 1.5). The repositioning of the MTOC and the Golgi apparatus provide direct supply of proteins and polymerized actin required at the leading front of the cell. At the leading edge of the cell, protrusions are established by substantial actin polymerization and the enriched production of surface receptors. Furthermore, secretory proteins such as MMPs are produced at the leading front of the cell to facilitate the cell invasion into the ECM. Since MTOC is where the microtubules are nucleated and the Golgi apparatus is where



the proteins are packaged and modified, the translocation of these two organelles facilitate cell movement (37).

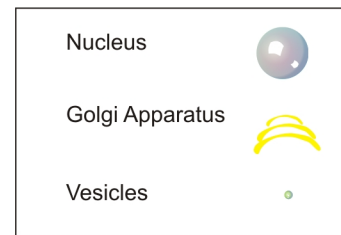




Direction of Movement

(A) Unpolarized cells

(B) Polarized cells



(Golgi image idea from Mellor H. Current Biology. 2004) ⁽³⁸⁾

Figure 1.5 Golgi reorientation in polarized cell during cell migration

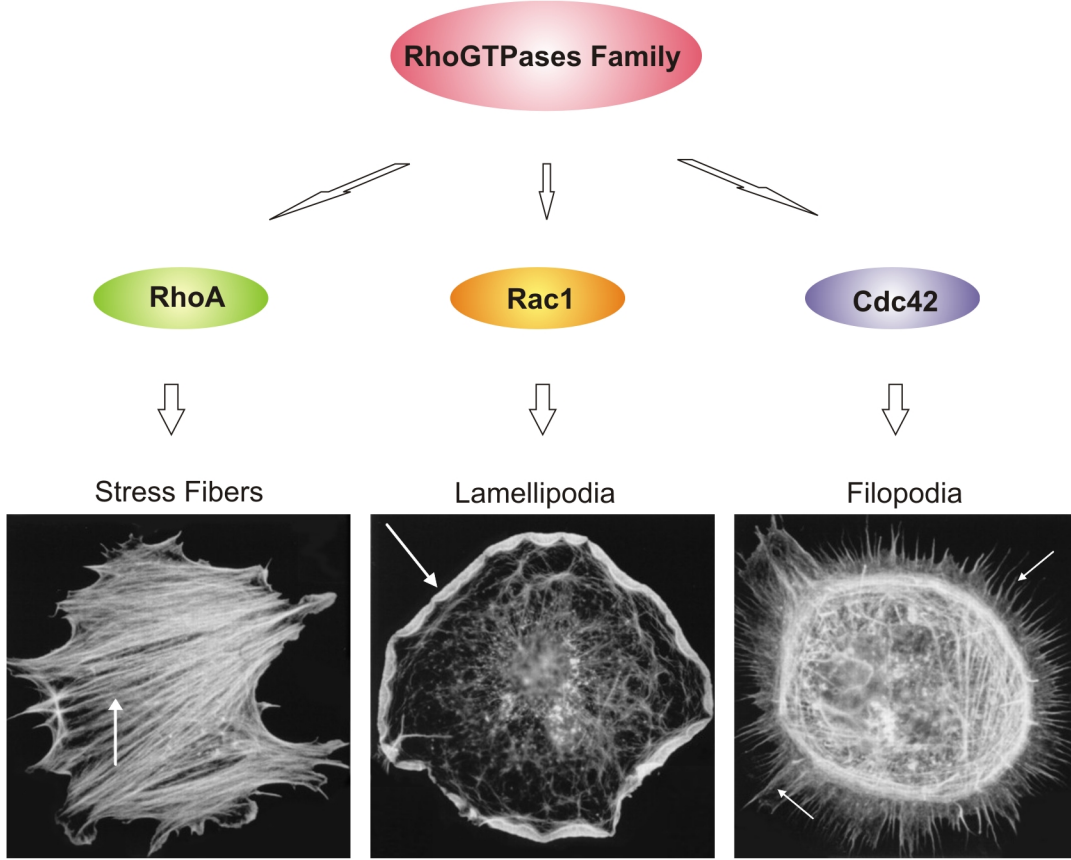
(A) The Golgi apparatus of unpolarized cells randomly distribute in the cell. (B) Upon stimulation, such as chemoattractant, the cell becomes polarized, and the Golgi apparatus realigns to the front of the nucleus towards the direction of movement. This is to facilitate secretion of components required to degrade the extracellular matrix and to package proteins for the membrane protrusions. After the Golgi apparatus has packaged the proteins, these proteins can be carried to the leading edge membrane promptly after the Golgi reorientation.

1.3 Rho-kinases (ROCK)

1.3.1 RhoGTPases and Rho-kinases (ROCK) in Cancer

Cell migration plays a pivotal role in tumor invasion and metastasis and a number of essential steps involve actin cytoskeleton rearrangement which is tightly controlled by Rho GTPases as mentioned in Section 1.2. The three best characterized Rho GTPases include RhoA, Rac1, and Cdc42; each executes separate function in actin rearrangement and they together regulate cell movement. By microinjecting the constitutive active forms of different Rho GTPases members, it was found that members of the Rho GTPases execute distinctive functions in actin rearrangement (39). RhoA stimulates assembly of contractile actin-myosin filaments, stress fibers (Figure 1.6) (39). Rac1 stimulates the assembly of actin filament formation at the cell periphery to produce actin rich membrane ruffles, lamellipodia (Figure 1.6) (39). Activation of Cdc42 stimulates actin-rich protrusions, filopodia (Figure 1.6) (39). Rho GTPases exchange between active from, GTP bound state, and inactive form, GDP bound state. Rho GTPases act as molecular switches and function through activation of their specific downstream effectors. Rho-kinase (ROCK) is the most well characterized downstream effector of RhoA and has been focused in this study. ROCK is the first discovered effector of RhoA. Activity of Rho-kinase is intimately and positively linked with the activity of RhoA. ROCK inhibitors and dominant negative ROCK were shown to abrogate Rho induced stress fibers and focal adhesions formation (40). ROCK mediates almost all of the cytoskeletal changes induced by RhoA. Both RhoA and ROCK are implicated in tumor progression especially in the metastatic aspects.





(Cell images from Hall AJ. Science. 1998) (39)

Figure 1.6 Members of the RhoGTPases family exhibited distinctive functions in the rearrangement of actin cytoskeleton

Activation of RhoA induced formation of actin rich filaments, stress fibers. Activation of Rac1 induced formation of actin rich membrane ruffles, lamellipodia. Activation of Cdc42 induced formation of actin rich protrusions, filopodia.

Unlike Ras, mutations in Rho proteins in human cancers are rare. Among all the Rho family members, RhoA is the best characterized member in cancers. RhoA was found to be significantly overexpressed in various cancers including HCC (41), breast (42), lung (43), colon (43), head and neck (44), testicular (45), and bladder cancers (46). ROCK was also shown to be involved in various cancer types. Overexpression of the two members of ROCK family, ROCK1 and ROCK2, was demonstrated in testicular and bladder cancer at the protein level (45, 46). Blockade of ROCK activity via ROCK inhibitor or overexpression of a dominant negative mutant of ROCK1 suppressed metastatic phenotypes such as cell migration, peritoneal invasion and intrahepatic metastasis in cellular and animal models (47-49). Besides, overexpression of RhoA and ROCK proteins was found to correlate with shortened disease-free survival, overall survival, and metastatic clinicopathological features in patients with bladder cancer (46). Of note, overexpression of RhoA and ROCK proteins was often found at the translational level (protein) rather than transcriptional level (mRNA expression). Only one study on gastric cancer indicated RhoA was overexpressed in tumorous tissues at mRNA level (50).

1.3.2 Background Information of ROCK

1.3.2.1 Identification of ROCK

There are two members in the ROCK family, ROCK1 and ROCK2. ROCK1 is located at chromosome 18, mapped to 18q11.1; whereas ROCK2 is located at chromosome 2, mapped to 2p24. Identification of ROCK1 and ROCK2 by different groups was based on using active Rho, RhoA-GTP, as binding probes. ROCK2, also named ROK α or p150ROCK, was first identified in year 1995 in an expression screening assay from rat



brain cDNA library with RhoA-GTP, active form of RhoA, as probe (51). Similarly, ROCK1, also named ROCK β or p160ROCK, was isolated and identified concurrently by two separate groups in year 1996 (52, 53). Using similar approach, ROCK1 was identified from expression screening assay from rat brain and liver library and bovine brain cDNA library (53). ROCK was quickly identified as autophosphorylating kinases as well as serine/threonine kinases, that are associated with cytoskeletal arrangements (51, 53, 54).

1.3.2.2 Tissue Distribution of ROCK

Both ROCK1 and ROCK2 are ubiquitously expressed in all tissues in mice and rats. With northern blot analysis, it was shown that ROCK1 mRNA was highly expressed in testis, liver, and lung while ROCK2 was abundantly expressed in brain and muscle (52). Of note, the differential tissue expression of ROCK1 and ROCK2 suggests their distinctive roles in these tissue types under normal physiological condition; nonetheless, how ROCK contributes to cancer is not clear.

1.3.2.3 Cellular Distribution of ROCK

Cellular distribution of ROCK in cells is dynamic depending on cell types and source of stimulation. Commonly, ROCK1 and ROCK2 were reported to localize mainly in cytosol and cell membrane (51, 53). The proportion of cytosolic and membranous localization of ROCK varies from cell type to cell type. Substantiated by cell fractionation and immunofluorescence analysis, it was reported that a portion of ROCK translocated to cell membrane upon RhoA expression and activation (51, 53). ROCK1 translocation to cell



membrane was shown to be driven by the binding with Integrin Cytoplasmic Domain-Associated Protein-1 (ICAP-1) (55). In addition, ROCK was also found to localize in the nucleus (56-58) upon growth factor stimulation (56, 57). Moreover, ROCK was also reported to localize at cleavage furrows (59, 60), intermediate filament network (61), centrosomal components (62), and stress fibers (63).

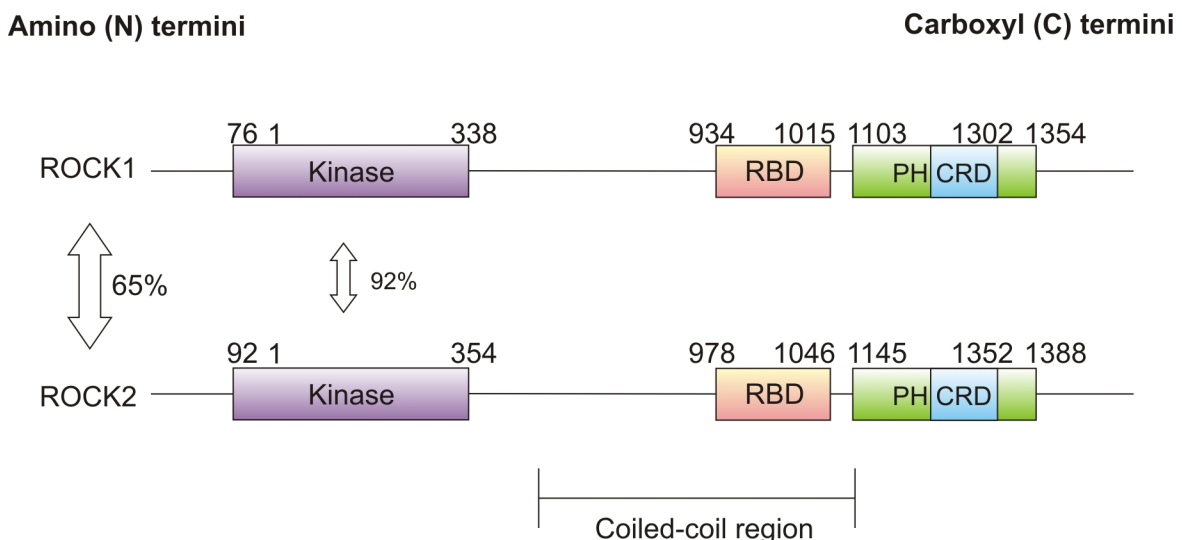
1.3.2.4 Molecular Structure of ROCK

Both ROCK1 and ROCK2 are approximately 160 kDa in molecular weight. They are highly homologous isoforms and their amino acid sequences, overall, share 65% identity. The amino acid sequences of their kinase domains share 92% identity and both are situated at the amino-terminus (N-terminus) (Figure 1.7). Besides the catalytic kinase domains they share in common, ROCK1 and ROCK2 share common coiled-coil forming region and similar auto-inhibitory carboxyl-terminus (C-terminus) (Figure 1.7). Rho-binding domain (RBD) is located after the kinase domain and within the coiled-coil forming region. Following the RBD is the pleckstrin-homology (PH) domain, which consists of a highly conserved cysteine/histidine rich region (Figure 1.7). The RBD and PH domains are located at the C-terminus while the kinase domain is located at the N-terminus (Figure 1.7).

1.3.2.5 Functions of ROCK Domains

ROCK encompasses several functional domains as illustrated in Figure 1.7, and each serves specific functions such as protein-protein interactions, cellular localization, and regulation of ROCK activity. Kinase domain is the most important domain of ROCK





(Modified and redrawn from Riento K. Nature Cell Biology Review. 2003) (113)

Figure 1.7 Molecular structure of ROCK

The kinase domain of ROCK is located at the amino terminus. The kinase domain of ROCK1 and ROCK2 are highly homologous (92%). The Rho binding domain (RBD) is the site where activated Rho binds to ROCK. The pleckstrin homology (PH) domain covers a cysteine rich domain (CRD). The region in between the kinase domain and the PH domain is the coiled-coil region where the autoinhibitory loop is formed. ROCK1 and ROCK2 overall share 65% homology in the amino acid sequences.

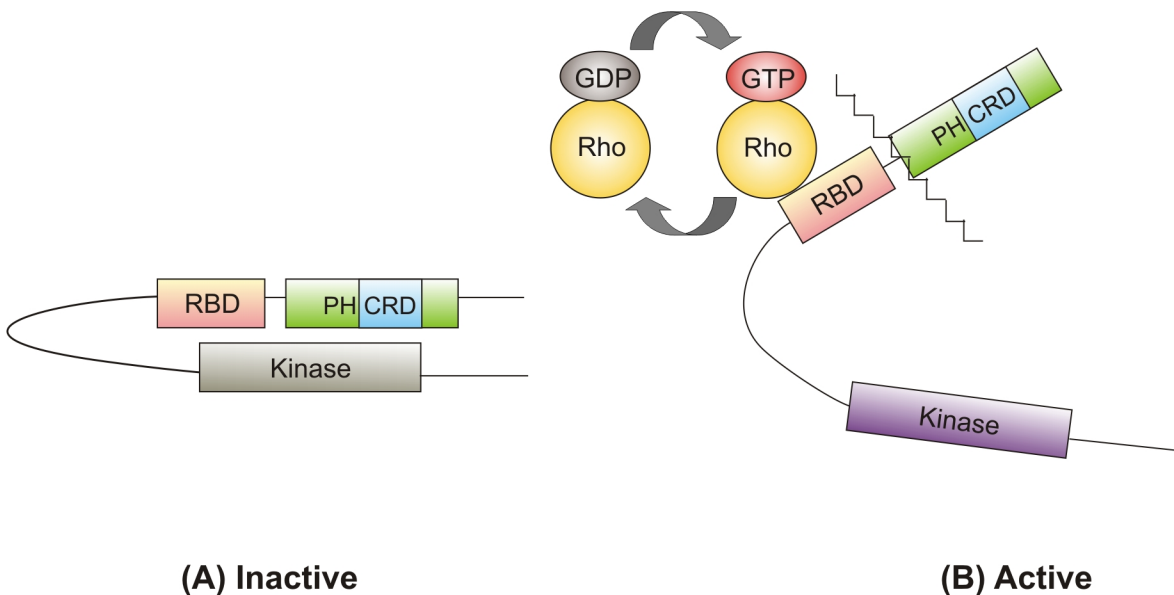


responsible for the central functions of ROCK including phosphorylation of its downstream targets to activate actomyosin contraction and regulate cell movement as will be discussed further in Chapter 3. Recent study has demonstrated that the PH domain is important for lipid binding and responsible for translocating ROCK2 to the cell membrane (64). PH domain of ROCK was also found to be associated with protein-protein interactions such as the interaction of ROCK with filamin A, an important protein related to actin cytoskeleton reorganization (65). An auto-inhibitory loop is formed when the C-terminus of ROCK protein binds to the N-terminus where the kinase domain is located (Figure 1.8). It was shown that the deletion of the C-terminus could release the autoinhibition of ROCK activity. Physiologically, the auto-inhibitory loop of ROCK can be released upon the binding of GTP-bound RhoA (active RhoA) with the RBD domain of ROCK. Also, ROCK1 and ROCK2 can be activated by cleavage of the C-terminal domain by caspase 3 and granzyme B, respectively (66, 67). Also, arachidonic acid and PI(3,4,5)P₃ were reported to activate ROCK by binding to the PH domain releasing the autoinhibitory loop open (68, 69).

1.3.2.6 Regulation of ROCK

As described above, the C-terminus exerts an inhibitory effect to the activity of ROCK by binding to the N-terminus forming an autoinhibitory loop at the coiled-coil region. The loop can be released by the active form of Rho (Figure 1.8). It was shown that RhoA, but not Cdc42 and Rac, bind to and activate ROCK (52). On the other hand, RhoE, a member of the Rho family which is devoid of RhoGTPase activity, bound to and inactivated ROCK and disrupted actin cytoskeleton and suppressed cell migration in MDCK cells





(Modified and redrawn from Riento K. Nature Cell Biology Review. 2003) (113)

Figure 1.8 Regulation of ROCK activity

(A) Inactive ROCK. The carboxyl terminus (RBD and PH domains) can bind to the amino terminus of ROCK and form an autoinhibitory loop. (B) Active ROCK. Active Rho (GTP bound Rho) binds to the rho binding domain (RBD) of ROCK and releases ROCK to an open conformation and releases the kinase domain resulting in the release of the catalytic activity. ROCK can also be activated when the carboxyl terminated is cleaved. The identified proteins that can cleave ROCK includes caspase 3 (ROCK1) and granzyme B (ROCK2).

(70, 71). Activity of RhoA is closely associated with ROCK activity, and the activity of RhoA is enhanced by RhoGEF (guanine exchange factor) and suppressed by RhoGAP (GTPase activating protein) (Figure 1.9). The activity of RhoA is determined by its binding to GTP or GDP (Figure 1.9). GTP bound RhoA is the active form whereas GDP bound RhoA is the inactive form. RhoA, like other members of the RhoGTPases family, itself possesses intrinsic GTPase activity which hydrolyzes GTP to GDP. Rho Guanine Nucleotide Exchange Factor (RhoGEF) activates RhoA by promoting the exchange of GDP to GTP, while Rho GTPase Activating Protein (RhoGAP) inactivates RhoA by promoting its intrinsic GTPase activity.

1.3.2.6.1 RhoGAP in HCC

So far, there is only one group of RhoGAP protein, Deleted in Liver Cancer (DLC), shown to be implicated in HCC. There are three identified members in the DLC1 family: DLC1, DLC2, and DLC3. Loss of DLC1 and DLC2 was shown to be associated with HCC and many other cancers and loss of DLC3 was shown to be associated with prostate cancer (72-77). Among these three members, DLC1 was the first one identified and its roles in HCC were the best characterized. Like other DLC members, DLC1 encodes RhoGAP protein (77). It is an important tumor suppressor gene in HCC that suppresses HCC cell migration (77). DLC1 possesses RhoGAP activity specific for RhoA and disrupts actin polymerization of HCC cells (77). DLC1 negatively regulates the activity of RhoA by enhancing intrinsic GTP hydrolytic activity of RhoA, thus catalyzing the conversion of RhoA from its GTP-bound active state to GDP-bound inactive state (76, 78). However, whether DLC1 regulates HCC cell migration and cytoskeletal



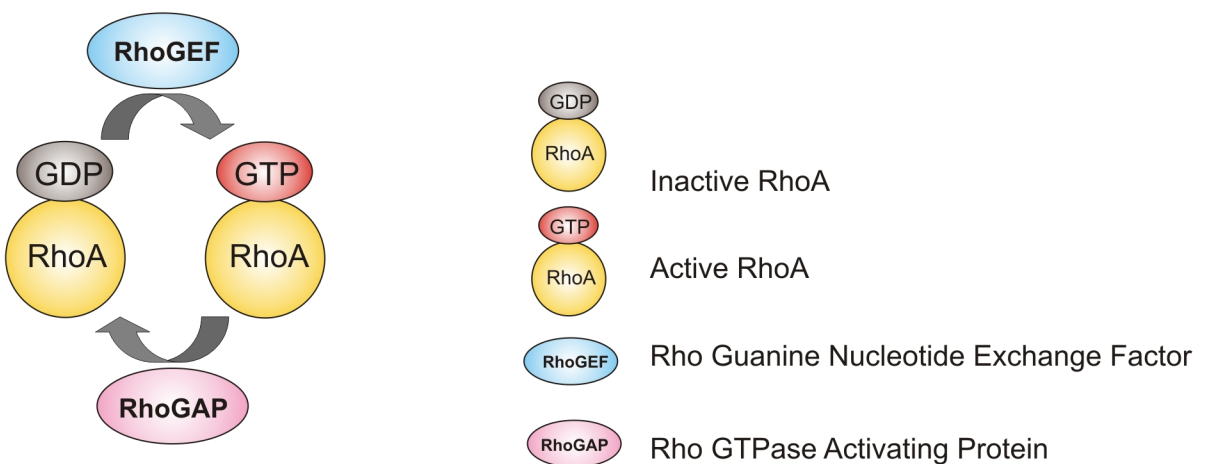


Figure 1.9 Regulation of Rho activity

RhoA, like other members of the RhoGTPases family, itself possesses intrinsic GTPase activity which constantly hydrolyzes GTP to GDP. GTP bound form of RhoA is the activated form while GDP bound form of RhoA is the inactivated form. Rho Guanine Nucleotide Exchange Factor (RhoGEF) activates RhoA by promoting the exchange of GDP to GTP. Rho GTPase Activating Protein (RhoGAP) inactivates RhoA by enhancing its intrinsic GTPase activity.

reorganization through ROCK is still unclear. Furthermore, the complete understanding of the DLC1/RhoA/ROCK signaling pathway and its implication in HCC has never been explored. We will further discuss and unveil this signaling pathway in HCC in Chapter 3.

1.3.2.7 Substrates of ROCK

The major characterized functional roles of ROCK are related to its kinase activity in phosphorylating downstream substrates. ROCK is a serine/threonine kinase which recognizes the consensus phosphorylation sequence RXXS/T or RXS/T. Basic amino acids such as arginine (R), is required to be adjacent to phosphorylation site of ROCK. Due to the high homology of ROCK1 and ROCK2, they phosphorylate common targets. The best known and most verified substrates of ROCK are myosin light chain 2 (MLC2) and myosin phosphatase 1 (MYPT1) and these phosphorylations were of crucial significance to actomyosin contraction, a key step for cell migration. In this section, these well characterized substrates as well as other reported substrates of ROCK will be discussed.

1.3.2.7.1 ROCK Phosphorylatable Substrates in the Regulations of Cytoskeleton Reorganization

ROCK activates myosin and mediated muscle contraction, neurite retraction, and other actomyosin contraction driven mechanisms such as cancer cell movement via phosphorylating two major substrates, myosin light chain 2 (MLC2) and myosin phosphatase 1 (MYPT1). ROCK phosphorylates and activates MLC2 at Thr 18 and Ser 19 while MYPT1 dephosphorylates and inactivates MLC2 at these sites (Figure 1.10)



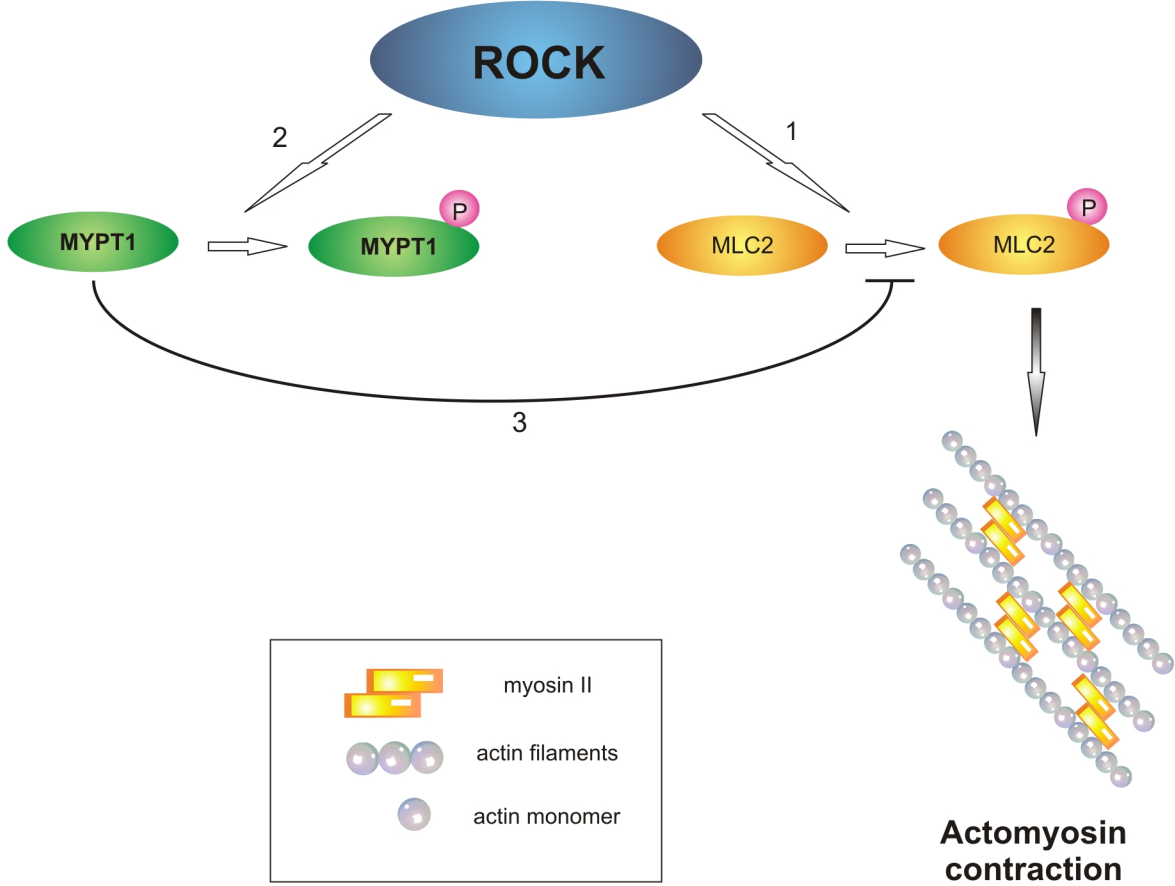


Figure 1.10 ROCK regulates phosphorylation of MLC2 and MYPT1 and regulates actomyosin contractility

ROCK activates MLC2 and induces actomyosin contraction by 1) phosphorylating MLC2 directly or 2) inactivating MYPT1 through phosphorylating MYPT1 since 3) MLC2 can be dephosphorylated by active MYPT1.

(79). MYPT1 and ROCK counteract each other in MLC2 phosphorylation status, but ROCK can inactivate MYPT1 by phosphorylating MYPT1 at Thr 697 and Ser 853 (80) (Figure 1.10). As mentioned, myosin and actin are two major components generating actomyosin contraction. Phosphorylation and activation of MLC2 by ROCK is important for actomyosin contraction and will be further discussed in Chapter 3.

In addition to MLC2 and MYPT1, mounting evidence has demonstrated that ROCK phosphorylates a number of substrates important for cytoskeletal related events (Table 1.1). ROCK has been shown to phosphorylate Thr 7, Ser 13, Ser 38 of human glial fibrillary acidic protein (GFAP), an astrocyte specific intermediate filament protein located at the cleavage furrow of cytokinetic cells. These phosphorylation sites were important for cytokinetic segregation of glial filaments (81). ROCK also phosphorylates another intermediate filament protein, vimentin at Ser 38 and Ser 71, and this ROCK-mediated vimentin phosphorylation abolishes *in vitro* filament formation (82). ROCK specific phosphorylation of vimentin occurs at the cleavage furrow in late mitotic stage. In addition, ROCK was found to phosphorylate adducin at Thr 445 and Thr 480. Adducin is classified as membrane skeletal protein that binds to fast growing ends of actin filaments (83-85). Adducin is responsible for spectrin-actin association beneath plasma membranes. Particularly, phosphorylation of Thr 445 is important for ROCK mediated membrane ruffling formation and cell movement (86). Besides, ROCK also phosphorylates calponin, actin binding protein, at Thr 170 and Thr 184. Phosphorylation of calponin via ROCK was shown to be involved in the abrogation of the binding between calponin and actin filaments (87). Furthermore, ROCK phosphorylates Tau,



microtubule-associated protein, at Ser 262 in regulating microtubule assembly and disassembly (88). Additionally, ROCK phosphorylates and activates LIM kinase 1 (LIMK1) at Thr 508 and LIM kinase 2 (LIMK2) at Thr 505 (89, 90). LIMK phosphorylates and inactivates cofilin, protein responsible for actin depolymerization; hence, activation of LIMK is important for actin cytoskeletal organization. Besides regulating cytoskeletal proteins directly, ROCK also regulates a group of proteins closely linked to the cytoskeleton, the ezrin/ radixin/ moesin (ERM) proteins, responsible for anchoring actin filaments to the plasma membrane. ROCK phosphorylates ezrin at Thr 567 (91, 92) and ROCK mediated ezrin Thr 567 phosphorylation was shown to be involved in focal adhesions formation (91).

1.3.2.7.2 ROCK Phosphorylatable Substrates in the Nervous System

ROCK also exhibits regulatory roles in nervous system and phosphorylates a specific group of substrates in the nervous system (Table 1.1). ROCK is able to phosphorylate a neuronal protein, Collapsin Response Mediator Protein 2 (CRMP2), at Thr 555 which is important for growth cone collapse (93). Neurofilament-L (NF-L), a chief component of neuronal cytoskeleton, was shown to be phosphorylated by ROCK at Ser 26 and Ser 57, indicating a role of neuronal signal transduction of ROCK (94). Furthermore, myristoylated alanine-rich C-kinase substrate (MARCKS), an actin binding protein in the nervous system, can also be phosphorylated by ROCK at Ser 159 (95). These signaling pathways are involved in the regulations of various neuronal functions including neuronal cell migration, dendritic spine morphology, axonal guidance and regeneration (96).



Table 1.1 ROCK Phosphorylatable Substrates

ROCK substrates	Phosphorylation site	Functions
Cytoskeletal or cytoskeletal related proteins		
Myosin Light Chain 2 (MLC2)	Thr 18, Ser 19	Actomyosin contraction
Myosin Phosphatase 1 (MYPT1)	Thr 697, Ser 853	Actomyosin contraction
Glial Fibrillary Acidic Protein (GFAP)	Thr 7, Ser 13, Ser 38	Cytokinetic segregation of glial filaments
Vimentin	Ser 38, Ser 71	<i>In vitro</i> filament formation
Adducin	Thr 445, Thr 480	Formation of membrane ruffles and cell movement
Calponin	Thr 170, Thr 184	Calponin and actin filaments binding
Tau	Ser 262	Microtubules assembly and disassembly
LIM Kinase 1	Thr 508	Actin polymerization
LIM Kinase 2	Thr 505	Actin polymerization
Ezrin	Thr 567	Focal adhesion formations
Cytoskeletal proteins in the nervous system		
Collapsin Response Mediator Protein 2 (CRMP2)	Thr 555	Growth cone collapse
Neurofilament-L (NF-L)	Ser 26, Ser 57	Neuronal intermediate filament reorganization
Myristoylated Alanine-Rich C-Kinase Substrate (MARCKS)	Ser 159	Actin binding in the nervous system



1.3.2.8 Functions of ROCK

Functions of ROCK largely rely on the kinase region of ROCK which phosphorylates downstream targets, mostly related to cytoskeleton reorganization. The following section will cover the reported functions of ROCK demonstrated in different cell systems.

1.3.2.8.1 ROCK Regulates Cytoskeletal Network of Cells

The most characterized and important function of ROCK is the formation of stress fibers which requires polymerization of actin and activation of myosin. Dominant negative ROCK or the treatment of ROCK inhibitor could suppress formation of stress fibers in smooth muscle cells and focal contacts in cervical cancer cells (HeLa) mediated by activated RhoA (97, 98). Overexpression of ROCK protein also promoted formation of focal adhesions and stress fibers demonstrated by microinjection of the protein in HeLa cells (52). ROCK is responsible for cell body contraction which requires high coordination of stress fibers and focal adhesions. ROCK phosphorylates a number of substrates, as discussed in the section 1.3.2.7, which contribute to the regulation of contractility.

1.3.2.8.2 ROCK Promotes Membrane Blebblings

ROCK was found to regulate formations of cellular membrane blebbing in a rho-independent manner (66, 99). Membrane bleb is transient actin-rich bubble-like protrusions formed from the plasma membrane. Cleavage of ROCK1 at DETD1113 amino acid sequence and ROCK2 at IGLD1131 by caspase 3 and granzyme B, respectively, resulted in constitutively activated ROCK due to the release of the



autoinhibitory loop (66, 99). This activation of ROCK induced membrane blebs formation in apoptotic cells (66, 99). However, this activation was shown to be a consequence rather than a cause of apoptosis (66, 99). Membrane blebs can be observed in apoptotic cells; however, non-apoptotic membrane blebs can also be formed and were reported to be involved cancer cell migration and invasion (100). The precise physiological regulation and role of membrane blebs remain largely unknown and we will further explore the relation of ROCK and membrane blebs formation in HCC in Chapter 4.

1.3.2.8.3 Nuclear Functions of ROCK

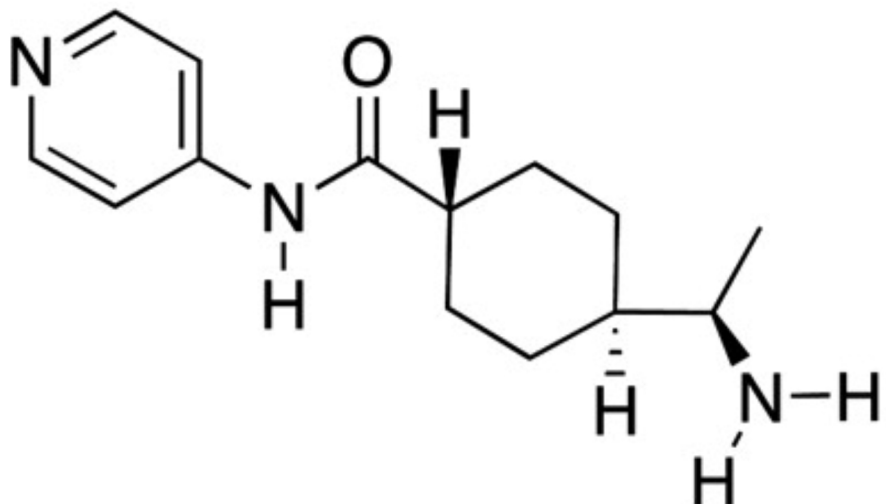
Despite most studies on ROCK focused on its cytoplasmic functions, two recent reports have demonstrated that ROCK functions in the nucleus. Nuclear function of ROCK2 was first discovered when it was found to be a binding partner of p300 acetyltransferase (58). p300 acetyltransferase was shown to interact with transcription factors and induced gene expression (101, 102). ROCK2 was shown to be able to phosphorylate p300 and this phosphorylation was crucial for its acetyltransferase activity *in vivo* and *in vitro* (58). This indicates that ROCK may be related to the functions of p300 acetyltransferase which has been implicated in a variety of other cellular activities, including the cell cycle, DNA repair, and apoptosis.



1.3.2.9 ROCK Inhibitors

As mentioned previously, ROCK plays an important role in many fundamental processes of cell migration, but aberrant activation of ROCK may contribute to disastrous physiological consequences such as cancer metastasis, blood vessels constriction, and extensive retraction of neurites. Over the years, pharmaceutical industry has been paying immense effort in search of ROCK-specific inhibitors. Two most common groups of ROCK inhibitors developed are the pyridine and the isoquinoline derivatives. These two groups of ROCK inhibitors are small molecule inhibitors both competing for the ATP binding sites of ROCK. Fasudil (HA1077) is the most widely used isoquinoline derivative. It is in clinical trial in the treatment of cerebral vasospasm, prolonged blood vessel constriction in the nervous system and other cardiovascular diseases. Fasudil was found to be a potent protein kinase inhibitor acting as a vessel dilator in treating cerebral vasospasm in 1993 and was later found to possess inhibitory effect on ROCK activity (103). Y27632 is the most widely used pyridine derivative (Figure 1.11) and was later discovered to exhibit a more selective inhibitory effect towards ROCK as compared to fasudil. Since Y27632 was shown to exhibit a much more significant and potent selectivity towards ROCK as compared to other protein kinases (104, 105), it has been extensively used as a tool to evaluate functions of the cellular and physiological functions of ROCK.





(Jacobs M et al. The Journal of Biological Chemistry. 2006) (106)

Figure 1.11 Chemical structure of Y27632

Y27632 is a pyrimidine-based small molecule inhibitor specific for ROCK. It competes with ATP for the ATP binding sites of ROCK.

1.4 Objectives

HCC is one of the most fatal cancers in the world and metastasis is the leading cause of death in HCC patients; therefore, detailed knowledge on the underlying molecular mechanisms involved in HCC metastasis is urgently warranted. Cancer cell migration is an essential step for cancer metastasis and ROCK controls the fundamental events in cell migration. Therefore, we wish to investigate the regulations and functions of ROCK in human HCC.

Previously, our team demonstrated that DLC1, a RhoGAP protein, was frequently underexpressed in human HCC. We also demonstrated that DLC1 suppressed HCC cell migration through inactivation of RhoA and disruption of actin cytoskeletal network. However, the detailed signaling pathway has not been explored. Since ROCK is an immediate downstream effector of RhoA, we hypothesized that DLC1 suppressed HCC cell migration via inhibiting the RhoA/ROCK signaling pathway. To address this question, we carefully observed the impact of DLC1 on the ROCK mediated cytoskeletal alterations such as formations of stress fibers and focal adhesions, and actomyosin contractility. We also observed the impact of DLC1/RhoA/ROCK pathway on cytoskeletal collapse and cell morphology.

We also hypothesized that ROCK was important for HCC cell motility and that deregulation of ROCK expression was implicated in HCC metastasis. To address these questions, we examined the expressions of the two members of ROCK, ROCK1 and ROCK2, in HCC. We found that only ROCK2 but not ROCK1 was overexpressed in



HCC. Therefore, we characterized the migratory functions of ROCK2 in HCC *in vitro* and *in vivo*. Furthermore, we further examined the effect of ROCK2 on the cytoskeletal and molecular impact on HCC cells.

We also wished to understand the mechanisms leading to the aberrant expression of ROCK in HCC. ROCK2 is frequently overexpressed in HCC at the protein but not the mRNA level. Therefore, we hypothesized that ROCK2 was deregulated translationally in HCC. To address the question, we examined the possible translational mechanisms such as ubiquitin-proteosomal degradation and microRNA mediated post-transcriptional modifications. We found an microRNA, miR139, was closely associated with ROCK2 expression in HCC. We hypothesized that underexpression of miR139 resulted in the overexpression of ROCK2 protein in human HCC. To answer this question, we correlated the expression of miR139 and expression of ROCK2 protein in our HCC samples. We also examined the effect of miR139 to ROCK2 protein expression, HCC cell migration and invasion, and the development of HCC.



Chapter 2

General Methodology

2.1 HCC Patients

2.1.1 Patients

Primary HCCs resected from patients between year 1991-2007 at Queen Mary Hospital were used in this study. All patients are Chinese and none received any other therapies including chemoembolization or chemotherapy before resection.

2.1.2 HCC and Non-Tumorous Liver Samples

Immediately after resection, tumors and their corresponding non-tumorous liver samples were snap-frozen in liquid nitrogen. Frozen samples were embedded with O.C.T compound (Tissue-Tek, Torrance, CA) and were stored at -80°C.

2.1.3 Clinical Pathological Study

Cellular differentiation was accessed based on the method of Edmondson and Steiner (Edmondson 1954) and was classified into Edmondson grade I, II, III, or IV. Edmondson grades I and II were to describe tumors with better cellular differentiation whilst Edmondson grades III and IV were to describe worse cellular differentiation. Tumor stages of HCC were classified based on pTNM classification and divided into pTNM stage I, II, III, or IV. Tumor size was measured at the largest diameter of the largest



tumor and was divided into small (≤ 5 cm) HCC and large (> 5 cm) HCC. The number of tumor nodules was determined macroscopically. Absence of tumor encapsulation, presence of venous invasion, and tumor microsatellite formation were studied and determined microscopically. Direct liver invasion was noted macroscopically and microscopically. Metastatic features of tumor were indicated by the absence of tumor encapsulation, presence of venous invasion (without differentiating into hepatic or portal veins), direct liver invasion into adjacent liver parenchyma, and tumor microsatellite formation. The hepatitis B surface antigen (HBsAg) status of the patients was provided from clinical records.



Table 2.1. Clinicopathological features of 71 HCC patients included in this study.

Parameters	Finding	No. of cases (%)
Gender	Male	55 (77.5%)
	Female	16 (22.5%)
Tumor size	≤ 5 cm	27 (38.0%)
	> 5 cm	44 (62.0%)
Tumor encapsulation	Present	26 (37.1%)
	Absent	44 (62.9%)
Number of tumor nodules	Solitary	53 (74.6%)
	≥ 2	18 (25.4%)
Venous invasion	Present	36 (50.7%)
	Absent	35 (49.3%)
Tumor microsatellite formation	Present	39 (54.9%)
	Absent	32 (45.1%)
Direct liver invasion	Present	25 (40.3%)
	Absent	37 (59.7%)
Cellular differentiation by Edmondson classification	Grade I & II	34 (47.9%)
	Grade III & IV	37 (52.1%)
Resection margin	Positive	1 (1.4%)
	Negative	70 (98.6%)
pTNM stage	Stage I & II	28 (39.4%)
	Stage III & IV	43 (60.6%)
Nontumorous liver	Normal	4 (5.6%)
	Chronic hepatitis	28 (40.8%)
	Cirrhosis	38 (53.5%)
HBsAg status	Positive	57 (76.1%)
	Negative	16 (22.5%)



2.2 Tissue Culture

2.2.1 Cell Lines

Human hepatoma cell lines including HepG2, Hep3B, HLE, WRL, PLC/PRF/5, SK-Hep-1, SNU-182, SNU-449, and SNU-475, human cervical cancer cell line HeLa, human embryonic fibroblast cell line, NIH3T3, human embryonic kidney cells HEK293, monkey kidney cell line COS7, Chinese hamster ovary cell line CHO were obtained from American Type Culture Collection. Human HCC cell lines H2P, H2M, BEL-7402, and SMMC-7721 and normal liver cell lines LO2 and MIHA were gifts from Shanghai Institute of Cell Biology, Chinese Academy of Sciences. Human HCC cell lines MHCC97L and MHCC97H were from Fudan University, Shanghai (Prof. Z.Y. Tang).



Table 2.2. Properties of HCC cell lines used in this study.

Cell Lines	Source	<i>In Vivo</i> Tumorigenecity (From Study of Subcutaneous Injection)	<i>In Vivo</i> Metastatic Capability (From Study of Orthotopic Liver Tumor Implantation)
BEL7402	Hepatocellular Carcinoma	Yes	Low (Local Invasion)
SMMC-7721	Hepatocellular Carcinoma	Yes	No
PLC/PRF/5	Hepatocellular Carcinoma	Yes	NA
MHCC97L	Hepatocellular Carcinoma	Yes	High (Lung Metastasis)
MHCC97H	Hepatocellular Carcinoma	Yes	High (Lung Metastasis)
Hep3B	Hepatocellular Carcinoma	Yes	NA
HepG2	Hepatoblastoma	No	NA
SK-Hep1	Adenoma	NA	NA

NA= No Information Available



2.2.2 Maintenance of Cells

HepG2, Hep3B, PLC, Sk-Hep-1, were grown in minimal essential medium (MEM) with 1 mM sodium pyruvate (GIBCO, NY, USA) and 10% fetal bovine serum (GIBCO). NIH3T3 was grown in Dulbecco's modified Eagle minimal high glucose essential medium (DMEM-HG) with 10% newborn calf serum (GIBCO). MHCC97L and MHCC97H were grown in DMEM-HG with 10% fetal bovine serum and 1 mM sodium pyruvate. SNU-182, SNU-449, SNU-475 were grown in RPMI medium (GIBCO). Other cell lines were maintained in DMEM-HG with 10% fetal bovine serum if not mentioned otherwise. All culture medium was added with penicillin and streptomycin. All cell cultures were kept in incubator at 37°C with 5% CO₂ and culture medium was refreshed every 3 days and confluent cells were split at ratio of 1:5 to 1:10.

2.2.3 Trypsinization

Confluent cells were washed with 1X phosphate buffered saline (PBS) (8.0 mg/mL NaCl, 1.4 mg/mL Na₂HPO₄, 0.2 mg/mL KCl, 0.2 mg/mL KH₂PO₄, pH 7.2). Then, 2 mL (for 100 mm culture dish) or 0.3 mL (for 35 mm culture dish) of trypsin/ EDTA (0.025% trypsin, 0.05% EDTA) was added to the culture and placed at 37°C CO₂ incubator for 5 minutes. After cells were detached from culture plates, trypsinized cells were suspended in culture medium with 10% serum (7mL for 100 mm and 0.7 mL for 35 mm) in order to inactivate the trypsin. For cell passaging, 1/5 or 1/10 of the suspended cells were added to new dish diluted with fresh culture medium.



2.2.4 Cell Counting

Cells were counted with hematocytometer or COULTER COUNTER® Cell and Particle Counter (Beckman Coulter). For cell counting with hematocytometer, cell suspension mentioned above was diluted with Trypan Blue dye (Sigma, St Louis, MO, USA) at 1:1 ratio and 10 uL of the mixture was used to load into the hematocytometer. Since Trypan Blue stained dead cells only, blue cells were not counted. Only viable cells (transparent) were counted under the phase contrast microscope in the hematocytometer. Precise cell number was calculated with the following equation:

$$\frac{\text{Total number of cell counts in 9 square units} \times \text{dilution factor} \times 10^4}{\text{Total number of square units counted}}$$

For cell counting with COULTER COUNTER® Cell and Particle Counter, 100 μ L of cell suspension was added to 10 mL of isoton II. Cell counter automatically calculated number of cells or concentration of cells with a dilution factor input of 100.

2.2.5 Transfection with Mammalian Cell Lines

Cells were transfected with FuGENE 6 (Roche, Indianapolis, IN, USA) for expression vectors or lipofectamine 2000 (Invitrogen, Carlsbad, CA, USA) for small RNAs including short interference RNAs and mature microRNAs according to manufacturers' protocols. 1×10^5 or 2×10^5 cells were seeded onto 18 mm plates or 35 mm plates, respectively, 1 day prior transfection. For expression vector transfection, plasmid DNA (2 - 4 μ g) was added to diluted FuGENE 6 in serum free medium. DNA and Fugene 6 was used in a 2 μ g: 3 μ L ratio. Mixture was finger vortexed and incubated at room temperature for 15 minutes, then added to cells evenly drop-wise. Transfected cells were



incubated for 24 - 48 hours in 37°C CO₂ incubator. For small RNA transfection, 100 nM of small RNAs and 1 µL of lipofectamine 2000 were diluted in serum free medium and incubated at room temperature for 5 minutes separately. Two mixtures were mixed together gently and further incubated at room temperature for 15 more minutes. The combined lipofectamine RNA mixture was added to cells evenly drop-wise and transfected cells were incubated for 2 - 4 days in 37°C CO₂ incubator. For microRNA transfection, 100-1000 pmol of microRNAs and 5 µL of lipofectamine 2000 were diluted in serum free medium and incubated at room temperature 5 minutes separately. Two mixtures were mixed together gently and further incubated at room temperature for 15 more minutes. The combined lipofectamine microRNA mixture was added to cells evenly drop-wise and transfected cells were incubated for 24 - 96 hours in 37°C CO₂ incubator.

2.2.6 Stocking and Thawing Cells

To stock cells from 100 mm plates in liquid nitrogen, cells were trypsinized as mentioned in 2.2.3 and centrifuged at 1500 x g for 5 minutes. Cell pellets were resuspended with 3 mL of anti-freezing medium (10% DMSO and 90% FBS) and placed in 1 mL cryogenic vials in cryogen box filled with 100% methanol. Cryogen box was placed in -80°C refrigerator for 24 hours and transferred to liquid nitrogen. To thaw frozen cells, cryogenic vials were placed at 37°C water bath. To wash way residual anti-freezing medium, thawed cell pellets were washed and resuspended in 1X PBS and centrifuged repeatedly three times. Finally, the pellets were resuspended in culture medium and placed into culture plates.



2.3 Preparation of RNA and cDNA Samples

2.3.1 Extraction of Total RNA from Frozen Tissues

0.1 µg of frozen tissues was resuspended in 3 mL TRIZOL Reagent (GIBCO). Tissue/TRIZOL mixture was centrifuged at 13,000 x g at 4°C for 5 minutes. Supernatant was added with 0.6 mL chloroform and incubated at room temperature for 3 more minutes. After centrifugation at 13,000 x g at 4°C for 15 minutes, upper aqueous phase (RNA containing) was removed into a clean tube followed by addition of 1.5 mL of 100% isopropanol and incubation at room temperature for 15 minutes. It was then centrifuged at 14,000 x g at 4°C for 15 minutes and the precipitate was washed with 70% ethanol thrice. Ethanol was removed through gentle suctioning and residual ethanol was removed by air-drying the precipitate in room temperature for 10 minutes. The RNA pellet was resuspended in DEPC-treated H₂O at 55°C heat block for 15 minutes. RNA concentration was measured by spectrophotometer at A₂₆₀.

2.3.2 Extraction of Total RNA from Cell Lines

1 mL of TRIZOL reagent was added directly to 35 mm plate cultured with confluent cells. TRIZOL started to lyse cells once added to well. TRIZOL lysing solution was transferred into a new tube after 5 minutes of incubation at room temperature. 0.2 mL chloroform was added to the TRIZOL lysed cells followed by 15 seconds of vigorous shaking. Tube was then incubated at room temperature for 3 minutes followed by centrifugation at 13, 000 x g for 15 minutes at 4°C. Aqueous phase (upper phase) was transferred to clean tube following with the addition 0.5 mL 100% isopropanol (IPA).



Tube was incubated at room temperature for 10 minutes and was then centrifuged at 13,000 x g for 10 minutes. The precipitate was washed with 1 mL 75% ethanol followed by vortexing. It was then centrifuged at 7500 x g for 5 minutes. Supernatant was then removed by gentle pipetting or suctioning and the pellet was then air-dried. Pellet (RNA) was dissolved with 50 µL DEPC-treated H₂O and was incubated at 55-60°C heat block for 10 minutes. RNA concentration was measured by spectrophotometer at A₂₆₀.

2.3.3 Complementary DNA Synthesis

Reverse transcription was carried out with GeneAmp RNA PCR kit (Applied Biosystems, Foster City, CA, USA) according to manufacturer's protocol. In general, 1 µg of total RNA was denatured at 65°C for 10 minutes and then incubated on ice for 5 minutes. It was used as template for reverse transcription with the addition of 1X PCR buffer II, 5 mM of MgCl₂, 4 mM of dNTPs mix, 2.5 µM of random hexamer, 1 unit of RNase inhibitor, and 2.5 unit of MuLv Reverse Transcriptase in a total volume of 20 µL of reaction mixture. The reaction mixture was incubated at room temperature for 10 minutes followed by reaction at 42°C for 60 minutes followed by 95°C for 10 minutes. Synthesized cDNA was ready and could be kept at -20°C for later use.



2.4 Western Blot Analysis

2.4.1 Extraction of Protein from Frozen Tissues

1 mm³ of frozen or fresh tissue was washed with 500 µL RIPA lysis buffer (50 mM Tris HCl, 1% NP40, 0.25% sodium deoxycholate, 150 mM NaCl, 1 mM EDTA, 1 mM NaF, pH 7.4) with 1X complete protease inhibitor (Roche) once and then homogenized in 250 µL RIPA buffer followed by incubation on ice for 10 minutes. It was then centrifuged at 14,000 x g 4°C for 30 minutes. Supernatant was transferred to new 1.5 mL tube.

2.4.2 Extraction of Protein from Cell Lines

2.4.2.1 Extraction by NETN Buffer

To extract protein by NETN buffer (5 mM Tris (pH 7.4), 0.15 mM of NaCl, 5 mM EDTA , 0.2%-1% NP40, 1X complete protease inhibitor) from cell lines, cells from plates were washed once with 1X PBS and were collected in PBS by cell scraper. Cells in PBS were then centrifuged at 14,000 rpm high speed at 4°C. Supernatant was removed and NETN was added to resuspend the pellets. For 100 mm dish, 0.5 – 1.0 mL of NETN buffer was used; for 60 mm dish, 0.3 mL of NETN buffer was used; for 35 mm dish, 0.1 mL of NETN buffer was used. After pellets were resuspended in NETN and were set in ice for 30 minutes, they were quickly centrifuged at 14,000 rpm at 4°C for 20 minutes. Supernatants were transferred to fresh 1.5 mL tubes.



2.4.2.2 Extraction by SDS Buffer

To extract protein by SDS buffer (0.175 M Tris base, 7.5% glycerol, 0.4% SDS), cells from plates were washed with 1X PBS and were added SDS buffer (150-200 µL for 35 mm plates). Cells were incubated with SDS buffer for 5 minutes at room temperature. Cells were lysed by SDS buffer and were collected by cell scraper. Cells were boiled at 95°C for 15-20 minutes before loading.

2.4.3 Measurement of Protein Concentration

Protein concentration was determined by Bradford protein assay (Bio-Rad, Hercules, CA, USA). Bradford dye reagent concentrate was diluted 1:5 with H₂O. Proteins were added to 1 mL of diluted Bradford solution and measured at absorbance 750 nm. 0 mg/ mL, 0.25 mg/ mL, 0.50 mg/ mL, 0.75 mg/ mL, 1.25 mg/ mL, 2.50 mg/ mL, 5.00 mg/ mL of BSA was prepared and measured to plot standard curve for the Bradford protein assay.

2.4.4 Polyacrylamide Gel Electrophoresis

2.4.4.1 Protein Preparation for Loading

When proteins are heated, SDS, negatively charged detergent, gives all molecules negative charges with the presence of DTT, a reducing agent which breaks disulfide bonds within and between polypeptides. The movement of a protein through a SDS-polyacrylamide gel depends primarily on its molecular size with elimination of the effects from protein charge and shape. Therefore, 6X SDS sample buffer (of 0.7 M Tris base,



30% glycerol, 1.67 % SDS, 0.12 mg/ mL bromophenol blue) was added into protein samples before protein samples were boiled at 95°C for 10 minutes before loading.

2.4.4.2 Polyacrylamide Gel Preparation

Polyacrylamide gel electrophoresis (PAGE) was used to separate proteins on the basis of size. Ammonium persulfate (APS) was the source of free radicals which initiated a chain reaction in which acrylamide monomers were polymerized into chains. TEMED (N,N,N',N'-tetramethylethylenediamine) was added to form and stabilize the free radicals. Bis-acrylamide (N,N' methylene-bisacrylamide) was added to polymerize and cross-link acrylamide chains into gel. The length of the acrylamide chains (dependent on the concentration of acrylamide) and the degree of cross-linking (dependent on the concentration of the bis-acrylamide) determined the porosity of a gel. For better resolution, discontinuous buffer system was employed for gel electrophoresis in which gel consisted of two layers poured one on top of the other. In this study, 10% acrylamide concentration was used as the lower separating (resolving) gel (pH 8.8) while 4% acrylamide concentration was used as the upper stacking gel (pH 6.8). 10% separating gel was composed of 10% acrylamide/bisacrylamide solution, 1X separating gel buffer, 0.75 mg/mL APS, 0.1% TEMED. 5X separating gel buffer was composed of 1.879 M Tris HCl, 0.5% Sodium dodecyl sulfate (SDS), and H₂O. 4% stacking gel was composed of 4% acrylamide/bisacrylamide solution, 1X stacking gel buffer, 0.75 mg/mL APS, 0.75% TEMED, and 3.26 mL H₂O were used. For this study, gels were run at 100 volts for 10 minutes (stacking gel layer) and 200 volts for 50-60 minutes in 1X running



buffer (25 mM Tris base, 192 mM glycine, 0.1% SDS). 4 µL of rainbow marker was added to mark protein size.

2.4.5 Immunoblotting

Immunoblotting techniques are based on the principles that antigens may be immobilized on a membrane and then probed with antibodies.

2.4.5.1 Western Transfer

In Western immunoblotting, after proteins were separated electrophoretically by SDS-PAGE, they were transferred to a solid support, nitrocellulose membrane. Western transfer was performed at 100 volts for 60 minutes in 1X transfer buffer (25 mM Tris base, 192 mM glycine, 20% methanol). After the transfer, membrane was incubated with 5% skim milk in 1X TBS (38 mM Tris HCl, 151 mM NaCl, pH 7.6) with 0.1% Tween 20 for 1 hour at room temperature to saturate unoccupied sites on the membrane to prevent non-specific binding with the antibodies. The membrane was then incubated with primary antibodies overnight at 4°C followed by incubation with secondary antibodies for 2 hours at room temperature. Protein expression was detected with the ECLTM detection system (GE Healthcare, Buckinghamshire, UK) according to the manufacturer's protocol. Images were scanned and intensity of bands was quantified with AlphaEaseFCTM software



2.4.5.2 Stripping and Reprobing of Western Blot

The membrane was washed in stripping buffer (100 mM β -mercaptoethanol, 2% SDS, 62.5 mM Tris HCl pH 6.7) at 65°C water bath for 30 minutes. After striping, membrane was washed with 1X TBST three times. Then, membrane was treated just as after transfer with 5% skim milk blocking followed by incubation with primary and secondary antibodies.



2.5 Gene Cloning

2.5.1 Cloning of PCR Products into pGEM-T Easy or pCR4-TOPO Vectors

PCR products were verified by gel electrophoresis in 0.8-2% agarose gel (according to expected product size) in 1X TBE buffer (69 mM Tris HCl, 89 mM boric acid, 310 µM EDTA). The band was cut from the gel and purified by the Gel Extraction Kit (Qiagen, Valencia, CA, USA) based on manufacturer's protocol. The purified PCR product was cloned into pGEM-T Easy Vector (Promega, Madison, WI, USA) or pCR4-TOPO vector (Invitrogen) based on manufacturer's protocol. For cloning using pGEM-T Easy, 5 µL of the purified PCR product was added to 0.5 µL pGEM-T Easy vector, 6 µL 2X ligation buffer, 1.5 µL T4 DNA ligase at 16°C or 4°C overnight. For cloning using pCR4-TOPO, 2 µL of the purified PCR product was added to 0.5 µL salt solution and 0.5 µL pCR4-TOPO vector at room temperature for 5-10 minutes. The ligation product was then transformed as described. 100 µL of cells were spread on LB agar plate with according antibiotics (ampicillin for pGEM-T Easy, ampicillin or kanamycin for pCR4-TOPO) together with 40 µg/ mL X-Gal and 0.1 mM IPTG, and grown at 37 °C incubator overnight. Plate was subjected to additional blue/white screening. Since the PCR insert disrupted the β galactosidase coding sequence and would disrupt the blue color produced, white colonies represented successful cloning of the PCR insert into the pGEM-T Easy vector or pCR4-TOPO vector and were picked and expanded.



2.5.2 Restriction Enzyme Digestion, Alkaline Phosphatase

Treatment, and DNA Ligation

Restriction enzymes were purchased from Amersham Biosciences (Uppsala, Sweden). 1 µg of DNA was digested with 1 unit of restriction enzyme with its according restriction enzyme buffer for 3 hours to 16 hours (based on individual enzyme cutting efficiency) at 37°C incubator. Vector DNA would be treated with 1 unit of calf intestinal alkaline phosphatase (CIAP) to prevent self-ligation at 37°C incubator if a single restriction enzyme was used. After restriction digestion, DNA would be subjected to gel electrophoresis (agarose) and specific bands would be excised from gel followed by DNA purification with Gel Extraction Kit (Qiagen). Ligation was established by mixing vector and insert (1:6 ratio), 1.5 µL ligase and 4 µL ligase buffer in a reaction total volume of 20 µL. Ligation reaction was incubated in 16°C water bath or 4°C cold room overnight.

2.5.3 Transformation

E. coli strain, DH5α, was spread on Luria-Bertani (LB) plate, and a single colony was picked to be inoculated in 3 mL of LB broth. After one overnight culture at 37°C shaker, the culture was inoculated in 100 mL new LB broth and grown to log phase at A₆₀₀ of 0.4. The cells were the centrifuged at 5000 x g for 5 minutes at 4°C and pellet was resuspended in 33 mL ice-chilled RF1 solution (50 mM MnCl₂•4H₂O, 30 mM potassium acetate, 10 mM CaCl₂•2H₂O, 100 mM KCl, 15% glycerol, pH 5.8). The solution was incubated on ice for 15 minutes, and then was centrifuged at 5000 x g for 5 minutes at 4°C. Pellet was resuspended in 8 mL of ice-chilled RF2 solution (75 mM CaCl₂•2H₂O, 10 mM MOPS, 10 mM KCl, 15% glycerol, pH 6.8). Competent bacterial cells were



aliquoted into 100 μ L and stored at -80°C. 10 μ L ligation product or plasmid (0.1-1 ng) was added to the aliquoted competent bacterial cells. After incubation on ice for 10 minutes, competent cells were subjected to heat shock transformation in 42°C water bath for 90 seconds followed by ice-chilling for 5 minutes. Then, 700-800 μ L of LB broth was added to the cells for 37°C culturing at shaker for 50 minutes. 100 μ L of cells were spread on LB agar plate with according antibiotics (28 mM ampicillin or 62 mM kanamycin) and grown at 37 °C incubator overnight.

2.5.4 Minipreparation and Midipreparation of Plasmid

DNA

Single colonies grown on the plates were picked and inoculated in 2 mL LB broth (antibiotics containing) at 37°C shaker for at least 8 hours. Culture could be used as starter culture for culture expanding for midi-prep kit (Qiagen) or for plasmid extraction by mini-prep kit (Qiagen) according to manufacturer's protocol. For expanding the culture, the 2 mL of bacterial cells was inoculated in 150 mL fresh LB broth (antibiotics containing) at 37°C shaker overnight and subjected to plasmid extraction by midi-prep kit (Qiagen) according to manufacturer's protocol. In general, for mini-prep, 2 mL of the bacterial culture was centrifuged at 14,000 x g for 1 minute. The pellet was resuspended in 0.25 mL cold P1 solution. Then, 0.25 mL P2 solution (alkaline lysis buffer) was added to lyse the bacterial cells through inverting the tubes rapidly 6-10 times. After the lysis, 0.35 mL P3 buffer solution was added to stop the lysis reaction through inverting the tubes vigorously. Lysed cells were centrifuged at 14,000 x g for 10 minutes and the supernatants were purified through columns from the mini-prep kit through washing by



0.7 mL PE solution and elution with 50 μ L H₂O. For midi-prep, 100-150 mL of the bacterial culture was centrifuged at 6000 \times g for 5 minutes at 4°C. The pellet was resuspended in 4 mL cold P1 solution. Then, 4 mL P2 solution (alkaline lysis buffer) was added to lyse the bacterial cells through inverting the cylinder rapidly 6-10 times followed by 5 minutes of incubation at room temperature. After the lysis, 4 mL P3 buffer solution was added to stop the lysis reaction through inverting the cylinder vigorously followed by 15 minutes of incubation on ice. The plasmid DNA and the cell debris were separated by centrifugation of 20,000 \times g at 4°C for 30 minutes. Then, plasmid DNA containing supernatant was added to the equilibrated column (equilibrated by 4 mL of QBE buffer). The column was washed with 10 mL of QC buffer twice and eluted with 5 mL of QF buffer. The eluted plasmid DNA containing solution was added with 3.5 mL 100% isopropanol followed by centrifugation of 15,000 \times g at 4°C for 30 minutes. The white precipitate was washed with 2 mL of 70% ethanol followed by centrifugation of 15,000 \times g at 4°C for 10 minutes. The white precipitate has to be air-dried for 5-10 minutes to remove residual ethanol. The dried pellet was dissolved in 200 μ L H₂O. Concentration of the DNA was measured by spectrophotometer at A_{260/280}. All plasmids were verified by restriction enzyme digestion, PCR, and DNA sequencing prior use if necessary.

2.5.5 DNA Sequencing

DNA sequencing reaction was performed with DYNaMic ET terminator cycle sequencing kit (Amersham Pharmacia Biotech, Cleveland, OH, USA). Reactions contained 10 nmol of primer, 1 μ L (mini prep or 1:20 diluted midi-prep) purified PCR product, and 4 μ L



sequencing reaction premix kit. Sequencing reaction was carried out for 35 cycles of 95°C 20 for seconds, 50°C for 15 seconds, 60°C for 60 seconds. Product was then precipitated with 40 µL 95% ethanol and 1 µL sodium acetate/ EDTA buffer. It was placed on ice for 30 minutes and then centrifuged at 13,000 x g for 15 minutes. Pellet was washed with 70% ethanol twice and air-dried. The pellet was sent to Human Genome Center (The University of Hong Kong) for resuspension in 2 µL of loading buffer (deionized formamide and 25 mM EDTA). It was then denatured at 95°C for 15 minutes and undergone electrophoresis in 5% Longer Ranger gel (Applied Biosystems, Foster City, CA, USA). Sequence was analyzed by Chromas 2.33 (Technelysium Pty Ltd, Helensvale, Queensland, Australia).



2.6 Cell Migration and Invasion Assays

2.6.1 Wound Healing Assay

1×10^6 (35 mm plates) and 2×10^6 (60mm plates) cells were seeded one night before the assay. Confluent cells were pretreated with 1 $\mu\text{g}/\text{mL}$ mitomycin C (Sigma) for 2 hours. A 10 μL plastic pipette tip was used to scratch a wound (space) on the confluent plate gently. Cells would be forced to move towards the space. Images of the wounds were captured at the same marked region at different time points.

2.6.2 Transwell Assay

Transwell Boyden chamber of polycarbonate membranes with pore size of 8.0 μm (Corning Inc., NY, USA) was used for transwell migration assay (Figure 2.1). 5×10^4 cells were resuspended in 300 μL serum free culture medium and added to the upper chamber. 500 μL 10% FBS culture medium was used as chemoattractant and was filled in the lower chamber. Cells were then incubated in CO₂ incubator at 37°C for 8-16 hours depending on cell lines. Cotton-tipped swabs were used to gently remove non-migrating cells in the interior upper chamber. Cells having migrated through the pores to the lower surface of the membrane were fixed by dipping the upper chamber into 100% methanol. After air drying, upper chamber was dipped into 0.1% crystal violet. Chambers were rinsed with tap water until wash off of excess crystal violent. Chambers were air dry. Photographs of 3 different fields of the stained cells were captured by a camera connected to a phase contrast microscope and cells were counted by AlphaEaseFC™ software.



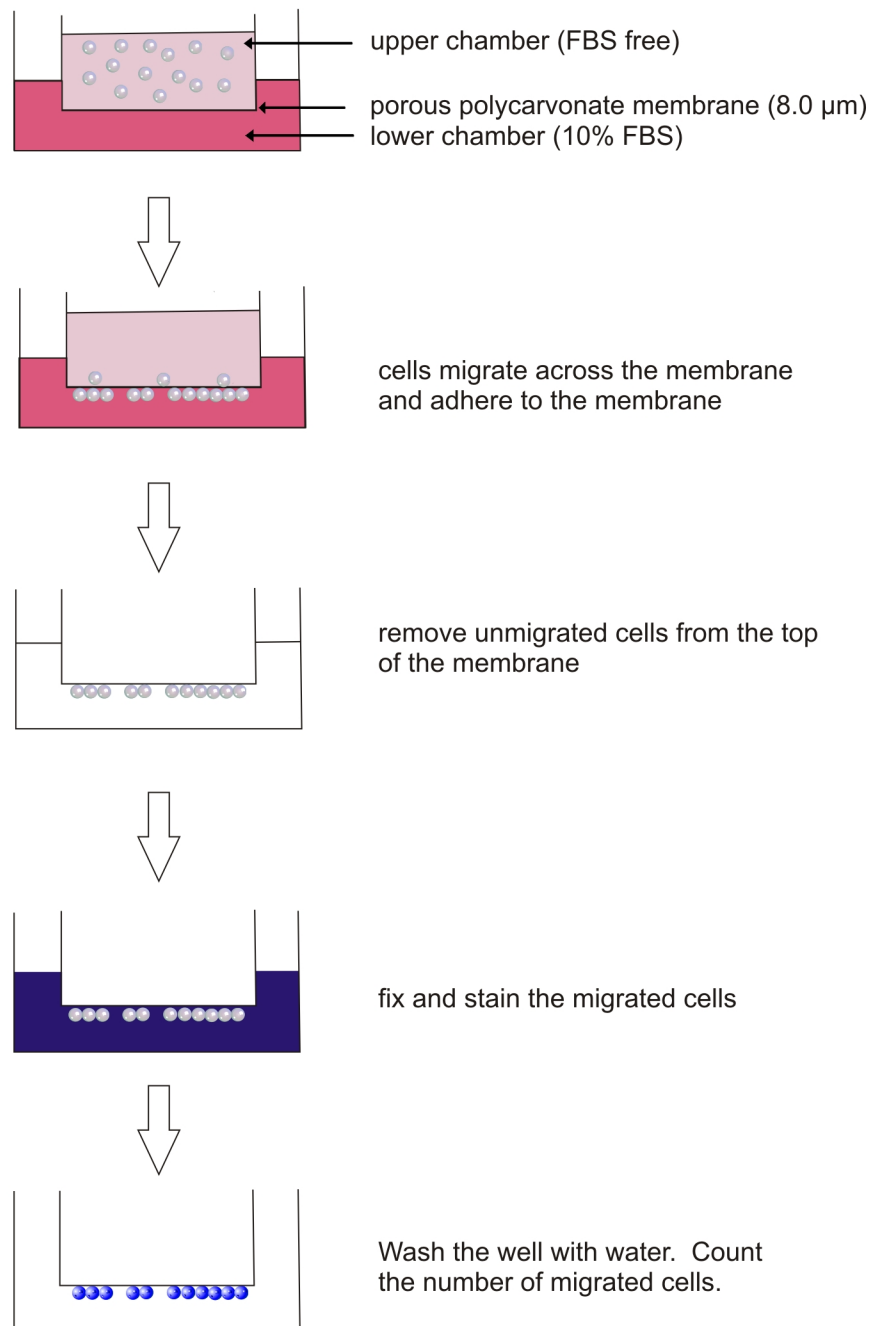


Figure 2.1 Cell migration assay (transwell)

Cells were resuspended in serum free medium and added to the transwell insert (upper chamber). Medium containing 10% of fetal bovine serum (FBS) was added to the lower well as chemoattractant. After incubation for a period of time, cells migrated through the pores across the membrane adhered to the bottom of the membrane. Migrated cells were then fixed by dipping the transwell insert into methanol and stained with crystal violet. The well was washed with water. After the well was air-dried, photo was captured under microscop and the number of migrated cells was counted.

2.6.3 Invasion Assay

Invasion assay was carried out similar to transwell migration assay with an addition of a thin layer of matrigel coated on top of the membrane of the inner chamber to mimic the extracellular matrix environment. Invasion assay was carried out with precoated cell invasion kit (Chemicon International, Temecula, CA, USA), or self coated matrigel BD MatrigelTM Matrix (BD Biosciences, Sparks, MD, USA). Matrigel (56% laminin, 31% collagen IV, 8% entactin) was thawed on ice in 4°C cold room overnight. Matrigel was diluted with equal volume of ice-cold serum free DMEM-HG culture medium. 10 µL of diluted matrigel was added to the inner membrane surface of the transwell chamber and incubated in 37°C CO₂ incubator for 60 minutes. After matrigel was set, 1 - 3 x 10⁵ cells were added to upper chamber as described in previous section. Rest of the steps were carried out like transwell migration assay except cells were incubated in CO₂ incubator at 37°C for 16-48 hours depending on cell lines

2.6.4 *In vivo* Metastasis Assay (Orthotopic Liver Implantation in Nude Mice)

To examine the metastatic potential of HCC cells *in vivo*, 1 – 4 × 10⁶ cells in 0.1 mL of phosphate-buffered saline, respectively, were injected subcutaneously into the flanks of BALB/C nude mice. After 4 weeks, the subcutaneous tumors were resected and cut into 1 mm³ cubes and implanted in the left lobes of the livers of the nude mice (4 per experimental group) (Figure 2.2). The animals were sacrificed and examined 6-12 weeks after implantation. Tumor metastasis of luciferase labelled xenografts was detected weekly with bioluminescent signaling during the course of study. 100 mg/kg D-luciferin



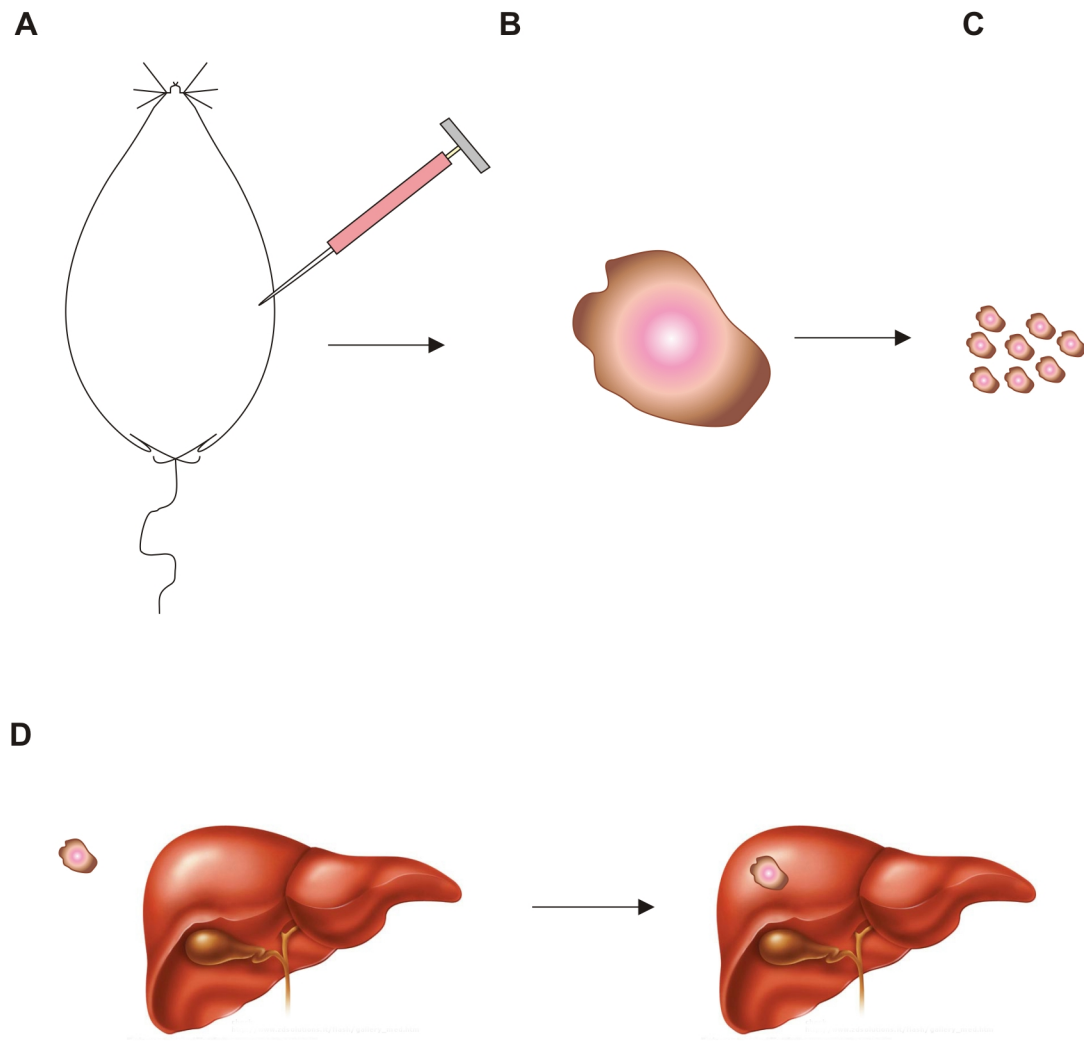


Figure 2.2 Orthotopic liver tumor implantation

(A) Cancer cells were injected into nude mice subcutaneously. (B) Subcutaneous tumors were harvested 3 weeks after injection. (C) Tumors were excised into 1 mm^3 . (D) Excised tumors were implanted to the left lobes of the livers of a new batch of nude mice.

(Xenogen, Hopkinton, MA) was injected into the peritoneal cavities of the mice and bioluminescence was detected by IVISTM100 Imaging System (Xenogen, Hopkinton, MA). For *ex vivo* organ imaging, mice were injected with 100 mg/kg D-luciferin 5 min intraperitoneally before necropsy and the excised organs were imaged. These experiments were performed according to the Animals (Control of Experiments) Ordinance (Hong Kong) and the Institute's guidance on animal experimentation.



Chapter 3

Regulation of ROCK: Signal Transduction Pathway

3.1 Introduction

As mentioned in Chapter 1, cell migration requires cycles of steps which begin from the formation of cell protrusion at the leading edge. At the sites of protrusion, focal adhesions are formed to attach the cytoskeleton, mainly actin and myosin, to the extracellular matrix. The cytoskeleton generates tension which results in actomyosin contractility to translocate the cell body. Finally, the tension releases the adhesions from the cell's trailing edge (33). Deregulation in any of the steps involved in cell migration can result in aberrant cell movement and, in cancer cells, metastasis (34). HCC is one of the most prevalent cancers worldwide and intrahepatic and extrahepatic metastasis is the leading cause of mortality in patients with this cancer. More thorough knowledge of the molecular mechanisms regulating HCC cell migration is still awaited for the development of novel targeted therapeutic intervention. As mentioned in Chapter 1, RhoA and ROCK are indispensable regulators to fundamental steps in cell migration and cancer metastasis. Rho-kinase (ROCK) is the best known downstream effector of RhoA (52, 53). Binding of RhoA releases ROCK from its autoinhibitory structure and activates ROCK-mediated cellular events (52, 97, 107, 108). ROCK is known to regulate cellular events related to cell motility. For example, ROCK was shown to control cell polarity by regulating PTEN/Akt signaling pathway in neutrophils (35) and control tail retraction in monocytes and prostate cancer cells (109-111). ROCK also enhances actomyosin contractility, a

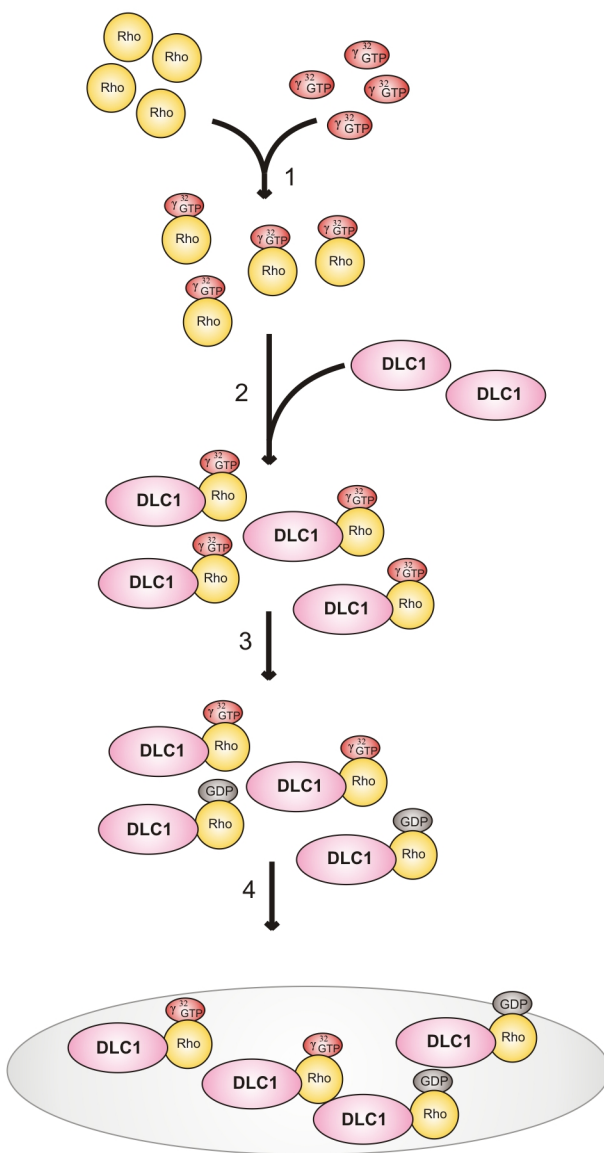
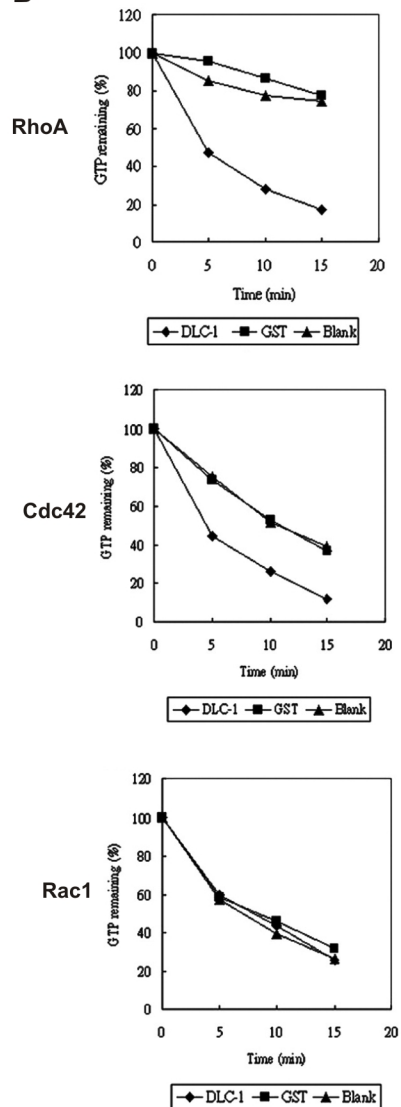


principal step of cell migration as described above (112). Importantly, ROCK is a kinase that phosphorylates and activates many downstream substrates such as LIMK and myosin light chain 2 (MLC2). Phosphorylation of these substrates is important in regulating cytoskeletal reorganization and cell migration (113, 114). Hyperactivation of the Rho/ROCK pathway is known to be associated with more aggressive tumor properties such as metastasis and invasion (46-49, 115-117). Deregulation of Rho/ROCK pathway may be consequentially related to its aberrant upstream regulatory pathway. We aimed to delineate their upstream regulators in order to have a better understanding on its signal transduction pathway.

3.1.1 DLC1 is a RhoGAP protein that Downregulates RhoA in HCC

Deleted in Liver Cancer 1 (DLC1) is a member of the RhoGTPase activating protein (RhoGAP) family and possesses RhoGAP activity specific for RhoA (76). By *in vitro* RhoGAP assay, we previously demonstrated that DLC1 negatively regulated the activity of RhoA by enhancing intrinsic GTP hydrolytic activity of RhoA, thus catalyzing the conversion of RhoA from its GTP-bound active state to GDP-bound inactive state (Figure 3.1). *In vitro* RhoGAP assay assessed the intrinsic RhoGTPases activity of Rho family members by pre-mixing the purified GST fusion RhoGTPases and radiolabelled GTP, and later loaded with purified GST fusion DLC1. Measurement of the remaining GTP at different time point represents the GTP hydrolytic rate (Figure 3.1A). Purified DLC1 was able to enhance the GTP hydrolytic ability of RhoA drastically and Cdc42 mildly, but with no effect on Rac1 (Figure 3.1B) (76). This result was also confirmed by other groups showing that DLC1 has the most specific RhoGAP effect on RhoA as compared



A**B**

(Wong CM et al. Cancer Research, 2003)

Figure 3.1 DLC1 possessed RhoGAP activity specific for RhoA

(A) *In vitro* RhoGAP assay. 1. GST Rho GTPases fusion proteins including GST RhoA, GST Cdc42, and GST RhoA were incubated with [γ^{32} P] labelled GTP. 2. GST DLC1 fusion proteins were added and the reactions were incubated. 3. DLC1 accelerated the intrinsic GTP hydrolysis of Rho GTPases. 4. The amount of radioactive GTP bound RhoGTPases was determined by the remaining radioactivity measured by scintillation counting. (B) Scintillation counting result showing GTP hydrolysis rate of RhoA, Rac1, or Cdc42 in the presence and absence of DLC1. GST DLC1 drastically reduced the remaining radioactive GTP bound to RhoA as compared to GST control. GST DLC1 mildly reduced the remaining radioactive GTP bound to Cdc42 as compared to GST control. GST DLC1 did not affect the GTP hydrolysis activity of Rac1.



to Cdc42 by *in vitro* RhoGAP assay (118). DLC1 was shown to possess RhoGAP activity towards RhoA in *in vivo* RhoGAP assay in non-small cell lung cancer model (118). *In vivo* RhoGAP assay involved a GST fusion of rhotekin, an effector of RhoA which only bound to activated RhoA. GST fusion rhotekin was purified and was used in pull down assay to detect the amount of activated RhoA in cell lysates by Western blot analysis.

3.1.2 Implications of DLC1 in HCC and Cancers

DLC1, a tumor suppressor gene, was first identified in primary HCC as a rat p122RhoGAP homolog (119). In HCC, DLC1 has been found to possess tumor suppressive abilities (77, 120, 121). Overexpression of DLC1 in HCC cell line suppressed subcutaneous tumor formation in nude mice (77). On the other hand, knockdown of DLC1, cooperated with myc, enhanced HCC formation and accelerated the HCC onset in mice (120).

DLC1 was underexpressed mainly through gene deletion and DNA methylation (75, 76, 122). From allelic loss of heterozygosity (LOH) study, our laboratory showed that DLC1 was frequently deleted in 44.1% to 50% of the HCC human samples tested (76). From methylation specific PCR (MS-PCR) study, our laboratory demonstrated that the promoter of DLC1 was methylated in 24% of the HCC human samples tested (76). Nevertheless, somatic mutation of DLC1 was found to be rare (0%) in HCC (76). Underexpression of DLC1 was also implicated in other cancers such as breast, lung, and prostate (122-127). DLC1 was also shown to be downregulated in metastatic cells compared to non-metastatic cells in breast and HCC models (128, 129). Ectopic expression of DLC1 was found to suppress cell migration and invasion in HCC, non-small cell lung cancer, breast cancer, lung cancer, ovarian cancer cell line models (77, 118, 128, 130-133), and overexpression of DLC1 in metastatic breast



cancer cell line could attenuate size and incidence of pulmonary metastases (128). However, the molecular mechanisms underlying this suppression of cell movement and cancer metastasis remain unclear.

3.1.3 Objectives

Our laboratory has previously demonstrated that DLC1 is a RhoGAP protein and it is therefore logical to speculate that DLC1 suppresses cancer cell metastasis through negatively regulating Rho/ROCK-mediated cytoskeletal rearrangement. However, this hypothesis has never been tested experimentally and the mechanistic basis of how DLC1 suppresses cancer cell metastasis has not been delineated. Hence, it is strategic to examine the possible functional links between DLC1 and Rho/ROCK pathway and their implications in HCC. In this study, we examined whether DLC1 could inhibit ROCK-mediated cytoskeletal events including formation of stress fiber and focal contact network and phosphorylation of MLC2 at cell cortex. Furthermore, whether these inhibitory effects of DLC1 depended on its RhoGAP activity was examined. In addition, we observed the effect of DLC1 and ROCK on the cytoskeleton and cell morphology.



3.2 Materials and Methods

3.2.1 Cell Lines and Plasmids

SMMC-7721 (SMMC), BEL7402, Hep3B, HepG2, WRL, HeLa, COS7, HEK 293T cell lines were employed in this study. Myc-tagged expression constructs (pCAG) carrying human wild-type ROCK, dominant active ROCK (1-725 amino acids), and dominant negative ROCK mutant (K105A, I1009A) were kindly provided by S. Narumiya (Faculty of Medicine, Kyoto University) (97). The human ROCK1 kinase domain (ROCK1 76-338 amino acids) was PCR amplified with forward primer 5' GCG GTA CCC TCG AGC TGG ATG GAT TGG ATG CTT T 3' and reverse primer 5' GCG GTA CCT TAA GCC CAC TGG TCA TTT TTG 3' and PCR product was cloned into pEGFPC3 vector using KpnI and XhoI digestion sites and was used as dominant active form of ROCK.

Full length wild-type DLC1, 3.5-kb of coding sequence, was amplified from normal liver tissue and cloned into pcDNA3.1(-) vector by BamHI and KpnI digestion. Full length DLC1 (1-1,091 amino acids) was subcloned into myc-tagged expression construct (pCS2+MT) by EcoRI single digestion and SalI and XhoI double digestion. DLC1 Δ SAM (1-292 amino acids) was then subcloned into myc-tagged expression constructs (pCS2+MT) by EcoRI digestion. DLC1 K714E construct was generated by PCR mutagenesis. A DLC1 fragment (1-804 amino acids) from pcDNA3.1(-) DLC1 plasmid was digested with EcoRI and a fragment (1-804 amino acids) was released and subcloned into pBluescript II SK(+) vector (pSK(+) vector). The site-specific mutation of DLC1 at K714E was then generated by PCR mutagenesis with three PCR amplifications. The first round of PCR reaction employed forward primer 5' GGA TGG ATG AGG AGA AGC



TG 3' and reverse primer 5' GAT CTC GAA AAT ACT GCT CCA 3' to generate the first PCR product from the DLC1 template (1-804 amino acids) and the forward primer 5' TGC TGG AGC AGT ATT TTC GAG 3' and reverse primer 5' TAA TAC GAC TCA CTA TAG GG 3' to generate the second PCR product from the DLC1 template (1-804 amino acids). Then, the first and second PCR products were used as template for the next round of PCR amplification with forward primer 5' GGA TGG ATG AGG AGA AGC TG 3' and reverse primer 5' TAA TAC GAC TCA CTA TAG GG 3'. This PCR product was then ligated back into pSK (+) DLC1 construct by NcoI and BamHI digestion and further replaced the wild-type fragment (1-804 amino acids) of the pCS2+MT DLC1 plasmid by EcoRI.

3.2.2 Drug Treatment and Transfection

ROCK-specific inhibitor Y27632 was obtained from Calbiochem (Darmstadt, Germany). For treatment in immunofluorescence study, cells were added Y27632 at 10 µM and incubated for 1 hour at 37°C. For treatment in the cell migration assay, cells were first pretreated with 10 µM Y27632 for 1 hour and fresh 10 µM Y27632 was added to top chamber. For transfection, 1×10^5 cells were seeded on coverslips in 35-mm plates one day before transfection. Indicated plasmids were transfected into cells with FuGene 6 reagent (Roche) according to manufacturer's instructions.

3.2.3 Immunofluorescence Microscopy

Mouse monoclonal antibody against phospho-myosin light chain 2 (Ser 19) was purchased from Cell Signaling Technology (Danvers, MA, USA). Mouse monoclonal



antibody against paxillin was obtained from Upstate (Lake Placid, NY, USA). Mouse monoclonal (9E10) and rabbit polyclonal (A14) antibodies against c-myc were obtained from Santa Cruz Biotechnology (Santa Cruz, CA, USA). Texas Red dye-conjugated AffiniPure goat anti-mouse IgG and fluorescein (FITC)-conjugated AffiniPure goat anti-rabbit IgG were purchased from Jackson Immuno Research Laboratories (West Grove, PA, USA). For immunofluorescence staining, cells were fixed in 4% paraformaldehyde, permeabilized with 0.2% TritonX, blocked with 3% bovine serum albumin and then incubated with indicated primary and secondary antibodies. Focal adhesions were probed with anti-paxillin antibody and stress fibers were stained with phalloidin TRITC (Sigma). Nuclear counterstaining was done with 4'-6-Diamidino-2-phenylindole (DAPI) (Calbiochem) and coverslips were mounted in 15 µL Vectashield antifade mountant (Vector Laboratories, Burlingame, CA, USA). Cells were counted under Leica Q550CW fluorescence microscope (x 100 magnification) and images were captured with a charge-coupled device camera connected to the microscope.

3.2.4 Cell Migration Assay

Transwell assay was performed with Transwell Boyden chamber as described in Chapter 2. 5×10^4 cells resuspended in serum free culture medium were added to the upper chamber whilst culture medium with 10% FBS was placed in the lower chamber as chemoattractant. Cells were incubated in CO₂ incubator at 37°C and were allowed to migrate for 16 hours. Cells having migrated were fixed and stained and counted as previously mentioned in Chapter 2. Photographs of 3 different fields of the stained cells



were captured and cells were counted. Experiment was repeated independently three times.

3.2.5 Cell Proliferation Assay

2×10^4 cells were seeded in 12 well plates. Cells were counted everyday with COULTER COUNTER® Cell and Particle Counter (Beckman Coulter) in triplicates and a 6-day growth curve was plotted. Cells were replenished with fresh medium (mock or Y27632) every other day.

3.2.6 mRNA Extraction, Protein Extraction, Western Blots

Total RNA was extracted and cDNA was synthesized as described in Chapter 2, and the expression of DLC1 mRNA was detected by RT-PCR with primers amplifying region 192–649 bp. The sequence of the forward primer is 5' AGC AAG GAT GCG TTG AGG 3' and the sequence of the reverse primer is 5' CAC CTC TTG CTG TCC CTT TG 3'. GAPDH was used as endogenous control gene and the expression of its mRNA was detected by RT-PCR with forward primer 5' ACG CAT TTG GTC GTA TTG GG 3' and reverse primer 5' TGA TTT TGG AGG GAT CTC GC 3'. For Western blot, cells were lysed with SDS buffer or NP40 in NET buffer. Proteins were resolved by SDS-PAGE and blotted onto a nitrocellulose membrane. The membrane was probed using anti-DLC1 antibody (BD Biosciences Pharmingen), anti-MYPT antibody or anti-phospho-MYPT (Thr 853) antibody (Upstate), followed by incubation with anti-mouse IgG or anti-rabbit IgG (GE Healthcare). Protein expression was detected and images were scanned and intensity of bands was quantified as described in Chapter 2.



3.3 Results

3.3.1 DLC1 Abolished Formation of ROCK-mediated Stress Fibers and Focal Adhesion Network

First, we queried if the formation of stress fibers and focal adhesions in HCC cells was ROCK-dependent. We found that, the stress fiber bundling arrays (stained with phalloidin stain) and focal adhesions (paxillin), particularly those in the central region that were linked to stress fibers, were abolished upon ROCK inhibitor treatment (Figure 3.2). This finding indicated that the formation of the stress fibers and focal adhesions in HCC cells is ROCK-dependent.

To investigate the regulatory function of DLC1 on ROCK-mediated stress fiber and focal adhesion formation in HCC, we transiently overexpressed DLC1 in DLC1-deficient SMMC-7721 and BEL7402 HCC cells and observed its effects on the network of stress fibers and focal adhesions. Overexpression of wild-type DLC1 significantly suppressed formation of stress fibers and focal adhesions in these cells, as indicated by phalloidin (Figure 3.3) and paxillin stains (Figure 3.4 and Figure 3.5), respectively. Analogous to ROCK inhibition, DLC1 abolished mainly the stress fiber-linked focal adhesions located in the central region of cells (Figure 3.6A). The loss of focal adhesions was further aggravated with ectopic expression of SAM domain-deleted mutant of DLC1 (Δ SAM) (Figure 3.6B), a DLC1 truncated construct that caused a more severe cell shrinkage and loss of stress fibers (77). In contrast, a RhoGAP-deficient mutant (DLC1 K714E) was unable to inhibit formation of both stress fibers and focal adhesions (Figures 3.3, 3.4 and



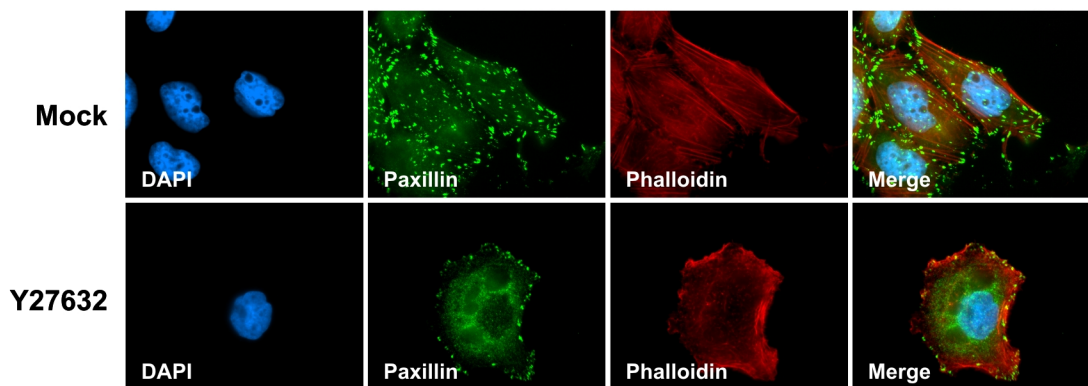
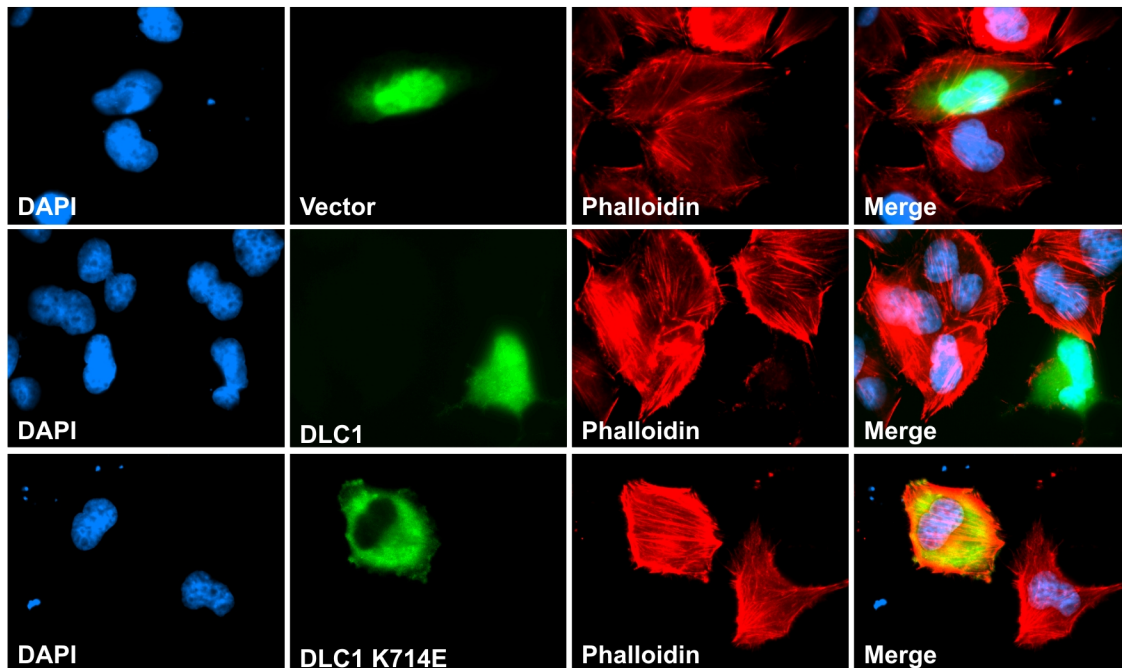


Figure 3.2 ROCK inhibitor suppressed formation of stress fiber and focal adhesion formation

ROCK inhibitor, Y27632, suppressed stress fiber and focal adhesion formation in HCC cells, SMMC-7721. Cells were seeded onto cover-slip one day before drug treatment. Stress fibers were stained with phalloidin stain (red) and focal adhesions with paxillin stain (green). Stress fibers could be clearly observed as bundles stretching across the cells and focal adhesions were attached to the stress fiber bundling arrays mock treated control. Treatment with ROCK inhibitor Y27632 at 10 μ M for 1 hour suppressed formation of stress fiber and focal adhesion network in SMMC-7721.



Stress Fibers

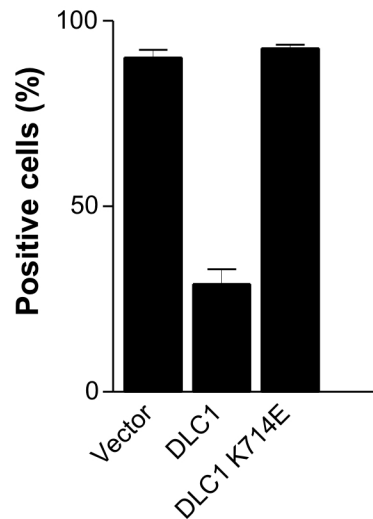
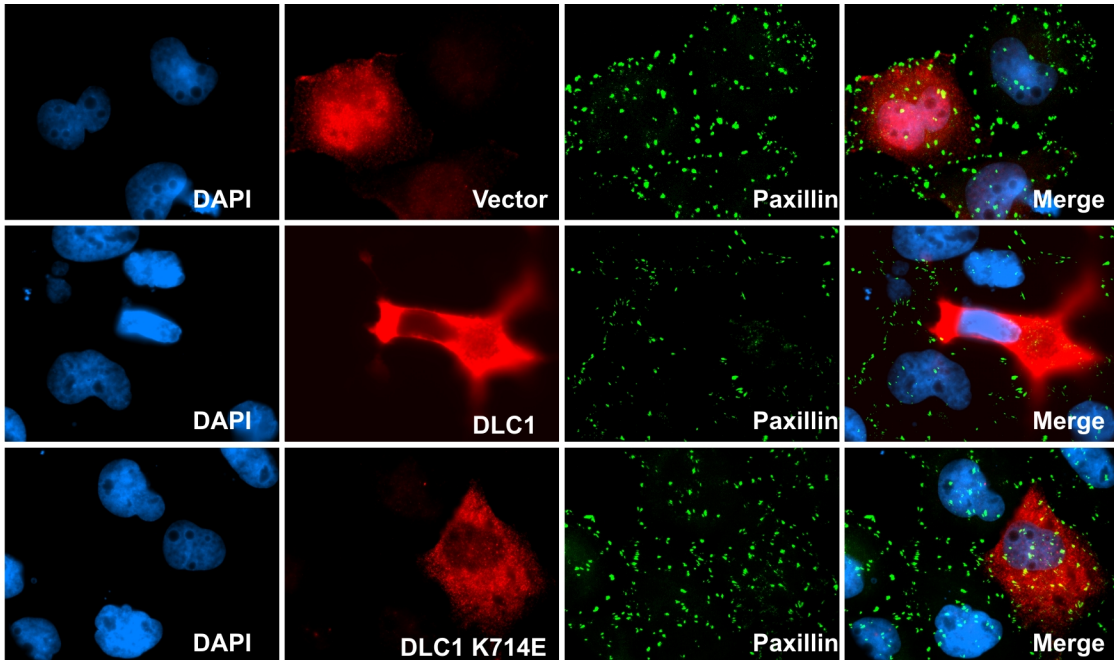


Figure 3.3 DLC1 suppressed ROCK-mediated stress fiber formation in HCC cells
 SMMC-7721 cells were transfected with myc-tagged expression plasmids, pCS2+MT, pCS2+MT/DLC1, pCS2+MT/DLC1 K714E, and recognized by anti-myc antibodies (9E10) (green). Stress fibers were stained with phalloidin (red). Wild-type DLC1, but not RhoGAP-deficient mutant (K714E), suppressed stress fiber formation in SMMC cells. Percentage of different DLC1 constructs transfected cells exhibiting stress fibers were presented in a bar graph. For each construct, total ~100 transfected cells were counted under microscope. Error bars represent standard deviation (SD) of data obtained from two independent experiments.



Focal Adhesions (SMMC)

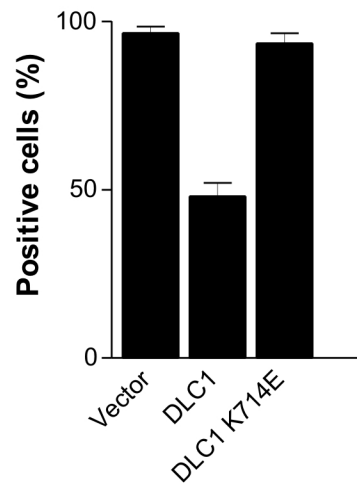
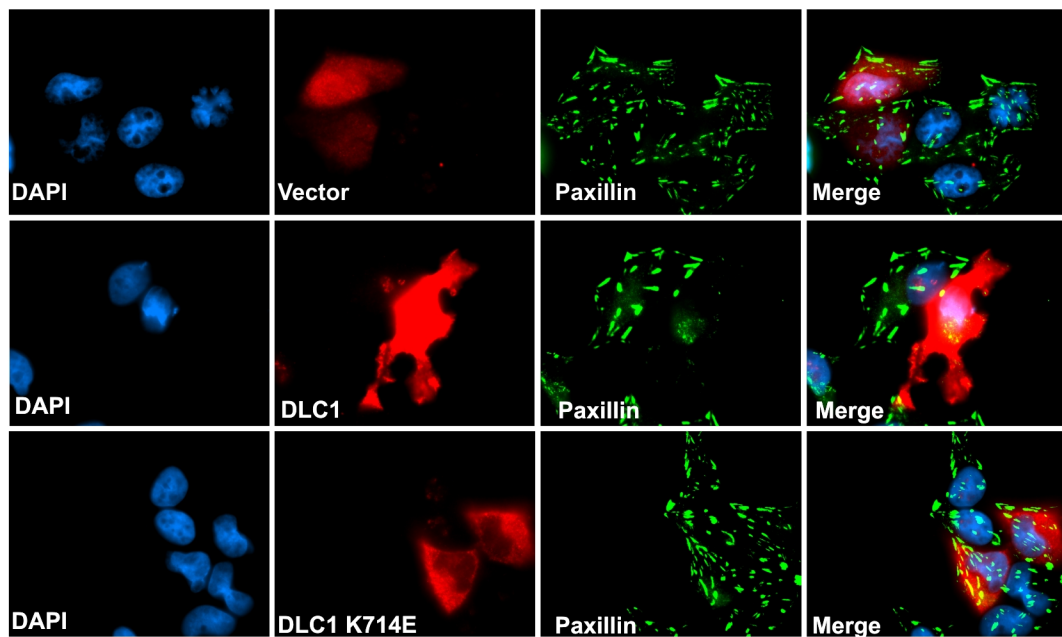


Figure 3.4 DLC1 suppressed ROCK-mediated focal adhesion formation in HCC cells (SMMC-7721)

SMMC-7721 cells were transfected with myc-tagged expression plasmids, pCS2+MT, pCS2+MT/DLC1, pCS2+MT/DLC1 K714E, and recognized by anti-myc antibodies (9E10) (red). Focal adhesions were stained with anti-paxillin antibody (green). Wild-type DLC1, but not RhoGAP-deficient mutant (K714E), reduced number of stress fiber-linked focal adhesions formed in SMMC-7721 cells. Percentage of different DLC1 constructs transfected cells exhibiting focal adhesions were presented in a bar graph. For each construct, total ~100 transfected cells were counted under microscope. Error bars represent standard deviation (SD) of data obtained from two independent experiments.



Focal Adhesions (BEL7402)

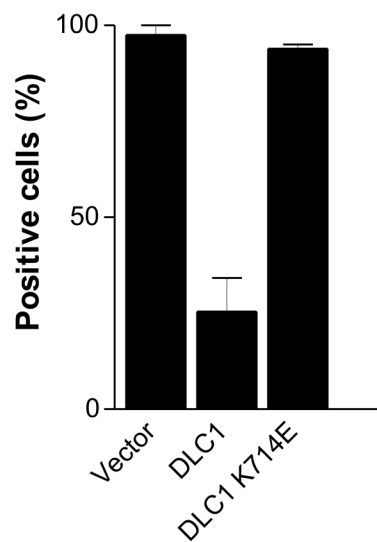


Figure 3.5 DLC1 suppressed ROCK-mediated focal adhesion formation in HCC cells (BEL7402)

BEL7402 cells were transfected with myc-tagged expression plasmids, pCS2+MT, pCS2+MT/DLC1, pCS2+MT/DLC1 K714E, and recognized by anti-myc antibodies (9E10) (red). Focal adhesions were stained with anti-paxillin antibody (green). Wild-type DLC1, but not RhoGAP-deficient mutant (K714E), reduced number of stress fiber-linked focal adhesions formed in SMMC-7721 cells. Percentage of different DLC1 constructs transfected cells exhibit focal adhesions were presented in a bar graph. For each construct, total 67-100 transfected cells were counted under microscope. Error bars represent standard deviation (SD) of data obtained from two independent experiments.

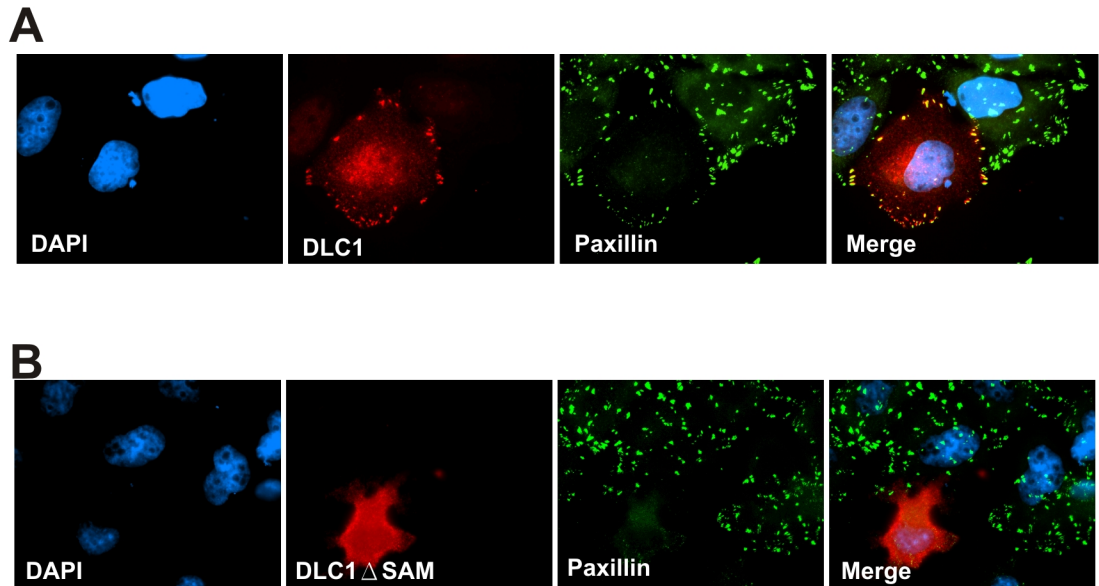


Figure 3.6 DLC1 and focal adhesions

(A) DLC1 localized to focal adhesions. SMMC cells transfected with pCS2+MT DLC1 (red) displayed a reduction of focal adhesions but the remaining focal adhesion molecules as represented by the paxillin stain (green) colocalized with DLC1 (red). (B) DLC1 Δ SAM induced a severe cell shrinkage and loss of focal adhesions. SMMC cells transfected with DLC1 Δ SAM displayed an intensive shrinkage and a loss of focal adhesions. Loss of focal adhesions is believed to be associated to cell shrinkage because cells with more severe cell shrinkage displayed more severe loss of focal adhesions.

3.5). These findings demonstrated that DLC1 inhibited ROCK-dependent stress fiber and focal adhesion formation via its RhoGAP activity.

3.3.2 DLC1 Abolished ROCK-mediated Cortical Myosin Light

Chain 2 Phosphorylation

Active ROCK specifically phosphorylates myosin light chain 2 (MLC2) at Ser 19; therefore, this ROCK-specific phosphorylation has been widely used as a surrogate marker of ROCK activity (79, 115, 134-136). Phosphorylation of MLC2 at Ser19 is important for the activity of myosin which is responsible for actomyosin contractility and hence cell migration (63). In this study, we observed that phospho-MLC2 staining of BEL7402 HCC cells was especially prominent at the cell cortex. However, when ROCK activity was blocked either by Y27632 (Figure 3.7) or ectopic expression of a dominant-negative ROCK mutant (Figure 3.8), this peripheral phosphorylation of MLC2 was completely abolished and the phosphorylation of MLC2 became a predominantly cytoplasmic pattern. In contrast, ectopic expression of dominant-active ROCK culminated in a substantial increase of MLC2 phosphorylation at actin bundles (Figure 3.8). These findings indicated that this distinctive phosphorylation pattern of MLC2 at cell cortex was tightly and positively regulated by ROCK activity.

We next investigated whether DLC1 could abolish this ROCK-specific MLC2 phosphorylation pattern in HCC cells. We first evaluated whether the cortical phospho-MLC2 staining pattern was related to the endogenous expression levels of DLC1 in different cell lines. We observed conspicuous phospho-MLC2 staining at the cell cortex



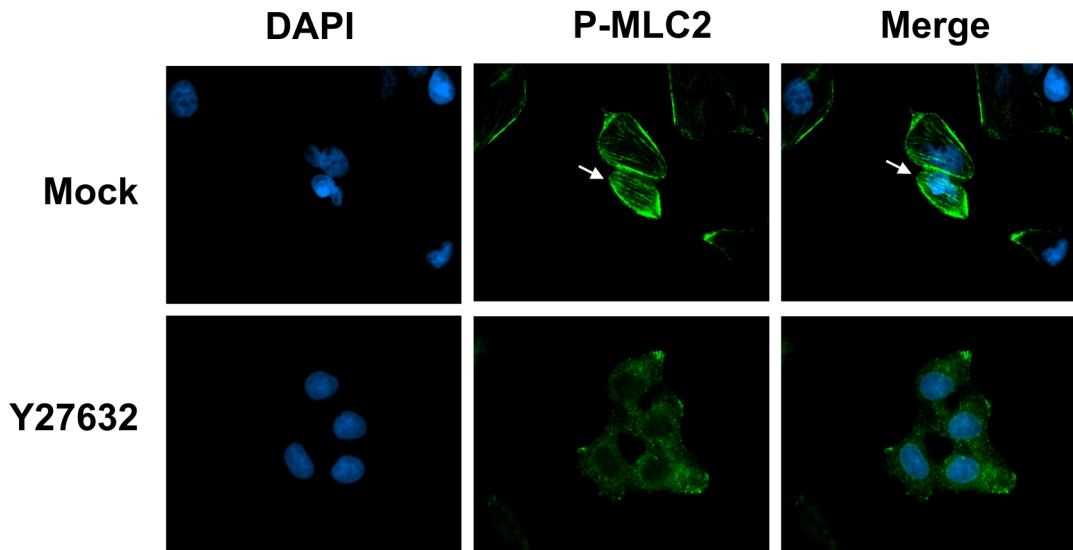


Figure 3.7 ROCK inhibitor suppressed cortical phosphorylation of MLC2.

BEL7402 HCC cells treated with mock control or ROCK inhibitor Y27632 were stained with mouse monoclonal antibody against phospho-MLC2 (Ser 19). Phospho-MLC2 (green) was mainly detected at the cell cortex of BEL7402 cells (arrow) and this cortical staining pattern was abolished upon ROCK inhibitor Y27632 treatment for 1 hour.

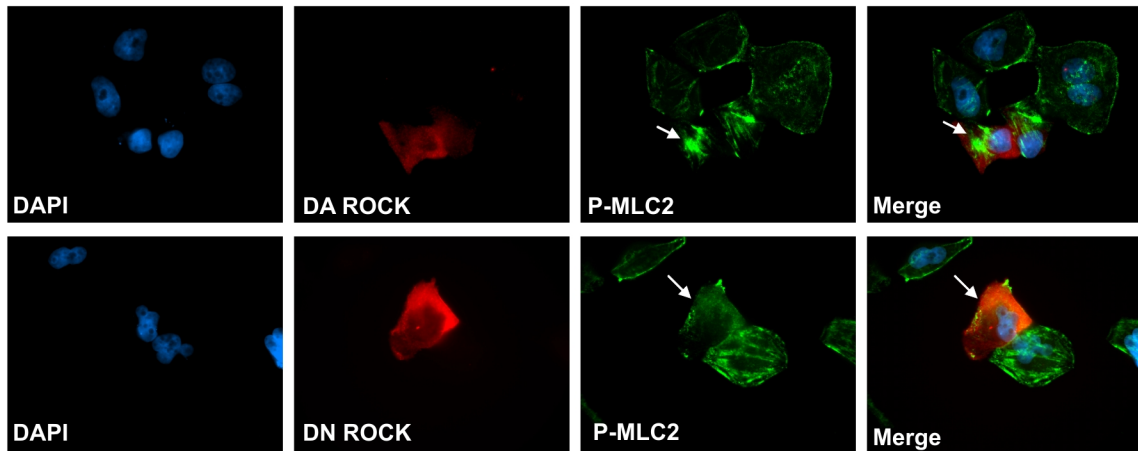


Figure 3.8 ROCK mediated cortical phosphorylation of MLC2

BEL7402 cells were transfected with myc-tagged (pcAG) dominant negative ROCK or dominant active ROCK constructs and detected with rabbit polyclonal antibody against myc-epitope (A14) (red). Dominant active (DA) ROCK caused intense phosphorylation of MLC2 (Ser 19) at the actin bundles (Percentage of cells exhibiting this phenomenon: 94.0% of the DA ROCK-transfected cells compared to 0% of the vector transfected cells. Arrow marks the actin bundles of the DA ROCK transfected cell where phosphorylation of MLC2 (Ser 19) was enhanced. Dominant negative (DN) ROCK suppressed cortical phosphorylation of MLC2 (Ser 19) (Percentage of cells exhibiting this phenomenon: 87.5% of the DN ROCK-transfected cells compared to 7.3% of the vector transfected cells). Arrow points at the cell cortex of the DN ROCK cell where phosphorylation of MLC2 (Ser 19) was lost. As shown, a tight regulation and an optimal level of ROCK activity were required to maintain cortical phosphorylation of MLC2 (Ser 19) in BEL7402 cells.

in SMMC-7721, BEL7402, and WRL HCC cell lines, and HeLa cervical cancer cell line, all of which had no expression of DLC1 (Figure 3.9, 3.10). On the other hand, HepG2 and Hep3B, the two HCC cell lines with DLC1 expression (Figure 3.9), displayed diffuse cytoplasmic phospho-MLC2 staining without any distinct cortical phosphorylation of MLC2 at cell periphery (Figure 3.10).

To verify that inhibition of cortical phospho-MLC2 was directly related to DLC1, we transiently expressed wild-type DLC1 and DLC1 RhoGAP-deficient mutant (K714E), respectively, in DLC1-null BEL7402 cells. Wild-type DLC1 substantially reduced the number of cells having phospho-MLC2 cortical staining (Figures 3.11), signifying the suppressive role of DLC1 on ROCK activity. On the other hand, DLC1 RhoGAP-deficient mutant (K714E) was unable to abolish phospho-MLC2 cortical staining (Figures 3.11). Our observation therefore suggested DLC1 inhibited ROCK-specific MLC2 phosphorylation in HCC cells, via its RhoGAP activity.

3.3.3 DLC1 Attenuated Myosin Phosphatase Activity by Reducing Phosphorylation of Myosin Phosphatase Target Subunit 1

Apart from phosphorylation of myosin, ROCK also increases myosin phosphorylation by phosphorylating myosin phosphatase target subunit 1 (MYPT1) at Thr 696 and Thr 853 and thereby inactivating it. Although Thr 696 of MYPT1 can be phosphorylated by other protein kinases, Thr 853 phosphorylation, on the other hand, is selectively regulated by ROCK (112). Moreover, MYPT1 Thr 853 phosphorylation has been shown to be a promising surrogate marker that reversely correlates with myosin phosphatase activity



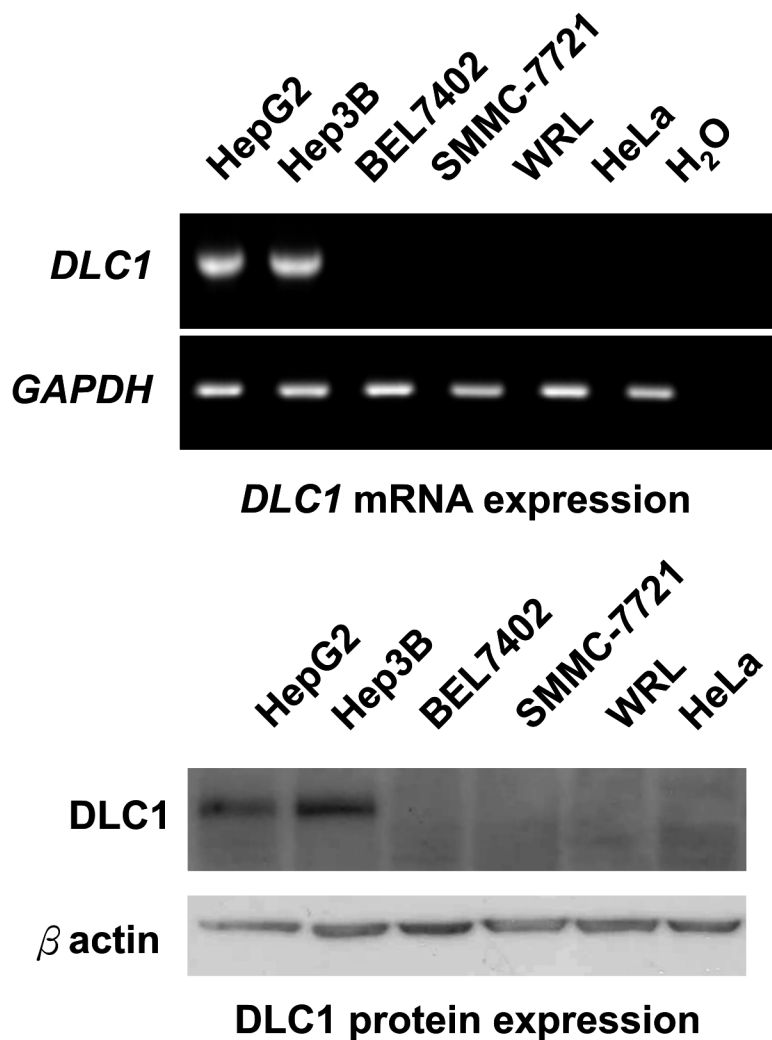
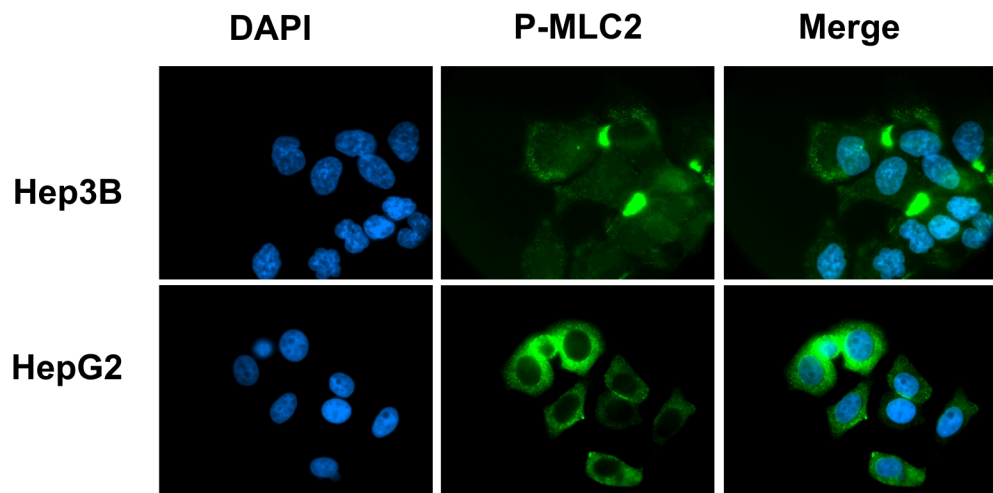


Figure 3.9 DLC1 expression in cell lines

DLC1 mRNA and protein expression in cell lines. DLC1 is expressed in HepG2, Hep3B, but not in BEL7402, SMMC-7721, WRL, and a cervical cancer cell line HeLa.

DLC1 Positive Cell Lines



DLC1 Negative Cell Lines

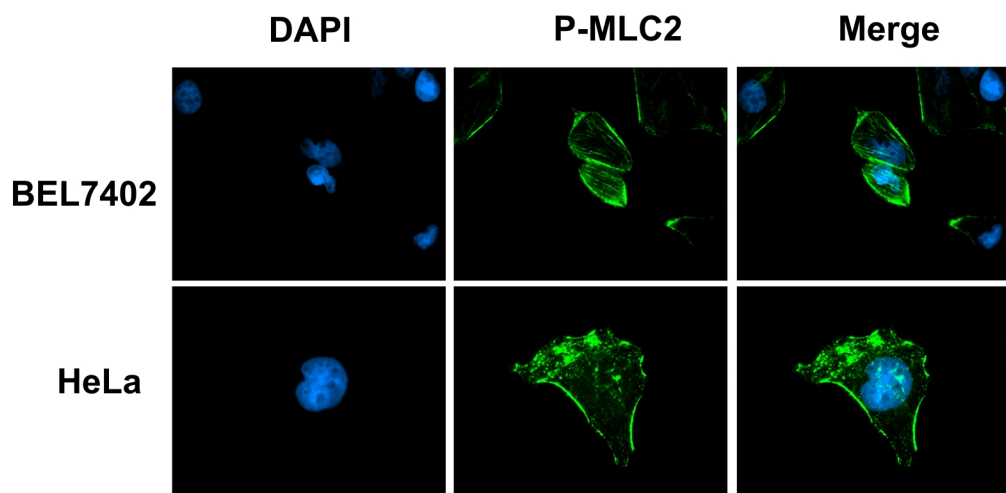


Figure 3.10 DLC1 expression was associated with phospho-MLC2 staining pattern
Representative pictures from DLC1-positive and DLC1-negative cells, respectively. DLC1-positive cells Hep3B and HepG2, displayed diffuse phosphorylation of MLC2, whereas DLC1-negative (non-expressing) BEL7402 and HeLa, displayed pronounced cortical phosphorylation of MLC2 at cell cortex.

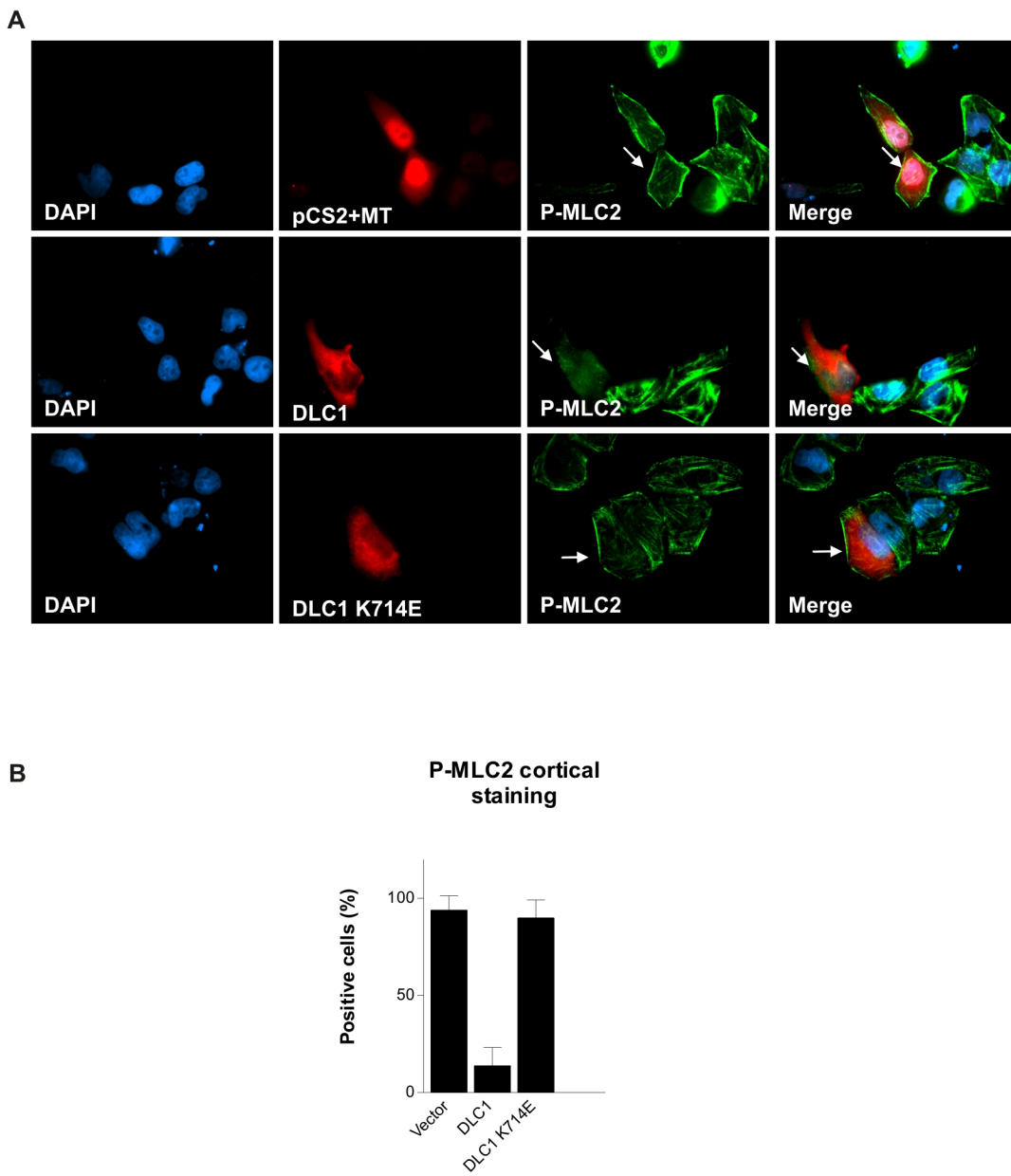


Figure 3.11 DLC1 RhoGAP was responsible for regulating cortical phosphorylation of MLC2

(A) pCS2+MT vector alone, pCS2+MT DLC1, pCS2+MT DLC1 K714E, respectively, were transfected into BEL7402 cells. Recognition of transfected cells was done by probing cells with c-myc (A14) rabbit antibody followed by staining with anti-rabbit antibody conjugated with Texas Red. Cells transfected with pCS2+MT vector alone displayed pronounced cortical phosphorylation of MLC2 as indicated by the arrows. Cells transfected with DLC1 displayed loss of cortical phosphorylation of MLC2. Cells transfected with DLC1 K714E , the RhoGAP-deficient mutant, still displayed pronounced cortical phosphorylation of MLC2 as indicated by the arrows. (B) Percentage of different DLC1 constructs exhibiting cortical phosphorylation of MLC2 at Ser 19 was calculated and presented in a bar graph. For each column, 80-100 transfected cells were counted and cortical MLC2 phosphorylation was recorded. Error bars represent standard deviation (SD) of data obtained from three independent experiments.

(79, 115, 134-136). In this study, we found that upon Y27632 treatment, the phosphorylation levels of MYPT1 (Thr 853) were reduced in all HCC cell lines tested (Figure 3.12), while the total MYPT1 levels remained unchanged. Similarly, overexpression of DLC1 attenuated phosphorylation of MYPT1 at Thr 853, indicating the loss of ROCK activity (Figure 3.13). Inactivation of myosin phosphatase (as reflected by increased MYPT1 phosphorylation) and activation of MLC2 are combined effects of ROCK, and these effects could be suppressed by DLC1, leading to a total decrease of myosin phosphorylation and a reduction of cell contractility.

3.3.4 ROCK Inhibitor Suppressed HCC Cell Motility

By ectopic expression of DLC1 in HCC cell line, we previously showed that DLC1 significantly repressed HCC cell migration and invasiveness (77). To substantiate our hypothesis that DLC1 suppressed cell migration via negatively regulating ROCK activity, we examined the effect of ROCK inhibitor on HCC cell migration with transwell assay. We observed that the ROCK inhibitor Y27632 suppressed migration of HCC cells, SMMC-7721 (Figure 3.14, left panels) and BEL7402 (Figure 3.14 left panels), as demonstrated by the decreased number of migrated cells in transwell assay. This finding indicated that ROCK activity was crucial for HCC cell migration. To eliminate any misinterpretation due to cell death caused by toxicity of the drug, we performed cell proliferation assay on the HCC cells. Cell proliferation assay demonstrated that Y27632 did not affect cell growth which confirmed that inhibition of ROCK only affected HCC cell migration (Figure 3.14, right panels).



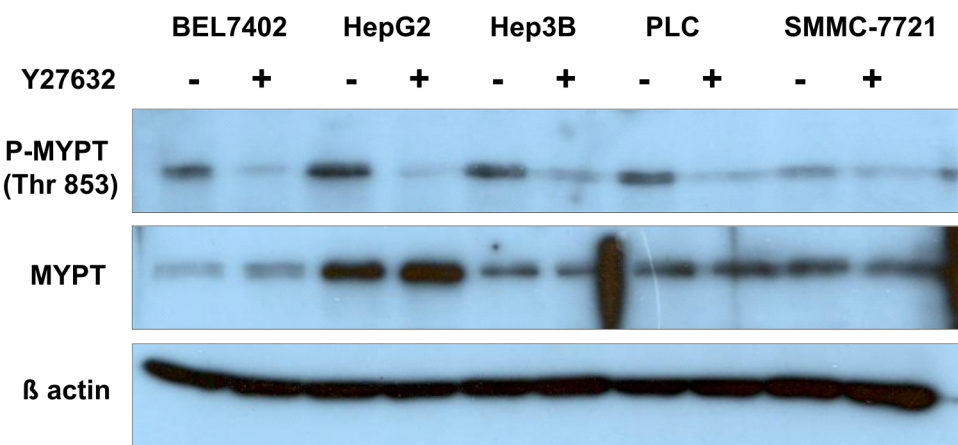


Figure 3.12 ROCK inhibitor suppressed MYPT phosphorylation

ROCK inhibitor Y27632 suppressed MYPT phosphorylation at Thr 853 in all HCC cell lines tested. Cells were treated with Y27632 for 1 hour.

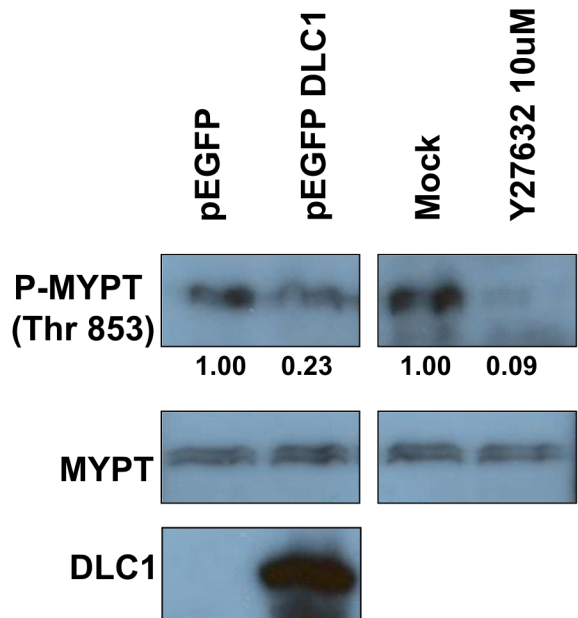


Figure 3.13 DLC1 and ROCK regulated MYPT phosphorylation

DLC1 suppressed MYPT phosphorylation at Thr 853 in 293T cells. Band intensity was analyzed by AlphaEaseFC™ and percentage was calculated from comparison with its according control (Total MYPT). ROCK inhibitor Y27632 suppressed MYPT phosphorylation after 1 hour treatment.

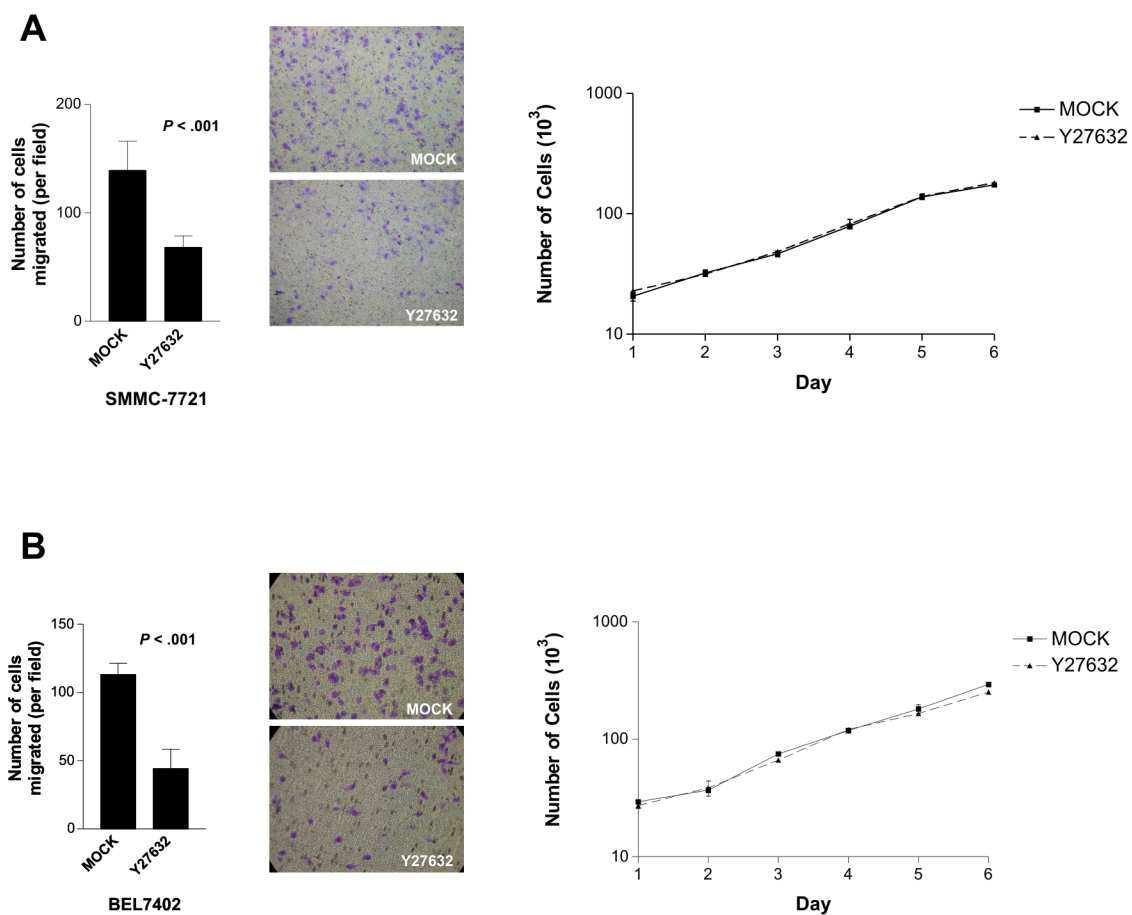


Figure 3.14 ROCK inhibitor suppressed HCC cell migration

ROCK inhibitor Y27632 suppressed HCC cell migration. Y27632 decreased number of migrated (A) SMMC-7721 cells ($P < .001$, *t*-test) and (B) BEL7402 cells ($P < .001$, *t*-test). Error bars represent standard deviation (SD) of data obtained from three microscopic fields. Experiments have been repeated three times. Cell Proliferation assay was shown on the right to compare growth rate of the mock control cells and Y27632 treated cells.

3.3.5 ROCK Reversed the Cell Morphological Alteration of DLC1

We previously demonstrated that DLC1 was able to induce cell morphological change with reduced stress fiber formation in HCC cells and fibroblasts (77). Since ROCK is a chief modulator in cytoskeletal signaling and cytoskeletal organization is a key determinant of cell morphology, we speculated that the cell morphological changes induced by DLC1 were via ROCK. To this end, we observed the cell morphology of DLC1 and ROCK co-transfected cells by immunofluorescence staining. We also counted the number of cells that exhibited cell collapse or shrinkage caused by collapse of cytoskeletal network, as described elsewhere (77, 137-139). In this study, we observed that overexpression of DLC1 in COS7 cells induced cytoskeletal collapse or cell shrinkage (Figure 3.15A-i, 3.16). Similar to our previous finding (77), cell shrinkage was intensified by ectopic expression of SAM domain-deleted mutant of DLC1 (Δ SAM) (Figure 3.15B-i, 3.16). Co-transfection of empty pEGFP vector could not rescue DLC1-induced cell morphological change, but cells with dominant active ROCK could overcome the inhibitory regulation from DLC1 (Figure 3.15A-ii, 3.16) and even DLC1 Δ SAM (Figure 3.15B-ii, 3.16) and released cells from DLC1-induced cell shrinkage. This experiment showed that ROCK was one of the downstream effectors of DLC1 in coordinating the morphological changes in HCC cells.



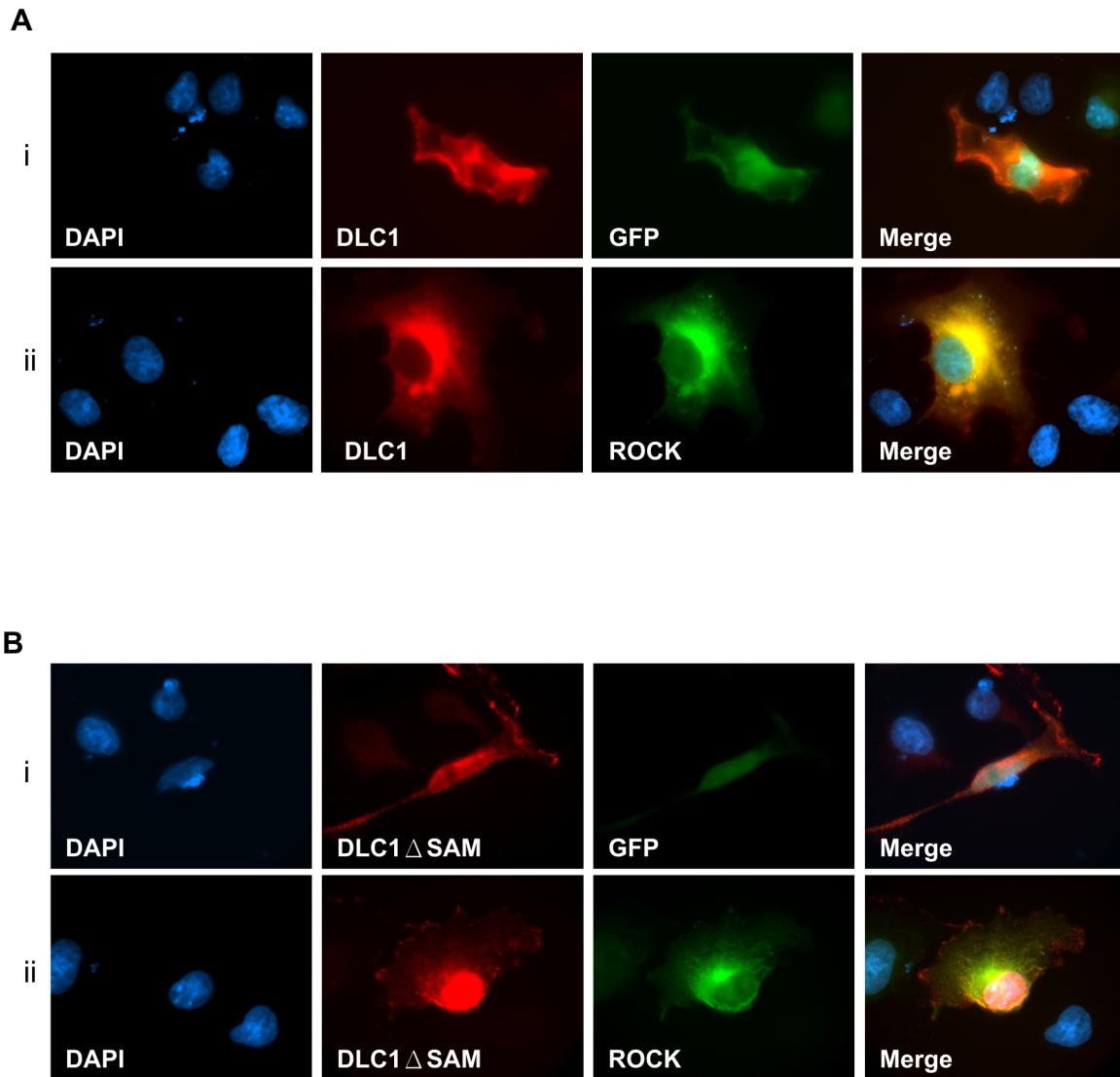
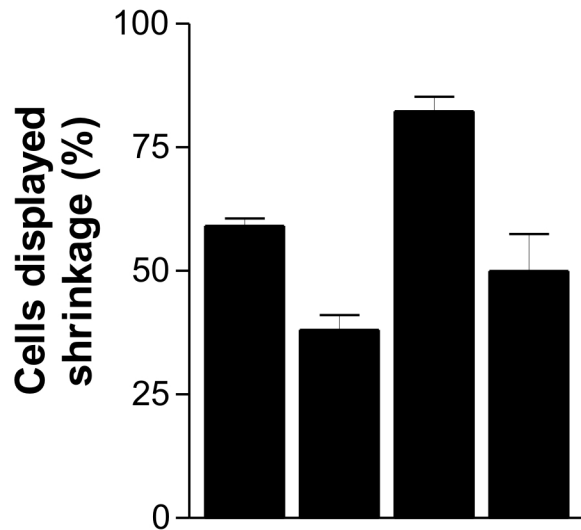


Figure 3.15 ROCK reversed the cell morphological alteration of DLC1

COS7 cells were co-transfected with (A) DLC1 and ROCK or (B) DLC1 SAM and ROCK, respectively. Cells transfected with pCS2+MT DLC1 or pCS2+MT DLC1 Δ SAM appeared red, while cells transfected with pEGFP or pEGFP ROCK appeared green. DLC1-induced cytoskeletal collapse or cell shrinkage (A-i), which was further enhanced and clearly demonstrated by SAM deleted construct, pCS2+MT DLC1 Δ SAM (B-i) ROCK was able to restore cells from DLC1-induced cell shrinkage (A-ii) and even from DLC1 SAM-induced intense cell shrinkage (B-ii).



DLC1	+	+	-	-
DLC1ΔSAM	-	-	+	+
GFP	+	-	+	-
GFP ROCK	-	+	-	+

Figure 3.16 ROCK reversed the cell morphological alteration of DLC1

Co-transfected cells were shown in Figure 3.15 were counted and their morphologies were recorded. The number of co-transfected cells displaying observable cell shrinkage (cell collapse) was divided by total number of co-transfected cells counted, to calculate the percentage of cells in displaying shrinkage as shown in the bar graph. For each column, 150-200 co-transfected cells were counted. Error bars represent standard deviation (SD) of data obtained from three independent experiments.

3.4 Discussion

One of the important roles of DLC1 is its ability in repressing cancer cell migration and invasion. In this study to elucidate the underlying mechanisms in the regulation of HCC cell migration and invasion by DLC1, we have shown that DLC1 suppressed HCC cell migration through regulating the ROCK mediated cytoskeletal rearrangement and actomyosin contraction. Also, we have shown that DLC1 functioned as a negative regulator of ROCK in controlling cell morphology.

3.4.1 DLC1 Negatively Regulated ROCK-mediated Actomyosin

Contractility

The contractile motion of cancer cells is generated by consecutive contractions of actomyosin bundles composed of actin and myosin called actomyosin. These actomyosin bundles, visualized as stress fibers, stretch across the cell body and create a tension to generate cell contraction to drive cell movement by connecting with the focal adhesion molecules (140). Based on the previous study on the inhibitory effect of DLC1 on stress fibers, herein we further found that the formation of stress fibers and focal adhesions network was dependent on DLC1 RhoGAP and ROCK activity in HCC cells. This finding further elucidated that stress fibers and focal adhesions worked hand in hand as described by Hall A. (39), and their formation was interdependent and tightly regulated by RhoGAP of DLC1 and ROCK activity. In addition, DLC1 decreased ROCK-mediated phosphorylation of MYPT1 (Thr 853) and phosphorylation of MLC2 (Ser19) and would consequently lead to a decrease of total myosin phosphorylation and cause a



reduction of stress fiber contractility (63). All these lines of evidence converged to explain that DLC1 controlled one of the pivotal migratory mechanisms, actomyosin contraction, similar to another member of the RhoGAP family, p190-RhoGAP (141).

3.4.2 DLC1 Abolished Focal Adhesion Formation but Localized to Focal Adhesion Complex

An intriguing issue of this finding about the inhibitory effect of RhoGAP on focal adhesion molecules has arisen. DLC1 and several members of the RhoGAP proteins including p122-RhoGAP and RC-GAP72 were found to be localized at the focal adhesions (137, 139). In fact, others and we have previously reported that DLC1 also localized to focal adhesions and interacted with members of the tensin family (131, 142, 143). In this study, we found that DLC1 suppressed stress fiber-linked focal adhesion formation by its RhoGAP activity. From immunofluorescence study, we observed that, in a portion of DLC1 transfected cells, DLC1 exhibited a focal adhesion localization pattern (Figure 3.6); whereas in some other DLC1 transfected cells, especially those displaying extensive cell shrinkage, an intensive loss of stress fiber-linked focal adhesions was observed (Fig 3.4, 3.5). DLC1 localization to focal adhesions and its inhibitory effect on focal adhesions are not mutually exclusive. We speculate that dosage effect might be one of the factors involved. When cells were transfected with a high dose of DLC1, DLC1 would extinguish all the stress fibers and the stress fiber-linked focal adhesions and result in extensive cell collapse (Fig 3.4, 3.5). On the other hand, when cells were transfected with a lower dose of DLC1, DLC1 would extinguish most of the stress fibers and stress fiber-linked focal adhesions but spare some focal adhesions not linked to stress fibers and



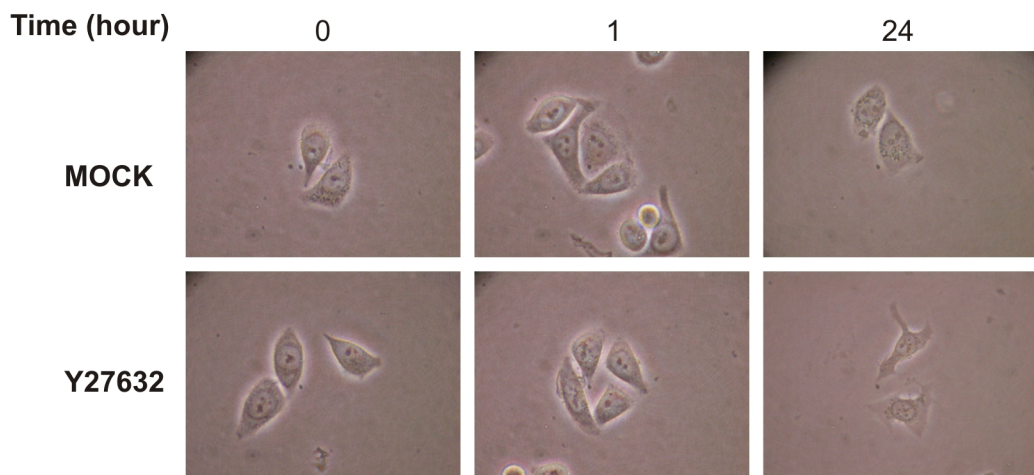
result in a milder cell collapse (Figure 3.6). Another speculation was that similar to RC-GAP72 (137), DLC1 might localize to focal adhesion to disintegrate the focal adhesion complexes.

3.4.3 Cytoskeletal Collapse Induced Cell Shrinkage and the Impact of DLC1 on Cytoskeletal Collapse

Focal adhesions and actomyosin stress fibers always work in inter-dependent manner and they together construct a scaffold to support an intact morphology of the cell (137). The disruptions of the abovementioned network caused by DLC1 led to an intensive cell cytoskeletal collapse resulting in cell shrinkage. This finding was similar to Barberis D *et al.*'s study on p190RhoGAP that loss of focal adhesions induced by p190RhoGAP preceded cell shrinkage (138). We observed that loss of focal adhesions and stress fibers took place an hour after ROCK inhibition by Y27632, but cells did not collapse immediately (Figure 3.17) until prolonged treatment of Y27632 up to 24 hours (Figure 3.17). From this observation, we conjecture that cell collapse caused by Y27632 treatment was ensued from loss of focal adhesion and stress fiber network. Upon inhibition of ROCK by Y27632, the cytoskeletal networks could not be formed and the cells could no longer endure the loss of cytoskeletal network and eventually undergo cell collapse, which we observed as cell shrinkage (Figure 3.18). The present study showed that the cytoskeletal collapse induced by DLC1, a RhoGAP which its downregulation is associated with HCC progression, could be partially reversed by active ROCK, further implying that DLC1 negatively regulated ROCK in controlling actomyosin contractility, cell morphology, and cell migration sequentially. Our previous study reported that DLC1



BEL7402



SMMC

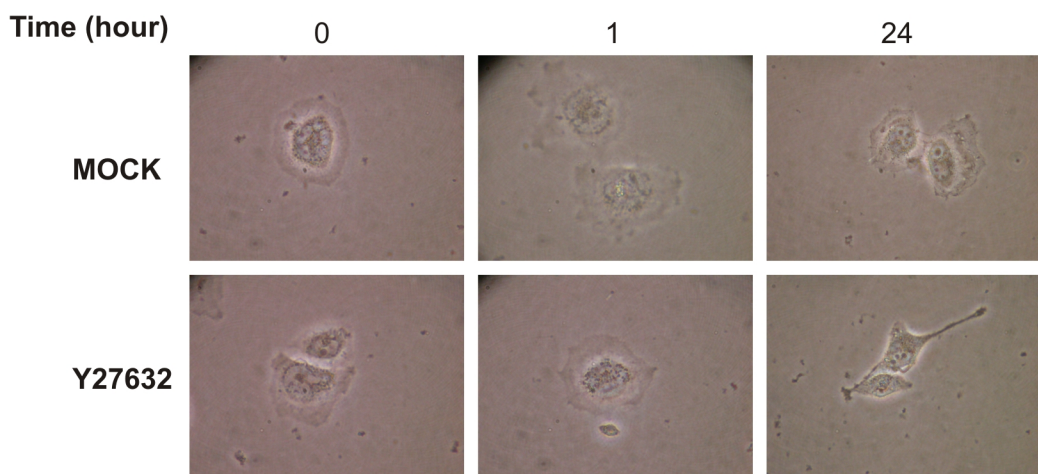


Figure 3.17 Prolonged ROCK inhibitor treatment induced HCC cell collapse
HCC cells, BEL7402 and SMMC, were treated with ROCK inhibitor, Y27632, as the indicated period of time. Short term inhibition of ROCK inhibitor (1 hour) did not cause cell collapse in both HCC cell lines. Long term inhibition of ROCK (24 hours) resulted in cell collapse.

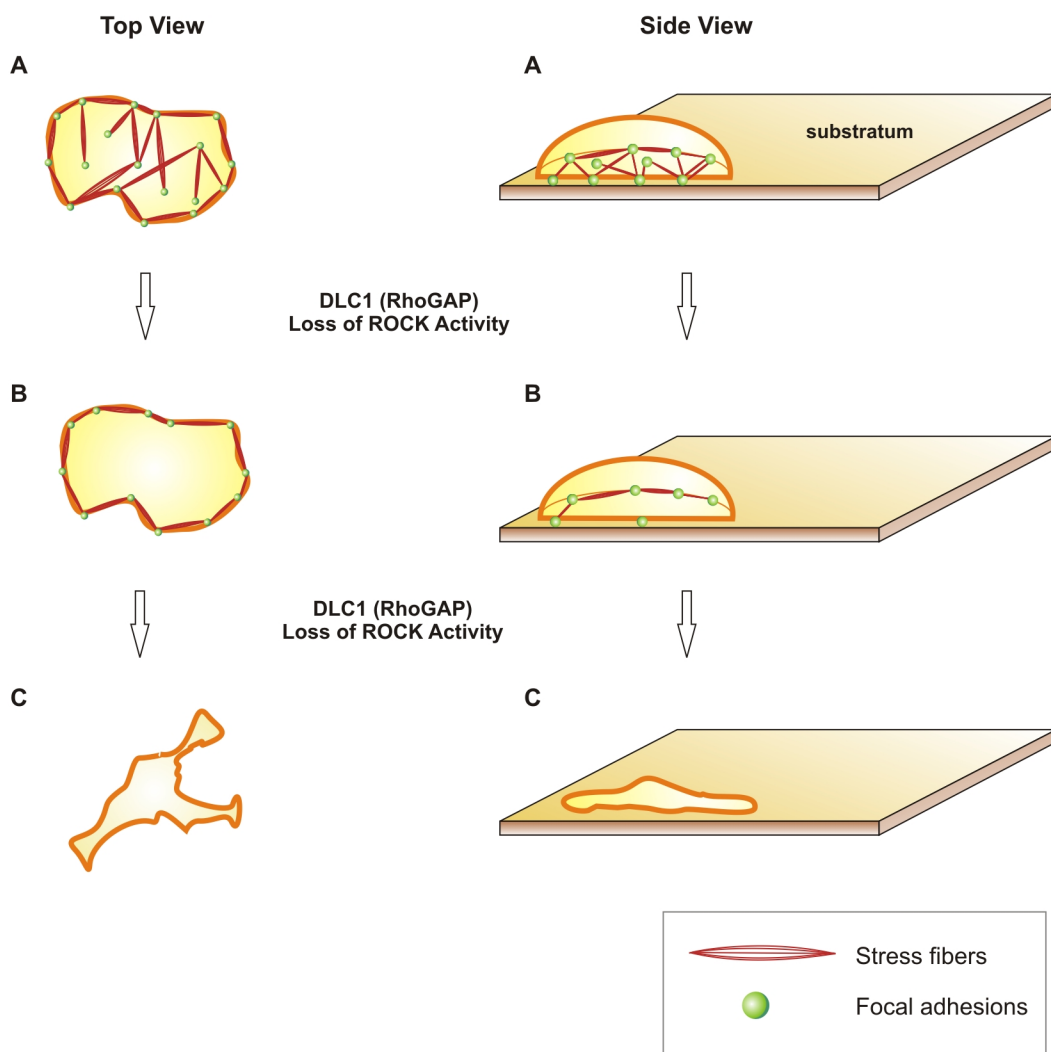


Figure 3.18 Model of DLC1 induced cytoskeletal collapse.

(A) Stress fibers were connected to focal adhesions forming a network. Stress fibers stretched across the cell to provide the cell an intact morphology. (B) DLC1 RhoGAP or loss of ROCK activity induced the loss of stress fibers and focal adhesions. A few focal adhesions and bundle of stress fibers remained. (C) A prolonged or severe loss of stress fiber and focal adhesion network caused by DLC1 RhoGAP or suppression of ROCK activity would result in intensive cytoskeletal collapse. All the stress fibers and focal adhesions were abolished.

not only suppressed cell migration but also cell invasion which involved extracellular matrix barrier. Sahai E *et al.* reported that cancer cell lines might possess different modes of cell motility and the rounded morphology cancer cell lines were more sensitive to ROCK inhibitor in 3-dimensional matrix (29). However, whether this model is applicable to HCC cells and whether other extracellular proteolytic pathways cooperatorate with the DLC1/Rho/ROCK/MLC pathway are still unknown and awaited to be addressed.

Our study demonstrated that ROCK inhibitor, Y27632, did not affect HCC cell proliferation at an efficient dosage that suppressed HCC cell migration. ROCK inhibitors have been widely used in animal models, such as rat and mice models, without causing major toxicity to the animals at efficient dosages (49, 144). Takamura M *et al.* demonstrated that Y27632 could inhibit intrahepatic metastasis of HCC (49) and recently, another ROCK inhibitor, fasudil, has been successfully applied in clinical trial for patients with cardiovascular diseases (145). These studies demonstrate that the toxicity of ROCK inhibitors to cells is limited (49). Accumulating knowledge indicates that ROCK is playing an important role in cancer metastasis, and the present study has enriched the knowledge on the DLC/Rho/ROCK signaling pathway in HCC. ROCK inhibitors such as Y27632 might be useful to the chemotherapeutic intervention in suppressing intrahepatic metastasis, a major cause of mortality in HCC patients, without causing much adverse effects to the patients. Further characterization of the efficacy of specific ROCK inhibitor and the impact of ROCK in HCC will be beneficial to the development of therapies for HCC patients. In Chapter 4, we will further characterize the functional implication of ROCK in HCC.



3.5 Summary

Deleted in liver cancer 1 (DLC1), a member of RhoGTPase activating protein (GAP) family, is known to have suppressive activities in tumorigenicity and cancer metastasis. However, the underlying molecular mechanisms of how DLC1 suppresses cell motility have not been fully elucidated. ROCK is an immediate down-stream effector of RhoA in mediating cellular cytoskeletal events and cell motility. In the present study, we aimed to investigate the effects of DLC1 on Rho/ROCK signaling pathway in HCC. We demonstrated that DLC1 negatively regulated ROCK-dependent actomyosin contractility. From immunofluorescence study, we found that ectopic expression of DLC1 abrogated Rho/ROCK-mediated cytoskeletal reorganization including formation of stress fibers and focal adhesions. It also downregulated cortical phosphorylation of myosin light chain 2 (MLC2). These inhibitory events by DLC1 were RhoGAP-dependent, as RhoGAP-deficient mutant of DLC1 (DLC1 K714E) abolished these inhibitory events. In addition, from western blot study, DLC1 inhibited ROCK-related myosin light chain phosphatase targeting unit 1 (MYPT1) phosphorylation at Threonine 853. By examining cell morphology under microscope, we found that ectopic expression of dominant-active ROCK released cells from DLC1-induced cytoskeletal collapse and cell shrinkage. In summary, our data suggested that DLC1 negatively regulated Rho/ROCK/MLC2 in regulating cell movement (Figure 3.19). This part of the study suggested a ROCK-mediated pathway of DLC1 in suppressing metastasis of HCC cells and enriches our understanding in the molecular mechanisms involved in the progression of HCC.



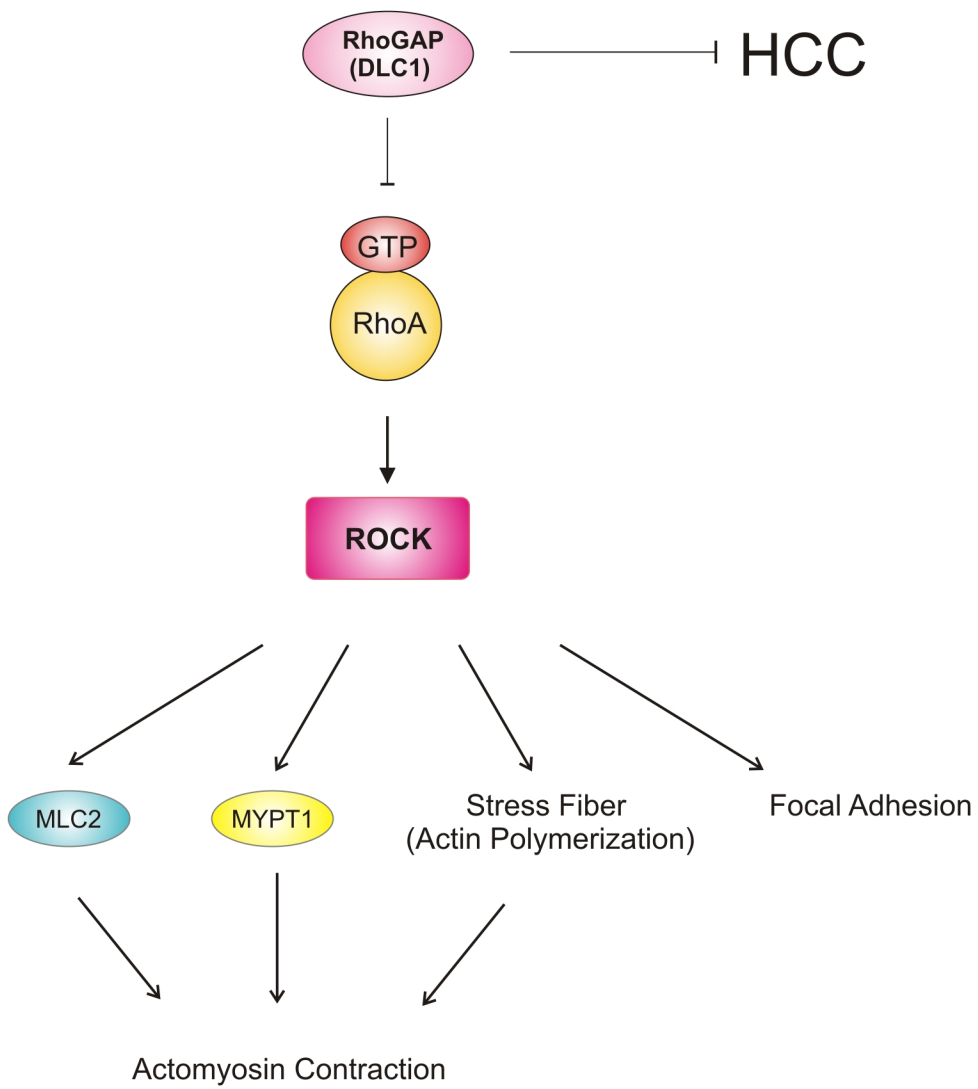


Figure 3.19 DLC1 suppressed RhoA/ROCK/MLC2 pathway

DLC1 downregulated activity of RhoA and suppressed ROCK mediated events including (1) the phosphorylation of myosin light chain 2 (MLC2) and myosin phosphatase target subunit 1 (MYPT1) which are important for actomyosin contraction (2) and the formation of stress fiber- focal adhesion bundling arrays.

Chapter 4

Functions of ROCK in Hepatocellular Carcinoma

4.1 Introduction

As aforementioned in Chapter 1, cancer metastases, both intrahepatic and extrahepatic, are major factors for the mortality of HCC patients. Nonetheless, the molecular mechanisms underlying HCC metastasis remain largely unclear. Cancer cell migration is essential for cancer metastasis. As mentioned in Chapter 3, DLC1/Rho/ROCK is an important pathway in HCC cell movement; thus, it is of importance to further elucidate the function of this pathway in HCC. ROCKs (ROCK1 and ROCK2) are immediate downstream effectors of Rho, a member of Rho family small GTPases. They play important roles in many physiological functions such as neurite growth retardation (146, 147), prenatal and postnatal development (148-150), and smooth muscle contractions (151). ROCK activity is regulated by distinct members of RhoGTPases (Rho), and the Rho/ROCK pathway also participates in regulating cytoskeletal signaling events and is crucial to cell motility (113). Deregulation of Rho/ROCK pathway has been recently implicated in tumor progression and, particularly, tumor metastasis. Among all the Rho family members, RhoA is the best characterized member in cancers and positively regulates ROCK activity. Overexpression of RhoA has been reported in various cancers including HCC (41), breast (42), lung (43), colon (43), head and neck (44), testicular (45), and bladder cancer (46). As well, overexpression of the two members of ROCK



family, ROCK1 and ROCK2, has been reported in testicular and bladder cancers at protein level (45, 46). In addition, ROCK inhibitor (Y27632) treatment was sufficient to abolish chemotactic migration in pancreatic cancer cell lines (111). Likewise, inhibition of ROCK activity either by Y27632 or overexpression of a dominant negative mutant of ROCK1 suppressed actomyosin activity, peritoneal invasion, and intrahepatic metastasis in rat and SCID mouse models (47-49). Although upregulation of Rho/ROCK is often associated with aggressive tumor behavior (116, 117), the exact roles of ROCK in HCC have not been fully elucidated.

4.1.1 Objectives

Since ROCK was often associated with aggressive tumor behaviors and cancer metastasis, we aimed to delineate the functional implications and molecular mechanisms of ROCK in HCC development and metastasis. In this regard, we examined the expression of ROCK (ROCK1 and ROCK2) in human HCCs and studied whether their expression patterns were associated with aggressive clinicopathologic features of HCC. We also investigated whether ROCK could promote HCC migration and invasion by *in vitro* and *in vivo* assays. We further investigated whether ROCK was responsible in regulating events associated with cell polarity establishment as indicated by Golgi reorientation and actin polymerization such as formation of filopodia and stress fibers.



4.2 Materials and Methods

4.2.1 Cell Lines and Patient Samples

BEL7402, CHO, SMMC-7721, and MHCC97L were employed. Human HCC and their corresponding non-tumorous liver samples were collected at the time of surgical resection at Queen Mary Hospital, the University of Hong Kong from 1991 to 2000. All samples, after collection from surgical resection, were snap-frozen in liquid nitrogen before storage at -80°C.

4.2.2 Semi-quantitative and Real time-quantitative PCR

cDNA was synthesized as mentioned in Chapter 2. ROCK1 was amplified with forward primer 5' TTG TCT GCC TCA AAT GCT TG 3' and reverse primer 5' CTG GGA AGA AAG GGA CAT CA 3'. ROCK2 was amplified with forward primer 5' TGC TGG ATG GCT TAA ATT CC 3' and reverse primer 5' GAG CAT GTT GTC AGG CTT CA 3'. GAPDH was used as endogenous control gene and the expression of its mRNA was detected by RT-PCR with primers indicated in Chapter 3. Real-time quantitative PCR of ROCK2 mRNA expression was performed with Applied Biosystems 7900HT Fast Real-Time PCR System with ROCK2 specific Taqman probe (Applied Biosystems, Foster City, CA, USA).

4.2.3 Antibodies

Anti-ROCK2 antibody used for protein expression analysis in human samples was purchased from Anaspec Inc. (San Jose, CA, USA) and anti-ROCK2 antibody for protein expression analysis in cell lines was purchased from Santa Cruz. Anti-MYPT antibody



and anti-phospho-MYPT (Thr 853) antibody were from Upstate, anti- β actin antibody was from Cell Signaling and anti-GFP and anti-ROCK1 antibodies were from Santa Cruz.

4.2.4 Protein Extraction and Western Blotting

For Western blotting, cells were lysed with SDS buffer (for detection of phospho-MYPT, MYPT) or NP40 in NET buffer (for the detection of ROCK1 and ROCK2). Proteins from human samples were extracted with RIPA buffer. Proteins were resolved by SDS-PAGE and blotted onto a nitrocellulose membrane. The membrane was incubated with the indicated primary antibody, followed by incubation with anti-mouse IgG or anti-rabbit IgG (GE Healthcare). Protein expression was detected with the ECLTM detection system (GE Healthcare) according to the manufacturer's protocol. Images were scanned and intensity of bands was quantified with AlphaEaseFCTM software.

4.2.5 Clinicopathologic Correlation and Statistical Analysis

Clinicopathologic features of HCC patients included tumor size, cellular differentiation according to the Edmondson grading, venous invasion without differentiation into portal or hepatic venules, direct liver invasion, tumor microsatellite formation, tumor encapsulation, number of tumor nodules, and serum hepatitis B surface antigen (HBsAg) status were analyzed by SPSS for Windows 14.4 (SPSS, Inc., Chicago, IL) as described previously in Chapter 2 (152). Categorical data were analyzed by Fisher's exact test, whereas independent *t* test was used for continuous data. Tests were considered significant when the *P* value was less than .05.



4.2.6 Plasmid Construction

Constitutively active ROCK2 (1-581 aa) was PCR amplified from HepG2 cDNA (forward primer: 5' CCG CTC GAG TAT GTT ATC CCA ATG CCA CTG A 3' and reverse primer: 5' AAC TGC AGT ATC AGA CTC TGT T 3'). Purified PCR product was then cloned into pEGFP vector by PstI and XhoI digestions. Vector-based short hairpin RNA (shRNA) specifically targeting ROCK2 was generated by PCR-based strategy based on the sequence of siRNA purchased from Dharmacon (Chicago, IL, USA). In brief, U6 promoter sequence served as template in which the short hairpin RNA sequence was included in the reverse primer (forward primer: 5' GAT TTA GGT GAC ACT ATT AG 3' and reverse primer: 5' AAA AAA GTT AGT GTC CTA TTA GTT TCC AAG CTT CGA AAC TAA TAG GAC ACT AAC GGT GTT TCG TCC TTT CCA CAA 3'). PCR product was cloned into pCR4-TOPO (Invitrogen) by EcoRI digestion and subsequently subcloned into pDSRed vector via Ase I digestion after klenow DNA polymerase treatment at 37°C.

4.2.7 Establishment of ROCK2 Stably Expressing Cells and ROCK2

Stable Knockdown Cells

2×10^5 cells were seeded onto 35-mm plates one day before transfection. Plasmids were transfected into cells with FuGene 6 reagent (Roche). After 24 hours, transfected cells were spread onto 100-mm culture dish at 1:100 dilution. To select for stable transfectants, cells were cultured in DMEM high glucose medium with 0.7 mg/mL G418 for 4 weeks. Clones with G418 resistance and fluorescent label (DSRed or GFP) were selected and



expanded. Stable overexpression and knockdown of ROCK2 were confirmed by Western blotting with anti-GFP and anti-ROCK2 antibodies, respectively.

4.2.8 Cell Migration and Invasion Assays

Transwell and wound healing assays were performed as described previously (77). Cell invasion assay was carried out with precoated cell invasion kit (Chemicon) or self coated Matrigel (BD Biosciences) on the upper surface of the transwell chamber. The invasive cells that had invaded through the extracellular matrix (ECM) layer to the lower surface of the membrane were fixed with methanol and stained with crystal violet. Photographs of three randomly selected fields of the fixed cells were captured and cells were counted. Experiments were repeated independently three times.

4.2.9 Immunofluorescence Microscopy and Scanning Electron

Microscopy

Cells were seeded onto coverslips and incubated overnight at 37°C CO₂ incubator. For immunofluorescence study, cells were fixed with 4% paraformaldehyde in PBS and permeabilized with 0.2% Triton X-100 in PBS. Fixed cells were incubated with 1:2,000 FITC-conjugated phalloidin (Sigma) or antibodies as indicated. Cells were counterstained with 4V,6-diamidino-2-phenylindole (DAPI) (Calbiochem) and mounted with Vectashield antifade mountant (Vector Laboratories). Images were captured under ×1,000 magnification by a fluorescence microscope connected to a charge-coupled device camera (Leica, Wetzlar, Germany). For scanning electron microscopy, cells were fixed with 1% osmium tetroxide and 2.5% glutaldehyde followed by stepwise ethanol



dehydration. After the step of critical point dry, slides were mounted on silver paste. Images were scanned and captured under $\times 5,000$ and $\times 8,000$ magnification by a scanning electron microscope stereoscan 440 (Oxford Instruments, Cambridge, UK).

4.2.10 Orthotopic Liver Implantation in Nude Mice

To examine the metastatic potential of ROCK2 stable knockdown clones, 1×10^6 cells (BEL7402) and 4×10^6 (MHCC97L) in 0.1 mL of phosphate-buffered saline, respectively, were injected subcutaneously into the flanks of BALB/C nude mice. After 4 weeks, the subcutaneous tumors were resected and diced into 1 mm^3 cubes, which were then implanted in the left lobes of the livers of the nude mice. For xenografts derived from BEL7402 and MHCC97L cells, the animals were sacrificed and examined 12 and 6 weeks, respectively, after implantation. For *in vivo* tracking, the MHCC97L cells were stably transfected with firefly luciferase. Tumor metastasis of MHCC97L xenografts was detected weekly with bioluminescent signaling during the course of study. 100 mg/kg D-luciferin (Xenogen, Hopkinton, MA) was injected into the peritoneal cavities of the mice and bioluminescence was detected by IVISTM100 Imaging System (Xenogen, Hopkinton, MA). For *ex vivo* organ imaging, mice were injected with 100 mg/kg D-luciferin 5 min intraperitoneally before necropsy and the excised organs were imaged. These experiments were performed according to the Animals (Control of Experiments) Ordinance (Hong Kong) and the Institute's guidance on animal experimentation.



4.2.11 Histologic Analysis

Livers and lungs of the sacrificed mice were harvested and fixed in 10% formalin followed by 75% ethanol before paraffin embedding. Five μm -thick paraffin sections were cut and stained with Hematoxylin & Eosin for histologic examination.

4.2.12 Golgi Reorientation Assay

Golgi reorientation assay was performed as described elsewhere (37). To record the position of the Golgi apparatus in migrating wound edge cells, wounds were created to confluent monolayers of BEL7402 cells on coverslips. Cells were then allowed to migrate for 5 hours. The Golgi apparatus and nucleus were stained with 10 $\mu\text{g}/\text{mL}$ lectin HPA Alexa Fluor® 488 conjugates (Invitrogen) and DAPI (Calbiochem, San Diego, CA), respectively. Wound edge cells were scored positive if the Golgi apparatus located in front of the nucleus in the direction towards the wound. Experiments were repeated independently three times. A range of 353 - 737 cells were counted in total for each wound column.



4.3 Results

4.3.1 Expression of ROCK1 and ROCK2 Expression in human HCC

First, we examined the ROCK1 and ROCK2 mRNA expression levels in human HCC samples using semi-quantitative PCR in 25 pairs of human HCC samples. Neither ROCK1 nor ROCK2 showed significant difference in mRNA expression between human HCC and their corresponding non-tumorous livers (Figure 4.1). We next examined the ROCK1 and ROCK2 protein expression levels in 41 pairs of human HCC and their corresponding non-tumorous livers by Western blotting. Intriguingly, ROCK2 was found to be overexpressed in 53.66% (22/41) of the HCC cases (Figure 4.2). In contrast, there was no significant difference in ROCK1 expression levels between HCCs and their non-tumorous livers (Figure 4.3). To confirm that ROCK2 was only overexpressed in protein level but not in mRNA level, we specifically examined the mRNA expression level in those human HCC cases which exhibited ROCK2 protein overexpression by real time-quantitative PCR. We found there was no significant difference in mRNA expression in these human HCC cases and their corresponding non-tumorous livers even their protein was profoundly overexpressed in human HCC (Figure 4.4). These data indicated that ROCK2 expression was deregulated in human HCC in a post-transcriptional manner.



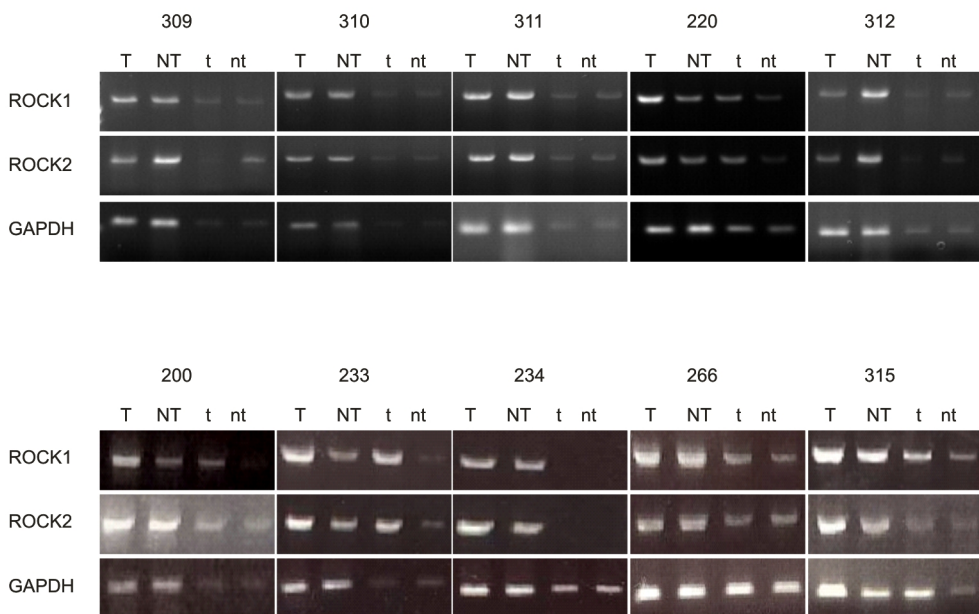


Figure 4.1 ROCK1 and ROCK2 mRNA expression in human HCC was assessed by semi-quantitative PCR

Semi-quantitative analysis showing representative HCC cases with ROCK1 and ROCK2 mRNA expression. cDNA from different cases of HCC samples (T) and their corresponding non-tumorous livers (NT) was used as template for PCR reaction with primers amplifying ROCK1 and ROCK2. GAPDH was used as endogenous control. t: 1/5X of T used for PCR reaction; nt: 1/5X of NT used for PCR reaction.

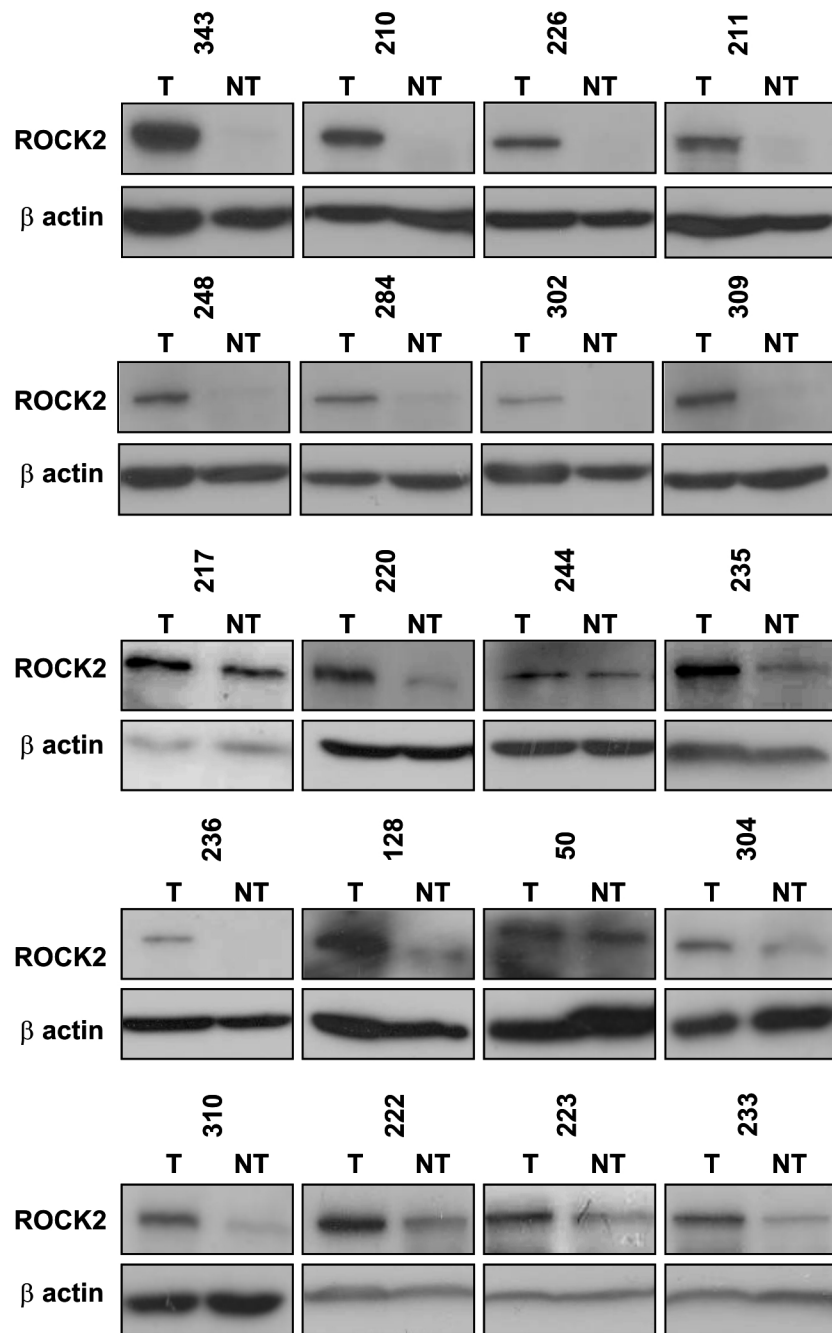


Figure 4.2 ROCK2 protein expression in human HCC

Western blot analysis showing representative HCC cases with ROCK2 overexpression. ROCK2 was significantly overexpressed in HCC. T, tumor; NT, non-tumorous liver
 β actin was used as a loading control.

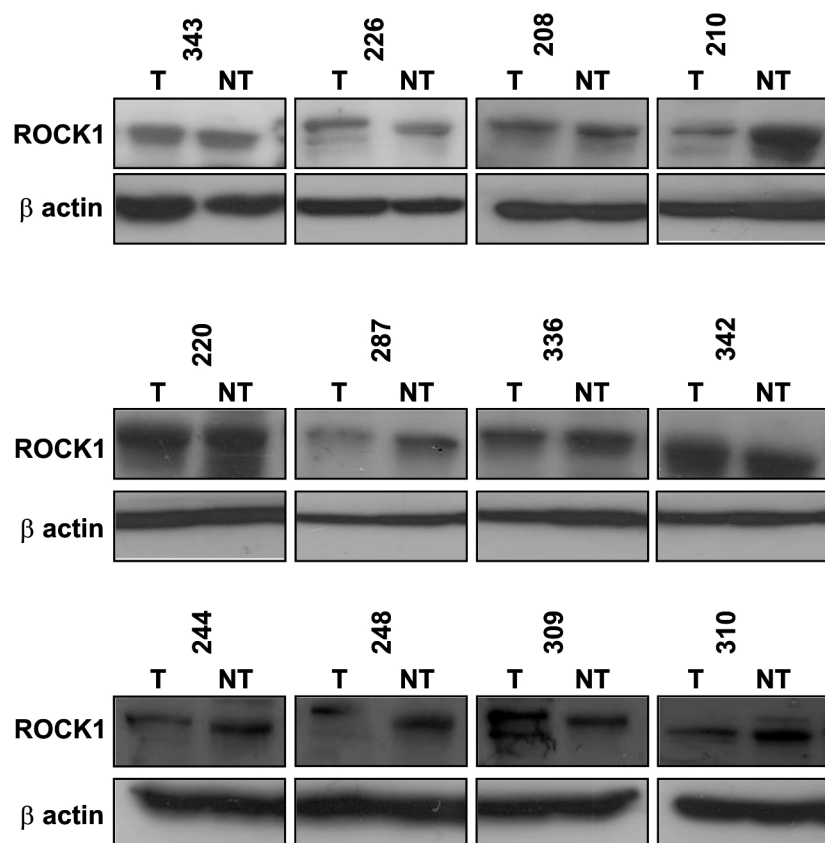


Figure 4.3 ROCK1 protein expression in human HCC

Western blot analysis showing representative HCC cases of ROCK1 expression. No significant change was observed between the expression of ROCK1 in T and NT. T, tumor; NT, non-tumorous liver. β actin was used as a loading control.

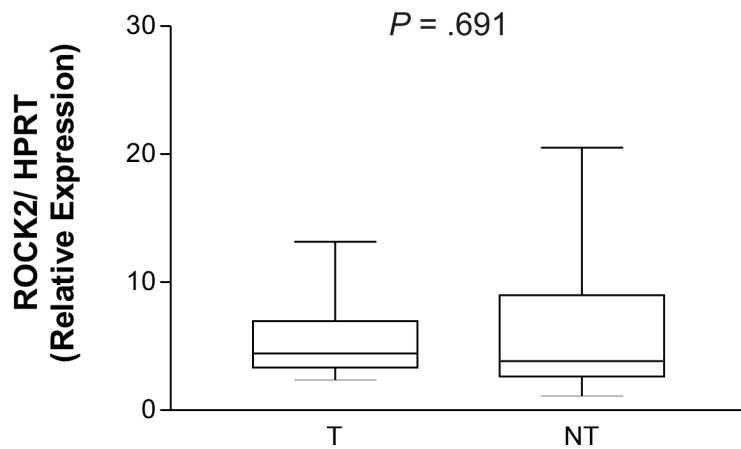


Figure 4.4 ROCK2 mRNA expression in human HCC was assessed by real-time quantitative PCR

The mRNA expression of ROCK2 in the 22 paired HCC cases which showed ROCK2 protein overexpression in the tumorous livers as compared to the non-tumorous livers was accessed by real-time quantitative PCR. There was no significant difference in ROCK2 mRNA expression between tumorous and non-tumorous livers. Paired non-parametric test (Wilcoxon signed rank test) was used to calculate P value.

4.3.2 Overexpression of ROCK2 in Human HCC was Associated with Aggressive Tumor Behavior

Upon clinicopathologic correlation analysis, overexpression of ROCK2 was found to be closely and positively associated with the presence of tumor microsatellite formation ($P = .005$, Fisher's exact test), which is a feature of intrahepatic metastasis (Table 4.1). These findings indicated that overexpression of ROCK2 was frequent in human HCCs and might be related to tumor metastasis.



Table 4.1. Clinicopathologic correlation of ROCK2 overexpression in human HCC.

		ROCK2			$P = .115$
		Without Overexpression		With Overexpression	
		(No. of cases)	(No. of cases)		
Tumor size	≤ 5 cm	6	2	$P = 1.000$	$P = .115$
	> 5 cm	13	20		
Number of tumor nodules	1	15	17	$P = .186$	$P = 1.000$
	≥ 2	4	5		
Tumor encapsulation	Absent	10	9	$P = .062$	$P = .186$
	Present	16	5		
Cellular differentiation by Edmondson grading	I-II	11	6	$P = .216$	$P = .062$
	III-IV	8	16		
Venous invasion	Absent	10	7	$P = 1.000$	$P = .216$
	Present	9	15		
Tumor microsatellite formation	Absent	12	4	$P = .005^*$	$P = .005^*$
	Present	7	18		
Direct liver invasion	Absent	10	12	$P = 1.000$	$P = 1.000$
	Present	7	9		
HBV surface antigen	Absent	3	4	$P = 1.000$	$P = 1.000$
	Present	16	18		

* $P < .05$



4.3.3 Expression of ROCK1 and ROCK2 Expression in HCC Cell Lines

We first examined the ROCK1 and ROCK2 expression levels in normal liver cell lines and HCC cell lines. Both the ROCK1 and ROCK2 protein expression exhibited no significant changes between normal liver cell lines: LO2 and MIHA, and the other hepatoblastoma and HCC cell lines: SNU182, SNU449, SNU475, Huh7, HepG2, Hep3B, HLE, PLC, BEL7402, SMMC, MHCC97L, and MHCC97H (Figure 4.5). Despite the important difference found in the ROCK2 expression in human HCC as compared to non-tumorous liver, there was no significant difference in ROCK2 protein expression between normal liver cell lines and HCC cell lines. Since LO2 and MIHA are immortalized normal liver cell lines, their properties might be altered and different from normal liver cells.

4.3.4 ROCK2 Enhanced Cell Migration and Invasion of HCC Cells *in Vitro*

To assess the effect of ROCK2 on HCC cell migration, constitutively active ROCK2 was stably transfected into BEL7402 HCC cell line and confirmed with Western blotting (Figure 4.6A). We found that ROCK2 stably expressing cells (GFP-ROCK2C11) displayed a significant increase in cell migration ability as compared with the vector control ($P < .001$, *t*-test) (Figure 4.6B). In addition, using invasion chamber coated with a thin layer of ECM, we further demonstrated that overexpression expression of ROCK2 substantially enhanced the invasiveness of HCC cells, as indicated by a marked increase in the number of invaded cells ($P < .001$, *t*-test) (Figure 4.6C). These findings were



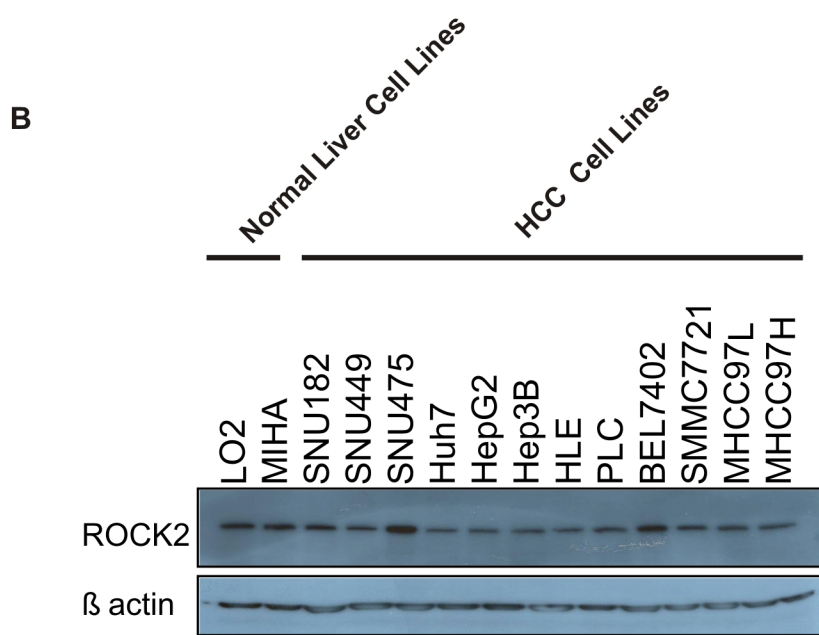
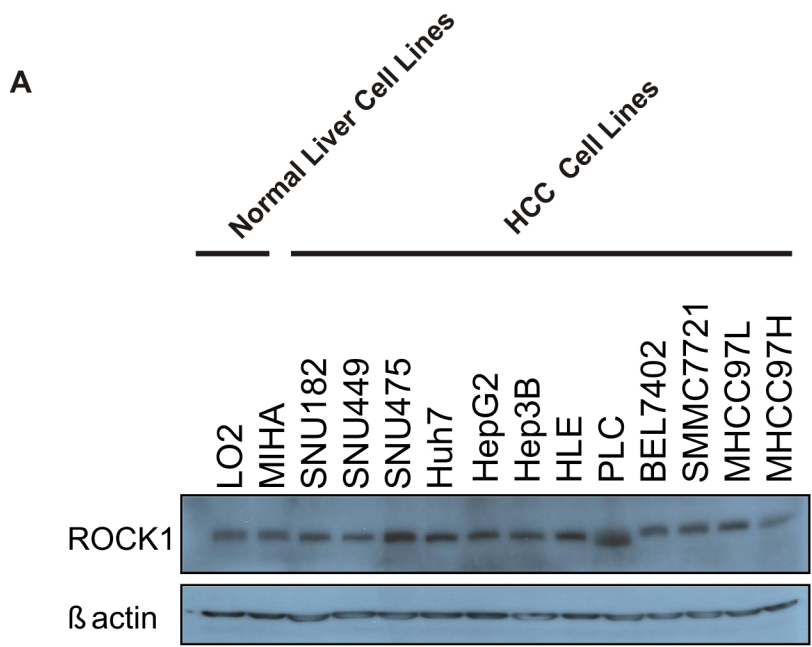


Figure 4.5 ROCK1 and ROCK2 protein expression in HCC cell lines

Western blot analysis showing (A) ROCK1 (B) ROCK2 protein expression in normal liver cell lines and HCC cell lines. β actin was used as loading control.



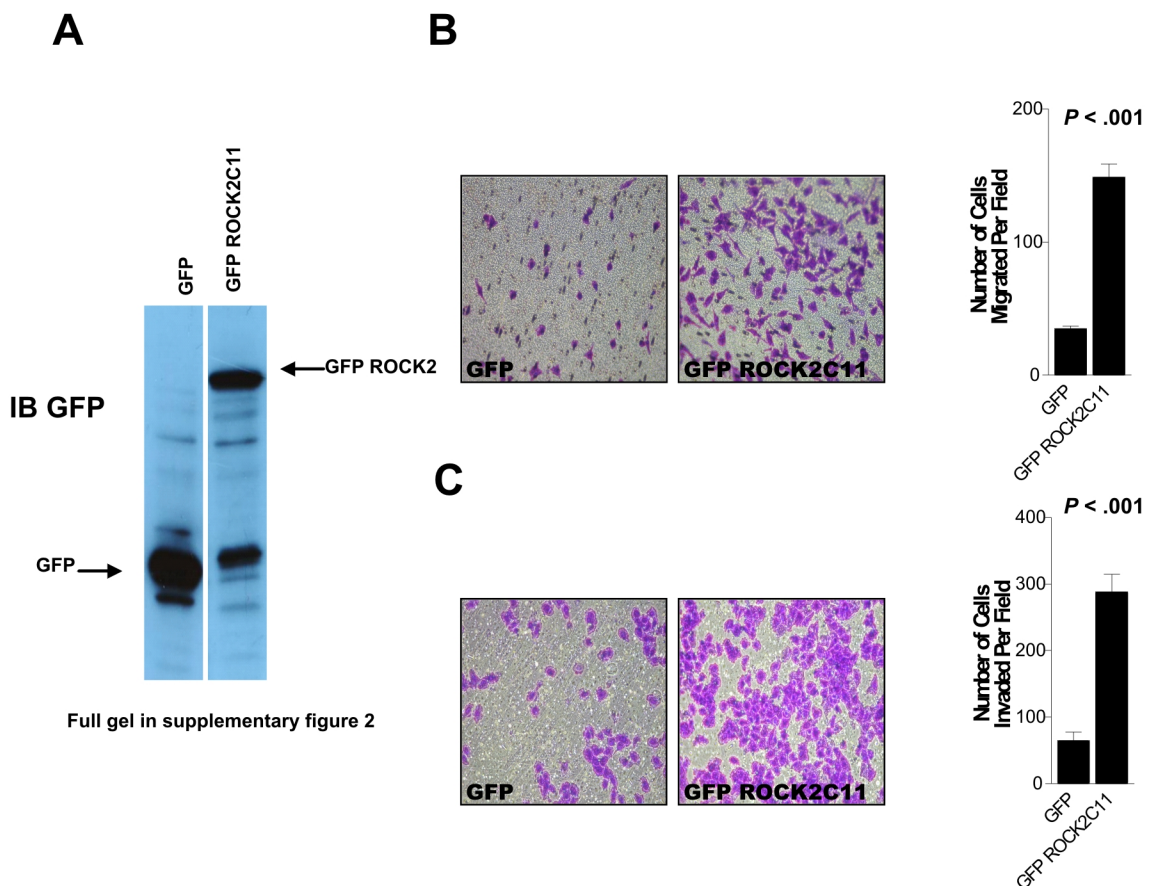


Figure 4.6 Overexpression of ROCK2 enhanced HCC cell migration and invasion

(A) Ectopic overexpression of GFP-ROCK2 fusion protein in BEL7402. GFP (lower left arrow) and GFP-ROCK2 fusion (upper right arrow) expression were confirmed by western blot analysis with GFP antibody. (B) Tranwell cell migration assay. 5×10^4 cells were seeded onto the upper chamber of the Transwell and allowed to migrate for 8 hours. The number of migrated cells was significantly increased in ROCK2 stable transfector (GFP ROCK2C11) as compared with vector control (GFP). (C) Invasion assay. 1×10^5 cells were seeded and allowed to invade through the ECM pre-coated invasion chamber kit for 24 hours. The number of invaded cells was significantly increased in ROCK2 stably overexpressing cells (GFP ROCK2C11) as compared with vector control (GFP). Error bars represent SEM.

consistent with the correlation we observed between overexpression of ROCK2 and the pathologic feature of intrahepatic metastasis in HCC patients and suggested that overexpression ROCK2 positively regulated HCC cell motility and invasiveness.

To further substantiate the notion that ROCK2 was implicated in HCC cell migration and invasion, we stably knocked down ROCK2 expression in BEL7402 by short hairpin RNA (Figure 4.7). In contrast to ROCK2 overexpression, stable knockdown of ROCK2 (ShROCK2-1 and ShROCK2-3) considerably decreased cell migration ability in BEL7402 as evidenced by Transwell assay ($P < .001$, *t*-test) (Figure 4.8) and wound healing assay (Figure 4.9). Of note, ROCK2 expression was almost completely knocked down in ShROCK2-1 and partially knocked down in ShROCK2-3 (Figure 4.7). Intriguingly, ShROCK2-1 displayed a drastic reduction of migrated cells as compared to ShROCK2-3, and this suggested a possible dosage effect of ROCK2 on HCC cell migration (Figure 4.7). Consistently, ROCK2 stable knockdown transfectant (ShROCK2-1) also exhibited a significant decrease in the number of invaded cells than its vector control ($P = .007$, *t*-test) (Figure 4.10). The results from the *in vitro* overexpression and knockdown cell models suggested that ROCK2 played a significant role in HCC cell migration and invasion.

4.3.5 Stable Knockdown of ROCK2 in HCC Cell Line Suppressed Invasion and Metastasis in Nude Mice

To investigate the functions of ROCK2 on HCC cell invasion and metastasis *in vivo*, orthotopic liver implantation was performed in nude mice with ROCK2 stable knockdown cell lines. To this end, the HCC cell line MHCC97L, which was shown to be



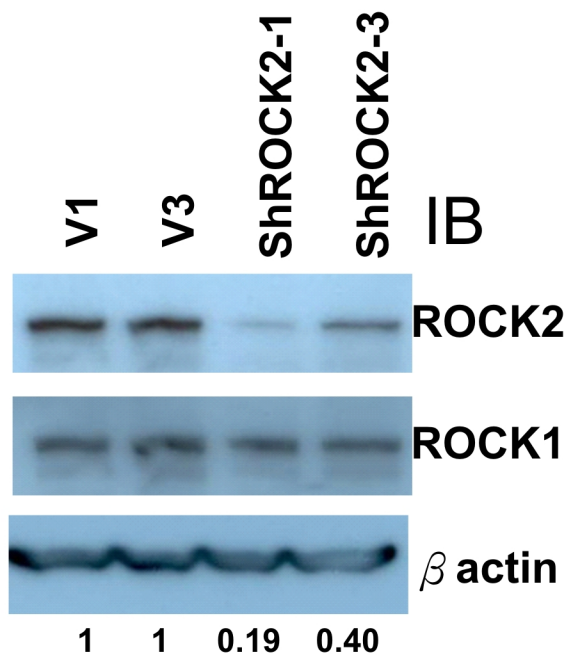


Figure 4.7 ROCK2 expression in BEL7402 ROCK2 stable knockdown cells.

ROCK2 expression in ROCK2 stable knockdown cells. Stable clones were generated from BEL7402 HCC cell line. Both ShROCK2-1 and ShROCK2-3 stable clones showed significant reduction of ROCK2 expression as compared with the vector stable clones V1 and V3. Protein bands were scanned and quantified by AlphaEaseFCTM software.

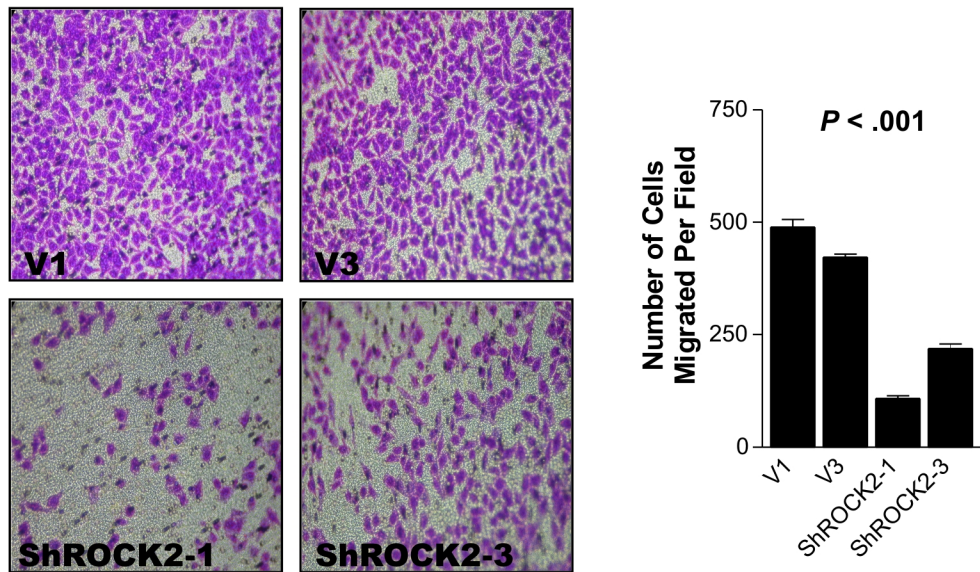


Figure 4.8 Knockdown of ROCK2 suppressed HCC cell migration (Transwell)
 Transwell cell migration assay. 1×10^5 cells were seeded onto the upper chamber of the transwell and allowed to migrate for 16 hours. The number of migrated cells was significantly reduced in ROCK2 stable knockdown cells (ShROCK2-1 and ShROCK2-3) as compared with vector controls (V1 and V3). Error bars represent SEM.

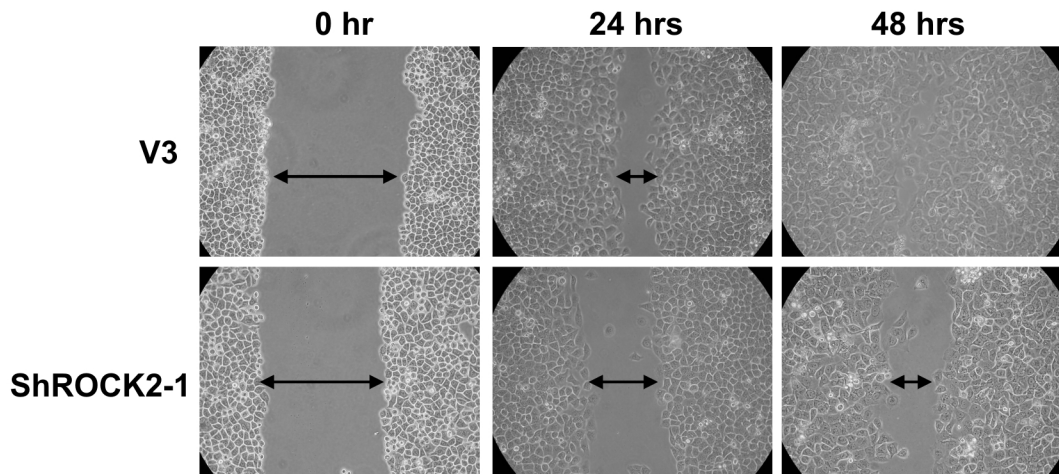


Figure 4.9 Knockdown of ROCK2 suppressed HCC cell migration (wound healing)

Wound closure was delayed in ROCK2 stable knockdown cells (ShROCK2-1) as compared with the vector control (V3) in both 24 and 48 hr time points.

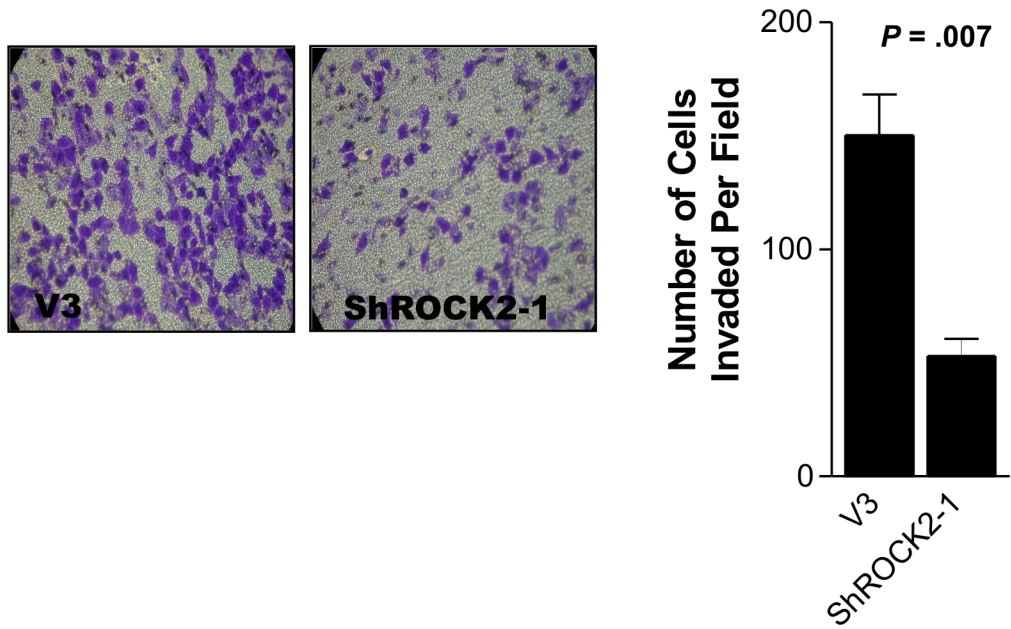


Figure 4.10 Knockdown of ROCK2 suppressed HCC cell invasion

3×10^5 cells were seeded onto Matrigel coated invasion chamber and allowed to invade for 24 hours. The number of invaded cells was significantly reduced in BEL7402 ROCK2 stably knockdown cells (ShROCK2-1) as compared with vector control (V3). Error bars represent SEM.

metastatic in orthotopic liver implantation model (153) was sequentially transfected with shRNA targeting ROCK2 and firefly luciferase reporter. Stable knockdown of ROCK2 was confirmed by Western blotting (Figure 4.11). After subcutaneous injection, tumors derived from MHCC97L ShROCK2 and vector clones were then resected and implanted into the livers of nude mice, with weekly monitoring of bioluminescent signals. After 6 weeks of implantation, the mice were sacrificed and their livers and lungs were examined. Pulmonary metastasis was found in one mouse from the vector group and none in the ShROCK2 group, as detected by the bioluminescence generated from the lung of the mouse and confirmed with histology (Figure 4.12 and 4.13A, Table 4.2). A more remarkable effect in HCC local invasion was found from histologic analysis of the tumors. In the orthotopic implanted livers, the tumor growth fronts from the MHCC97L vector group were invasive and irregular, whereas the tumor growth fronts from the MHCC97L ShROCK2 group were found to be bulging, more regular and less invasive (Figure 4.13B). In addition, tumor microsatellite formation was found in 3 of the 4 mice in the vector group, whereas none was found in the ShROCK2 group (Figure 4.13C and Table 4.2). Moreover, the incidence of venous invasion was slightly reduced in the tumors derived from MHCC97L ShROCK2 clone (Table 4.2). Of note, only a single focus of venous invasion was found in each of the two tumors of ShROCK2 clone, as compared with multiple foci of venous invasion found in the MHCC97L vector clone (Figure 4.13D).

We also repeated similar orthotopic liver implantation experiment using subcutaneous tumor xenografts derived from BEL7402 vector clone (V3) and BEL7402 ROCK2



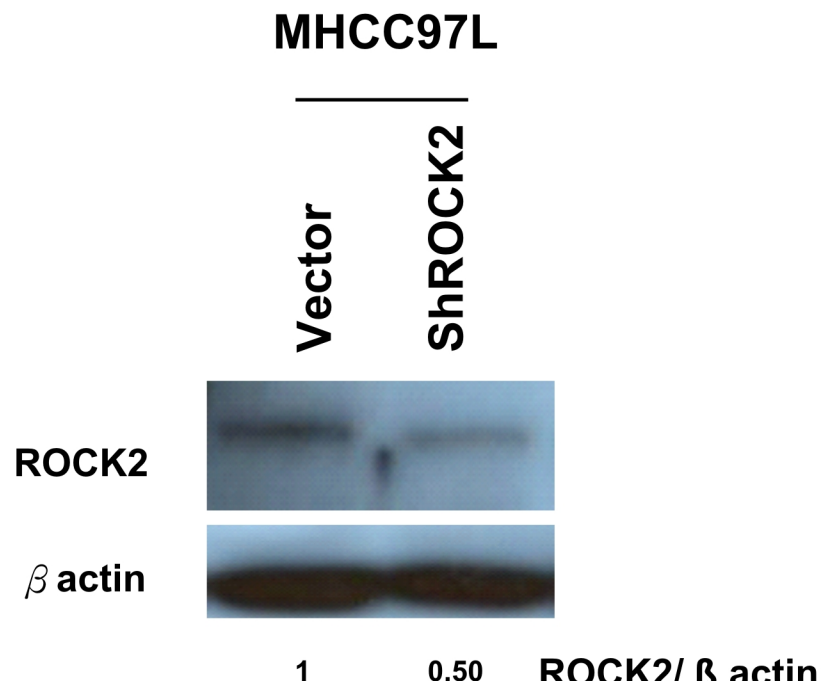


Figure 4.11 ROCK2 expression in MHCC97L ROCK2 knockdown stable clone

ROCK2 expression was significantly reduced in the ROCK2 stable knockdown HCC cell line, MHCC97L. Protein bands were scanned and quantified by AlphaEaseFC™ software.

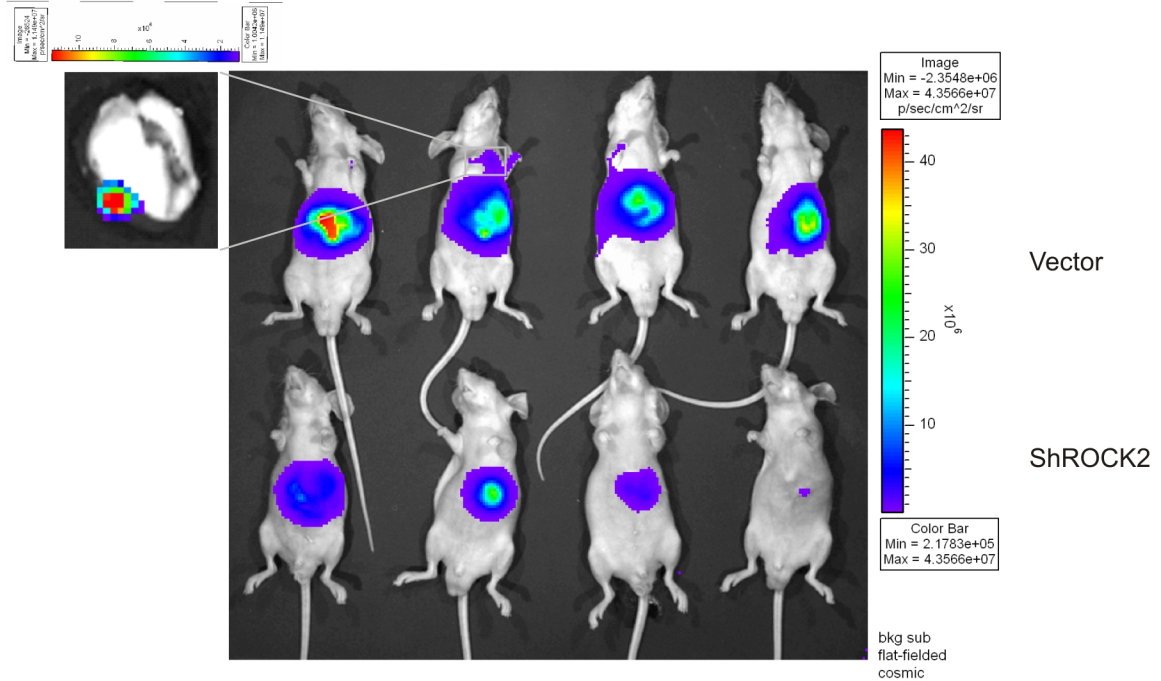


Figure 4.12 Knockdown of ROCK2 suppressed HCC metastasis *in vivo*

Luciferase signal was generated from the luciferase-labeled MHCC97L xenografts. Luciferase signal was observed in the livers of the nude mice where the xenografts were implanted. Stronger signals were observed in the vector control group. One mouse from the vector group displayed lung metastasis, highlighted in the white rectangular box. Lungs were dissected out and luciferase signal was measured separately. Positive luciferase signal was detected from the lung, which is indicative of lung metastasis.

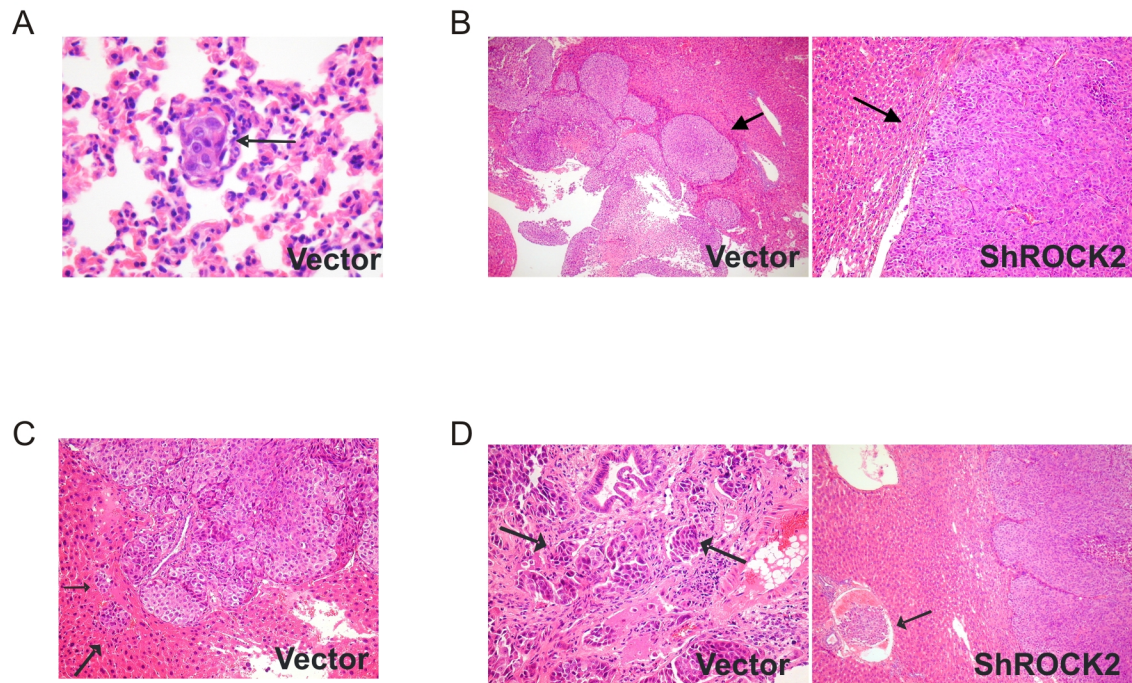


Figure 4.13 Histologies showing knockdown of ROCK2 in MHCC97L suppressed HCC invasion *in vivo*

(A) Lung metastasis (arrow) found in the vector group was confirmed by histologic analysis in H&E staining. (B) Tumors formed in livers from MHCC97L vector control clone displayed an irregular invasive tumor front whereas tumors formed in liver from MHCC97L ShROCK2 clone displayed a bulging growth front (H&E sections). Arrows mark the tumor fronts. (C) Tumor microsatellite formation (arrows) around the main tumor was observed in the mice of the vector control group but not in those of the ShROCK2 group. (D) Multiple foci of venous invasion (arrows) were detected in the livers of the MHCC97L vector control group while only a single focus of venous invasion (arrow) was detected in each of the two livers of the MHCC97L ShROCK2 group.

Table 4.2. Results of orthotopic liver implantation from MHCC97L vector and ROCK2 knockdown clones.

	No. of tumors with invasive growth front	No. of tumors with venous invasion	No. of tumors with microsatellite formation	No. of tumors with lung metastasis
Vector	4/4	3/4 (multiple foci in all)	3/4	1/4
ShROCK2	1/4	2/4 (single focus in both)	0/4	0/4



knockdown ROCK2 clone (ShROCK2-1). Similarly, tumors formed from BEL7402 vector control clone displayed frequent venous invasion than that of BEL7402 ShROCK2 clone (ShROCK2-1) (Figure 4.14 and Table 4.3). Overall, we demonstrated that stable knockdown of ROCK2 was able to suppress HCC cell invasion both *in vitro* and *in vivo*.

In the livers of the mice, we observed a slight reduction of tumor size derived from MHCC97L ShROCK2 cell line as compared to the MHCC97L vector control cell line. Nevertheless, no difference was observed in the *in vitro* cell proliferation rate (Figure 4.15A left panel and 4.15B left panel) and *in vivo* subcutaneous tumor size when ROCK2 was knocked down in both HCC cell lines (Figure 4.15A right panel and 4.15B right panel). Although the precise reason needs to be elucidated, these observations could be explained by the disparate growth environments, and we speculate that ROCK2 may also be important to the tumor development of HCC cells in mouse livers which mimics the natural microenvironment of HCC growth.



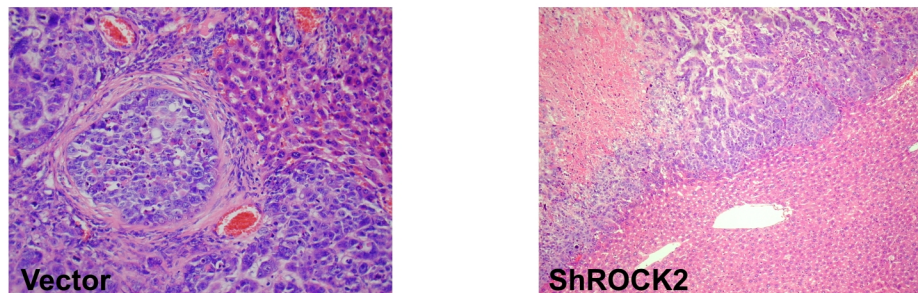


Figure 4.14 Knockdown of ROCK2 in BEL7402 suppressed HCC invasion *in vivo*

BEL7402 vector (V3) and BEL7402 ShROCK2 (ShROCK2-1) stable transfectants were used for orthotopic liver nude mice implantation. Representative pictures of H&E stained slides showing histology of the tumors formed in the livers of the mice. Left: Tumors derived from vector cells exhibited venous invasion. Right: Tumors derived from ShROCK2 cells exhibited no venous invasion nor microsatellite formation.

Table 4.3. Results of orthotopic liver implantation from BEL7402 vector and ROCK2 knockdown clones.

	No. of tumors with venous invasion	No. of tumors with microsatellite formation
Vector	3/4	1/4
ShROCK2	0/4	0/4



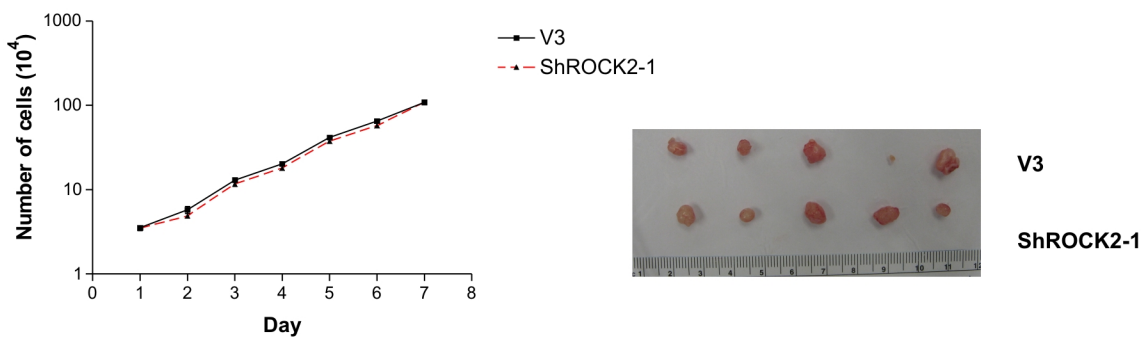
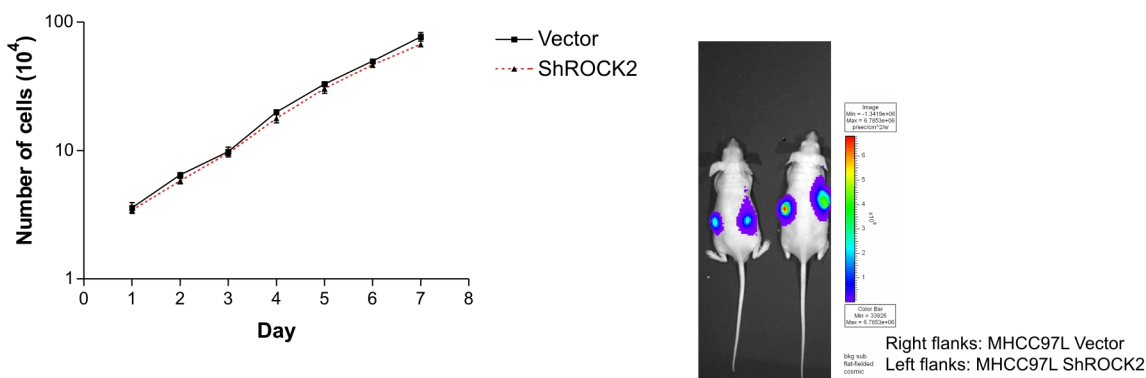
A**BEL7402****B****MHCC97L**

Figure 4.15 Knockdown of ROCK2 did not affect HCC cell proliferation *in vitro* and *in vivo*

(A) Left: BEL7402 V3 and BEL7402 ShROCK2-1 stable transfectants exhibited no difference in cell proliferation in *in vitro* cell proliferation assay. Right: Nude mice subcutaneous injection of BEL7402 V3 and BEL7402 ShROCK2-1 stable transfectants. Tumors were harvested 4 weeks after injection and tumors derived from vector and ShROCK2 clones showed no difference in tumor size. (B) Left: Luciferase labelled MHCC97L Vector and MHCC97L ShROCK2 stable transfectants exhibited no difference in *in vitro* cell proliferation assay. Right: Nude mice subcutaneous injection of MHCC97L Vector and MHCC97L ShROCK2 stable clones. Tumors were harvested 4 weeks after injection and tumors derived from vector and ShROCK2 clones showed no significant difference in tumor size as reflected by the bioluminescence.



4.3.6 Knockdown of ROCK2 Inhibited Stress Fiber Formation and Attenuated Phosphorylation of Myosin Phosphatase Target Subunit (MYPT1)

To investigate the molecular mechanisms of ROCK2 in regulating cell motility and cancer metastasis, we examined stress fiber formation and polymerized actin in ROCK2 stable knockdown cells. Cytoskeletal reorganization exemplified by the formation of stress fiber bundling arrays is essential for the contractile motion of cancer cells. Using phalloidin staining, we found that stress fiber formation was suppressed in ROCK2 stable knockdown transfectant ShROCK2-1 (Figure 4.16).

Previous studies have indicated that phosphorylation of MYPT1 at Thr 853 was essential for phosphorylation of myosin II and crucial for cell contractility (154). To further delineate the roles of ROCK2 on actomyosin contractility, the MYPT1 phosphorylation level in ROCK2 stable knockdown transfectant ShROCK2-1 was assessed. With Western blotting, we demonstrated that the phosphorylation level of MYPT1 (Thr 853) of ROCK2 knockdown stable transfectant was significantly reduced as compared to the vector control (Figure 4.17), suggesting that ROCK2 was important for mediating cytoskeletal reorganization in HCC cells via regulating actomyosin contraction.



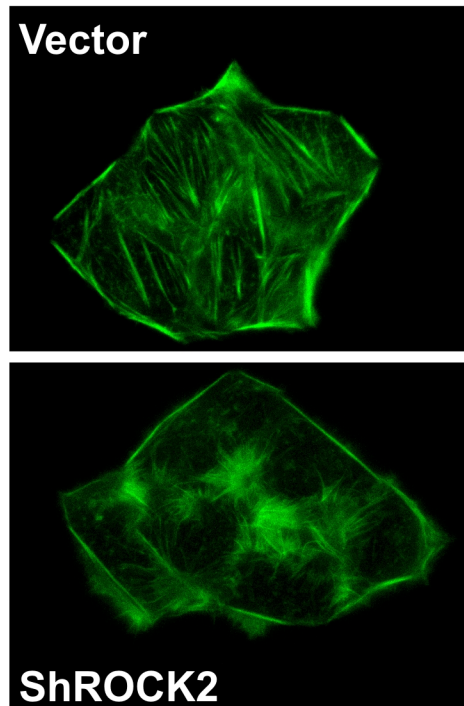


Figure 4.16 Knockdown of ROCK2 impaired stress fibers formation

BEL7402 ROCK2 knockdown stable clone (ShROCK2-1) and vector control clone (V3) were used. Knockdown of ROCK2 disrupted stress fiber network. Stress fibers (polymerized actin) and actin filaments, were demonstrated by phalloidin staining (green). Top panel: vector control transfectant (V3) of BEL7402 cells exhibited clear stress fibers, whereas ROCK2 knockdown stable transfectant (ShROCK2-1) exhibited loss of stress fibers (fluorescence microscopy; X1000 magnification)

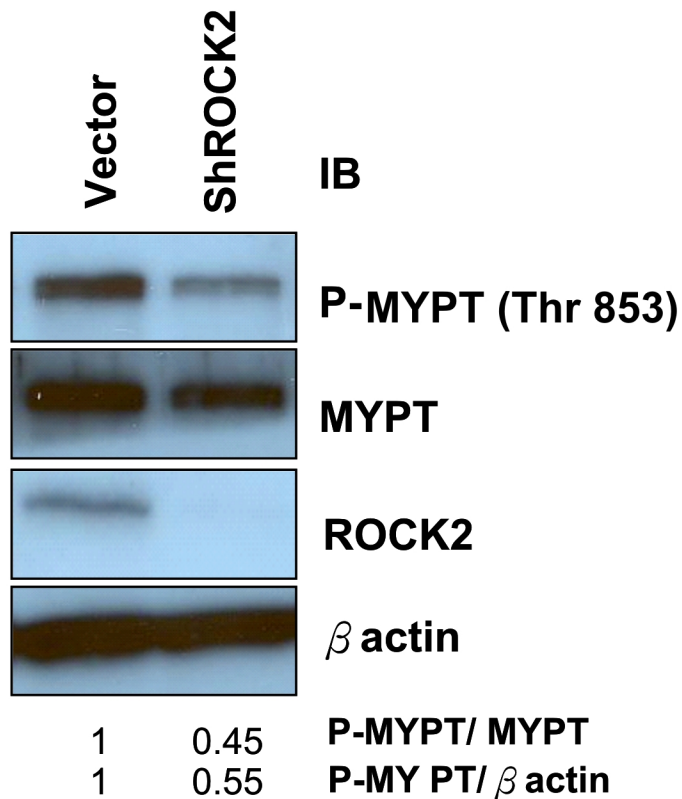


Figure 4.17 Knockdown of ROCK2 inhibited MYPT phosphorylation at Thr 853
 BEL7402 ROCK2 knockdown stable clone (ShROCK2-1) and vector control clone (V3) were used. With Western blot analysis, ShROCK2 stable transfectant (ShROCK2-1) displayed a reduction in MYPT phosphorylation (Thr853), indicative of impairment of actomyosin contractility.

4.3.7 Knockdown of ROCK2 Inhibited Filopodia and Membrane Bleb Formation

To further understand the impact of ROCK2-mediated cytoskeletal reorganization on migratory and invasive related cellular changes in HCC cells, we compared the cell morphology of vector and ShROCK-2 stably transfected BEL7402 cells. Under scanning electron microscopy, we observed a significant reduction of filopodia (spiky cell protrusions) and membrane blebs (rounded cell protrusions) on the cell surfaces of ROCK knock down cells as compared to the vector control cells (Figure 4.18). Filopodia and membrane blebs are dynamic cellular features on cell membrane surfaces, require actin polymerization, and are involved in cancer cell invasion (39, 100). Our results indicated that ROCK2 might play an important role in regulating the cellular events related to cancer invasion and metastasis.

4.3.8 Knockdown of ROCK2 Disrupted HCC Cell Polarity

Next, we investigated the effect of ROCK2 on HCC cell polarity by the Golgi reorientation assay (37). The establishment of cell polarity is essential for migrating cells to coordinate directional movement through protruding at the anterior end of the membrane and retracting from the posterior end of the cell, which also plays an important role in cancer invasion and metastasis. A polarized cell shows realignment of the Golgi apparatus to the front of the nucleus in the direction of movement in order to direct membrane protrusion (37, 38). We first examined whether HCC cells exhibited this phenomenon. We confirmed our observations with CHO fibroblast cells, SMMC-7721, and BEL7402 parental cells for the Golgi reorientation assay. We found that Golgi



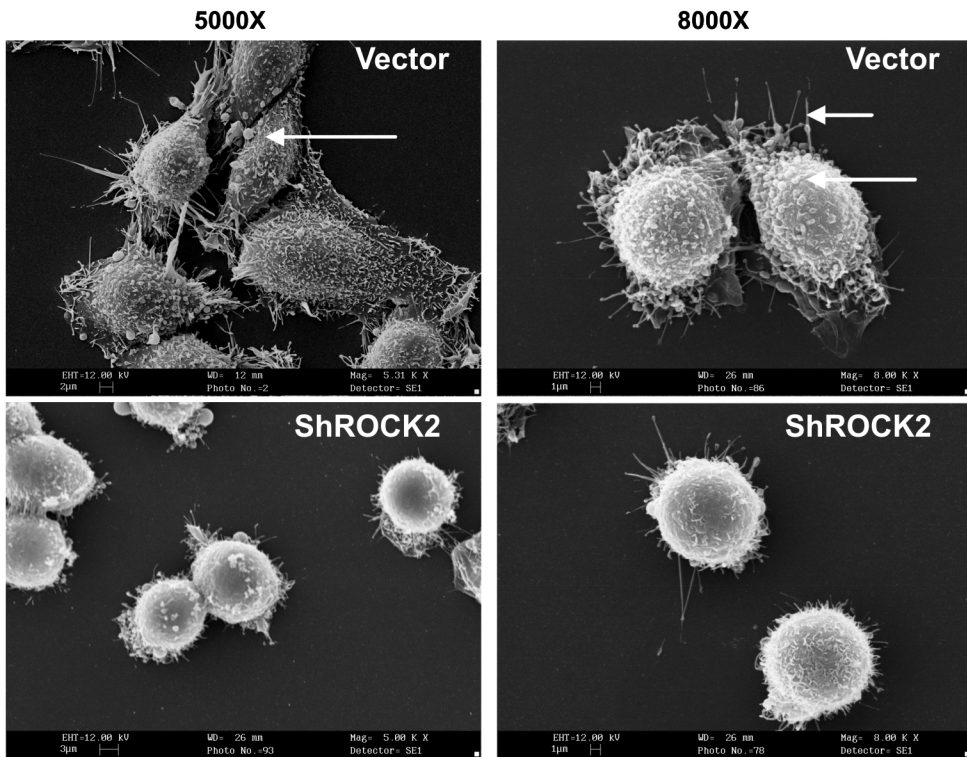


Figure 4.18 Knockdown of ROCK2 suppressed formation of membrane blebs and filopodia

BEL7402 ROCK2 knockdown stable clone (ShROCK2-1) and vector control clone (V3) were used. Knockdown of ROCK2 suppressed suppressed formation of membrane blebs (rounded protrusions) and filopodia (spiky protrusions) (arrows) (scanning electron microscope; X5000 magnification [left panel] and X8000 magnification [right panel]).

reorientation was specific in certain HCC cell lines. We found the Golgi realigned to the front of the nucleus towards the wound in BEL7402 (Figure 4.19A & B) but not in SMMC-7721 cells (Figure 4.20A & B) 6 hours after the wounds were created. Using CHO fibroblasts as positive control (155), we found that CHO fibroblasts (Figure 4.21A & B) exhibited a greater ability in Golgi repositioning (~75%) when compared to BEL7402 parental HCC cells (~54 %) 6 hours after wound creation. Having included the positive control (CHO cells) and the negative control (SMMC-7721), we confirmed that BEL7402 can reposition its Golgi apparatus. Although BEL7402 exhibited less Golgi repositioning as compared to CHO fibroblasts, we observed a significant number of BEL7402 cells having ability to realign the Golgi apparatus. Therefore, we examined the effect of ROCK2 in cell polarity by comparing the abilities of BEL7402 V3 and BEL7402 ShROCK2-1 cells in Golgi apparatus repositioning. At zero time point, the random values of cells scoring positive for the Golgi reorientation assay in both groups were 15% (Figure 4.22A). Five hours after the wound was created, 55% of the cells from the BEL7402 V3 clone scored positive, as compared to 28% cells from the BEL7402 ShROCK2-1 cells ($P = .001$) (Figures 4.22A & B). Our results showed that knockdown of ROCK2 significantly impaired the ability of HCC cells to establish cell polarity.



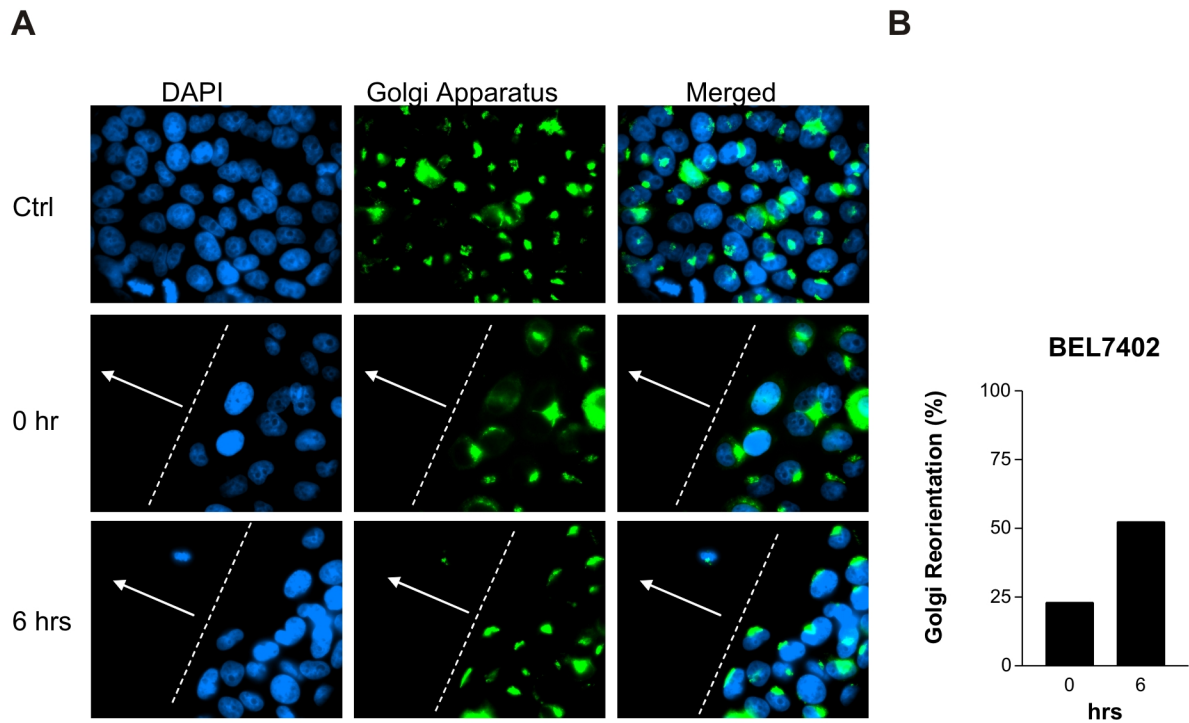


Figure 4.19 BEL7402 cells exhibited golgi reorientation 6 hours after wound creation

A wound was created on confluent BEL7402 cells. Cells were fixed and stained at the given time points (0 hour, 6 hours). Unscratched BEL7402 cells were used as control (Ctrl). The nuclei were stained with DAPI (blue) whilst the Golgi apparatus were stained with lectin (green). Arrows marked the direction of movement. (B) Percentage of cells that exhibited golgi reorientation was shown in the graph. 142-147 wound edge cells were counted at different time points. There was significant increase of cells that exhibited Golgi reorientation to the front of the nucleus towards the direction of movement at 0 hour time point and 6 hours time point.

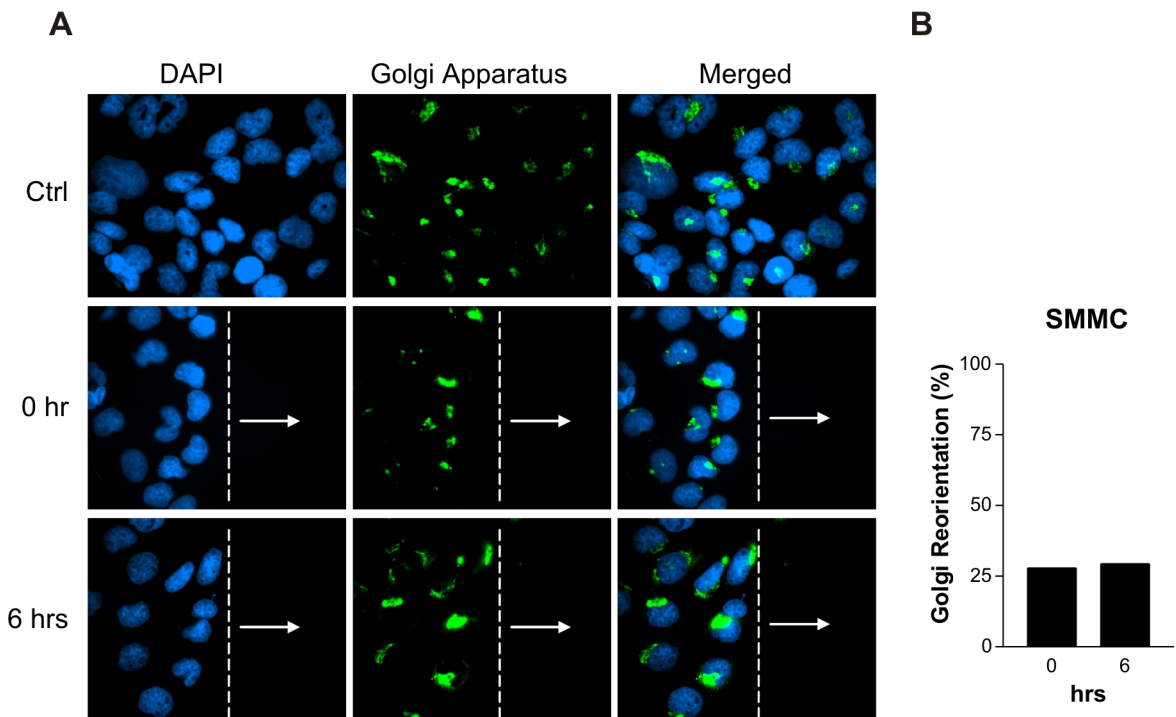


Figure 4.20 SMMC-7721 cells did not exhibit golgi reorientation 6 hours after wound creation

A wound was created on confluent SMMC-7721 cells. Cells were fixed and stained at the given time points (0 hour, 6 hours). Unscratched SMMC-7721 cells were used as control (Ctrl). The nuclei were stained with DAPI (blue) whilst the Golgi apparatus were stained with lectin (green). Arrows marked the direction of movement. (B) Percentage of cells that exhibited golgi reorientation was shown in the graph. 86-126 wound edge cells were counted at different time points. There was no significant difference between the percentage of cells that exhibited Golgi reorientation to the front of the nucleus towards the direction of movement at 0 hour time point and 6 hours time point.

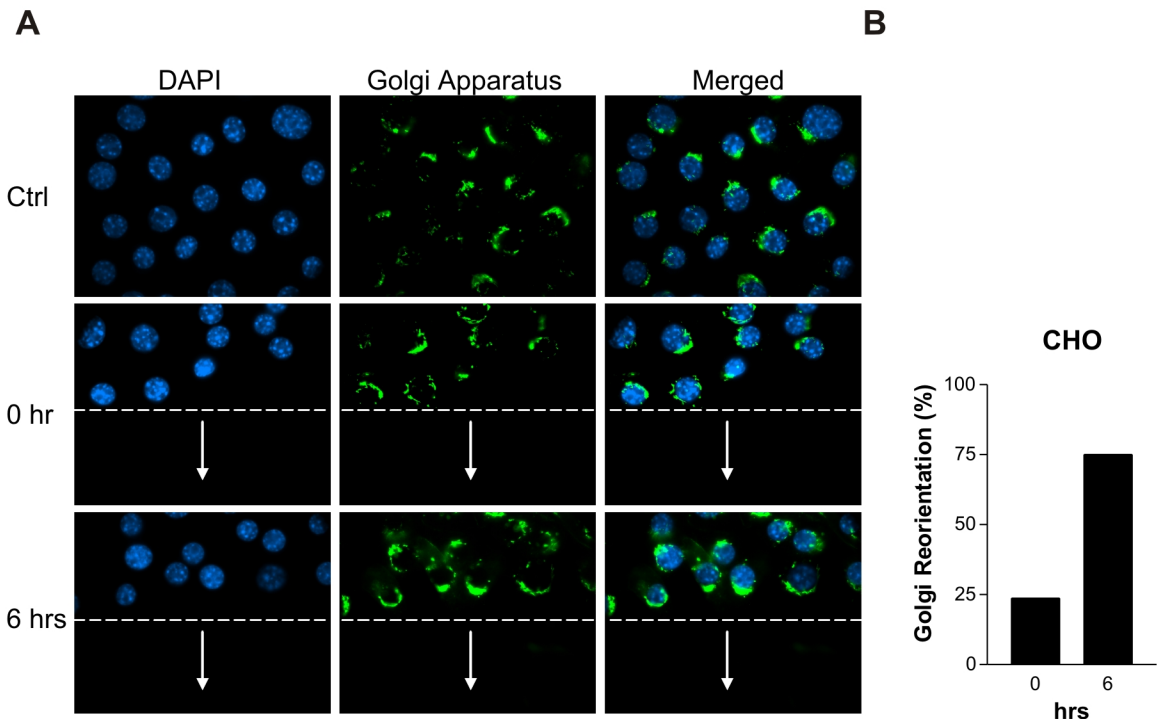
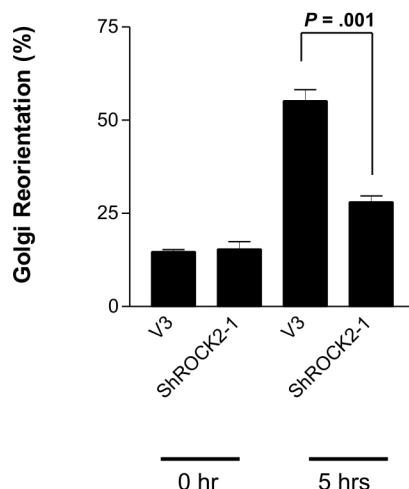
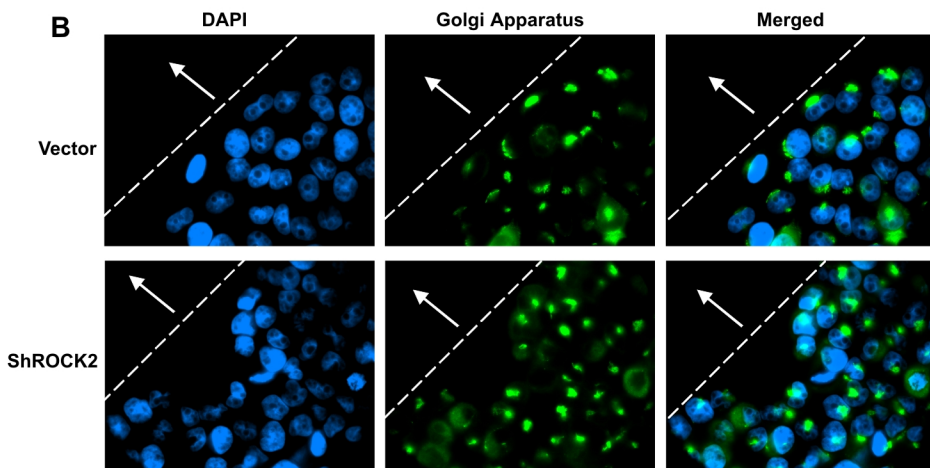


Figure 4.21 CHO cells exhibited golgi reorientation 6 hours after wound creation

(A) A wound was created on confluent CHO cells. Cells were fixed and stained at the given time points (0 hour, 6 hours). Unscratched CHO cells were used as control (Ctrl). The nuclei were stained with DAPI (blue) whilst the Golgi apparatus were stained with lectin (green). Arrows marked the direction of movement. (B) Percentage of cells that exhibited golgi reorientation was shown in the graph. 97-114 wound edge cells were counted at different time points. There was remarkable increase of cells that exhibited Golgi reorientation to the front of the nucleus towards the direction of movement at 0 hour time point and 6 hours time point.

A

0 hr 5 hrs

B**Figure 4.22 Knockdown of ROCK2 suppressed HCC cell polarity**

(A) Percentage of cells exhibited the repositioning of their Golgi to the front of the nucleus towards the direction of movement at a given time point after wounds were created. A range of 353-737 cells in total were counted for each column. Error bars represent SEM obtained from three independent experiments. (B) Representative pictures of Golgi repositioning 5 hours after wound was created in BEL7402 vector control transfectant (V3) (top panel) and BEL7402 ShROCK2 stable transfectant (ShROCK2-1) (bottom panel). The Golgi apparatus was stained with lectin HPA Alexa Fluor 488 conjugates (green) and the nuclei were stained with DAPI (blue). The wounds were marked with white lines and arrows indicate the direction of cell movement. The BEL7402 ShROCK2 stable transfectant (ShROCK2-1) showed significant reduction in the ability of the Golgi apparatus to realign to the front of the nuclei at the direction towards the wound, as compared with the BEL7402 vector control transfectant (V3) 5 hours after the wound was created.

4.4 Discussion

In this study, we found that ROCK2 was frequently overexpressed in human HCC. Importantly, overexpression of ROCK2 significantly correlated with tumor microsatellite formation in human HCCs, which is a pathologic feature of intrahepatic metastasis in HCC. Furthermore, we found that overexpression of ROCK2 promoted HCC cell motility and invasiveness of HCC cells *in vitro*. This mirrored the findings of ROCK2 overexpression in human HCC samples and its association with more frequent tumor microsatellite formation. Reversely, when we knocked down the endogenous ROCK2 specifically by short hairpin RNA approach in HCC cells, the mobility and invasiveness of HCC cells were significantly reduced, indicating that ROCK2 is closely involved in HCC invasion. Importantly, our *in vivo* animal model using orthotopic liver implantation also confirmed that ROCK2 was associated with tumor invasiveness and (pulmonary) metastasis. The specific roles of ROCK2 in HCC have never been addressed and thus our findings are of significance. Reduction of ROCK2 expression might be a potential target for antagonizing tumor metastasis in HCC.

Studies have shown that inhibition of Rho-kinase activity by ROCK specific inhibitor Y27632 could suppress HCC cell migration, invasiveness and intrahepatic metastasis of HCC (47-49), as well as tumor recurrence after liver transplantation (156). Nevertheless, Y27632 inhibits the kinase activity of both ROCK1 and ROCK2 and even other kinases; therefore, ROCK inhibitor does not specifically distinguish the contributions of ROCK1 and ROCK2 in hepatocarcinogenesis. From the parallel examination of ROCK1 and ROCK2 protein expression in human HCC, we found the particular significance of



ROCK2 in human HCC. This would shed light into the development of more specific anti-HCC drugs that target ROCK2 exclusively.

The two members of the Rho-kinases family, ROCK1 and ROCK2, share 65% sequence homology in amino acid level (113). Although ROCK1 and ROCK2 were both identified as the downstream targets of RhoA (51, 53), mounting studies have confirmed that they are regulated and processed by different participants and not functionally redundant (66, 67, 69). Knockout mice models have provided significant evidence distinguishing their individual physiological roles. ROCK1 and ROCK2 homozygous knockout (ROCK1^{-/-} and ROCK2^{-/-}, respectively) mice displayed distinct phenotypes. ROCK1^{-/-} mice manifested EOB (eyelid open at birth) and omphalocele phenotypes (149), whilst ROCK2^{-/-} mice manifested not only EOB, but also thrombus formation, placental dysfunction, and intrauterine growth retardation (150). Furthermore, most ROCK2^{-/-} mice were embryonic fatal (150), whereas most ROCK1^{-/-} mice could survive till adulthood (149). On top of this growing body of evidence, the present study adds a new layer of evidence showing a distinctive role of ROCK2 in human HCC. This indicates that, among the two members of Rho-kinases family, ROCK2 may play a more important role in hepatocarcinogenesis.

Many studies have evidenced and depicted the roles of Rho/ROCK pathway in the regulation of cytoskeletal events. Rho/ROCK pathway is indispensable for cell movement including the coordination of actomyosin contraction (69), rear end retraction (110), turnover of focal adhesions, and formation of stress fibers in fibroblasts (40).



Hereinbefore, our data substantiated that ROCK2 was a key mediator regulating the phosphorylation of MYPT1 and thereby actomyosin contraction. We further demonstrated that specific knockdown of ROCK2 in BEL7402 significantly suppressed the formation of stress fiber, filopodia, membrane blebs, and establishment of cell polarity. The establishment of cell polarity is important for a cell to move to a designated direction with cooperation of continuous actin polymerization and depolymerization that allow the cell to protrude at the anterior front, undergo consecutive actomyosin contractions, and de-adhere from the posterior end. Formation of stress fiber, filopodia and membrane blebs all require actin polymerization, and loss of these features is indicative of inability in actin polymerization. Altogether, our data have demonstrated that ROCK2 is important for the multiple events in HCC cell migration.

Taken together, ROCK2 was overexpressed in human HCCs and this overexpression was associated with a more aggressive biologic behavior. Our results showed that ROCK2, specifically, played a significant role in HCC progression and invasion by regulating cytoskeletal reorganizations and enhancing the invasive and motility properties of HCC cells both *in vitro* and *in vivo*.



4.5 Summary

Deregulation of Rho family small GTPases has been implicated in human carcinogenesis. Rho-kinases are downstream effectors of Rho GTPases in the regulation of cytoskeletal reorganization and cell motility. However, their functions in human cancers remain elusive. In this study, we aimed to investigate the role of Rho-kinases in HCC tumor progression and metastasis. We first examined the expression of the two members of Rho-kinases, ROCK1 and ROCK2, in human HCC, and found that ROCK2 was frequently overexpressed in primary HCCs (22/41, 53.66%). Clinicopathologic analysis revealed that overexpression of ROCK2 was significantly associated with the presence of tumor microsatellite formation ($P = .005$), suggesting that deregulation of ROCK2 may contribute to the intrahepatic metastasis of HCC. Consistently, we demonstrated that stable overexpression of ROCK2 significantly enhanced cell motility and invasiveness in HCC cells. Reversely, stable knockdown of ROCK2 by shRNA approach remarkably reduced HCC cell migration and invasion. Moreover, using orthotopic liver xenograft models, we further demonstrated that stable knockdown of ROCK2 suppressed HCC invasion and metastasis *in vivo*. Stable knockdown of ROCK2 in HCC cells significantly inhibited Golgi reorientation, myosin phosphatase phosphorylation, and formation of stress fibers, filopodia and membrane blebs; these molecular and cellular events are crucial for cell motility and cancer metastasis. In summary, our results indicated that ROCK2 was overexpressed in human HCCs and this overexpression was associated with a more aggressive biological behavior. Our findings also demonstrated that ROCK2 played a significant role in regulating cytoskeletal events and contributed to the metastasis of HCC.



Chapter 5

Post-transcriptional Regulation of ROCK2 in HCC

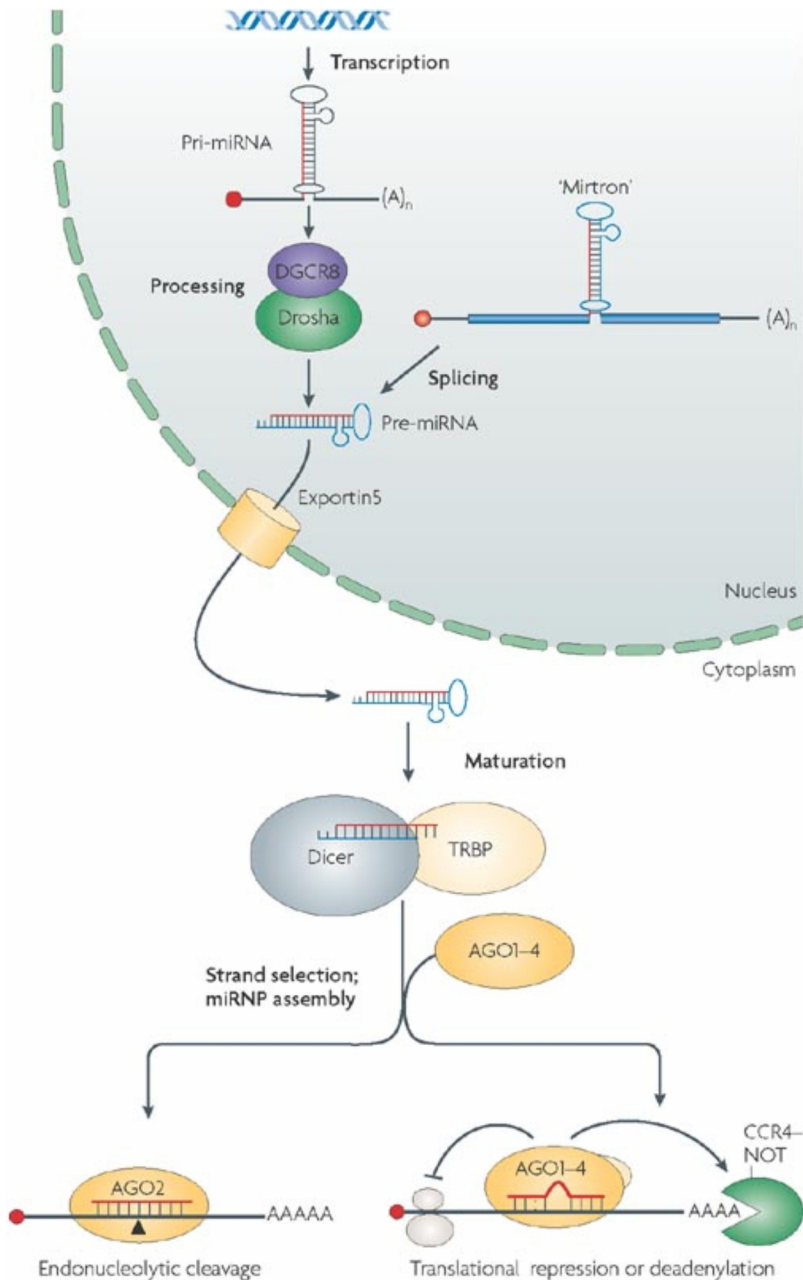
5.1 Introduction

In Chapter 4, we demonstrated that ROCK2 was significantly associated with aggressive tumor behavior in HCC. Overexpression of ROCK2 in HCC enhanced HCC cell migratory and invasive ability. Knockdown of ROCK2 profoundly suppressed invasive features of HCC including venous invasion, microsatellite tumor formation, and incidence of lung metastasis *in vivo* in the orthotopic liver nude mouse model. Interestingly, overexpression of ROCK2 in human HCC was found only in the protein level but not in the mRNA level (Figure 4.1, 4.2, 4.4). This finding suggested a possible post-transcriptional deregulation of ROCK2 expression in human HCC. Recently, a group of non-coding RNAs, microRNAs, was identified to regulate gene expression post-transcriptionally and was found to be often deregulated in human cancers. Hence, we aimed to explore the post-transcriptional deregulation of ROCK2 in HCC and to investigate the potential microRNAs that were involved in this mechanism.

5.1.1 MicroRNA Biogenesis

MicroRNAs (miRNAs) belong to a class of non-coding RNAs controlling gene expression. miRNAs are transcribed by RNA polymerase II and the initial transcript is called the primary miRNA (pri-miRNA) (Figure 5.1) (157). In the nucleus, Drosha, a





(Filipowicz W et al. Nature Genetics. 2008) (161)

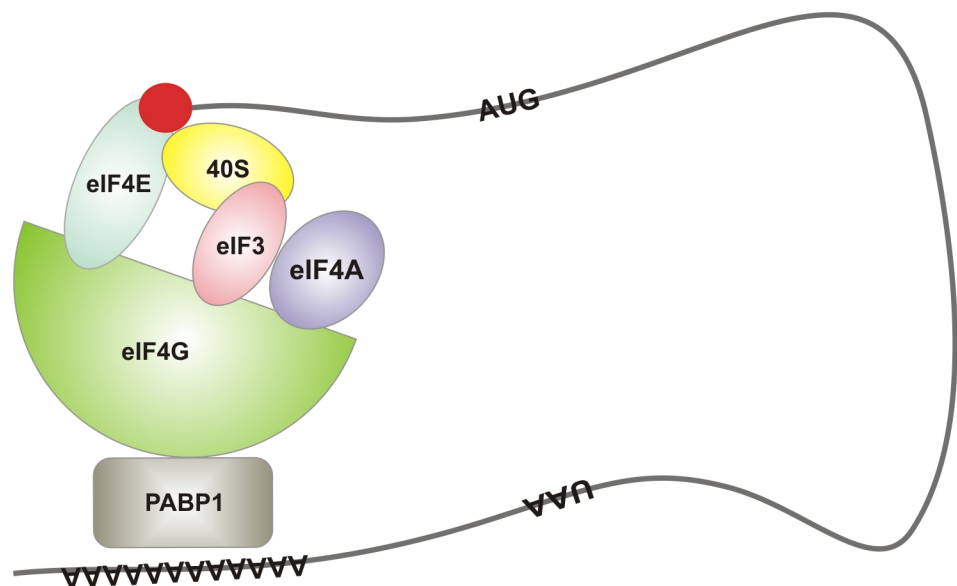
Figure 5.1 Biogenesis of microRNAs

microRNAs (miRNAs) derived from precursor molecules (pri-miRNAs). One pri-miRNA is comprised of a couple of sequences of separate miRNAs. The Drosha-DGCR8 complex cleaves pri-miRNAs to pre-miRNAs (~70 nucleotides). Pre-miRNAs are exported to the cytoplasm by exportin 5. In the cytoplasm, pre-miRNAs are further cleaved by Dicer into double stranded miRNAs (~20 nucleotides). One strand of the miRNA functions as the mature miRNA which associates with the proteins of Argonaute (AGO) family and forms miRNA-induced silencing complex (miRISC). miRISC binds to its target binding sites and initiates either endonucleolytic cleavage (more often in plants with perfect matches) or translational repression (more often in mammals which imperfect matches).



ribonuclease, cleaves the pri-miRNA into precursor miRNA (pre-miRNA) hairpin of about 90 nucleotides in size (Figure 5.1) (158). Pre-miRNA is then exported to the cytoplasm by exportin 5. Then, pre-miRNA is digested by Dicer, RNaseIII, into mature miRNA (159). Mature miRNAs are short single stranded RNAs, approximately 18-25 nucleotides long, incorporate into miRNA induced silencing complex (miRISC) (160), forming perfect or imperfect matches with the 3'UTR of their target mRNAs, causing mRNA degradation or translational repression, respectively (Figure 5.1). Argonaute (Ago) protein is the key catalytic component of the miRISC and is responsible for mRNA degradation or translational repression. Ago possesses endonucleolytic activity against the complementary mRNA strands for direct cleavage (161). Also, Ago was reported to be responsible for translational repression (161). In fact, the precise mechanisms to elucidate how imperfect match of mature miRNA and 3'UTR of mRNA induces translational repression are still elusive. Several groups provided evidence for potential explanations of such phenomenon. It was reported that Ago protein competed with eukaryotic translation initiation factor 4E (eIF4E) for the 5'-terminal 7-methylguanosine cap (5' cap) binding and suppresses the translation of capped mRNAs (162, 163). Besides, Filipowicz W *et al.* suggested that miRISC complex enhanced deadenylation of the poly A tails of the mRNAs which would abolish the binding between 3' poly A tail and the 5' cap of the mRNA (161). The interaction of 3' poly A tail and the 5' cap is important for translation because subunit of eIF, eIF4E, binds to the 5' cap of the mRNA and another subunit of eIF, eIF4G, interacts with the 3' poly A tail (Figure 5.2). The mRNA circularization stimulates translation initiation and recycling of ribosomes (164, 165). Therefore, the miRISC complex abolished the circularization of the mRNA and





(Modified and redrawn from Filipowicz W et al. Nature Genetics. 2008.) (161)

Figure 5.2 Interaction of 5' cap and 3' poly A tail induced circularization of mRNA

Initiation of translation of mRNA begins when eukaryotic initiation factor (eIF) 4E subunit binds to the 5' terminal 7-methylguanosine cap (5' cap) (red circle). eIF4G subunit acts as a scaffold for recruitment of other translation initiation complex subunits such as eIF3, eIF4A, and 40S. eIF4G interacts with the poly (A) binding protein (PABP1) which binds to the 3' poly (A) tail of the mRNA strand. This interaction circularizes the mRNA to stimulate translation initiation and facilitate the recycling of ribosomes. The interaction between miRNA and the 3'UTR of its target gene may affect the circularization of the mRNA and the translational efficiency.

reduced eIF4E binding affinity for the mRNA and suppressed translation (161, 166). In plants, miRNAs usually form perfect complementary base pairing with the target mRNAs and induce endonucleolytic mRNA cleavage (161). In animals, miRNAs generally form imperfect complementary base pairing with the target mRNAs. Therefore, it is believed that miRNAs mainly regulate gene translation in animals (161).

5.1.2 MicroRNA and Cancers

miRNAs are found to direct a wide repertoire of biological mechanisms such as cell cycle control, apoptosis, cell proliferation, cell polarity, and cell migration. Genome wide miRNA profiling has revealed that each type of cancer harbors a differential profile of miRNA expressions (167). Accumulating studies demonstrated that miRNAs contributed to the aberrant gene expression in cancer initiation and progression. For example, let-7, a miRNA suppressed RAS expression, was shown to act as tumor suppressor in lung cancer (168). miR203 suppressed BCR-ABL fusion protein expression and acts as the tumor suppressor in T cell lymphoma (169). Moreover, underexpression of miR223 was demonstrated to contribute to HCC and miR223 was shown to downregulate stathmin1, a microtubule destabilizing protein important for mitotic spindle formation (2). Furthermore, in HCC, miR21 was found to suppress PTEN expression and was shown to act as an oncogene in HCC (170). In addition to oncogene and tumor-suppressor gene expression, studies evidenced that miRNAs also modulate metastatic gene expression. For example, miR10b, a miRNA upregulated by Twist, promoted breast cancer cell invasion through inhibition of homeobox D10 causing upregulation of RhoC (171), a member of the Rho family involved in cancer metastasis (172). A recent study



demonstrated that loss of miR-200 expression enhanced cancer cell migration and invasion because miR-200 could inhibit expression of E-cadherin repressor, zinc finger E-box binding homeobox (ZEB), leading to inhibition of epithelial mesenchymal transition (173).

5.1.3 MicroRNA Signature in HCC

The first comprehensive study to examine the implications of miRNAs and HCC was performed by microarray study using synthetic probes corresponding to 180 mature human miRNAs and 206 precursor human miRNAs to compare the expression profiles of 25 pairs of HCC and their corresponding non-tumorous livers (174). It was shown in this array data that HCC and non-tumorous liver tissues exhibited distinct miRNA expression profiles (174). Specifically, the miRNA profiles of livers of chronic hepatitis and cirrhosis were shown to be significantly different. Furthermore, the underexpression of several miRNAs was found to be associated with poorly differentiated HCC (174). Recently, a more comprehensive study on the miRNA profiles of 241 pairs of HCC and their corresponding non-tumorous livers was performed (175). This study further revealed a distinct metastatic signature of 20 miRNAs that could differentiate tissues with venous metastasis from metastasis-free solid HCC by supervised algorithm and a clinically well-defined cohort of 131 cases (175). Furthermore, this distinctive metastatic signature was also found to be correlated with survival and relapse in HCC patients (175).



5.1.4 Objectives

As aforementioned, ROCK2 expression was deregulated in the protein level but not in the mRNA level in HCC. It is logical to speculate that ROCK2 expression was deregulated in a translational manner. miRNAs could induce translational repression by forming imperfect matches with the 3'UTR of their target genes and deregulation of miRNAs as abovementioned is undoubtedly associated with cancer development. We therefore undertook the investigation on the potential translational regulation of ROCK2 expression by miRNAs in HCC. By *in silico* study, we analyzed the 3'UTR of ROCK2 and searched for the miRNAs that potentially interact with ROCK2. Next, we aimed to validate the effects of the potential miRNAs on ROCK2 expression by overexpression of the identified miRNAs in HCC cells. We aimed to validate the expression level of these identified miRNAs in human HCC and investigate whether there is an inverse correlation of ROCK2 protein expression in human HCC. Since we found that ROCK2 was closely associated with aggressive HCC, we also aimed to further analyze the expression of these miRNAs and the clinicopathologic correlation in HCC patients to see whether their expression is associated with aggressive HCC behaviors. Besides clinicopathologic statistical analysis, we wished to investigate whether these miRNAs are further deregulated in metastatic HCC tissues.



5.2 Materials and Methods

5.2.1 Luciferase Reporter Assay

5×10^4 PLC cells were seeded onto wells of the 24 well plate overnight. Cells were transfected with 1.33 µg of total DNA plasmids including Renilla luciferase plasmid and Firefly luciferase plasmid in 1:100 ratio with 2 µL Fugene 6 transfection reagent. 48 hours after transfection, luciferase assay was performed by Dual-luciferase Reporter Assay System (Promega, Madison, WI, USA). Three independent transfections were performed in each experiment and three independent experiments were performed. Cells were lysed with 100 µL 1X passive lysis buffer for 15 minutes at room temperature in the shaker. 20 µL of the cell lysates were loaded onto luciferase 96 well plate for luciferase reporter assay. Luciferase Assay Reagent II and Stop & Glo Reagent were prepared as indicated in the manufacturer's protocol and were diluted 1:1 with H₂O for assay. 50 µL of diluted Luciferase Assay Reagent II and 50 µL of Stop & Glo Reagent were used for the assay. Firefly luciferase reading was normalized with the corresponding Renilla luciferase reading.

5.2.2 Bioinformatics

Algorithms from TargetScan 4.2 (<http://www.targetscan.org>) and miRanda (<http://www.microrna.org>) were employed to predict the human miRNAs that target the 3' untranslated region of ROCK2. It was further assessed and verified under the criteria suggested by Filipowicz W *et al* (161).



5.2.3 Cell Lines, Plasmids, microRNA Precursors, and Drug Treatment

Human HCC cell lines BEL7402, SMMC-7721, PLC/PRF/5 were employed in this study. miRNA precursor of hsa-miR139 were purchased from Dharmacon. pRL-CMV Vector (Promega) which carries Renilla Luciferase reporter gene and pCDNA3.1 (+) Hygro Firefly Luciferase Vector which carries Firefly Luciferase reporter gene were used in Luciferase Assay. pCDNA3.1 (+) Hygro Firefly Luciferase Vector was constructed by subcloning the Firefly Luciferase reporter gene from pSP-luc+NF Fusion Vector (Promega) to pCDNA3.1 (+) Hygromycin Vector (Invitrogen) by KpnI and XhoI digestion. Full length of ROCK2 3'UTR was PCR amplified from normal liver cell line, LO2, and was subsequently cloned into pCDNA3.1 (+) Hygro Firefly Luciferase construct via XhoI digestion. Orientation and sequence were confirmed by DNA sequencing. For MG132 (Calbiochem) treatment, 2×10^5 BEL7402 cells were seeded onto 6 well plates overnight. For time point treatment, cells were treated with 10 μM MG132 for 0, 6, 18 hours. For dosage treatment, cells were treated with 0 μM , 5 μM , 10 μM , 20 μM , 30 μM for 6 hours.

5.2.4 HCC Patient Samples and Microdissection

Human HCC and their corresponding non-tumorous liver samples were collected at the time of surgical resection at Queen Mary Hospital, The University of Hong Kong from 1991 to 2008. All samples for RNA extraction, after collection from surgical resection, were snapped frozen in liquid nitrogen before storage at -80°C as previously described in Chapter 2. The samples for paraffin embedding were fixed in 10% formalin. Venous invasion in HCC was confirmed by pathologist (IOL Ng) and paraffin slides were



dewaxed in 100% xylene repeatedly 3 times followed by stepwise rehydration in 100% EtOH, 95% EtOH, 80% EtOH, 50 % EtOH, and H₂O sequentially. Slides were slightly stained with hematoxylin and rinsed in H₂O. The HCC cells which had invaded into the veins as tumor thrombi were microdissected by a 27-gauge needle under the dissecting microscope and were resuspended in RNase free H₂O. Corresponding tumorous and non-tumorous liver tissues were microdissected in parallel with the venous tumor thrombus samples. Extrahepatic metastases were confirmed by pathologist and the tumor cells were microdissected with a 27-gauge needle under microscope. Corresponding tumorous and non-tumorous liver tissues were isolated in parallel with the extrahepatic metastasis samples.

5.2.5 Clinicopathologic Correlation and Statistical Analysis

The clinicopathologic features of the patients were analyzed by SPSS for Windows 14.4. Fisher's exact test was used for the analysis of categorical data, whereas independent *t* test was used for continuous parametric data. Mann Whitney *U* test was used for continuous non-parametric data. Tests were considered significant when the *P* value was less than .05. The clinicopathologic features of the patients analyzed included tumor size, cellular differentiation according to the Edmondson grading, venous invasion without differentiation into portal or hepatic venules, direct liver invasion, tumor microsatellite formation, tumor encapsulation, cirrhosis, and serum hepatitis B surface antigen (HBsAg) status, as described previously (152). HCC patients samples (tumorous and non-tumorous livers) and normal liver samples were further categorized into normal liver with no



disease background, liver with chronic hepatitis, liver with cirrhosis (cirrhotic liver), liver of stage I/II HCC, and liver of stage III/IV HCC according to patients' record.

5.2.6 microRNA Extraction and microRNA Reverse Transcription and microRNA Real-time Quantitative PCR

miRNA extraction from frozen tissues was performed by TRIZOL Reagent (GIBCO) as described. miRNA extraction from paraffin sections was performed by 95°C 10 minutes heat boiling in H₂O or by miRNeasy FFPE Kit (Qiagen) and concentration of RNA was detected by Quant-iTTM RiboGreen RNA kit (Invitrogen) according to manufacturers' guidelines. Reverse transcription was performed by Taqman® MicroRNA Reverse Transcription (RT) Kit (Applied Biosystems) according to manufacturer's protocol. In general, 10 ng of RNA was added for each miRNA reverse transcription reaction with the addition of 1X miRNA specific primers, 1X RT buffer, 15 mM dNTPs, 3.8 unit of RNase inhibitor, 50 unit MultiScribe RT enzyme. Reactions were kept on ice for 5 minutes and RT was performed at 16°C for 30 minutes, 42°C for 30 minutes, 85°C for 5 minutes. Expression level of mature miR-139 was examined by real time quantitative PCR with Taqman® MicroRNA Assays (Applied Biosystems) in 7900HT Fast Real-Time PCR System (Applied Biosystems). Each reaction was set up with the addition of 1X Taqman universal PCR master mix buffer, 1X Taqman miRNA RT probe, and 1.33 μL of the miRNA RT product.



5.3 Results

5.3.1 3'UTR of ROCK2 Regulated Translational Control of Gene Expression

miRNAs are small non-coding RNAs that can affect the translational control of tumor progression by interaction with the 3' UTRs of their target genes without influencing the mRNA expression level. Therefore, we first wished to examine whether the 3'UTR region of ROCK2 could regulate gene translation. In this regard, we employed the Luciferase reporter assay to examine the effect of the 3'UTR of ROCK2 in gene translation. 3'UTR of ROCK2 was inserted to the end of the Firefly luciferase construct that was driven by a CMV promoter. 3'UTR of ROCK2 profoundly suppressed Firefly Luciferase activity as compared to the vector control in HCC cell line, PLC/PRF/5 up to 6.73 fold (Figure 5.3). As implicated by the decrease of Luciferase reporter activity, this demonstrated that 3'UTR of ROCK2 could regulate gene expression in a translational level.

5.3.2 Expression of ROCK2 was Deregulated in Post-transcriptional Level and miR139 Potentially Targets 3' Untranslated Region (3'UTR) of ROCK2

We demonstrated that ROCK2 was overexpressed in human HCC in protein but not in mRNA level. This suggested a post-transcriptional modification of ROCK2 proteins in human HCC (Chapter 4). Since we confirmed that the 3'UTR of ROCK2 exhibited inhibitory function in gene translation, we next aimed to investigate the potential



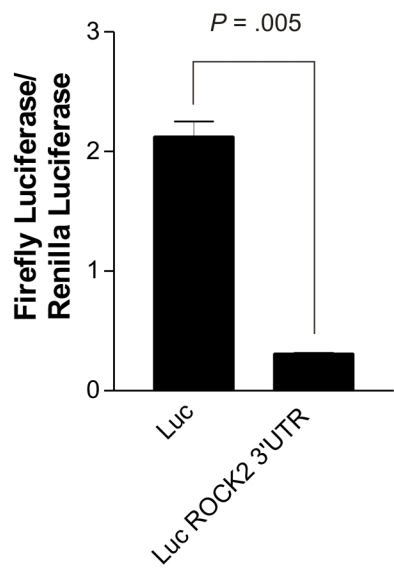
A**B**

Figure 5.3 The 3' Untranslated Region (3'UTR) of ROCK2 suppressed gene translation

(A) 3' UTR of ROCK2 was inserted into Firefly luciferase plasmid as shown. (B) PLC cells were transfected with Firefly luciferase empty vector (Luc) and Firefly luciferase ROCK2 3'UTR (Luc ROCK2 3'UTR). Renilla luciferase vector was transfected with firefly luciferase vectors in 1:100 ratio as transfection control. 3'UTR of ROCK2 significantly suppressed firefly luciferase reading for 6.73 fold. Error bar represents SEM from three independent transfections.

miRNAs that are involved in regulating the aberrant expression of ROCK2 in HCC. To this end, we performed *in silico* study to find the miRNAs that potentially target the 3'UTR of ROCK2 by bioinformatics algorithms, TargetScan and miRanda. From these two algorithms, miR139 was the miRNA commonly computed by the two programs to target position 1156-1163 bp of ROCK2 3'UTR. We further verified the binding possibility according to the principles suggested by Filipowicz W *et al* (161) (Figure 5.4). First, miR139 formed perfect and contiguous base pairing with 3'UTR of ROCK2 at (1156 -1163 bp) from miRNA nucleotides 1-8 which satisfied the criteria of the seeding region (Figure 5.4). This seeding region was predicted to initiate the miRNA and mRNA interaction (161). Second, bulge, formed by base pairing mismatches, was found in the central region of the miRNA-mRNA duplex (Figure 5.4) and this bulge was expected to prevent endonucleolytic cleavage of mRNA mediated by Ago protein (161). Third, the 3' end of miR139 was partially complementary to the mRNA of ROCK2 3'UTR. Nucleotides 14-18 of miR139 are complementary to the mRNA of ROCK2 3'UTR (1151-1155 bp) (Figure 5.4) and this was believed to further stabilize the miRNA and mRNA interaction (161).

5.3.3 Overexpression of miR139 Caused a Decrease in ROCK2 Protein Expression and Suppressed HCC Cell Migration and Invasion

Since we hypothesized that the overexpression of ROCK2 protein in human HCC is associated with the downexpression of miR139, we tested the effect of miR139 on ROCK2 protein expression in HCC cell line. Thus, we transiently transfected miR139 precursor into SMMC-7721 cells. Overexpression of miR139 precursor into SMMC-7721



A



B

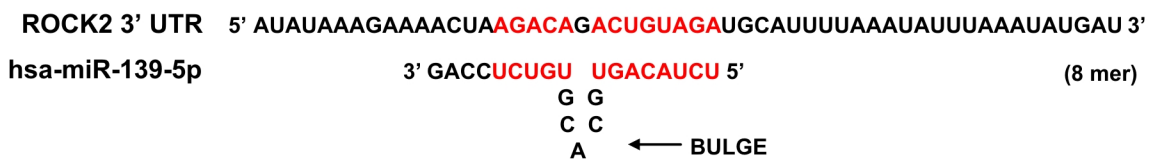


Figure 5.4 Predicted binding site of miR139 on the 3'UTR of ROCK2

In silico study demonstrated that miR139 has the potential binding sequence of 3'UTR of ROCK2. The 1-8 nucleotides of miR139 forms the seeding binding with 3'UTR of ROCK2 at 1156-1163 bp, followed by a bulge formation of the 9-13 nucleotides of the miR139, followed by perfect match of 14-18 nucleotides of miR139 at 1151-1155 bp of the 3'UTR ROCK2.

HCC cells (Figure 5.5A) resulted in a slight reduction of ROCK2 protein expression (Figure 5.5B). This finding supported that ROCK2 protein expression was associated with miR139 expression in HCC cell system. Since ROCK2 controlled HCC cell migration and invasion as demonstrated in Chapter 4 and its expression was negatively associated with miR139, we hypothesized that miR139 antagonistically regulated HCC cell migration through downregulation of ROCK2. Hence, we tested the migratory and invasive abilities of HCC cells upon miR139 overexpression. Overexpression of miR139 precursor substantially suppressed the invasive ability of HCC cells, SMMC-7721, as indicated by the decrease of invaded cells (Figure 5.6). To further verify whether miR139 regulates HCC cell migration through ROCK2, we made use of a HCC cell line which ROCK2 was knocked down via short hairpin approach (BEL7402 ShROCK2-1). Overexpression of mature miR139 profoundly impeded cell migration in BEL7402 vector control cells (BEL7402 V3) but failed to impede cell migration in BEL7402 ShROCK2-1 cells. The cell line devoid of ROCK2 was insensitive to miR139 overexpression in cell migration, further demonstrated that miR139 suppressed HCC cell migration via ROCK2 (Figure 5.7).

5.3.4 Expression of miR139 in HCC Inversely Correlated with Expression of ROCK2 Protein in Human HCC Samples

In HCC cell models, we demonstrated that 3'UTR of ROCK2 regulated gene expression in a translational manner and overexpression miR139 downregulated ROCK2 protein expression. Next, we analyzed the correlation of miR139 and ROCK2 protein expression in human HCC samples. Therefore, we examined the expression of mature form miR139



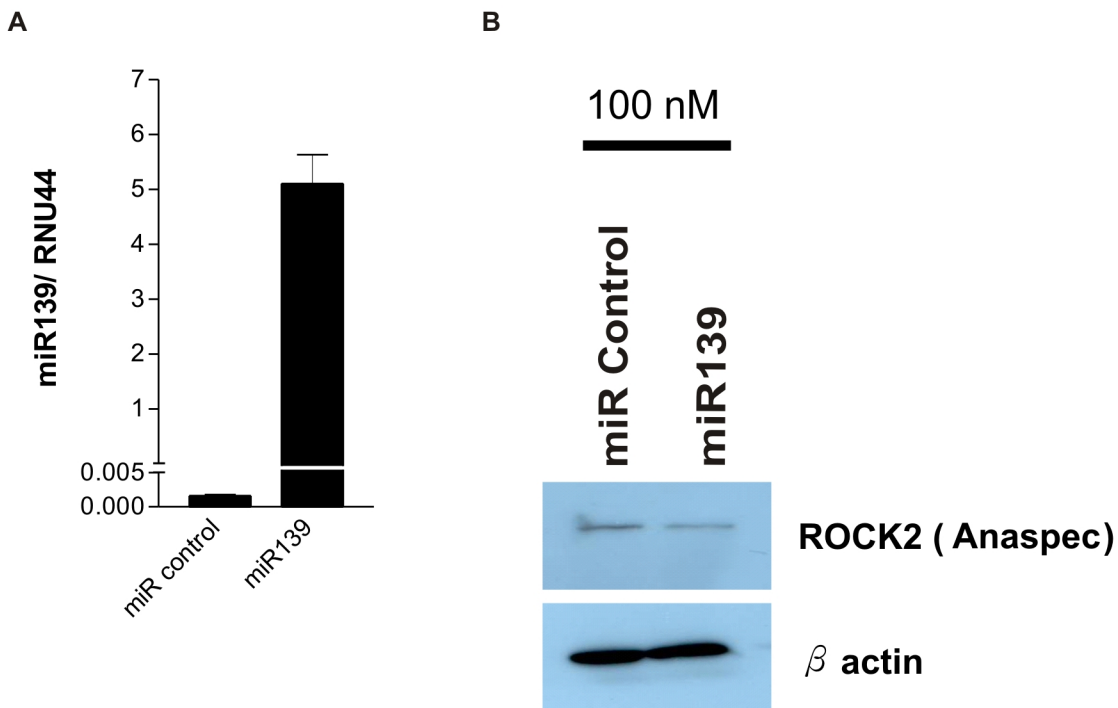


Figure 5.5 miR139 suppressed ROCK2 protein expression

(A) miR139 mimic (precursor) was transfected into SMMC cells for 48 hours. Real-time quantitative PCR confirmed miR139 mimic transfected cells exhibited 3700 fold mature form miR139 more than the miR control transfected cells. (B) miR139 mimic transfected cells exhibited a decreased of ROCK2 protein expression as shown in the Western Blot.

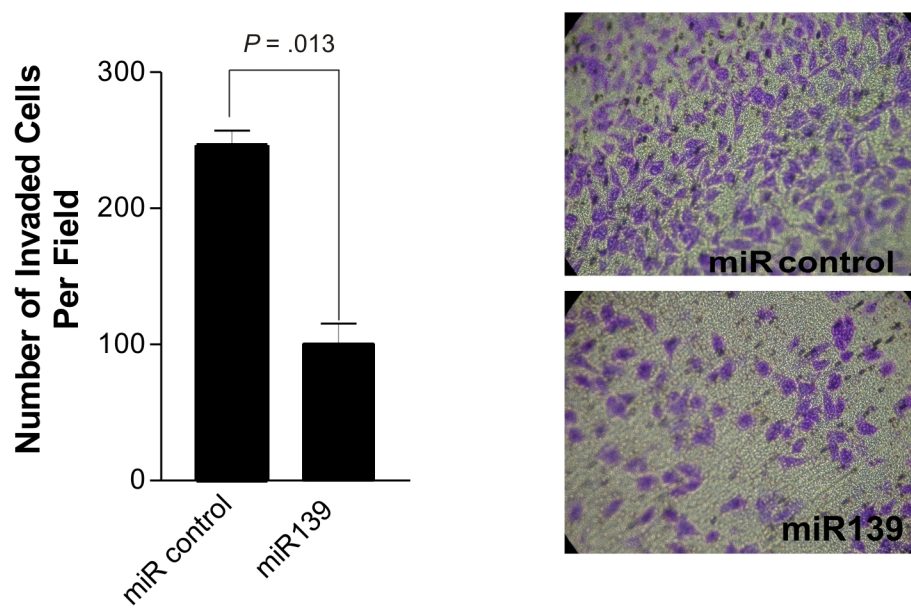


Figure 5.6 miR139 suppressed HCC cell invasion

3×10^5 SMMC cells were seeded onto Matrigel coated invasion chamber and allowed to invade for 24 hours. The number of invaded cells was significantly reduced in miR139 overexpressed (miR139) as compared with control (miR control). Error bars represent SEM.

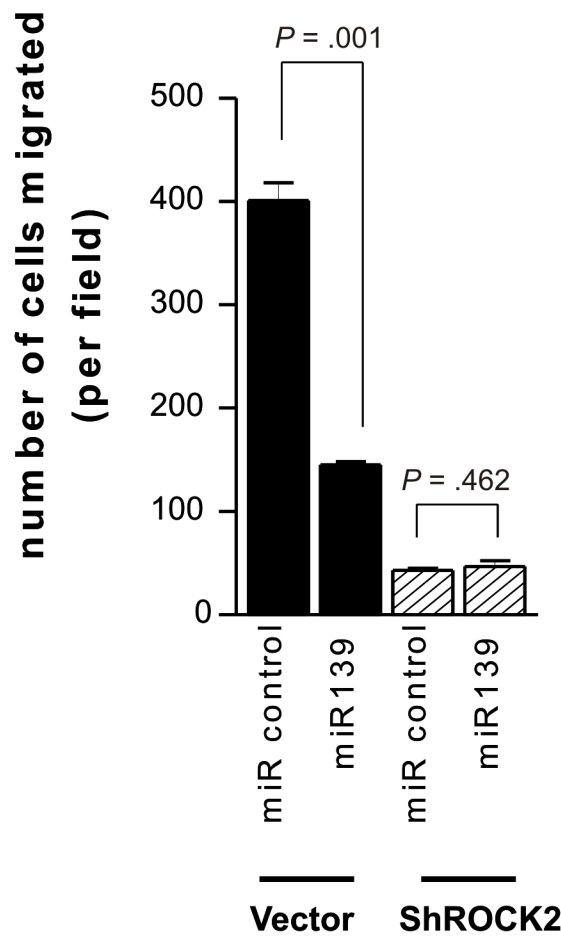
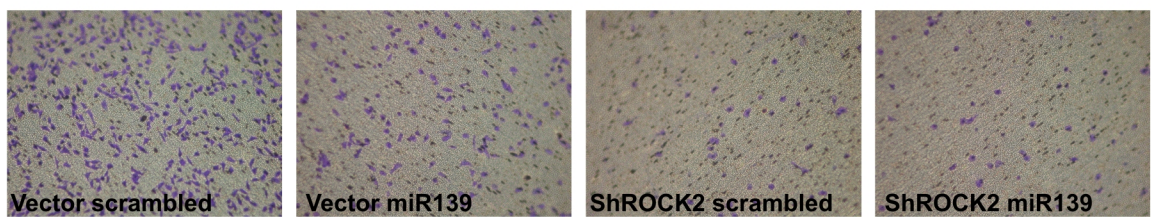


Figure 5.7 miR139 could not suppress cell migration in ROCK2 knockdown HCC cells

5×10^4 BEL7402 cells were seeded onto transwell chamber and allowed to migrate for 16 hours. The number of migrated cells was significantly reduced in miR139 overexpressed (miR139 mimic) as compared with control (miR control) in BEL7402 vector cell line. Overexpression of miR139 did not affect cell migration in BEL7402 ShROCK2 cell line. Error bars represent SEM.

in our paired human HCC samples by real-time quantitative PCR. Among 67 pairs of HCC cases we tested, 77.8% of the patients expressed at least 4 fold decrease of miR139 expression in the tumorous livers as compared to the corresponding adjacent non-tumorous livers ($P < .001$, Mann Whitney U test) (Figure 5.8). We then correlated the expression of miR139 and protein expression of ROCK2 in our human HCC samples by statistical analysis. We found that underexpression of miR139 mature form was closely associated with ROCK2 protein overexpression in human primary HCC ($P = .03$) (Table 5.1).



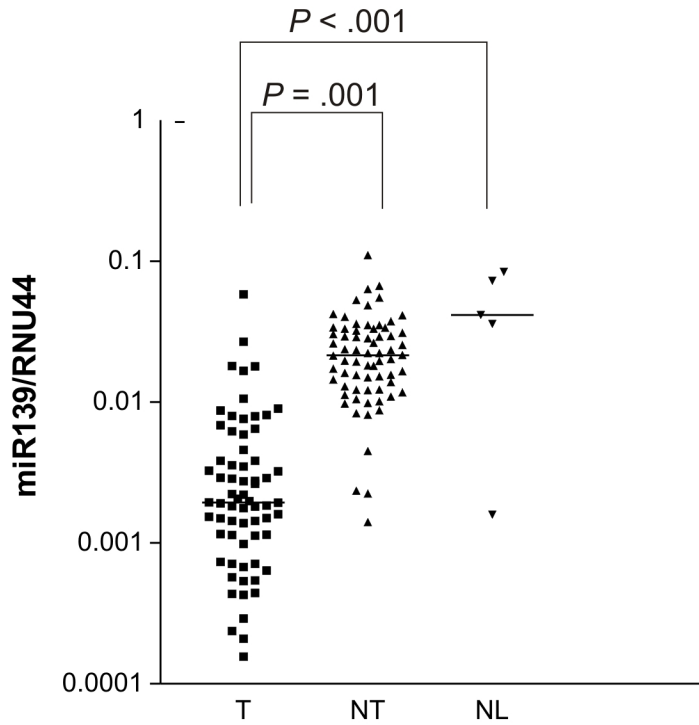


Figure 5.8 Underexpression of miR139 in HCC

Mature miR139 expression was assessed in 68 paired HCC samples (T: tumorous liver and NT: corresponding non-tumorous liver) and 5 normal liver samples (NL). miR139 was significantly underexpressed in T as compared with NT ($P < .001$ Mann Whitney U test) and NL ($P = .001$ Mann Whitney U test).

Table 5.1. Expression of miR139 reversely correlated with ROCK2 protein expression in human HCC

ROCK2	miR139				$P = .03^*$	
	Without		With			
	Underexpression (No. of cases)	Underexpression (No. of cases)	With	Without		
Without Overexpression (No. of cases)	6	9				
With Overexpression (No. of cases)	1	17				

* $P < .05$



5.3.5 Underexpression of miR139 Correlated with Aggressive Human HCC and Hepatocarcinogenesis

Since miR139 regulated ROCK2 protein expression and overexpression of ROCK2 was found to be correlated with aggressive human HCC, we studied the expression of miR139 and its clinicopathologic correlation with HCC patients. From the clinicopathologic analysis (Table 5.2), underexpression of miR139 was significantly associated with aggressive HCC pathologic features including presence of venous invasion ($P = .002$), presence of tumor microsatellite formation ($P = .014$), absence of tumor encapsulation ($P = .005$), and poor cell differentiation of the tumor (Edmondson Grading III/IV) ($P = .005$).

Development of HCC is a multistep process, like many other cancers, involved the accumulation of genetic and epigenetic alterations. It is not uncommon that livers of chronic hepatitis develop into cirrhosis, early stages HCC, and eventually to late stages HCC. Therefore, we hypothesized that progressive loss of miR139 was associated with multistep hepatocarcinogenesis. To this end, we categorized the patients into four groups: those with normal livers and no disease background, livers with chronic hepatitis, livers with cirrhosis (cirrhotic livers), and HCCs of pTNM stage I/II, and HCCs of stages III/IV. We found that miR139 expression progressively decreased through hepatocarcinogenesis from normal, chronic hepatitis, cirrhosis, early-staged HCCs (stages I/II), and eventually to advance-staged HCCs (stages III/IV) (Figure 5.9) (Table 5.3). This data provided support that underexpression of miR139 was involved in multistep hepatocarcinogenesis.



Table 5.2. Clinicopathologic Correlation of miR139 Underexpression in Human HCC.

		miR139		
		Without Underexpression (No. of cases)	With Underexpression (No. of cases)	
Tumor size	≤ 5 cm	7	19	<i>P</i> = .543
	> 5 cm	7	30	
Tumor encapsulation	Absent	4	35	<i>P</i> = .005*
	Present	10	14	
Cellular differentiation by Edmondson grading	I-II	12	20	<i>P</i> = .005*
	III-IV	2	29	
Venous invasion	Absent	12	19	<i>P</i> = .002*
	Present	2	32	
Tumor microsatellite formation	Absent	11	19	<i>P</i> = .014*
	Present	3	30	
Direct liver invasion	Absent	8	25	<i>P</i> = .284
	Present	2	19	
HBV surface antigen	Absent	5	8	<i>P</i> = .146
	Present	9	40	
Nontumorous liver	Normal &	0	4	<i>P</i> = .567
	Chronic			
	Hepatitis			
	Cirrhosis	14	45	
Gender	Male	11	40	<i>P</i> = 1.000
	Female	3	9	

**P* < .05



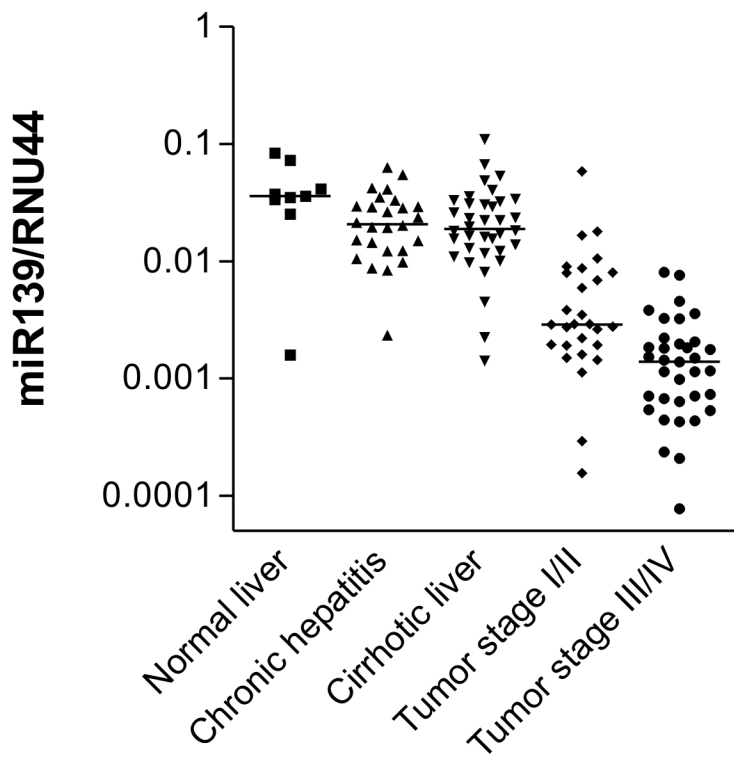


Figure 5.9 Expression of miR139 progressively decreased in hepatocarcinogenesis

Expression of mature miR139 was assessed by real-time quantitative PCR. miR139 was progressively lost from normal livers, to livers with chronic hepatitis, to cirrhotic livers, to livers of tumor stage I/II HCC, and eventually to livers of tumor stage III/IV.

Table 5.3. miR139 Underexpression is associated with multistep hepatocarcinogenesis.

	Normal liver	Chronic hepatitis	Cirrhotic liver	Tumor stage I/II	Tumor stage III/IV
Normal liver					
Chronic hepatitis	.029				
Cirrhotic liver	.017	.859			
Tumor stage I/II	< .001	< .001	< .001		
Tumor stage III/IV	< .001	< .001	< .001	< .001	

* $P < .05$



5.3.6 Expression of miR139 was Further Decreased in Venous Invasion and Extrahepatic Metastases

Clinicopathologic study demonstrated that underexpression of miR139 was associated with more aggressive HCC behavior, and *in vitro* invasion study showed that miR139 suppressed HCC cell invasion. To substantiate these findings in human samples, we directly compared miR139 expression level in tissues of primary HCCs and metastatic HCCs. We studied 3 HCC cases that had venous invasion, with the tumor thrombi representing tumor metastases. After microdissecting the tumor cells that had invaded the veins microscopically on the paraffin sections (Figure 5.10), we quantified miR139 expression in these metastatic HCC cells and compared with the miR139 expression in their corresponding primary HCCs and non-tumorous livers. Consistent with our previous findings in the fresh frozen HCC samples, miR139 was found to be significantly underexpressed in tumorous livers (primary HCC) as compared to their corresponding non-tumorous livers in paraffin-embedded tissues. Notably, 3 of the 3 cases exhibited a mild reduction of miR139 expression in venous invasion as compared to their corresponding primary HCCs (Figure 5.10). We further compared miR139 expression in non-tumorous livers, their corresponding tumorous livers and extrahepatic metastases. Extrahepatic metastases cases used in this study included HCC tumors formed in distant organs: intraperitoneal cavity, diaphragm, portal vein, and bone (Figure 5.11). A slight reduction of miR139 expression was observed in 3 of the 4 cases of extrahepatic metastases as compared to the primary HCC. Extrahepatic metastases showing further loss of miR139 included metastases found in the intraperitoneal cavity, diaphragm, and portal vein as compared to the primary HCC (Figure 5.11). However, the miR139



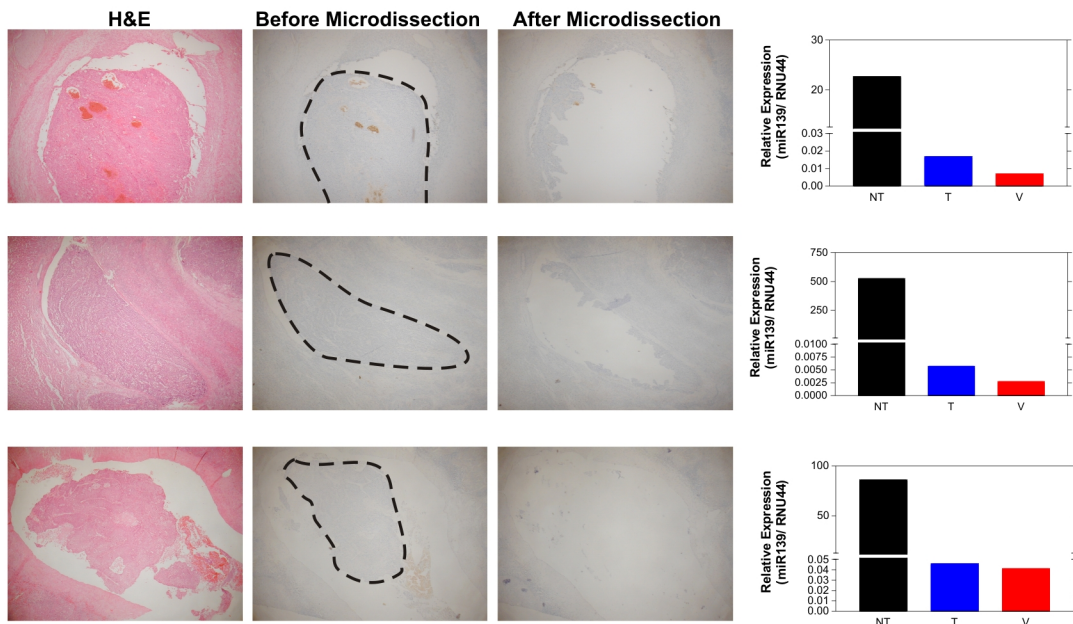


Figure 5.10 miR139 was further downregulated in veins invaded HCC

(A) Venous Invasion of HCC. HCC cells that had invaded into the veins were microdissected for microRNA expression assessment. (B) Expression of mature miR139 in NT, non-tumorous livers, T, tumorous livers, and V, veins invaded HCC were assessed by real-time quantitative PCR. Expression of mature miR139 further decreased in veins invaded HCC.

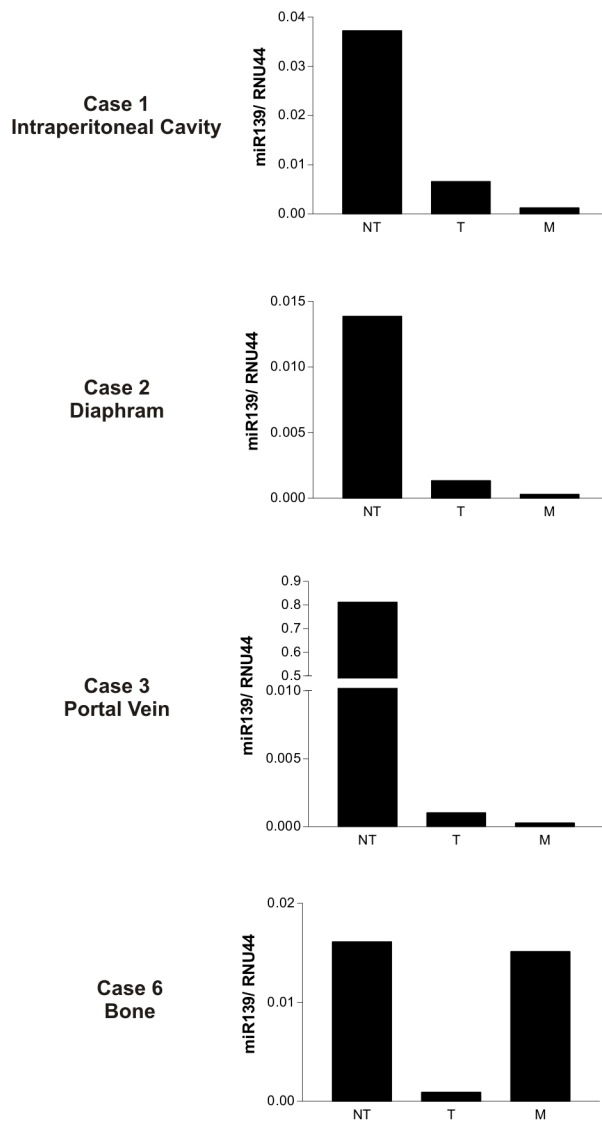


Figure 5.11 miR139 was further downregulated in extrahepatic metastases

Expression of mature miR139 in NT, non-tumorous livers, T, tumorous livers, and M, extrahepatic metastases were assessed by real-time quantitative PCR. Expression of mature miR139 further decreased in extrahepatic metastases as compared to HCC.

expression rebound in the extrahepatic metastases found in the bone. Because bone RNA requires decalcification before extraction, decalcification of the bone might affect this adverse result. Better extraction method of this set of samples is required to confirm the result. In general, the slight reduction of miR139 expression in venous tumor thrombi and extrahepatic metastases demonstrated that underexpression of miR139 might be associated with HCC metastasis. Examination of a larger sample size of metastatic tissues will be performed to confirm the result. Furthermore, whether expression of miR139 is associated with sites of metastases will be investigated by comparing miR139 expression in HCC metastases found in different organs.



5.4 Discussion

Protein overexpression of ROCK2 in human HCC suggested an intriguing hint of the possible translational modification of ROCK2 in cancers. Post-transcriptional modifications including ubiquitination and miRNAs mediated protein degradation may result in aberrant protein expression in cancers. Overexpression of Wnt/β-catenin in cancers is a well-studied model demonstrating the contributions and alterations of ubiquitin-proteosome degradation pathway in the development of cancers (176-180). Wnt signals are reported to be abundant in cancers which prevent β-catenin from being phosphorylated by GSK3β (176-180); hypophosphorylated β-catenin does not undergo ubiquitin-proteosome degradation and thus eventually results in the accumulation of β-catenin in cancers (176-180). MG132, a proteosome inhibitor, was not able to alter ROCK2 protein expression (Figure 5.12), and this finding excluded our speculation that ROCK2 was regulated by ubiquitin-proteosome degradation pathway. As increasing evidence demonstrated the regulatory roles of miRNAs on translational modification, we investigated the possible miRNAs regulatory roles on ROCK2 in HCC.

In this study, we found that the 3'UTR of ROCK2 could downregulate gene expression using firefly luciferase as readout. Furthermore, by *in silico* analysis, we found that the 3'UTR of ROCK2 harbored potential binding site complementary to miR139. Transient overexpression of miR139 reduced ROCK2 protein level in HCC cells. Statistical analysis demonstrated that underexpression of miR139 was associated with increased of ROCK2 protein expression and other aggressive HCC features. We further examined miR139 expression in human HCC tissues and metastatic HCC tissues and we found that



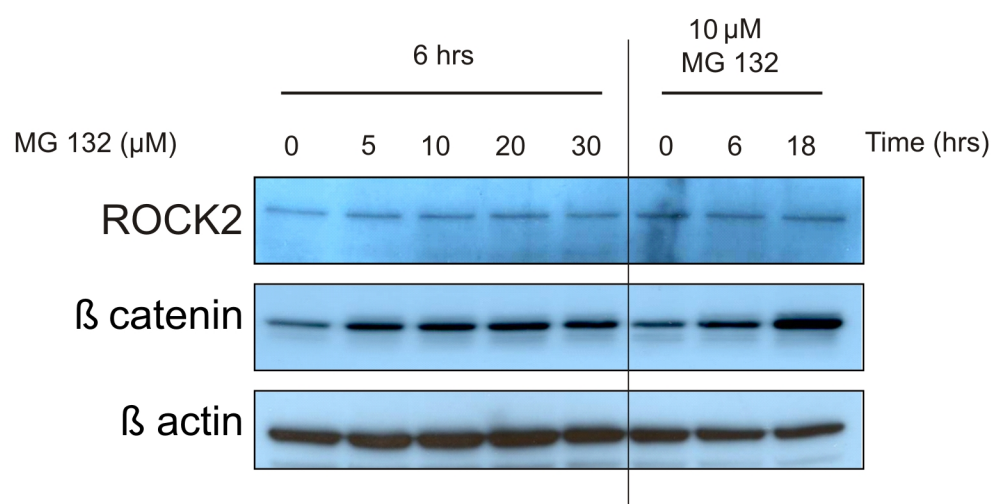


Figure 5.12 ROCK2 was not affected by MG132 treatment

HCC cells, BEL7402, was treated with 0, 5, 10, 20, 30 μ M of MG132 for 6 hours or 10 μ M MG132 for 0, 6, 18 hrs. ROCK2 protein expression was not affected by MG132 in dosage nor time dependent manners. β catenin was a positive control of the MG132 treatment. β actin was the loading control.

miR139 was further underexpressed in metastatic HCCs. This finding is of particular importance since metastasis is the leading cause of death in solid tumors including HCC. The limited availability of metastatic tissues from patients often hinders research on metastasis. The limitation was related to the clinical and surgical practice in HCC. When HCC patients are diagnosed with metastatic HCC or advanced HCC, surgical resection is in general not a preferable curative treatment for patients. Therefore, only a small number of extrahepatic tissues are available for investigation.

Real-time quantitative PCR of miRNA from paraffin-embedded tissues can partially overcome the above hindrance. By extracting miRNA from formalin-fixed paraffin-embedded (FFPE) tissues, we could retrieve valuable information from archival FFPE specimens and this may increase the sample size for examining metastatic HCC. Second, since the miRNA quantitative PCR assay is specific for the mature form of miRNA, information on the expression of miRNA can be assessed in a tiny amount of start up miRNA. Using the combination of these two techniques, we were able to quantify the expression of mature miRNA from archival FFPE specimens which provided us valuable information about the miRNA expression in limited amount tissues and archival materials.

Recently, ROCK1 protein was found to be suppressed by miR146a in human prostate cancer cell line (181). In this part of the present study, we identified that miR139 contributed to aggressive HCC and regulated ROCK2 expression in HCC. Different cancers have different miRNA profile expressions and result in different gene expression



profile (167). The basis of this study relied on the finding that ROCK2 was only overexpressed in the protein level but not in the mRNA level; it is however possible that multiple miRNAs and multiple translational modifications synergistically exert an effect on ROCK2 protein expression level. We believe our findings on miR139 enrich the current understandings on the underlying molecular mechanisms involved in the deregulation of ROCK2 and in HCC metastasis.



5.5 Summary

In search of possible post-transcriptional regulations of ROCK2 expression in HCC, we identified a miRNA, miR139, responsible for ROCK2 deregulated expression in HCC. We first demonstrated that the 3' UTR of ROCK2 suppressed gene translation. Next, through *in silico* analysis, we identified a miR139 possessing potential binding sites on the 3'UTR of ROCK2. Overexpression of miR139 in HCC cells reduced ROCK2 protein expression and ROCK2 dependent cell migration. miR139 was profoundly underexpressed in human HCC. Statistical analysis demonstrated that underexpression of miR139 was significantly associated with overexpression of ROCK2 protein in human HCC samples. Clinicopathologic correlation demonstrated that underexpression of miR139 in human HCC was closely associated with multistep hepatocarcinogenesis and aggressive HCC features including presence of venous invasion, presence of tumor microsatellite formation, absence of tumor encapsulation, and poorly differentiated HCC. Expression of miR139 was progressively lost along multistep hepatocarcinogenesis and was found to be further decreased in metastatic HCC tissues. In summary, our findings demonstrated that ROCK2 protein expression was regulated by miR139 in hepatocarcinogenesis and suggested a translational mechanism involved in the deregulation of ROCK2 leading to the development of human cancers.



Chapter 6

General Summary

HCC, the most common primary liver cancer, is the fifth most prevalent malignancy in the world. Incidence of HCC is especially high in China, Southeast Asia, and Sub-Saharan Africa. In Hong Kong, HCC is the third most common cancer and is the second major cause of cancer deaths. Multiple risk factors, including HBV or HCV infection, alcohol abuse, cirrhosis, and aflatoxin B1 intake, are associated with the development of HCC. Hepatocarcinogenesis is a multistep process, often advancing from chronic hepatitis and cirrhosis to HCC. HCC is tightly associated with HBV infection as reflected by the overlapping geographical distributions of HCC incidence and HBV infection. HBV infection may result in chronic liver diseases and eventually leading to cirrhosis, and about 80% - 90% of HCC cases are found with livers with cirrhotic background (17).

HCC has a high mortality rate and is largely attributed to metastasis. Cancer metastasis accounts for 90% of mortality in solid cancers. Intrahepatic metastasis and extrahepatic metastasis are the major cause of liver failure and mortality in HCC patients. Although vascular invasion and extrahepatic metastasis are two classic features of advanced HCC, there are no chemotherapeutic treatments aimed at targeting HCC metastasis. In Hong Kong, tumor resection remains the most efficient and preferable treatment for HCC patients at early stages. However, tumor resection is not applicable to patients of advanced stages HCC. Also, even the tumors can be resected in early stages, the 5-year recurrence rate reaches 70% - 100%. The high recurrence rate is often resulted from



intrahepatic metastasis or multicentric hepatocarcinogenesis in the liver remnants (182). Knowledge on the detailed underlying molecular mechanisms may enrich our understanding on cancer metastasis. Cancer metastasis is a complicated process in which cancer cells acquire the ability to invade into the extracellular matrix, extravasate and survive in the circulatory system, extravasate and colonize in new tissues either at the same organ or distant organs.

Acquisition of cell migratory and invasive ability is essential for cancer metastasis which involves complicated changes in gene expression. Different genes are deregulated in HCC and such deregulations contribute to HCC metastasis. A group of proteins called matrix metalloproteinases (MMPs) have been shown to be involved in cancer invasion and metastasis. Overexpression of MMP2 and MMP9 in HCC may be involved in increased tumor recurrence or metastasis after tumor resection (183). Particularly, MMP9 was demonstrated to increase the invasive potential of HCC and was involved in capsular filtration in HCC (184). Osteopontin (OPN), a secreted phosphoglycoprotein which binds to integrin receptors, has been shown to be frequently overexpressed in HCC and involved in *in vitro* invasion and *in vivo* lung metastasis through the upregulation of MMP2 and a serine proteinase, urokinase (uPA) (185). Furthermore, TWIST, a transcriptional factor, was found to be correlated with HCC metastasis through downregulation of E-cadherin (186). These reported proteins are known to be important for various steps involved in cancer metastasis such as invasion into the extracellular matrix and loss of cell-cell adhesions. As mentioned in Chapter 1, cell motility plays critical roles in many steps of cancer metastasis. ROCK is important for reorganizing the



actin cytoskeleton, key to cell motility. In this study, we explored the regulations and functions of ROCK in HCC.

Previously, we demonstrated that a tumor suppressor gene, DLC1, was implicated in HCC. DLC1 was found to be frequently underexpressed in HCC mainly through gene deletion and promoter hypermethylation. Interestingly, DLC1 suppressed HCC cell migration and invasion. DLC1 was found to be a RhoGAP protein that specifically suppressed the activity of RhoA and actin polymerization. RhoA was found to be active when bound to GTP and inactive when bound to GDP. *In vitro* RhoGAP assay demonstrated that DLC1 accelerated the intrinsic GTP hydrolysis and turned RhoA inactive. RhoA carried out almost all functions related to cytoskeletal rearrangement through regulating its immediate downstream effector ROCK. In this study, we demonstrated that DLC1 suppressed ROCK mediated cytoskeletal reorganization events including the formation of stress fiber and focal adhesion network and phosphorylation of MLC2 and MYPT1. Due to the breakdown of the cytoskeletal network, DLC1 induced cell shrinkage. We demonstrated that dominant active ROCK could rescue the cell from DLC1 induced cell shrinkage. In the first part of the study, we reported a general cell signaling pathway DLC1/RhoA/ROCK/MLC2 in cell migration. Since DLC1 suppressed RhoA which activated both ROCK1 and ROCK2, we believe that DLC1 could suppress both ROCK1 and ROCK2. Thus, in this part of our study, we mainly employed ROCK inhibitor, Y27632, which does not discriminate ROCK1 or ROCK2. ROCK1 and ROCK2 kinase domains share 92% homology in amino acid sequences. So far, there is no report showing ROCK1 and ROCK2 possess different substrates. Therefore, we



believe that both ROCK1 and ROCK2 can participate in DLC1/RhoA/ROCK/MLC2 pathway to control HCC cell motility.

DLC1 was found to be frequently underexpressed in 67.50 % (75, 76) and ROCK2 was found to be overexpressed in 52.66 % of human HCC. However, no significant correlation between DLC1 expression and ROCK expression in human HCC samples was found. This is a reasonable finding because DLC1 regulates the activities but not the expressions of RhoA and ROCK. Nevertheless, it is technically challenging to access the activities of RhoA and ROCK in human samples. RhoA possesses intrinsic GTP hydrolyzing activity and undergoes a fast endothermic reaction. First, it is difficult to preserve the RhoGTPase activity during tumor resection and extraction. Second, thawing of the extracts provides energy for the fast RhoGTPase reaction. Similarly, the kinase activity of ROCK is also difficult to access and preserve in human HCC samples. Both the activities of RhoA and ROCK would quickly decline after resection and extraction from tissues.

DLC1 is underexpressed mainly through gene deletion and DNA methylation (75, 76, 122). From loss of heterozygosity (LOH) study, DLC1 was found to be frequently deleted in 44.1% to 50% of human HCCs (76). From methylation-specific PCR (MS-PCR) study, DLC1 was found to be methylated in 24% of human HCCs (76). However, ROCK2 overexpression was found to be at the protein level but not mRNA level. ROCK2 overexpression in HCC, a post-transcriptional modification, was significantly associated with the underexpression of miR139. These lines of evidence demonstrated that the expressions of DLC1 and ROCK were regulated by independent mechanisms.



Intriguingly, only ROCK2 but not ROCK1, was profoundly overexpressed in human HCC. Knockout mice models have distinguished their separate physiological roles. ROCK1 and ROCK2 homozygous knockout mice shared several common and several different phenotypes. With both manifested EOB (eyelid open at birth) (149), $\text{ROCK2}^{-/-}$ mice manifested more severe physiological defects such as thrombus formation, placental dysfunction, and intrauterine growth retardation (150). Also, most $\text{ROCK2}^{-/-}$ mice were embryonic lethal (150), whilst most $\text{ROCK1}^{-/-}$ mice live till adulthood (149). ROCK1 and ROCK2 may have redundant functions as they share common downstream targets. However, their difference in physiological localization may confer the variations in the knockout mice models. The regulation of the tissue expression of ROCK1 and ROCK2 is still unclear. ROCK1 protein was expressed both in HCC and non-tumorous livers without much difference in expression levels. Although ROCK2 was mildly expressed in non-tumorous livers, ROCK2 protein expression was profoundly upregulated in HCC. Increased ROCK2 expression was associated with the tumor microsatellite formation, which is a metastatic feature of HCC, and conferred HCC cells a higher capability of migratory and invasive abilities as demonstrated by the ROCK2 overexpression HCC cell model. The consistent results from ROCK2 knockdown HCC cell models *in vitro* and *in vivo* confirmed that ROCK2 contributed to increased HCC cell motility and HCC invasion. The ROCK2 knockdown HCC cells displayed a loss of actomyosin contraction as demonstrated by loss of actin stress fibers and decreased MYPT1 phosphorylation level. More intriguingly, ROCK2 knockdown HCC cells exhibited a loss of spiky protrusions, filopodia, on the cell surface. Hall A. suggested that Cdc42 induced formation of filopodia while RhoA induced formation of actin stress fibers (39).



However, in HCC cell model, we found that knockdown of ROCK2 impaired both the formation of actin stress fibers and filopodia. Hall A. employed microinjection of dominant active form of Cdc42 and RhoA proteins or treatment of LPA to induce activation of RhoA into fibroblasts (39). These discrepancies can be ascribed to several reasons. First, we employed different cell types and different cell models. More importantly, we employed different methodologies in examining the cellular impact on actin reorganization. Microinjection of proteins or treatment of LPA induced prompt responses of a cell within a few hours or even minutes and reflected a quick effect on the cell. In contrary, the effect of our stable ROCK2 knockdown model is more continuing. Our model reflected the cellular effect of the constant loss of ROCK2. Furthermore, emerging evidence has shown that different members of the RhoGTPases cross talk and regulate the activities of one another (35). Therefore, long-term suppression of ROCK might result in affecting the activities of other RhoGTPases. Hepatocarcinogenesis, like many other cancers, is a multistep process and involves the accumulation of multiple genetic and epigenetic alterations. Overexpression of ROCK2 in HCC is not a temporary event; therefore, stable overexpression or knockdown ROCK2 models may reveal a closer model to demonstrate the impact of ROCK2 in cancers.

Our work shed light on the molecular bases of tumor microsatellite formation around primary HCC. This problem is of major interest in HCC as it conditions many cases of tumor recurrence after surgery. Our clinicopathologic study demonstrated that overexpression of ROCK2 was significantly associated with tumor microsatellite formation or microsatellite metastasis formation around HCC, and was further confirmed



by the *in vivo* orthotopic liver nude mouse model. Besides microsatellite metastasis formation, ROCK2 was shown to be important in other invasive features of HCC including the presence of venous invasion and invasive growth fronts. Since liver has rich systemic venous drainage, pulmonary metastasis is common in HCC. One mouse from our *in vivo* study exhibited lung metastasis in the vector group while none was found in the ROCK2 knockdown group. From the *in vivo* mouse model results, ROCK2 seemed to be more important for HCC local invasion as compared to distant metastasis. Overall, in human HCCs and orthotopic liver implantation nude mouse model, ROCK2 was important in metastasis as well as local invasion in HCC.

Of particular note, deregulation of ROCK2 expression was found in the post-transcriptional level. Since the 3'UTR of ROCK2 suppressed gene expression, we further investigated the microRNA mediated translational suppression. miR139 was frequently underexpressed in human HCC and was associated with overexpression of ROCK2 protein. Coherent with ROCK2 overexpression, we further characterized miR139 as anti-migratory and invasive microRNA. miR139 was progressively lost through hepatocarcinogenesis. Among all stages of hepatocarcinogenesis, miR139 showed the most drastic reduction from cirrhotic livers to early stages of HCC. It is reasonable because the most drastic changes lie in the transformation of non-malignant hepatocytes into malignant HCC cells. Different microRNAs might be implicated in the development of different stages of HCC; therefore, it is of particular interest to unveil the microRNA expression profiles of different stages of HCC.



To conclude, we showed that ROCK-mediated cytoskeletal reorganization was antagonistically regulated by DLC1. We previously showed that underexpression of DLC1 was implicated in human HCC and significantly suppressed HCC cell migration. Our study delineated the DLC1/RhoA/ROCK/MLC2 pathway in HCC cell movement which is an important property of cancer metastasis. Despite the high homology of ROCK1 and ROCK2, only ROCK2 but not ROCK1 was significantly overexpressed in HCC. Overexpression of ROCK2 in HCC was significantly associated with HCC metastasis and invasiveness, as indicated by the clinicopathologic correlation and orthotopic liver nude mouse model. We confirmed that ROCK2 conferred the enhanced migratory and invasive phenotypes by regulating the cytoskeletal reorganization including actin polymerization and myosin activation. In HCC, ROCK2 was deregulated in the translational level and we showed that the 3'UTR of ROCK2 profoundly suppressed gene expression. miR139 suppressed ROCK2 protein expression and expressions of miR139 and ROCK2 was reversely associated in human HCC. Consistent with knockdown of ROCK2, overexpression of miR139 also exerted anti-migratory and invasive effects on HCC cells. We believe that deregulation of miR139 contributes to overexpression of ROCK2 in HCC. This finding has enriched the understanding of DLC1/RhoA/ROCK pathway, characterized the functional roles of ROCK2 in HCC, and partially elucidated the aberrant translational regulation of ROCK2 in HCC. Our finding has enriched the knowledge of the underlying molecular mechanisms involved in HCC metastasis which might be beneficial to the development and intervention of chemotherapeutic treatment for HCC patients in the future.



References

1. Parkin DM, Bray F, Ferlay J, Pisani P. Estimating the world cancer burden: Globocan 2000. *Int J Cancer* 2001;94:153-156.
2. Wong QW, Lung RW, Law PT, Lai PB, Chan KY, To KF, Wong N. MicroRNA-223 is commonly repressed in hepatocellular carcinoma and potentiates expression of Stathmin1. *Gastroenterology* 2008;135:257-269.
3. El-Serag HB, Rudolph KL. Hepatocellular carcinoma: epidemiology and molecular carcinogenesis. *Gastroenterology* 2007;132:2557-2576.
4. Stroffolini T, Andreone P, Andriulli A, Ascione A, Craxi A, Chiaramonte M, Galante D, et al. Characteristics of hepatocellular carcinoma in Italy. *J Hepatol* 1998;29:944-952.
5. Feitelson MA, Lee J. Hepatitis B virus integration, fragile sites, and hepatocarcinogenesis. *Cancer Lett* 2007;252:157-170.
6. Fourel G, Trepo C, Bougueret L, Henglein B, Ponzetto A, Tiollais P, Buendia MA. Frequent activation of N-myc genes by hepadnavirus insertion in woodchuck liver tumours. *Nature* 1990;347:294-298.
7. Hussain SP, Schwank J, Staib F, Wang XW, Harris CC. TP53 mutations and hepatocellular carcinoma: insights into the etiology and pathogenesis of liver cancer. *Oncogene* 2007;26:2166-2176.
8. Zhang X, Zhang H, Ye L. Effects of hepatitis B virus X protein on the development of liver cancer. *J Lab Clin Med* 2006;147:58-66.
9. Park IY, Sohn BH, Yu E, Suh DJ, Chung YH, Lee JH, Surzycki SJ, et al. Aberrant epigenetic modifications in hepatocarcinogenesis induced by hepatitis B virus X protein. *Gastroenterology* 2007;132:1476-1494.
10. Donato F, Tagger A, Gelatti U, Parrinello G, Boffetta P, Albertini A, Decarli A, et al. Alcohol and hepatocellular carcinoma: the effect of lifetime intake and hepatitis virus infections in men and women. *Am J Epidemiol* 2002;155:323-331.
11. Takano S, Yokosuka O, Imazeki F, Tagawa M, Omata M. Incidence of hepatocellular carcinoma in chronic hepatitis B and C: a prospective study of 251 patients. *Hepatology* 1995;21:650-655.
12. Ray RB, Lagging LM, Meyer K, Ray R. Hepatitis C virus core protein cooperates with ras and transforms primary rat embryo fibroblasts to tumorigenic phenotype. *J Virol* 1996;70:4438-4443.
13. Ray RB, Steele R, Meyer K, Ray R. Transcriptional repression of p53 promoter by hepatitis C virus core protein. *J Biol Chem* 1997;272:10983-10986.
14. Kato N, Lan KH, Ono-Nita SK, Shiratori Y, Omata M. Hepatitis C virus nonstructural region 5A protein is a potent transcriptional activator. *J Virol* 1997;71:8856-8859.
15. Kato N, Yoshida H, Ono-Nita SK, Kato J, Goto T, Otsuka M, Lan K, et al. Activation of intracellular signaling by hepatitis B and C viruses: C-viral core is the most potent signal inducer. *Hepatology* 2000;32:405-412.
16. Moriya K, Fujie H, Shintani Y, Yotsuyanagi H, Tsutsumi T, Ishibashi K, Matsuura Y, et al. The core protein of hepatitis C virus induces hepatocellular carcinoma in transgenic mice. *Nat Med* 1998;4:1065-1067.



17. Leong TY, Leong AS. Epidemiology and carcinogenesis of hepatocellular carcinoma. *HPB (Oxford)* 2005;7:5-15.
18. Bressac B, Kew M, Wands J, Ozturk M. Selective G to T mutations of p53 gene in hepatocellular carcinoma from southern Africa. *Nature* 1991;350:429-431.
19. Turner PC, Sylla A, Diallo MS, Castegnaro JJ, Hall AJ, Wild CP. The role of aflatoxins and hepatitis viruses in the etiopathogenesis of hepatocellular carcinoma: A basis for primary prevention in Guinea-Conakry, West Africa. *J Gastroenterol Hepatol* 2002;17 Suppl:S441-448.
20. Kondo F, Wada K, Nagato Y, Nakajima T, Kondo Y, Hirooka N, Ebara M, et al. Biopsy diagnosis of well-differentiated hepatocellular carcinoma based on new morphologic criteria. *Hepatology* 1989;9:751-755.
21. Qian GS, Ross RK, Yu MC, Yuan JM, Gao YT, Henderson BE, Wogan GN, et al. A follow-up study of urinary markers of aflatoxin exposure and liver cancer risk in Shanghai, People's Republic of China. *Cancer Epidemiol Biomarkers Prev* 1994;3:3-10.
22. De Maria N, Manno M, Villa E. Sex hormones and liver cancer. *Mol Cell Endocrinol* 2002;193:59-63.
23. Yu MC, Tong MJ, Govindarajan S, Henderson BE. Nonviral risk factors for hepatocellular carcinoma in a low-risk population, the non-Asians of Los Angeles County, California. *J Natl Cancer Inst* 1991;83:1820-1826.
24. Nguyen DX, Massague J. Genetic determinants of cancer metastasis. *Nat Rev Genet* 2007;8:341-352.
25. Norton L, Massague J. Is cancer a disease of self-seeding? *Nat Med* 2006;12:875-878.
26. El-Serag HB, Marrero JA, Rudolph L, Reddy KR. Diagnosis and treatment of hepatocellular carcinoma. *Gastroenterology* 2008;134:1752-1763.
27. Tan C, Costello P, Sanghera J, Dominguez D, Baulida J, de Herreros AG, Dedhar S. Inhibition of integrin linked kinase (ILK) suppresses beta-catenin-Lef/Tcf-dependent transcription and expression of the E-cadherin repressor, snail, in APC-/ human colon carcinoma cells. *Oncogene* 2001;20:133-140.
28. Deryugina EI, Quigley JP. Matrix metalloproteinases and tumor metastasis. *Cancer Metastasis Rev* 2006;25:9-34.
29. Sahai E, Marshall CJ. Differing modes of tumour cell invasion have distinct requirements for Rho/ROCK signalling and extracellular proteolysis. *Nat Cell Biol* 2003;5:711-719.
30. Yang J, Mani SA, Donaher JL, Ramaswamy S, Itzykson RA, Come C, Savagner P, et al. Twist, a master regulator of morphogenesis, plays an essential role in tumor metastasis. *Cell* 2004;117:927-939.
31. Steeg PS. Tumor metastasis: mechanistic insights and clinical challenges. *Nat Med* 2006;12:895-904.
32. Muller A, Homey B, Soto H, Ge N, Catron D, Buchanan ME, McClanahan T, et al. Involvement of chemokine receptors in breast cancer metastasis. *Nature* 2001;410:50-56.
33. Ananthakrishnan R, Ehrlicher A. The forces behind cell movement. *Int J Biol Sci* 2007;3:303-317.
34. Yamazaki D, Kurisu S, Takenawa T. Regulation of cancer cell motility through actin reorganization. *Cancer Sci* 2005;96:379-386.



35. Li Z, Dong X, Wang Z, Liu W, Deng N, Ding Y, Tang L, et al. Regulation of PTEN by Rho small GTPases. *Nat Cell Biol* 2005;7:399-404.
36. Xu J, Wang F, Van Keymeulen A, Herzmark P, Straight A, Kelly K, Takuwa Y, et al. Divergent signals and cytoskeletal assemblies regulate self-organizing polarity in neutrophils. *Cell* 2003;114:201-214.
37. Kupfer A, Louvard D, Singer SJ. Polarization of the Golgi apparatus and the microtubule-organizing center in cultured fibroblasts at the edge of an experimental wound. *Proc Natl Acad Sci U S A* 1982;79:2603-2607.
38. Mellor H. Cell motility: Golgi signalling shapes up to ship out. *Curr Biol* 2004;14:R434-435.
39. Hall A. Rho GTPases and the actin cytoskeleton. *Science* 1998;279:509-514.
40. Amano M, Chihara K, Kimura K, Fukata Y, Nakamura N, Matsuura Y, Kaibuchi K. Formation of actin stress fibers and focal adhesions enhanced by Rho-kinase. *Science* 1997;275:1308-1311.
41. Fukui K, Tamura S, Wada A, Kamada Y, Sawai Y, Imanaka K, Kudara T, et al. Expression and prognostic role of RhoA GTPases in hepatocellular carcinoma. *J Cancer Res Clin Oncol* 2006;132:627-633.
42. Fritz G, Brachetti C, Bahlmann F, Schmidt M, Kaina B. Rho GTPases in human breast tumours: expression and mutation analyses and correlation with clinical parameters. *Br J Cancer* 2002;87:635-644.
43. Fritz G, Just I, Kaina B. Rho GTPases are over-expressed in human tumors. *Int J Cancer* 1999;81:682-687.
44. Abraham MT, Kuriakose MA, Sacks PG, Yee H, Chiriboga L, Bearer EL, Delacure MD. Motility-related proteins as markers for head and neck squamous cell cancer. *Laryngoscope* 2001;111:1285-1289.
45. Kamai T, Yamanishi T, Shirataki H, Takagi K, Asami H, Ito Y, Yoshida K. Overexpression of RhoA, Rac1, and Cdc42 GTPases is associated with progression in testicular cancer. *Clin Cancer Res* 2004;10:4799-4805.
46. Kamai T, Tsujii T, Arai K, Takagi K, Asami H, Ito Y, Oshima H. Significant association of Rho/ROCK pathway with invasion and metastasis of bladder cancer. *Clin Cancer Res* 2003;9:2632-2641.
47. Genda T, Sakamoto M, Ichida T, Asakura H, Kojiro M, Narumiya S, Hirohashi S. Cell motility mediated by rho and Rho-associated protein kinase plays a critical role in intrahepatic metastasis of human hepatocellular carcinoma. *Hepatology* 1999;30:1027-1036.
48. Itoh K, Yoshioka K, Akedo H, Uehata M, Ishizaki T, Narumiya S. An essential part for Rho-associated kinase in the transcellular invasion of tumor cells. *Nat Med* 1999;5:221-225.
49. Takamura M, Sakamoto M, Genda T, Ichida T, Asakura H, Hirohashi S. Inhibition of intrahepatic metastasis of human hepatocellular carcinoma by Rho-associated protein kinase inhibitor Y-27632. *Hepatology* 2001;33:577-581.
50. Pan Y, Bi F, Liu N, Xue Y, Yao X, Zheng Y, Fan D. Expression of seven main Rho family members in gastric carcinoma. *Biochem Biophys Res Commun* 2004;315:686-691.



51. Leung T, Manser E, Tan L, Lim L. A novel serine/threonine kinase binding the Ras-related RhoA GTPase which translocates the kinase to peripheral membranes. *J Biol Chem* 1995;270:29051-29054.
52. Leung T, Chen XQ, Manser E, Lim L. The p160 RhoA-binding kinase ROK alpha is a member of a kinase family and is involved in the reorganization of the cytoskeleton. *Mol Cell Biol* 1996;16:5313-5327.
53. Matsui T, Amano M, Yamamoto T, Chihara K, Nakafuku M, Ito M, Nakano T, et al. Rho-associated kinase, a novel serine/threonine kinase, as a putative target for small GTP binding protein Rho. *EMBO J* 1996;15:2208-2216.
54. Ishizaki T, Maekawa M, Fujisawa K, Okawa K, Iwamatsu A, Fujita A, Watanabe N, et al. The small GTP-binding protein Rho binds to and activates a 160 kDa Ser/Thr protein kinase homologous to myotonic dystrophy kinase. *EMBO J* 1996;15:1885-1893.
55. Stroeken PJ, Alvarez B, Van Rheenen J, Wijnands YM, Geerts D, Jalink K, Roos E. Integrin cytoplasmic domain-associated protein-1 (ICAP-1) interacts with the ROCK-I kinase at the plasma membrane. *J Cell Physiol* 2006;208:620-628.
56. Bhowmick NA, Ghiassi M, Aakre M, Brown K, Singh V, Moses HL. TGF-beta-induced RhoA and p160ROCK activation is involved in the inhibition of Cdc25A with resultant cell-cycle arrest. *Proc Natl Acad Sci U S A* 2003;100:15548-15553.
57. Lu J, Landerholm TE, Wei JS, Dong XR, Wu SP, Liu X, Nagata K, et al. Coronary smooth muscle differentiation from proepicardial cells requires rhoA-mediated actin reorganization and p160 rho-kinase activity. *Dev Biol* 2001;240:404-418.
58. Tanaka T, Nishimura D, Wu RC, Amano M, Iso T, Kedes L, Nishida H, et al. Nuclear Rho kinase, ROCK2, targets p300 acetyltransferase. *J Biol Chem* 2006;281:15320-15329.
59. Kosako H, Goto H, Yanagida M, Matsuzawa K, Fujita M, Tomono Y, Okigaki T, et al. Specific accumulation of Rho-associated kinase at the cleavage furrow during cytokinesis: cleavage furrow-specific phosphorylation of intermediate filaments. *Oncogene* 1999;18:2783-2788.
60. Yokoyama T, Goto H, Izawa I, Mizutani H, Inagaki M. Aurora-B and Rho-kinase/ROCK, the two cleavage furrow kinases, independently regulate the progression of cytokinesis: possible existence of a novel cleavage furrow kinase phosphorylates ezrin/radixin/moesin (ERM). *Genes Cells* 2005;10:127-137.
61. Sin WC, Chen XQ, Leung T, Lim L. RhoA-binding kinase alpha translocation is facilitated by the collapse of the vimentin intermediate filament network. *Mol Cell Biol* 1998;18:6325-6339.
62. Chevrier V, Piel M, Collomb N, Saoudi Y, Frank R, Paintrand M, Narumiya S, et al. The Rho-associated protein kinase p160ROCK is required for centrosome positioning. *J Cell Biol* 2002;157:807-817.
63. Katoh K, Kano Y, Amano M, Onishi H, Kaibuchi K, Fujiwara K. Rho-kinase-mediated contraction of isolated stress fibers. *J Cell Biol* 2001;153:569-584.
64. Miyazaki K, Komatsu S, Ikebe M. Dynamics of RhoA and ROKalpha translocation in single living cells. *Cell Biochem Biophys* 2006;45:243-254.
65. Ueda K, Ohta Y, Hosoya H. The carboxy-terminal pleckstrin homology domain of ROCK interacts with filamin-A. *Biochem Biophys Res Commun* 2003;301:886-890.



66. Coleman ML, Sahai EA, Yeo M, Bosch M, Dewar A, Olson MF. Membrane blebbing during apoptosis results from caspase-mediated activation of ROCK I. *Nat Cell Biol* 2001;3:339-345.
67. Sebbagh M, Hamelin J, Bertoglio J, Solary E, Breard J. Direct cleavage of ROCK II by granzyme B induces target cell membrane blebbing in a caspase-independent manner. *J Exp Med* 2005;201:465-471.
68. Feng J, Ito M, Kureishi Y, Ichikawa K, Amano M, Isaka N, Okawa K, et al. Rho-associated kinase of chicken gizzard smooth muscle. *J Biol Chem* 1999;274:3744-3752.
69. Yoneda A, Multhaupt HA, Couchman JR. The Rho kinases I and II regulate different aspects of myosin II activity. *J Cell Biol* 2005;170:443-453.
70. Foster R, Hu KQ, Lu Y, Nolan KM, Thissen J, Settleman J. Identification of a novel human Rho protein with unusual properties: GTPase deficiency and in vivo farnesylation. *Mol Cell Biol* 1996;16:2689-2699.
71. Guasch RM, Scambler P, Jones GE, Ridley AJ. RhoE regulates actin cytoskeleton organization and cell migration. *Mol Cell Biol* 1998;18:4761-4771.
72. Ching YP, Wong CM, Chan SF, Leung TH, Ng DC, Jin DY, Ng IO. Deleted in liver cancer (DLC) 2 encodes a RhoGAP protein with growth suppressor function and is underexpressed in hepatocellular carcinoma. *J Biol Chem* 2003;278:10824-10830.
73. Durkin ME, Ullmannova V, Guan M, Popescu NC. Deleted in liver cancer 3 (DLC-3), a novel Rho GTPase-activating protein, is downregulated in cancer and inhibits tumor cell growth. *Oncogene* 2007;26:4580-4589.
74. Leung TH, Ching YP, Yam JW, Wong CM, Yau TO, Jin DY, Ng IO. Deleted in liver cancer 2 (DLC2) suppresses cell transformation by means of inhibition of RhoA activity. *Proc Natl Acad Sci U S A* 2005;102:15207-15212.
75. Ng IO, Liang ZD, Cao L, Lee TK. DLC-1 is deleted in primary hepatocellular carcinoma and exerts inhibitory effects on the proliferation of hepatoma cell lines with deleted DLC-1. *Cancer Res* 2000;60:6581-6584.
76. Wong CM, Lee JM, Ching YP, Jin DY, Ng IO. Genetic and epigenetic alterations of DLC-1 gene in hepatocellular carcinoma. *Cancer Res* 2003;63:7646-7651.
77. Wong CM, Yam JW, Ching YP, Yau TO, Leung TH, Jin DY, Ng IO. Rho GTPase-activating protein deleted in liver cancer suppresses cell proliferation and invasion in hepatocellular carcinoma. *Cancer Res* 2005;65:8861-8868.
78. Hall A. Signal transduction through small GTPases--a tale of two GAPs. *Cell* 1992;69:389-391.
79. Amano M, Ito M, Kimura K, Fukata Y, Chihara K, Nakano T, Matsuura Y, et al. Phosphorylation and activation of myosin by Rho-associated kinase (Rho-kinase). *J Biol Chem* 1996;271:20246-20249.
80. Kawano Y, Fukata Y, Oshiro N, Amano M, Nakamura T, Ito M, Matsumura F, et al. Phosphorylation of myosin-binding subunit (MBS) of myosin phosphatase by Rho-kinase in vivo. *J Cell Biol* 1999;147:1023-1038.
81. Yasui Y, Amano M, Nagata K, Inagaki N, Nakamura H, Saya H, Kaibuchi K, et al. Roles of Rho-associated kinase in cytokinesis; mutations in Rho-associated kinase phosphorylation sites impair cytokinetic segregation of glial filaments. *J Cell Biol* 1998;143:1249-1258.
82. Goto H, Kosako H, Tanabe K, Yanagida M, Sakurai M, Amano M, Kaibuchi K, et al. Phosphorylation of vimentin by Rho-associated kinase at a unique amino-terminal



- site that is specifically phosphorylated during cytokinesis. *J Biol Chem* 1998;273:11728-11736.
83. Kuhlman PA, Hughes CA, Bennett V, Fowler VM. A new function for adducin. Calcium/calmodulin-regulated capping of the barbed ends of actin filaments. *J Biol Chem* 1996;271:7986-7991.
84. Li X, Matsuoka Y, Bennett V. Adducin preferentially recruits spectrin to the fast growing ends of actin filaments in a complex requiring the MARCKS-related domain and a newly defined oligomerization domain. *J Biol Chem* 1998;273:19329-19338.
85. Mische SM, Mooseker MS, Morrow JS. Erythrocyte adducin: a calmodulin-regulated actin-bundling protein that stimulates spectrin-actin binding. *J Cell Biol* 1987;105:2837-2845.
86. Fukata Y, Oshiro N, Kinoshita N, Kawano Y, Matsuoka Y, Bennett V, Matsuura Y, et al. Phosphorylation of adducin by Rho-kinase plays a crucial role in cell motility. *J Cell Biol* 1999;145:347-361.
87. Kaneko T, Amano M, Maeda A, Goto H, Takahashi K, Ito M, Kaibuchi K. Identification of calponin as a novel substrate of Rho-kinase. *Biochem Biophys Res Commun* 2000;273:110-116.
88. Amano M, Kaneko T, Maeda A, Nakayama M, Ito M, Yamauchi T, Goto H, et al. Identification of Tau and MAP2 as novel substrates of Rho-kinase and myosin phosphatase. *J Neurochem* 2003;87:780-790.
89. Ohashi K, Nagata K, Maekawa M, Ishizaki T, Narumiya S, Mizuno K. Rho-associated kinase ROCK activates LIM-kinase 1 by phosphorylation at threonine 508 within the activation loop. *J Biol Chem* 2000;275:3577-3582.
90. Sumi T, Matsumoto K, Nakamura T. Specific activation of LIM kinase 2 via phosphorylation of threonine 505 by ROCK, a Rho-dependent protein kinase. *J Biol Chem* 2001;276:670-676.
91. Tran Quang C, Gautreau A, Arpin M, Treisman R. Ezrin function is required for ROCK-mediated fibroblast transformation by the Net and Dbl oncogenes. *Embo J* 2000;19:4565-4576.
92. Matsui T, Maeda M, Doi Y, Yonemura S, Amano M, Kaibuchi K, Tsukita S, et al. Rho-kinase phosphorylates COOH-terminal threonines of ezrin/radixin/moesin (ERM) proteins and regulates their head-to-tail association. *J Cell Biol* 1998;140:647-657.
93. Arimura N, Inagaki N, Chihara K, Menager C, Nakamura N, Amano M, Iwamatsu A, et al. Phosphorylation of collapsin response mediator protein-2 by Rho-kinase. Evidence for two separate signaling pathways for growth cone collapse. *J Biol Chem* 2000;275:23973-23980.
94. Hashimoto R, Nakamura Y, Goto H, Wada Y, Sakoda S, Kaibuchi K, Inagaki M, et al. Domain- and site-specific phosphorylation of bovine NF-L by Rho-associated kinase. *Biochem Biophys Res Commun* 1998;245:407-411.
95. Sasaki Y. New aspects of neurotransmitter release and exocytosis: Rho-kinase-dependent myristoylated alanine-rich C-kinase substrate phosphorylation and regulation of neurofilament structure in neuronal cells. *J Pharmacol Sci* 2003;93:35-40.
96. Schmandke A, Strittmatter SM. ROCK and Rho: biochemistry and neuronal functions of Rho-associated protein kinases. *Neuroscientist* 2007;13:454-469.



97. Ishizaki T, Naito M, Fujisawa K, Maekawa M, Watanabe N, Saito Y, Narumiya S. p160ROCK, a Rho-associated coiled-coil forming protein kinase, works downstream of Rho and induces focal adhesions. *FEBS Lett* 1997;404:118-124.
98. Uehata M, Ishizaki T, Satoh H, Ono T, Kawahara T, Morishita T, Tamakawa H, et al. Calcium sensitization of smooth muscle mediated by a Rho-associated protein kinase in hypertension. *Nature* 1997;389:990-994.
99. Sebbagh M, Renvoize C, Hamelin J, Riche N, Bertoglio J, Breard J. Caspase-3-mediated cleavage of ROCK I induces MLC phosphorylation and apoptotic membrane blebbing. *Nat Cell Biol* 2001;3:346-352.
100. Fackler OT, Grosse R. Cell motility through plasma membrane blebbing. *J Cell Biol* 2008;181:879-884.
101. Kasper LH, Fukuyama T, Biesen MA, Boussouar F, Tong C, de Pauw A, Murray PJ, et al. Conditional knockout mice reveal distinct functions for the global transcriptional coactivators CBP and p300 in T-cell development. *Mol Cell Biol* 2006;26:789-809.
102. Vo N, Goodman RH. CREB-binding protein and p300 in transcriptional regulation. *J Biol Chem* 2001;276:13505-13508.
103. Shibuya M, Suzuki Y. [Treatment of cerebral vasospasm by a protein kinase inhibitor AT 877]. *No To Shinkei* 1993;45:819-824.
104. Davies SP, Reddy H, Caivano M, Cohen P. Specificity and mechanism of action of some commonly used protein kinase inhibitors. *Biochem J* 2000;351:95-105.
105. Ishizaki T, Uehata M, Tamechika I, Keel J, Nonomura K, Maekawa M, Narumiya S. Pharmacological properties of Y-27632, a specific inhibitor of rho-associated kinases. *Mol Pharmacol* 2000;57:976-983.
106. Jacobs M, Hayakawa K, Swenson L, Bellon S, Fleming M, Taslimi P, Doran J. The structure of dimeric ROCK I reveals the mechanism for ligand selectivity. *J Biol Chem* 2006;281:260-268.
107. Chen XQ, Tan I, Ng CH, Hall C, Lim L, Leung T. Characterization of RhoA-binding kinase ROKalpha implication of the pleckstrin homology domain in ROKalpha function using region-specific antibodies. *J Biol Chem* 2002;277:12680-12688.
108. Amano M, Chihara K, Nakamura N, Kaneko T, Matsuura Y, Kaibuchi K. The COOH terminus of Rho-kinase negatively regulates rho-kinase activity. *J Biol Chem* 1999;274:32418-32424.
109. Alblas J, Ulfman L, Hordijk P, Koenderman L. Activation of Rhoa and ROCK are essential for detachment of migrating leukocytes. *Mol Biol Cell* 2001;12:2137-2145.
110. Worthylake RA, Lemoine S, Watson JM, Burridge K. RhoA is required for monocyte tail retraction during transendothelial migration. *J Cell Biol* 2001;154:147-160.
111. Somlyo AV, Bradshaw D, Ramos S, Murphy C, Myers CE, Somlyo AP. Rho-kinase inhibitor retards migration and in vivo dissemination of human prostate cancer cells. *Biochem Biophys Res Commun* 2000;269:652-659.
112. Pellegrin S, Mellor H. Actin stress fibres. *J Cell Sci* 2007;120:3491-3499.
113. Riento K, Ridley AJ. Rocks: multifunctional kinases in cell behaviour. *Nat Rev Mol Cell Biol* 2003;4:446-456.
114. Hagerty L, Weitzel DH, Chambers J, Fortner CN, Brush MH, Loiselle D, Hosoya H, et al. ROCK1 phosphorylates and activates zipper-interacting protein kinase. *J Biol Chem* 2007;282:4884-4893.



115. Wilkinson S, Paterson HF, Marshall CJ. Cdc42-MRCK and Rho-ROCK signalling cooperate in myosin phosphorylation and cell invasion. *Nat Cell Biol* 2005;7:255-261.
116. Yoshioka K, Matsumura F, Akedo H, Itoh K. Small GTP-binding protein Rho stimulates the actomyosin system, leading to invasion of tumor cells. *J Biol Chem* 1998;273:5146-5154.
117. Yoshioka K, Nakamori S, Itoh K. Overexpression of small GTP-binding protein RhoA promotes invasion of tumor cells. *Cancer Res* 1999;59:2004-2010.
118. Healy KD, Hodgson L, Kim TY, Shutes A, Maddileti S, Juliano RL, Hahn KM, et al. DLC-1 suppresses non-small cell lung cancer growth and invasion by RhoGAP-dependent and independent mechanisms. *Mol Carcinog* 2008;47:326-337.
119. Yuan BZ, Miller MJ, Keck CL, Zimonjic DB, Thorgeirsson SS, Popescu NC. Cloning, characterization, and chromosomal localization of a gene frequently deleted in human liver cancer (DLC-1) homologous to rat RhoGAP. *Cancer Res* 1998;58:2196-2199.
120. Xue W, Krasnitz A, Lucito R, Sordella R, Vanaelst L, Cordon-Cardo C, Singer S, et al. DLC1 is a chromosome 8p tumor suppressor whose loss promotes hepatocellular carcinoma. *Genes Dev* 2008;22:1439-1444.
121. Yuan BZ, Zhou X, Durkin ME, Zimonjic DB, Gumundsdottir K, Eyfjord JE, Thorgeirsson SS, et al. DLC-1 gene inhibits human breast cancer cell growth and in vivo tumorigenicity. *Oncogene* 2003;22:445-450.
122. Yuan BZ, Durkin ME, Popescu NC. Promoter hypermethylation of DLC-1, a candidate tumor suppressor gene, in several common human cancers. *Cancer Genet Cytogenet* 2003;140:113-117.
123. Guan M, Zhou X, Soulitzis N, Spandidos DA, Popescu NC. Aberrant methylation and deacetylation of deleted in liver cancer-1 gene in prostate cancer: potential clinical applications. *Clin Cancer Res* 2006;12:1412-1419.
124. Plaumann M, Seitz S, Frege R, Estevez-Schwarz L, Scherneck S. Analysis of DLC-1 expression in human breast cancer. *J Cancer Res Clin Oncol* 2003;129:349-354.
125. Seng TJ, Low JS, Li H, Cui Y, Goh HK, Wong ML, Srivastava G, et al. The major 8p22 tumor suppressor DLC1 is frequently silenced by methylation in both endemic and sporadic nasopharyngeal, esophageal, and cervical carcinomas, and inhibits tumor cell colony formation. *Oncogene* 2007;26:934-944.
126. Ullmannova V, Popescu NC. Expression profile of the tumor suppressor genes DLC-1 and DLC-2 in solid tumors. *Int J Oncol* 2006;29:1127-1132.
127. Yuan BZ, Jefferson AM, Baldwin KT, Thorgeirsson SS, Popescu NC, Reynolds SH. DLC-1 operates as a tumor suppressor gene in human non-small cell lung carcinomas. *Oncogene* 2004;23:1405-1411.
128. Goodison S, Yuan J, Sloan D, Kim R, Li C, Popescu NC, Urquidi V. The RhoGAP protein DLC-1 functions as a metastasis suppressor in breast cancer cells. *Cancer Res* 2005;65:6042-6053.
129. Song LJ, Ye SL, Wang KF, Weng YQ, Liang CM, Sun RX, Zhao Y, et al. [Relationship between DLC-1 expressions and metastasis in hepatocellular carcinoma]. *Zhonghua Gan Zang Bing Za Zhi* 2005;13:428-431.
130. Kim TY, Lee JW, Kim HP, Jong HS, Jung M, Bang YJ. DLC-1, a GTPase-activating protein for Rho, is associated with cell proliferation, morphology, and



- migration in human hepatocellular carcinoma. *Biochem Biophys Res Commun* 2007;355:72-77.
131. Qian X, Li G, Asmussen HK, Asnaghi L, Vass WC, Braverman R, Yamada KM, et al. Oncogenic inhibition by a deleted in liver cancer gene requires cooperation between tensin binding and Rho-specific GTPase-activating protein activities. *Proc Natl Acad Sci U S A* 2007;104:9012-9017.
132. Syed V, Mukherjee K, Lyons-Weiler J, Lau KM, Mashima T, Tsuruo T, Ho SM. Identification of ATF-3, caveolin-1, DLC-1, and NM23-H2 as putative antitumorigenic, progesterone-regulated genes for ovarian cancer cells by gene profiling. *Oncogene* 2005;24:1774-1787.
133. Zhou X, Thorgerisson SS, Popescu NC. Restoration of DLC-1 gene expression induces apoptosis and inhibits both cell growth and tumorigenicity in human hepatocellular carcinoma cells. *Oncogene* 2004;23:1308-1313.
134. Ueda K, Murata-Hori M, Tatsuka M, Hosoya H. Rho-kinase contributes to diphosphorylation of myosin II regulatory light chain in nonmuscle cells. *Oncogene* 2002;21:5852-5860.
135. Totsukawa G, Yamakita Y, Yamashiro S, Hartshorne DJ, Sasaki Y, Matsumura F. Distinct roles of ROCK (Rho-kinase) and MLCK in spatial regulation of MLC phosphorylation for assembly of stress fibers and focal adhesions in 3T3 fibroblasts. *J Cell Biol* 2000;150:797-806.
136. Sturge J, Wienke D, Isacke CM. Endosomes generate localized Rho-ROCK-MLC2-based contractile signals via Endo180 to promote adhesion disassembly. *J Cell Biol* 2006;175:337-347.
137. Lavelin I, Geiger B. Characterization of a novel GTPase-activating protein associated with focal adhesions and the actin cytoskeleton. *J Biol Chem* 2005;280:7178-7185.
138. Barberis D, Casazza A, Sordella R, Corso S, Artigiani S, Settleman J, Comoglio PM, et al. p190 Rho-GTPase activating protein associates with plexins and it is required for semaphorin signalling. *J Cell Sci* 2005;118:4689-4700.
139. Kawai K, Yamaga M, Iwamae Y, Kiyota M, Kamata H, Hirata H, Homma Y, et al. A PLC δ 1-binding protein, p122RhoGAP, is localized in focal adhesions. *Biochem Soc Trans* 2004;32:1107-1109.
140. Kaverina I, Krylyshkina O, Small JV. Regulation of substrate adhesion dynamics during cell motility. *Int J Biochem Cell Biol* 2002;34:746-761.
141. Peacock JG, Miller AL, Bradley WD, Rodriguez OC, Webb DJ, Koleske AJ. The Abl-related gene tyrosine kinase acts through p190RhoGAP to inhibit actomyosin contractility and regulate focal adhesion dynamics upon adhesion to fibronectin. *Mol Biol Cell* 2007;18:3860-3872.
142. Yam JW, Ko FC, Chan CY, Jin DY, Ng IO. Interaction of deleted in liver cancer 1 with tensin2 in caveolae and implications in tumor suppression. *Cancer Res* 2006;66:8367-8372.
143. Liao YC, Si L, deVere White RW, Lo SH. The phosphotyrosine-independent interaction of DLC-1 and the SH2 domain of cten regulates focal adhesion localization and growth suppression activity of DLC-1. *J Cell Biol* 2007;176:43-49.



144. Nakagawa H, Yoshioka K, Miyahara E, Fukushima Y, Tamura M, Itoh K. Intrathecal administration of Y-27632, a specific rho-associated kinase inhibitor, for rat neoplastic meningitis. *Mol Cancer Res* 2005;3:425-433.
145. Vicari RM, Chaitman B, Keefe D, Smith WB, Chrysant SG, Tonkon MJ, Bittar N, et al. Efficacy and safety of fasudil in patients with stable angina: a double-blind, placebo-controlled, phase 2 trial. *J Am Coll Cardiol* 2005;46:1803-1811.
146. Monnier PP, Sierra A, Schwab JM, Henke-Fahle S, Mueller BK. The Rho/ROCK pathway mediates neurite growth-inhibitory activity associated with the chondroitin sulfate proteoglycans of the CNS glial scar. *Mol Cell Neurosci* 2003;22:319-330.
147. Borisoff JF, Chan CC, Hiebert GW, Oschipok L, Robertson GS, Zamboni R, Steeves JD, et al. Suppression of Rho-kinase activity promotes axonal growth on inhibitory CNS substrates. *Mol Cell Neurosci* 2003;22:405-416.
148. Komagome R, Kimura K, Saito M. Postnatal changes in Rho and Rho-related proteins in the mouse brain. *Jpn J Vet Res* 2000;47:127-133.
149. Shimizu Y, Thumkeo D, Keel J, Ishizaki T, Oshima H, Oshima M, Noda Y, et al. ROCK-I regulates closure of the eyelids and ventral body wall by inducing assembly of actomyosin bundles. *J Cell Biol* 2005;168:941-953.
150. Thumkeo D, Keel J, Ishizaki T, Hirose M, Nonomura K, Oshima H, Oshima M, et al. Targeted disruption of the mouse rho-associated kinase 2 gene results in intrauterine growth retardation and fetal death. *Mol Cell Biol* 2003;23:5043-5055.
151. Van Eyk JE, Arrell DK, Foster DB, Strauss JD, Heinonen TY, Furmaniak-Kazmierczak E, Cote GP, et al. Different molecular mechanisms for Rho family GTPase-dependent, Ca²⁺-independent contraction of smooth muscle. *J Biol Chem* 1998;273:23433-23439.
152. Ng IO, Lai EC, Fan ST, Ng MM, So MK. Prognostic significance of pathologic features of hepatocellular carcinoma. A multivariate analysis of 278 patients. *Cancer* 1995;76:2443-2448.
153. Li Y, Tang ZY, Ye SL, Liu YK, Chen J, Xue Q, Gao DM, et al. Establishment of cell clones with different metastatic potential from the metastatic hepatocellular carcinoma cell line MHCC97. *World J Gastroenterol* 2001;7:630-636.
154. Velasco G, Armstrong C, Morrice N, Frame S, Cohen P. Phosphorylation of the regulatory subunit of smooth muscle protein phosphatase 1M at Thr850 induces its dissociation from myosin. *FEBS Lett* 2002;527:101-104.
155. Yvon AM, Walker JW, Danowski B, Fagerstrom C, Khodjakov A, Wadsworth P. Centrosome reorientation in wound-edge cells is cell type specific. *Mol Biol Cell* 2002;13:1871-1880.
156. Ogawa T, Tashiro H, Miyata Y, Ushitora Y, Fudaba Y, Kobayashi T, Arihiro K, et al. Rho-associated kinase inhibitor reduces tumor recurrence after liver transplantation in a rat hepatoma model. *Am J Transplant* 2007;7:347-355.
157. Lee Y, Jeon K, Lee JT, Kim S, Kim VN. MicroRNA maturation: stepwise processing and subcellular localization. *EMBO J* 2002;21:4663-4670.
158. Lee Y, Ahn C, Han J, Choi H, Kim J, Yim J, Lee J, et al. The nuclear RNase III Drosha initiates microRNA processing. *Nature* 2003;425:415-419.
159. Yi R, Qin Y, Macara IG, Cullen BR. Exportin-5 mediates the nuclear export of pre-microRNAs and short hairpin RNAs. *Genes Dev* 2003;17:3011-3016.



160. Hutvagner G, Zamore PD. A microRNA in a multiple-turnover RNAi enzyme complex. *Science* 2002;297:2056-2060.
161. Filipowicz W, Bhattacharyya SN, Sonenberg N. Mechanisms of post-transcriptional regulation by microRNAs: are the answers in sight? *Nat Rev Genet* 2008;9:102-114.
162. Kiriakidou M, Tan GS, Lamprinaki S, De Planell-Saguer M, Nelson PT, Mourelatos Z. An mRNA m7G cap binding-like motif within human Ago2 represses translation. *Cell* 2007;129:1141-1151.
163. Richter JD, Sonenberg N. Regulation of cap-dependent translation by eIF4E inhibitory proteins. *Nature* 2005;433:477-480.
164. Derry MC, Yanagiya A, Martineau Y, Sonenberg N. Regulation of poly(A)-binding protein through PABP-interacting proteins. *Cold Spring Harb Symp Quant Biol* 2006;71:537-543.
165. Wells SE, Hillner PE, Vale RD, Sachs AB. Circularization of mRNA by eukaryotic translation initiation factors. *Mol Cell* 1998;2:135-140.
166. Wakiyama M, Takimoto K, Ohara O, Yokoyama S. Let-7 microRNA-mediated mRNA deadenylation and translational repression in a mammalian cell-free system. *Genes Dev* 2007;21:1857-1862.
167. Lu J, Getz G, Miska EA, Alvarez-Saavedra E, Lamb J, Peck D, Sweet-Cordero A, et al. MicroRNA expression profiles classify human cancers. *Nature* 2005;435:834-838.
168. Johnson CD, Esquela-Kerscher A, Stefani G, Byrom M, Kelnar K, Ovcharenko D, Wilson M, et al. The let-7 microRNA represses cell proliferation pathways in human cells. *Cancer Res* 2007;67:7713-7722.
169. Bueno MJ, Perez de Castro I, Gomez de Cedron M, Santos J, Calin GA, Cigudosa JC, Croce CM, et al. Genetic and epigenetic silencing of microRNA-203 enhances ABL1 and BCR-ABL1 oncogene expression. *Cancer Cell* 2008;13:496-506.
170. Meng F, Henson R, Wehbe-Janek H, Ghoshal K, Jacob ST, Patel T. MicroRNA-21 regulates expression of the PTEN tumor suppressor gene in human hepatocellular cancer. *Gastroenterology* 2007;133:647-658.
171. Ma L, Teruya-Feldstein J, Weinberg RA. Tumour invasion and metastasis initiated by microRNA-10b in breast cancer. *Nature* 2007;449:682-688.
172. Hakem A, Sanchez-Sweatman O, You-Ten A, Duncan G, Wakeham A, Khokha R, Mak TW. RhoC is dispensable for embryogenesis and tumor initiation but essential for metastasis. *Genes Dev* 2005;19:1974-1979.
173. Korpal M, Lee ES, Hu G, Kang Y. The miR-200 family inhibits epithelial-mesenchymal transition and cancer cell migration by direct targeting of E-cadherin transcriptional repressors ZEB1 and ZEB2. *J Biol Chem* 2008;283:14910-14914.
174. Murakami Y, Yasuda T, Saigo K, Urashima T, Toyoda H, Okanoue T, Shimotohno K. Comprehensive analysis of microRNA expression patterns in hepatocellular carcinoma and non-tumorous tissues. *Oncogene* 2006;25:2537-2545.
175. Budhu A, Jia HL, Forgues M, Liu CG, Goldstein D, Lam A, Zanetti KA, et al. Identification of metastasis-related microRNAs in hepatocellular carcinoma. *Hepatology* 2008;47:897-907.
176. Aberle H, Bauer A, Stappert J, Kispert A, Kemler R. beta-catenin is a target for the ubiquitin-proteasome pathway. *EMBO J* 1997;16:3797-3804.



177. Hart MJ, de los Santos R, Albert IN, Rubinfeld B, Polakis P. Downregulation of beta-catenin by human Axin and its association with the APC tumor suppressor, beta-catenin and GSK3 beta. *Curr Biol* 1998;8:573-581.
178. Kitagawa M, Hatakeyama S, Shirane M, Matsumoto M, Ishida N, Hattori K, Nakamichi I, et al. An F-box protein, FWD1, mediates ubiquitin-dependent proteolysis of beta-catenin. *EMBO J* 1999;18:2401-2410.
179. Munemitsu S, Albert I, Souza B, Rubinfeld B, Polakis P. Regulation of intracellular beta-catenin levels by the adenomatous polyposis coli (APC) tumor-suppressor protein. *Proc Natl Acad Sci U S A* 1995;92:3046-3050.
180. Yost C, Torres M, Miller JR, Huang E, Kimelman D, Moon RT. The axis-inducing activity, stability, and subcellular distribution of beta-catenin is regulated in *Xenopus* embryos by glycogen synthase kinase 3. *Genes Dev* 1996;10:1443-1454.
181. Lin SL, Chiang A, Chang D, Ying SY. Loss of mir-146a function in hormone-refractory prostate cancer. *RNA* 2008;14:417-424.
182. Poon RT, Wong J. Long-term disease-free survival after resection of hepatocellular carcinoma: both tumor behavior and surgeon's performance are important determinants. *Ann Surg Oncol* 2003;10:834-836.
183. Jiang YF, Yang ZH, Hu JQ. Recurrence or metastasis of HCC:predictors, early detection and experimental antiangiogenic therapy. *World J Gastroenterol* 2000;6:61-65.
184. Arii S, Mise M, Harada T, Furutani M, Ishigami S, Niwano M, Mizumoto M, et al. Overexpression of matrix metalloproteinase 9 gene in hepatocellular carcinoma with invasive potential. *Hepatology* 1996;24:316-322.
185. Sun BS, Dong QZ, Ye QH, Sun HJ, Jia HL, Zhu XQ, Liu DY, et al. Lentiviral-mediated miRNA against osteopontin suppresses tumor growth and metastasis of human hepatocellular carcinoma. *Hepatology* 2008;48:1834-1842.
186. Lee TK, Poon RT, Yuen AP, Ling MT, Kwok WK, Wang XH, Wong YC, et al. Twist overexpression correlates with hepatocellular carcinoma metastasis through induction of epithelial-mesenchymal transition. *Clin Cancer Res* 2006;12:5369-5376.



List of Publications

Journals

Wong CC, Wong CM, Lee JM, Ng IO. Frequent underxpression of miR139 and its implication in hepatocellular carcinoma metastasis. Manuscript in preparation.

Wong CC, Wong CM, Tung EK, Man K, Ng IO. Rho-kinase 2 (ROCK2) is frequently over-expressed in hepatocellular carcinoma and involved in tumor invasion.

Hepatology. In Press.

Wong CC, Wong CM, Ko FC, Chan LK, Ching YP, Yam JW, Ng IO. Deleted in liver cancer 1 (DLC1) negatively regulates Rho/ROCK/MLC pathway in hepatocellular carcinoma. **PLoS ONE.** 2008 July 23; 3(7): e2779.

Wong CC, Ng IO. Gene Expression in Different Stages of Hepatocarcinogenesis. **Journal of Gastroenterology and Hepatology.** 2008 Jan;23(1):1-3.

Au SL, **Wong CC, Wong CM, Ng IO.** Upregulation of enhancer of Zeste Homolog 2 (EZH2) in human HCC. Manuscript in preparation.

Wong CM, **Wong CC, Ng YL, Ko FC, Ng IO.** Transcriptional repressive H3K9 and H3K27 methylations are essential for DNMT1-mediated DNA methylation recovery. Manuscript in preparation.



Lung HL, Lo CC, **Wong CC**, Cheung AK, Cheong KF, Wong N, Kwong FM, Chan KC, Law EW, Tsao SW, Chua D, Sham JS, Cheng Y, Stanbridge EJ, Robertson GP, Lung ML. **International Journal of Cancer**. 2008 Mar 15;122(6):1288-96.

Wong CM, Ng YL, Lee JM, **Wong CC**, Cheung OF, Chan CY, Tung EK, Ching YP, Ng IO. Tissue factor pathway inhibitor-2 as a frequently silenced tumor suppressor gene in hepatocellular carcinoma. **Hepatology**. 2007 May;45(5):1129-38.



Abstract Proceedings

Wong CC, Wong CM, Tung EK, Lee JM, Man K, Ng IO. Rho-kinase 2 (ROCK2) is involved in invasion and metastasis of hepatocellular carcinoma. The 13th Postgraduate Symposium, Faculty of Medicine, The University of Hong Kong. 2008.

Wong CC, Ng IO. Rho-kinase 2 (ROCK2) is involved in hepatocellular carcinoma progression, metastasis, and invasion. The International Liver Cancer Associate Annual Conference. 2008.

Wong CC, Ng IO. Overexpression of Rho-kinase 2 (ROCK2) is involved in invasion and metastasis of hepatocellular carcinoma. Joint Metastasis Research Society-AACR Conference on Metastasis. 2008. p. 97. C43.

Wong CC, Ng IO. Deleted in liver cancer 1 (DLC1) negatively regulates Rho/ROCK/MLC pathway in hepatocellular carcinoma. Hong Kong Shanghai International Liver Congress. Hepatology International. 2008. p. S49. YI20.

Wong CC, Ng IO. Rho-kinase 2 (ROCK2) is involved in migration and invasion of hepatocellular carcinoma cells by regulating actomyosin contractility. Hong Kong International Cancer Congress. 2007.



Wong CC, Ching YP, Ng IO. Roles and regulations of rho-kinase (ROCK) in hepatocellular carcinoma. American Association for Cancer Research Annual Meeting. 2007. p. 147. 1340.

Wong CC, Ching YP, Ng IO. The regulation and function of ROCK in hepatocellular carcinoma. The 11th Postgraduate Symposium, Faculty of Medicine, The University of Hong Kong. 2006.

Au SL, **Wong CC**, Wong CM, Ng IO. Upregulation of enhancer of Zeste Homolog 2 (EZH2) in human HCC. The 13th Postgraduate Symposium, Faculty of Medicine, The University of Hong Kong. 2008.



List of Academic Awards

(In Chronological Order)

The Croucher Foundation Fellowship

The Croucher Foundation

2009/2010

Best Presentation Award

The 13th Postgraduate Symposium, Faculty of Medicine, The University of Hong Kong
2008

Young Investigator Award

Hong Kong Shanghai International Liver Congress
2008

Swire Travel Grant

The University of Hong Kong
2008

Mary Sun Postgraduate Medical Scholarship

The University of Hong Kong
2007-2008

Wong Ching Yee Postgraduate Medical Scholarship

The University of Hong Kong
2007-2008

Swire Scholarship

The University of Hong Kong
2007-2008

Young Investigator Award

The 14th Hong Kong International Cancer Congress
2007

Outstanding Presentation Award

Cancer, Cell Biology and Musculoskeletal System Session
The 11th Postgraduate Symposium, Faculty of Medicine, The University of Hong Kong
2006

Best Presentation Award

The 3rd Postgraduate Retreat, Department of Pathology, The University of Hong Kong
2006

